AN EXPLORATION OF THERAPEUTIC APPLICATIONS FOR DINITROSYL IRON COMPLEXES (DNIC'S)

A Dissertation

by

DALE CHASE PECTOL

Submitted to the Graduate and Professional School of
Texas A&M University
in partial fulfillment of the requirements for the degree of

DOCTOR OF PHILOSOPHY

Chair of Committee,	Marcetta Y. Darensbourg
Committee Members,	David Barondeau
	Paul Lindahl
	Michael Nippe
Head of Department,	Simon W. North

August 2021

Major Subject: Chemistry

ABSTRACT

The therapeutic nature and mechanisms of *in vitro* nitric oxide (NO) release from dinitrosyl iron complexes (DNICs) are explored herein. First, the ideal primary coordination environment for the sustained liberation of NO while limiting the toxicity related to iron and NO was investigated. Dimeric RRE-type $\{Fe(NO)_2\}^9$ complexes, SPhRRE $[(\mu\text{-SPh})Fe(NO)_2]_2$ and TGTA-RRE, $[(\mu\text{-S-TGTA})Fe(NO)_2]_2$ (TGTA = 1-thio-β-d-glucose tetraacetate), were found to deliver NO with the lowest effect on cell toxicity (i.e., highest IC_{50}) with TGTA-RRE delivering a higher concentration of NO to the cytosol of SMCs. Monomeric DNICs with bulky N-heterocyclic carbenes (NHC), namely 1,3-bis(2,4,6-trimethylphenyl)imidazolidene (IMes), have IC_{50}'s of ~7 μM, but didn't release NO into SMCs. The reduced, mononuclear $\{Fe(NO)_2\}^{10}$ neocuproine-based DNIC increased intracellular NO.

Given the efficacy of TGTA-RRE, instead of redesigning entirely new DNICs, the release rate of NO was tuned with the addition of biomolecules histidine and glutathione. From the Griess assay and X-band EPR data, decomposition of the histidine-cleaved dimer, $[(TGTA)(N_{His})Fe(NO)_2]$, generated Fe(III) and increased the NO release rate compared to the TGTA-RRE precursor. In contrast, increasing concentrations of glutathione generated the stable $[(TGTA)(GS)Fe(NO)_2]^-$ and depressed the NO release rate. This work provides insight into tuning NO release beyond the design of DNICs, through the incubation with biomolecules.

A structure activity relationship between thiolate identity and expected protease inhibition was investigated *in silico* and *in vitro* via AutoDock 4.2.6 (AD4) and FRET protease assays respectively. AD4 was validated for coordinatively unsaturated DNIC binding using a crystal structure of a protein-bound DNIC, PDB – 1ZGN (calculation RMSD = 1.77). The dimeric DNICs TGTA-RRE and TG-RRE, $[(\mu\text{-}S\text{-TG})Fe(NO)_2]_2$ (TG = 1-thio-β-d-glucose), were identified as leads via the *in silico* study. Computations suggest inhibition at the catalytic Cys_{145} of $SC2M^{pro}$. *In vitro* studies indicate inhibition of protease activity upon TGTA-RRE treatment, with an IC_{50} of 38 μM for TGTA-RRE and 33 μM for TG-RRE. This study presents a simple computational method for predicting DNIC-protein interactions as well as validating the *in silico* leads *in vitro*.

DEDICATION

To my mother for making sure I was busy doing something productive as a kid.

To my dad for showing me how to channel my excitement.

To my wife for motivating me to make a better future for us.

And to my dog for putting up with me, I wish you were still here.

ACKNOWLEDGEMENTS

It has been a long, weird road to get where I actually am right now. Before grad school I had already cycled through a couple of potential careers: high school teacher (please, please don't suggest anyone to go into secondary school teaching unless they truly care about the education of the future. It can be a soul crushing profession), radio DJ and science talk-show host (I can credit my co-hosts for fine-tuning my speaking skills), and whatever you're supposed to do with an American Studies undergraduate degree (I was a door to door canvasser for Environment Texas for about a month before I realized I was awful at it). All that experience could not properly prepare me for what graduate school had in store for me: projects that would fail and fail again, then work when I had almost given up hope, a global pandemic, the Trump presidency, meeting my fiancée, making new friends and connections at conferences, getting married, crippling anxiety, and graduate research honors, just to name a few. I could not have made it through it all without the help of my advisor, my advisor, my committee members, our collaborators, my friends, my labmates, my family, and my wife.

I would like to extend my gratitude to Dr. Marcetta Y. Darensbourg. It is truly impressive that she was able to build a career in science academia as a woman in a male dominated field dating back to the 1970s, but also impressive that she was able to put up with my shenanigans for the last 6 years. She helped me hone my knowledge and intuition into the scientist I am today thanks to her attention to detail, skepticism, and tutelage. She has shown me that at its core, science is a rigorous, thorough search for truth. I will be forever grateful for her guidance these last few years.

I would also like to thank my committee members have helped me in various ways. Dr. Lindahl inadvertently played the matchmaker for me and my wife Dr. Donna Iadarola, since we met in his and Dr. Gohil's journal club. Who knew iron and copper disease states could be so romantic? Dr's Barondeau and Nippe were available for counsel throughout my graduate career and have offered helpful career and professional advice along the way. Dr. Lim for advising me during the more biochemical portions of our research, ensuring that I was able to make the appropriate connections for collaboration. Other Texas A&M staff that have been of great service include Yohannes Rezenom who aided me in the experimental design of a number of mass spectral experiments, and Nattamai Bhuvanesh, for the invaluable service that he provides for me and everyone else in the chemistry department with his work in the X-ray crystallography lab. Additionally, Dr. Elmo Mawk has been a constant guiding force in my teaching experience at Texas A&M, allowing me quite a bit of freedom in Quantitative Analysis.

Our collaborators have been a huge help and source of inspiration throughout graduate school. Dr's Hunstad and Wooley demonstrated the applicability of Ag^{+} coordination complexes in the development of potential antibacterial agents, and openly welcomed our inorganic chemistry group into the medicinal field. During the pandemic, the Liu and Fierke groups were instrumental in beginning our journey into protease inhibition with Zn complexes and DNICs.

Graduate school comes built in with friends in the form of study sessions, TA meetings, and lab mates. I was fortunate enough to cultivate quality, life-long friends in my years here. We helped each other through the roller coaster of graduate life in more

ways that one. In no particular order, I'd like to specifically thank Dr. Jeremy Willman, Dr. David Parobek, Christopher DeLaney, and Richard Carranza.

In the first two-ish years, I was the junior student in a lab full of 4+ year grad students, but that quickly changed in year 2, when I became the senior-most student in the lab after they all graduated. I would like to thank Dr.'s Rachel Chupik, Allan Lunsford, Jason Denny, and Pokraj Ghosh for their advice on how to navigate graduate school before they left; and I would like to thank Chris DeLaney, Dr. Xuemei Yang, Manuel Quiroz, Trung Le, Lindy Elrod, Dilshan Kariyawasam, and Paulina Guerrero for being there for me and for supporting each other through these last five years to make sure that the lab ran as well as it could.

I would like to thank my family for their continued support throughout this whole ordeal, and for finally stop asking, "so when are you going to be through?" In all seriousness though, watching my family grow has truly been a source of delight and motivation. My sister Chelsea's children (Trace and Jordie) have grown from toddlers to curious children. Trace, my nephew, came to visit the lab and when I asked him what he thought the glove box was, he paused with a pensive look on his face. Suddenly a wave of excitement rushed across his face, "It's a hug machine!" That's one of the first thoughts I have when I look at any glove box now. My mom and my dad have encouraged me when times got harder over the quarantine or during prelim times. Both of you have done a great job of pushing me to be the best version of myself.

And finally, the person who has made my time in College Station truly magical, my wife Dr. Donna Iadarola. I am so excited to be there to support you through the rest

of our lives together. This next chapter in Philadelphia will be an adventure and I cannot wait to see what's in store, but I know whatever happens will be even more special because I will not be on that journey alone. None of this would be possible without you.

CONTRIBUTORS AND FUNDING SOURCES

Contributors

The work reported within this dissertation was supported by a dissertation committee consisting of Professor Marcetta Y. Darensbourg, advisor, Professors Michael Nippe, and David Barondeau both of the Department of Chemistry, Dr. Soon-mi Lim, and Professor Paul Lindahl, of the Department of Biophysics and Biochemistry and Department of Chemistry.

Crystallographic data was collected and solved by Nattamai Bhuvanesh at the X-Ray diffraction laboratory at Texas A&M University. The data presented in Chapter III & IV was done in collaboration with the research group of Prof. Karen Wooley. Namely, the viability assays were performed in conjunction with Sarosh Khan and Mahmoud Elsabahy, and the immunotoxicity assays were performed by Dr. Mahmoud Elsabahy. Dr. Soon-mi Lim served as an advisor throughout the manuscript preparation process. Dr. Rachel Chupik helped lay the academic foundation for the data collected. Chapter V was a collaboration between the labs of Prof. Carol Fierke, Prof. Wenshe R. Liu, and Dr. Thomas Meek. The FRET assays reported in Chapter V were carried out by Christopher DeLaney and Jinye Zhu, a graduate student of in the Meek lab. Portions of the polymeric work reported in Chapter VI were carried out in collaboration with Dr. Gulzar Bhatt, of the Dr. Donald J. Darensbourg research group. All experiments were performed at Texas A&M University.

All other work reported in this dissertation was completed independently, under the supervision of Marcetta Y. Darensbourg of the Department of Chemistry.

Funding Sources:

This work was made possible in part from grants from the Welch Foundation and the National Science Foundation. Graduate studies were also supported by Texas A&M University.

The contents of this dissertation are solely the responsibility of the authors and do not necessarily represent the official views of the Welsh Foundation or the National Science Foundation.

NOMENCLATURE

AFM: Antiferromagnetic

CIP: chelatable iron pool

CVEC: coronary venular endothelial cells

DCM: dichloromethane

DEANO: 1,1-diethyl-2-hydroxy-2-nitroso-hydrazine sodium salt

DMEM/F12: Dulbecco's modified Eagle media – F12

DMSO: dimethylsulfoxide

DNIC: dinitrosyl iron complex

DNIU: dinitrosyl iron unit

EIC: extracted ion chromatogram

eNOS: endothelial nitric oxide synthase

EPR: electron paramagnetic resonance

ESI-MS: electrospray ionization mass spectrometry

FMOC: fluorenylmethyloxycarbonyl

FT-IR: Fourier transform infrared spectroscopy

GSH: glutathione

GSNO: *S*-nitrosoglutathione

GST: glutathione transferase

His: histidine

HisF: Nα-FMOC-N(im)-trityl-L-histidine

IL-X: interleukin-X

IMes: 1,3-bis(2,4,6-trimethylphenyl)imidazolidene

iNOS: inducible nitric oxide synthase

IpI: isopropylimidazole

L-NNA: L-N^G-Nitroarginine

MTS: 3-(4,5-dimethylthiazol-2-yl)-5-(3-carboxymethoxyphenyl)-2-(4-sulfophenyl)-2*H* tetrazolium

MRP1: multidrug resistance protein 1

NHC: *N*- heterocyclic carbene

nNOS: neuronal nitric oxide synthase

NO: nitric oxide

NOR: nitric oxide reductase

NORM: nitric oxide release molecule

RNS: reactive nitrogen species

RRE: Roussin's red ester

SARS-CoV: severe acute respiratory syndrome associated coronavirus

SGluc: 1-thio-β-d-glucose tetraacetate

sGC: soluble guanylate cyclase

SGlucRRE: $[(\mu\text{-}S$ 1- thio-β-d-glucose tetraacetate$)Fe(NO)_2]_2$

SMC: smooth muscle cell(s)

SNAP: *S*-nitroso-*N*-acetyl-DL -penicillamine

SNO: *S*-nitrosothiol

SPh: thiophenol

TG: 1- thio-β-d-glucose

TGTA: 1- thio-β-d-glucosetetraacetate

TNIC: trinitrosyl iron complex

TABLE OF CONTENTS

Page

LIST OF FIGURES

Page

LIST OF TABLES

Page

CHAPTER I : INTRODUCTION

I.1 Introduction to Nitric Oxide

The simple diatomic nitric oxide (NO), presents as one of the most ubiquitous signals in mammalian biology,[1-5] as well as a highly versatile tool in a synthetic inorganic chemist's toolbox.[6-9] Nitric oxide research, as it relates to biology in the timeline below (Figure I-1), took off in the early 1970's upon the discovery that it was the bioactive molecule in nitrates, a historically prescribed medication for heart conditions.[10] Soon thereafter, one of the first deliberate NO release molecule (NORM), sodium nitroprusside $[Fe(CN)_5(NO)]^{2-}$, was developed as a therapeutic for hypotension.[11] Studies continued into the 1980's where pioneers in the medicinal field, Furchgott, Ignarro, and Murad, made the discoveries that would gain them the joint Nobel Prize in Medicine in 1998.[12-17]

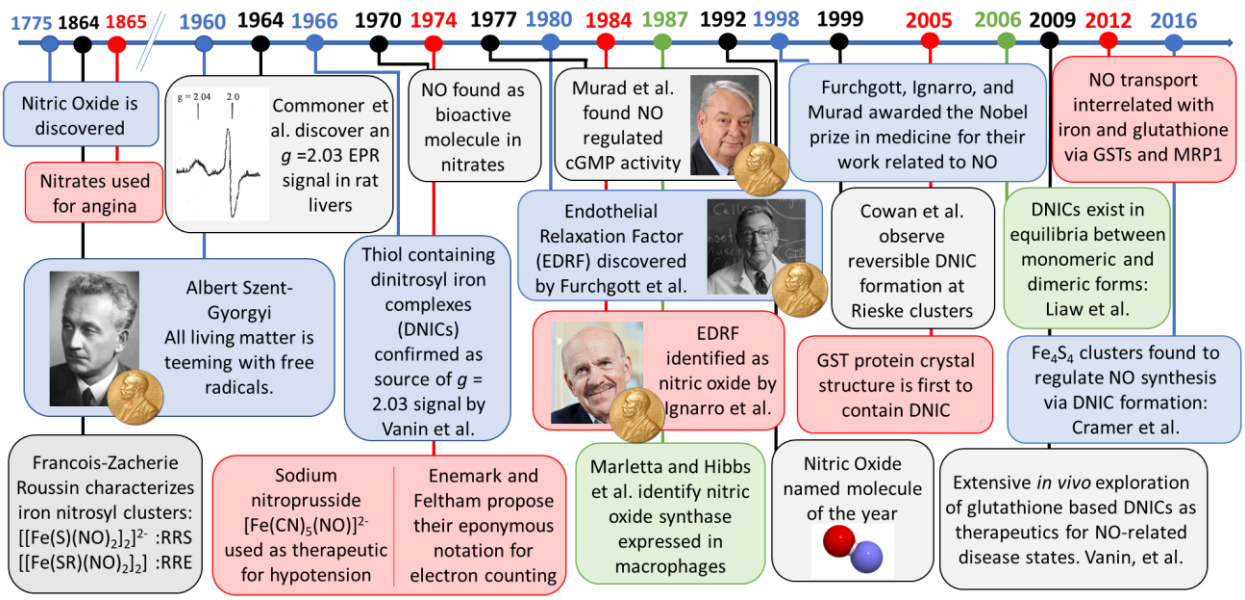

Figure I-1: Timeline of notable discoveries in nitric oxide and dinitrosyl iron complex research. A pictorial representation of the history of DNICs expressed in the review by Anatoly Vanin.[18] An expansion from 2016 to 2021 is given in Figure 4.

Furchgott discovered the existence of an endothelial derived relaxation factor (EDRF) responsible for smooth muscle cell relaxation.[19] Murad found that NO regulated cyclic GMP activity (the first step in a cascade of actions that ultimately causes smooth muscle relaxation),[20] and Ignarro connected the dots and identified the EDRF as nitric oxide.[21] After their discoveries, the labs of Marletta and Hibbs found that there were three different isoforms of nitric oxide synthase (NOS) which synthesized NO from L-Arginine in an NAD(P)H dependent manner.[22-24] The first is responsible for the delivery of NO from the endothelia to smooth muscle cells, endothelial NOS (eNOS). Neuronal NOS (nNOS) generates NO at neurons to send signals throughout the nervous system; and, finally, inducible NOS (iNOS) generates a high concentration of nitric oxide as a way to destroy physiologically perceived threats such as invading bacteria or infected cells.

Nitric oxide's characteristic odd electron is key to its involvement in these myriad processes. At lower concentrations (~50 nM – 1 μM), akin to what eNOS or nNOS would generate, this radical quickly reacts in the area where it is released, generating localized responses in cells or tissues such as smooth muscle relaxation, and wound healing, amongst numerous regulatory processes. However, at higher concentrations (~100 μM) such as those utilized by iNOS, this reactivity becomes deleterious (Figure I-2).[25-28] Nitric oxide combines with other reactive species such as thiolates, tyrosine, reactive oxygen species, metal hemes, DNA, the chelatable iron pool, and iron sulfur clusters.[29-36] Many of these are intermediates along the path of NO transport; others represent the final target. Perhaps the most critical and well-studied of iron-NO interactions is the porphyrin-

Fe(NO), which is found in soluble guanylate cyclase (sGC), the protein responsible for initiating the a cascade of actions that ultimately ends in smooth muscle relaxation. Other porphyrin-Fe(NO) related proteins include nitric oxide reductases, lipoxygenases, heme-oxygenase 1, and hemoglobin, amongst others.

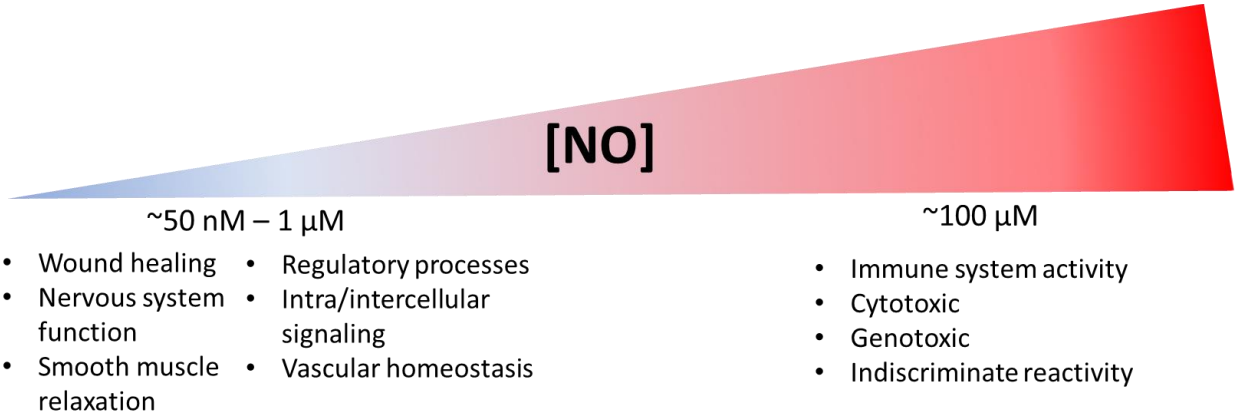

Figure I-2: Graphic identifying differing functions of nitric oxide based on its concentration in a biological setting.

Since NO is such a ubiquitous signaling agent, there are a number of disease states that can arise from misregulation of NO homeostasis, such as asthma, erectile dysfunction, ineffectual wound healing in diabetics, Parkinson's disease, cartilage degeneration, etc.[37-41] Scientists have sought to treat these disease states with simple NO release molecules like sodium nitroprusside, nitroglycerin, diazeniumdiolates, and amyl nitrites.[42-44] There are many excellent reviews of nitric oxide release molecules (NORMs) that highlight the importance of NO delivery.[45-50] However, many NORMs experience the same issue as free nitric oxide in that they quickly decompose in aerobic, aqueous environments.[51] To

combat that, these moieties have been incorporated into larger macromolecular frameworks to depress their NO release rate.[52] There are only a few NORMs in clinical use, but they are primarily used for a quick burst of NO to alleviate conditions like hypotension.[53] This results begs the question: how does biology tame the reactive radical NO so that it can be transported to and from tissues without spontaneous decomposition that hampers the development of NO release molecules? One such hypothesis that has gained traction is that the concentration of "free" NO in the body is always small, and most is bound to a version of their known cellular targets such as thiolates, Fe-S clusters, etc., awaiting liberation or transfer when contacted by a more suitable binding site.[54-56] Arguably, the most common of these intracellular adducts of nitric oxide is the dinitrosyl iron complex, or DNIC, typically comprised of two thiolate donors, commonly glutathione *in vivo,* and the $[Fe(NO)_2]$ dinitrosyl iron unit (DNIU).[57]

I.2 DNICs as the *in vivo* "working form" of NO (storage, transport and targeted release)

Before the biological significance of nitric oxide was revealed, NO had long been recognized by inorganic/coordination chemists for its versatile metal-binding properties. Some of the first metal nitrosyl complexes were characterized in the 1850s and 1860s by Francois Zacharie Roussin, who proceeded to name all of the Fe(NO) complexes after himself: the neutral, dimeric, thiolate bridged DNIC Roussin's Red Ester (RRE) $[Fe(NO)_2(\mu\text{-}SR)]$, the charged sulfide bridged dimer Roussin's Red Salt (RRS)

$[Fe(NO)_2(\mu\text{-}S)]_2^{2-}$, and the sulfide-bridged tetramer Roussin's Black Salt (RBS) is of the formula $[(Fe(NO)_2)_3(Fe(NO))(\mu\text{-}S)_3]$.[58] It was later specified that when bound to iron or other metals, nitric oxide can serve as a "non-innocent" ligand, tuning the redox level of the metal it is bound to by delocalization of the metal d-orbital electrons into the π* orbitals of NO.[59-61] The extent of delocalization can lead to difficulty in the formal assignment of oxidation states, so an eponymous methodology was coined by Enemark and Feltham in 1974: $\{M(NO)_x\}^y$ where x is the number of nitrosyl ligands and y is the number of electrons in the M *d*-orbitals and the π* manifold of the nitrosyl.[62]

There is a rich literature that has evolved around the chemical study of dinitrosyl iron complexes. Due to the "non-innocence" of the NO ligand, the DNIU has two stable redox levels: the EPR active oxidized $\{Fe(NO)_2\}^9$, and the reduced EPR silent $\{Fe(NO)_2\}^{10}$.[63-66] This unique and characteristic EPR g = 2.03 signal led to the identification of DNICs in 1964-5 from rat livers under heavily carcinogenic conditions.[67-68] This signal would later be identified by Vanin and coworkers as a dinitrosyl iron complex with two glutathione ligands, $[Fe(NO)_2(SG)_2]^-$.[69] This discovery is likely the foundation for biological studies as related to dinitrosyl iron complexes.[70-72]

Monomeric species spontaneously form in the presence of ferric iron, NO, and glutathione (GSH).[73] The NO comes from any of the NOS's and the glutathione is intracellularly ubiquitous (concentrations vary from 1-10 mM depending on the type of cell).[74-75] Once formed, the monomeric species is in an equilibrium with a dimeric Roussin's Red Ester DNIC where the bridging thiolates are likely glutathione.[76-77] These

equilibria have been observed biologically by the Vanin group, and in chemical studies by the Liaw group. The latter demonstrated the interconversion of monomeric mononitrosyl complexes (MNIC), monomeric DNICs, and dimeric DNICs using differing ratios of NO and tert-butyl thiol (Figure I-3).[78-79]

Cowan, Ding and coworkers demonstrated reversible DNIC formation with Fe-S clusters in Endonuclease III (EndoIII) and in ferredoxin (Fdx) with the aid of cysteine desulfurase.[80-84] Subsequently, the J.K. Barton lab showed that the DNIC formation in EndoIII was dependent on the presence of iron and nitric oxide. Further examination with HYSCORE, EPR, isotopic labeling studies using ^{15}NO, protein film electrochemistry, and gel electrophoresis proved that the resulting degradation product from nitrosative stress was two protein-bound DNICs, one RRE and one monomeric DNIC, at the site of the Fe_4S_4 cluster.[85] This DNIC formation led to a decrease in DNA repair that was attributed to a drastic 800 mV negative shift in reduction potential of the cluster, rather than a conformational shift in the enzyme (Figure I-3). Cysteine desulfurase can reduce the DNICs, liberating NO, and reforming the iron-sulfur cluster.[82,83,86]

Besides DNA repair enzymes, DNICs have also been implicated in the inhibition of cysteine aspartic acid proteases (Caspases) through the nitrosylation of the catalytic cysteine forming a cysteine-based nitrosylthiol (RSNO).[87] Caspases are a part of the "caspase cascade" which initiates apoptosis through the proteolysis of DNA repair enzymes, preventing the natural cycle of cell death via inhibition which leads to cancers.[88]

This inhibition is not permanent, since NO is readily liberated from RSNOs in the presence of trace metal ions, namely Cu^{+} and ferrous iron.[89-90]

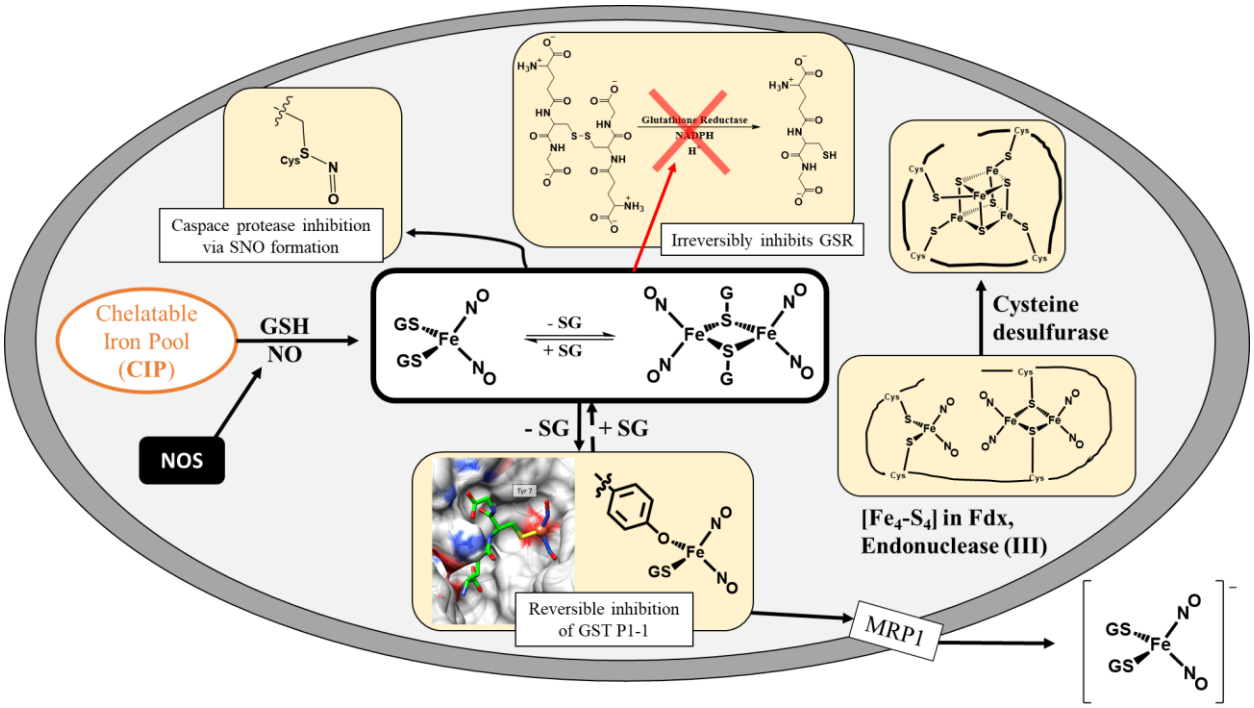

Figure I-3: Depiction of the likely roles of DNICs in biology. The grey concentric ovals indicate the membrane of a non-descript living cell. DNICs are formed via a spontaneous reaction with the CIP, NO via nitric oxide synthase (NOS), and GSH, whereupon they enter an equilibrium between dimeric and monomeric DNICs.[73,139] It is not clear which of these species is ultimately responsible for the inhibition or modification of the enzymes listed. These DNICs are found to inhibit, starting from the top left, working clockwise, Caspase,[87] glutathione reductase (GSR),[92] ferredoxin (FdX),[82] Endonuclease III (EndoIII),[85] and glutathione transferase (GST P1-1).[91] The beige boxes contain the chemical structures based on known modes of inhibition for Caspase, GST P1-1, and EndoIII. The chemical structure of the repaired Fe_4S_4 of EndoIII via cysteine desulfurase is shown for comparison. The protein crystal structure of DNIC inhibited GST[91] is depicted next to its chemical structure counterpart.

I.3 DNICs as related to glutathione homeostasis

DNICs have been found to inhibit enzymes related to glutathione homeostasis in an NO independent manner: Glutathione Reductase (GSR) and Glutathione Transferase (GST) (Figure I-3).[91-92] Glutathione is a tripeptide of γ-glutamate, cysteine, and glycine; it is regarded as the ubiquitous redox regulator in biology.[93-94] By balancing the concentration of the oxidized disulfide of glutathione with the protonated thiol, the redox potential (E') of cells is reported to be modulated from -245 mV to -366 mV depending on the GS-SG/GSH ratio.[95-98] One of the key enzymes in maintaining this redox balance is GSR, which catalyzes the reduction of GS-SG to GSH in an NADPH dependent process.[99] The active site of this enzyme contains two catalytic thiolates, Cys_{63} and Cys_{58}.[100] The catalytic thiolates reduce the disulfides in oxidized glutathione, liberating two equivalents of reduced glutathione, and forming a disulfide bond between Cys_{63} and Cys_{58}. The enzyme disulfide is then re-reduced to a pair of thiols with the aid of NAPDH and an FAD at the active site. It is not known which step in the catalytic cycle is inhibited by the monomeric DNICs, but it is accepted that the inhibition happens irreversibly at the active site cysteines with an IC_{50} of 5 μM.[92]

Another function of glutathione is the removal of compounds known to form reactive oxygen species (ROS) from the cytosol, such as metal ions and peroxides.[101-104] This avenue of detoxification is mediated by two enzymes, Glutathione Transferase (GST) and the Multidrug Resistant Protein (MRP1).[106-108] Glutathione attached to these potential toxins binds to the active site of cytosolic GST, whereupon it is transported to MRP1 and

expelled from the cell. This is the mechanism by which cancer cells become "immune" to platinum-based chemotherapeutics.[109-110] DNICs function as reversible inhibitors for GST; however they are not expelled from the cell immediately upon binding as are other metal-containing toxins.[111] There are equilibria established between monomeric DNICs, dimeric DNICs and GST bound DNICs resulting in a drastic extension of the lifetime of nitric oxide. On combining all of these different DNIC forms, DNICs are argued to be the most abundant adduct of nitric oxide.[57] The interaction between GST, glutathione, and DNICs is the crux of the hypothesis that DNICs are the "working form" of nitric oxide in biology.[18,112]

I.4 DNICs as therapeutics

Because of these DNIC specific interactions with proteins, variations on the naturally occurring motifs were developed as potential therapeutics that would allow for phenotypes not available for nitric oxide release molecules or drugs that block alternate functions of sGC, which mimics an increase in intracellular NO concentration.[113-115] The most extensively studied of these DNIC-based therapeutics is Oxacom®, or [(μ-S-Glutathione)$Fe(NO)_2]_2$.[78,112,116-119] The Vanin group deliberately synthesized the naturally occurring RRE-type DNIC, and showed that it abates a number of conditions associated with NO misregulation. That is, as a source of NO, it alleviates erectile dysfunction, promotes diabetic wound healing, decreases platelet aggregation, and lowers mean arterial blood pressure. Unfortunately, treatment the effect glutathionyl DNIC treatment is not

always beneficial since treatment of mice with Lewis carcinoma with Oxacom increased the size of the cancerous tissue due to activation of angiogenesis by the DNIC's.[120-123]

The Liaw group has investigated another type of water soluble RRE-DNIC that was built upon bridging thioethanol ligands, $[(\mu\text{-}SCH_2CH_2OH)Fe(NO)_2]_2$, that was found to release NO over the course of 24+ hours in solution.[124] This same DNIC notably increased the lifespan of *Caenorhabditis elegans* (roundworms are commonly used as the model organism for longevity),[125-127] and also promoted diabetic wound healing in mice (Figure I-4). When the RRE DNIC above was cleaved with a cysteamine zwitterion ($S^-CH_2CH_2NH_3^+$) generating the neutral $[(SCH_2CH_2NH_3^+)(SCH_2CH_2OH)Fe(NO)_2]$, the therapeutic nature of the DNIC was drastically reduced.[124] The $t_{1/2}$ of NO release was decreased from 27.4 h to 0.5 h. This rapid decomposition of NO led to cellular outcomes associated with a large excess of nitric oxide which allowed for the DNIC to now function as an anti-cancer agent via the activation of the Stress Associated Protein Kinases and Jun Amino-terminal Kinases (SAPK/JNK), ultimately leading to cancer cell apoptosis.[124,128]

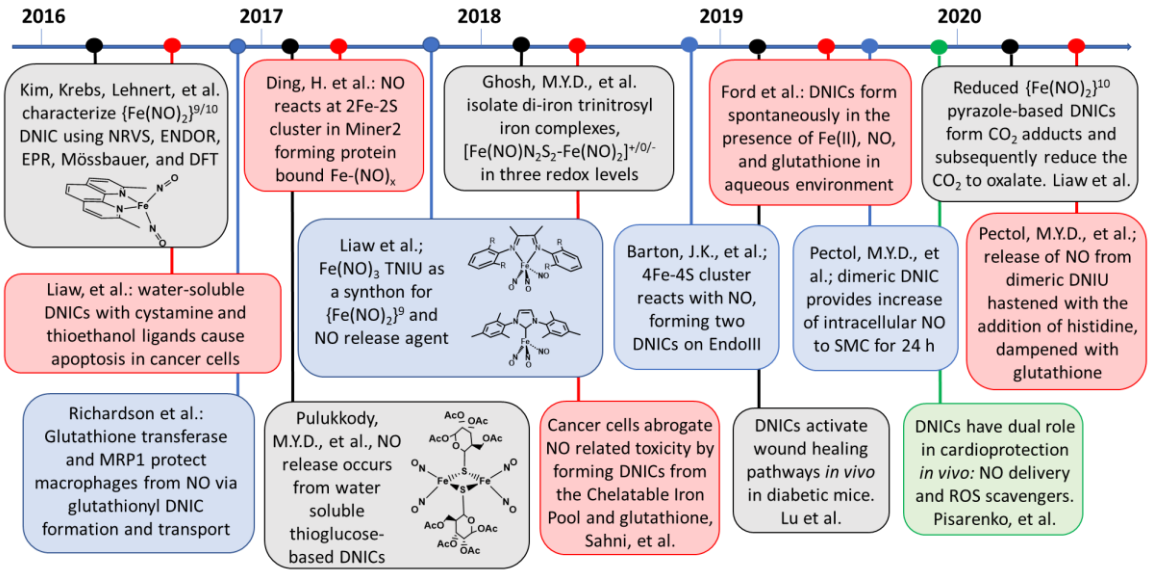

Figure I-4: Timeline showing recent advances in chemistry and biochemistry related to dinitrosyl iron complexes. Chemical structure of DNICs shown correspond to DNICs used in the corresponding studies. References from left to right on the timeline: Ref 177, 124, 102, 141, 81, 149, 176, 34, 85, 156, 73, 189, 190, 143, and 66.

Other efforts have been made to engineer a trigger into the DNIC that might control the liberation of NO. Ford and coworkers attached a photosensitizer (protoporphyrin-IX - PPIX) to the bridging thiolate groups in a Roussin's Red Ester DNIC.[129] The photo-excited electron from PPIX is transferred to the dimeric DNIUs causing one of the four NOs to be released forming a putative $Fe_2(NO)_3(\mu\text{-}SR)_2$ that spontaneously decomposes in aerobic aqueous conditions releasing 4 moles of NO per mole of PPIX-DNIC. The same effect was achieved when PPIX was replaced with Fluorescein in subsequent investigations.[131-132]

The group of Eunsuk Kim has investigated the use of L-L type DNICs as NO-release prodrugs. This unique 5-coordinate DNIC is metastable in an aqueous environment until the iodide dissociates which causes spontaneous decomposition.[130] The dissociation was proposed to happen intracellularly, where a number of ligands (glutathione, histidine, etc.) could potentially outcompete the iodide. The expression levels of two proteins was taken as evidence that *in vitro* in RAW 264.7 macrophage cells, intracellular NO release occurred .

Increased levels of Nitric Oxide are known to be a potent stimulant for the increase in the expression of heme oxygenase-1 (HO-1). The decrease in the expression of iNOS indicated that there was an increase in the concentration of intracellular NO due to a known negative feedback mechanism.[130] Additionally, these reduced $\{Fe(NO)_2\}^{10}$ DNICs were found to cause phenol nitration of tyrosine, presumably due to the enhanced O_2 reactivity of the DNIU.[133-134]

Most of these investigations of DNICs as therapeutics emulate the dimeric, thiolate-bridged motifs observed through biochemical characterization of DNICs. The M.Y. Darensbourg group posited that the introduction of abiotic, inorganic ligands would provide alternative routes to tune the release of NO from the DNIC via the addition of steric bulk and π backbonding from the mesityl-flanked *N*-heterocyclic carbene.[66] In contrast to the expected result, in all cases, the monomeric DNICs degraded rapidly in aerobic aqueous conditions, and the dimeric DNICs were sustained sources of NO (up to

24 h). In the dimeric form, the DNICs were much less toxic, and did not artificially stimulate the production of cytokines from macrophage cells.

Based on the rich history of DNICs in synthetic inorganic chemistry, its known that imidazoles and thiols could cleave the DNIC dimer to generate a monomer.[138] The most abundant sources of imidazoles and thiolates expected to be in the cell are histidine and glutathione respectively. The dimeric DNIC, $[(\mu\text{-S-TGTA})Fe(NO)_2]_2$; TGTA = 1-thio-β-d-glucose tetraacetate, was treated with increasing concentrations of histidine and glutathione to observe if there was any change in the rate of NO release.[189] Interestingly, there were two different outcomes. As was expected, upon cleavage with histidine, the DNIU is destabilized, and degrades, causing an increase in the rate of NO release inside and outside the cell. However, upon cleavage with glutathione, the rate of NO release decreases. The excess of glutathione cleaves and stabilizes the DNIU which allows for the more stable RRE-dimer to reform with a mixed thiolate environment, $[(\mu\text{-S-TGTA})(\mu\text{-S-Glutathione})(Fe(NO)_2)_2]$. This imparted stability reduced the amount of NO released in media, and intracellularly. Furthermore, since the addition of external chemical reductant abolished intracellular NO release, it was concluded that this stability was due to coordination and not redox modulation of the DNIU by GSH.

I.5 A Short History of Synthetic Inorganic Chemistry of DNICs

Based on what is known about DNIC and biology, there are questions that intrigue the inorganic chemist. As shown above, there is mounting evidence that DNICs are the "working form" of nitric oxide due to its interrelated nature to glutathione biochemistry, and that DNICs can provide therapeutic outcomes that are independent of treatment with nitric oxide alone.[18,29,91,102,111,112,135-137] But how is the NO released or transferred from the DNIC? Which form is more reactive, monomer or dimer? Does redox level control the stability/release of NO? In attempts to uncover the molecular basis of such properties, synthetic inorganic chemists have developed of an extensive library of DNICs with variable coordination environments. Using abiotic ligands, such DNICs were used to explore novel functions as related to physical and spectroscopic properties of the DNIU that would better inform biological characterization.

Monomeric DNICs with the formula $[(L/X)_2(Fe(NO)_2)]$ have been synthesized, where L = $:CR_2/:NR_2/:PR_3/:SR_2$ and $X^- = SR^-/OR^-/Cl^-/Br^-/I^-/PR_2^-$, in the reduced $\{Fe(NO)_2\}^{10}$ and oxidized $\{Fe(NO)_2\}^9$ forms.[138] They are generated either from a mixture of Fe^{II} salts with excess NO gas in the presence of ligand,[139] or from subsequent ligand substitution reactions using a convenient synthon, $Fe(CO)_2(NO)_2$.[140,141] Due to the ease of purification and reproducibility of synthetic results, $Fe(CO)_2(NO)_2$ is a popular synthon, isolated as a pure liquid to produce desired coordination complexes (Figure I-5). This neutral four-coordinate $\{Fe(NO)_2\}^{10}$ DNIU undergoes a number of nucleophilic substitution reactions and reacts readily with oxidized disulfides, yielding a dimeric,

oxidized $\{Fe(NO)_2\}^9$ DNIU bridged by thiolates.[142] The reductive power of the $\{Fe(NO)_2\}^{10}$ DNIU is not limited to reaction with disulfides, it can generate H_2 upon the addition of pyrazole, HPR_2, or RSH yielding the corresponding dimeric bridging pyrazolate, phosphide, or thiolate $\{Fe(NO)_2\}^9$ complexes.[143-148] Alternatively, the $\{Fe(NO)_2\}^{10}$ unit may be directly oxidized with the addition of a suitable oxidant.[149-150] Nitrosonium salts are the preferred oxidants since the byproduct is additional gaseous NO that can be easily removed from the reaction mixture and will not interfere with the metal bound nitrosyls.

There is a binding preference when it comes to the formation of nucleophilically substituted pseudotetrahedral $[(L/X)_2\{Fe(NO)_2\}^{10}]^{0/-}$ complexes.[138] The most favorable of the binding partners to the electronically diffuse DNIU are aliphatic and phenyl thiolates with a slight preference towards the aliphatic, followed by imidazolate, phenoxide, methoxide, nitrite, and finally CO.[151-154] Oxidized $\{Fe(NO)_2\}^9$ monomeric DNICs are either neutral or anionic depending on the identity of the ligands in the primary coordination sphere. Regardless of ligand field, all $\{Fe(NO)_2\}^9$ DNIUs display a characteristic EPR signal around $g = 2.03$.

For simple bidentate chelates, the coordination preference remains similar to what was stated above, with the most preferred being thiolate-based chelates, followed by mixed thiol-carboxylate/carboxamide, then pyridine-based chelates (i.e. - bipy, phen, etc.), followed by phosphines, and finally amines.[138] Because of this, TMEDA, sparteine, and Diphos $\{Fe(NO)_2\}^{10}$ DNICs have been used as precursors to other chelates via a ligand

displacement reaction. [63,155-157] A coordination number of 5 is reachable for the DNIU, and requires tridentate chelating ligands like pyridinediimidazole (PDI) or trispyridylmethylamine (TPA), or the conversion of NO to κ-2 nitrite or κ-2 nitrate in the presence of oxygen, or halides.[158-162]

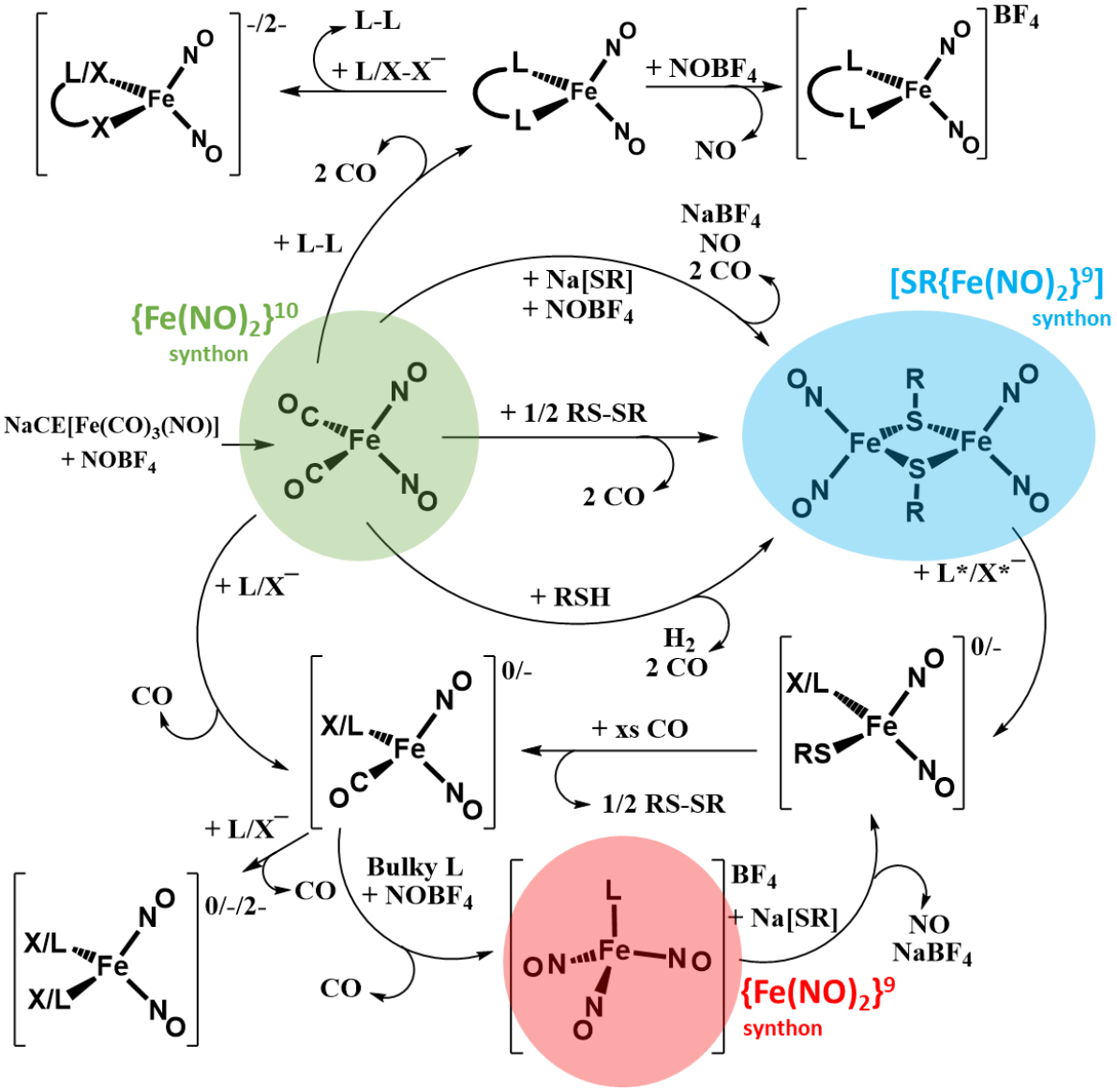

Figure I-5: Representations of DNIC synthesis routes for dinitrosyl iron complexes. Synthetically useful donors for the $\{Fe(NO)_2\}^{10}$, $\{Fe(NO)_2\}^{9}$, and $[SR\{Fe(NO)_2\}^{9}]$ units are indicated in green, red, and blue respectively. Based on the review by Tsai-Te Lu and coworkers.[138] L = :CR_2/:NR_3/:PR_3/:SR_2/Imidazole and X^- = SR^-/OR^-/Cl^-/Br^-/I^-/PR_2^-, L*/X* = SR^-/Imidazole/N-heterocyclic carbene (NHC). L-L = N/P bidentate chelates. L/X-X = :NR_3/OR^- /SR^-/:SR_2/PR_2^-/:PR_3 bidentate chelates. $NOBF_4$ was oxidant of choice for the figure due to its ability to donate NO and oxidize the $\{Fe(NO)_2\}^{10}$. Any suitable oxidant can replace $NOBF_4$ in any step that does not require NO donation as well as oxidation.

I.6 Biomimetic inorganic chemistry with DNICs

Besides the number of abiotic ligands described above, there have been investigations of the DNIU using a ligand field closer to what might be seen in nature. Chemists found inspiration in a number of metal binding motifs like histidine, cysteine, glutathione, and the Cys-Gly-Cys tripeptide. Li *et al.* synthesized methyl-imidazole DNIC derivatives from the $Fe(CO)_2(NO)_2$ synthon and found that the *N*-heterocycle was incapable of stabilizing reduced $\{Fe(NO)_2\}^{10}$ DNICs, but would readily stabilize the oxidized $\{Fe(NO)_2\}^9$ form.[7,163,164] From the M.Y. Darensbourg group, imidazolyl DNIC derivatives were converted into *N*-heterocyclic carbenes (NHCs) upon deprotonation of the imidazole in the presence of an alkylating agent.[165] Due to the weak π-backbonding and strong σ-donation offered by the NHC, the resulting DNICs were stable and isolable in the reduced and oxidized forms. Furthermore, when bulky substituents such as mesityls flank the *N*-heterocyclic carbene, it was possible to add another nitrosyl, forming a trinitrosyl (TNIC) $\{Fe(NO)_3\}^{10}$ complex, which serves as a convenient donor of the $\{Fe(NO)_2\}^9$ subunit (Figure I-5).[166-167] The mechanism of the loss of NHC and NO from the TNIC remains unknown.

As mentioned in the previous section, the Vanin group has thoroughly characterized both cysteinyl- and glutathionyl-based DNICs; he has as well as determined the biological activity of the DNICs.[78] There are a number of labs that have investigated other RRE-type dimeric DNICs, and the Liaw group found that both of the iron centers undergo reversible redox processes to generate three isolable redox states: the

antiferromagnetically (AFM) coupled, EPR silent $\{Fe(NO)_2\}^9$-$\{Fe(NO)_2\}^9$, the EPR active $[\{Fe(NO)_2\}^9$-$\{Fe(NO)_2\}^{10}]^-$, and the fully reduced $[\{Fe(NO)^{10}$-$\{Fe(NO)_2\}^{10}]^{2-}$ (Figure 6).[79,168,169] The key to stabilizing the reduced DNIUs was the geometric reorganization to aid in the delocalization of electron density across the bridging thiolates, i.e. a flat $Fe_2(\mu\text{-}SR)_2$ core in the neutral and anionic vs. a puckered dianion.

In the M.Y. Darensbourg lab, significant effort has been made in characterizing DNICs based on the Cys-Gly-Cys motif.[170,171] The dianionic tetradentate N_2S_2 chelate bis-mercaptoethyl-diazacyclooctane (bme-daco) was used to emulate this tripeptide.[172] The identity of the N to N linker, affects the rigidity of the chelate as well as changes the solubility of the resulting coordination complex.[173-175] Despite synthetic efforts to generate a number of indefinitely stable DNICs from this biomimetic scaffold, there was a certain thermodynamic sink of a complex that insisted to form: the bimetallic trinitrosyl complex of the formula $[\{Fe(NO)\}^7(2\mu\text{-}S\text{-}N_2S_2)\{Fe(NO)_2\}^9]^+$ (Figures I-4,I-6).[176]

With the added flexibility gained from exchanging the diazacyclooctane with the more flexible, open-chain *N-N'*-dimethylethylenediamine linker, the $Fe_2(NO)_3$ complex was isolated in three distinct oxidation levels as well.[176] Just as was the case with the RRE type DNICs obtained in three oxidation states, the thiolates, in concert with the DNIU were stablized due to their cooperative structural alterations that facilitated the distribution of electron density across the thiolates, irons, and nitrosyls.

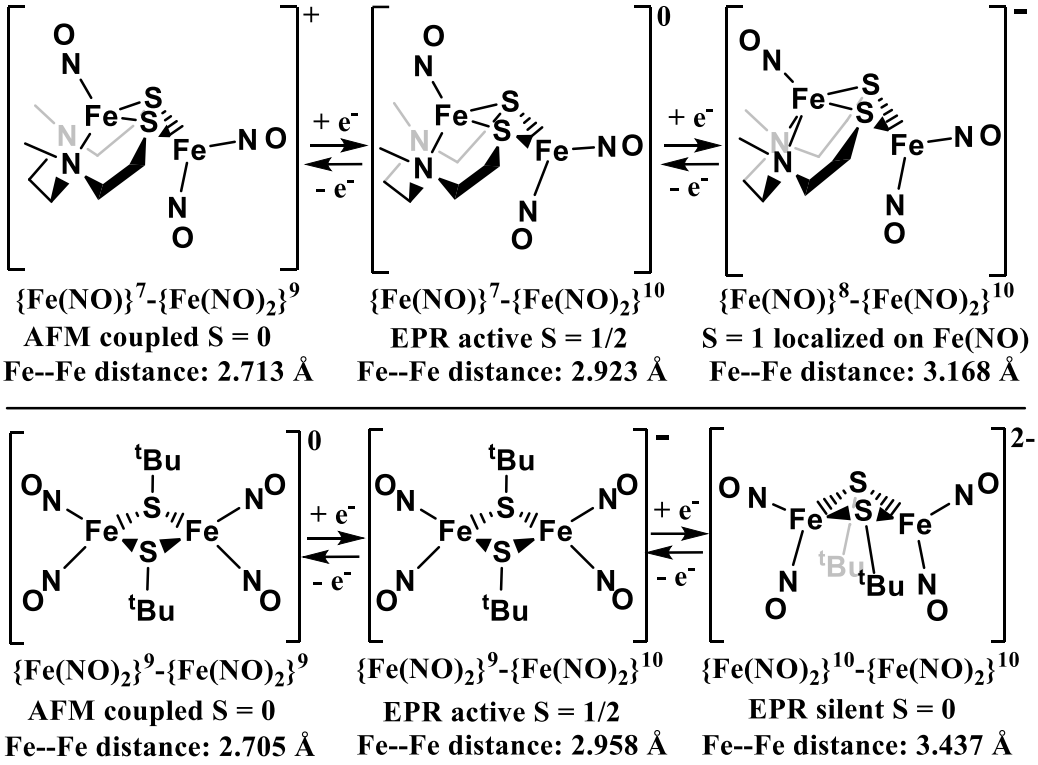

Figure I-6: Representations of dinitrosyl iron complexes successfully isolated in three oxidation states.[79,168,176] Relevant findings related to electronic spin state and Fe--Fe distance are indicated below each structure.

I.7 Beyond Enemark-Feltham notation: defining electronic occupancy of the DNIU

Recent studies have probed more accurate identification of the redox state of the substituents in the dinitrosyl iron unit. The simple Enemark-Feltham notation provides useful inferences about the redox level of the DNIU, but as spectroscopic and computational tools progress, the scientific community is better suited to answer the ambiguity associated with the electronic distribution in DNICs. The $\{Fe(NO)_2\}^9$ unit has been characterized using Raman, NRVS, Mössbauer, V2C XES, EPR, and XAS.[36,64,177-

[182] With a tetrahedral primary coordination environment filled with harder (i.e., smaller and less polarizable) ligands like phenoxide, alkoxides, and imidazoles, the DNIU is defined as an Fe^{III} coordinated to two nitroxyl (NO^{-}) ligands, with an EPR active S = ½ signal around g = 2.03.[157,168,183] With a softer primary coordination environment (i.e., larger and more polarizable ligands like alkyl and aryl thiolates), the DNIU may be considered as a resonance structure between two states: $Fe^{III}(NO^{-})(NO^{-})$, and $Fe^{II}(NO\cdot)(NO^{-})$, based on the electronic occupancy of the NO ligands as determined by V2C XES and the oxidation state of the iron as determined by XAS (Figure I-7).[139,184]

In the dimeric RRE state, a majority of the electron density is localized in the diamond Fe-S core, giving the NO's more nitrosyl ($NO\cdot$) character than nitroxyl (NO^{-}) character.[142,185-188] Upon reduction to $\{Fe(NO)_2\}^{10}$, the electronic assignments are much less ambiguous, yielding an EPR silent S = 0, tetrahedral, Fe^{II} coordinated by two nitroxyl ligands.[168] These variable electronic environments allow for DNIUs to serve as donors of NO in all three oxidation states (NO^{-}, $NO\cdot$, and NO^{+}).[142] Most importantly, the preference of the NO acceptor in competition with that of the donor will determine the overall course and thermodynamic outcome of the final transfer reaction.

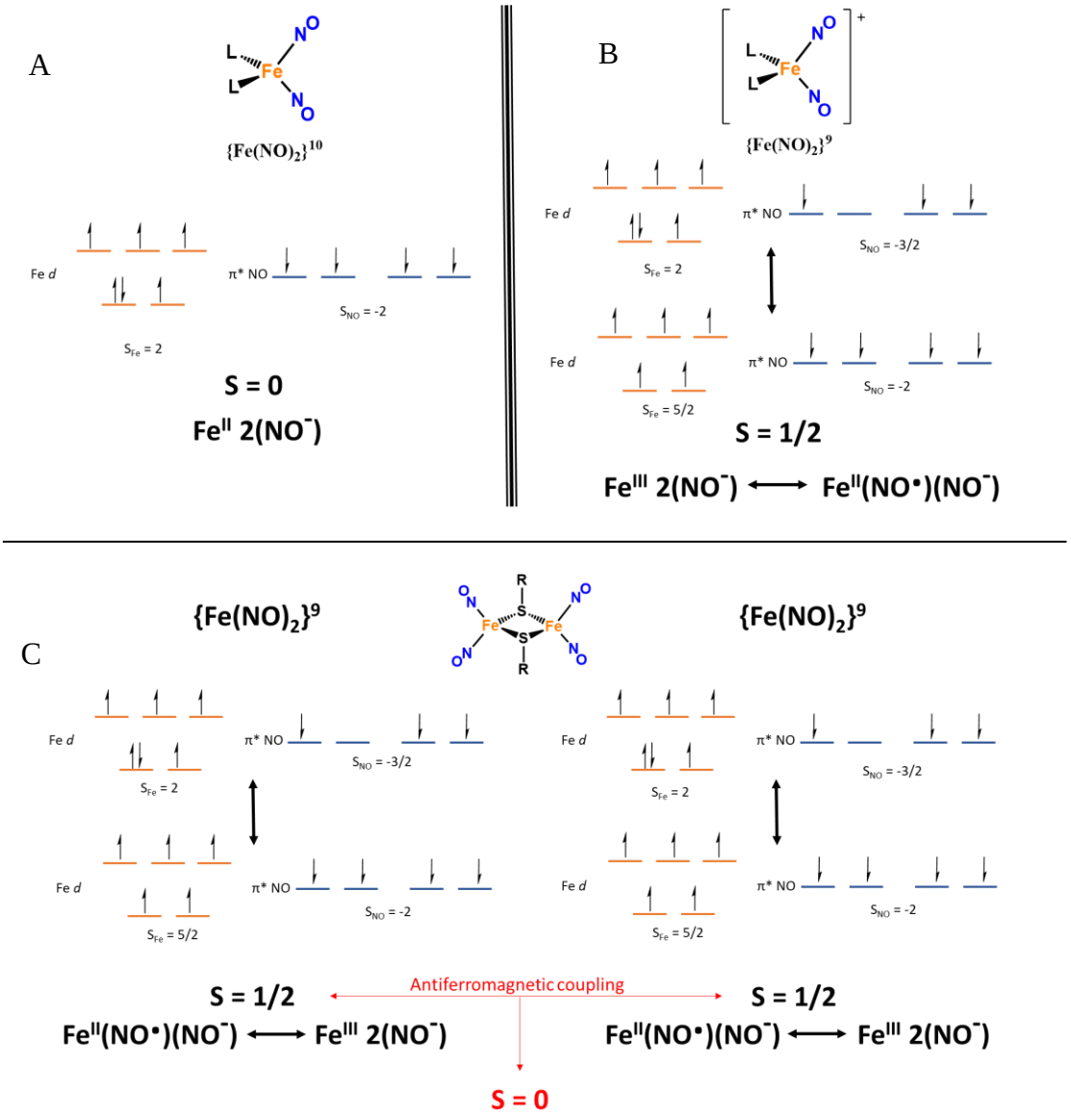

Figure I-7: Electronic assignments of the DNIU in the (A) reduced monomeric$\{Fe(NO)_2\}^{10}$, (B) oxidized monomeric $\{Fe(NO)_2\}^9$, and (C) oxidized dimeric $\{Fe(NO)_2\}^9$ forms. The orange lines represent the tetrahedral *d*-orbital splitting pattern of the iron, and the blue lines are the π^* orbitals of the two NO ligands. The half arrows indicate electronic occupancy. S_{Fe} and S_{NO} indicate the local spin states for the iron and NO respectively, and the bolded black **S** at the bottom of each section indicates the total spin for that DNIU. The red lettering indicates the change in total spin due to antiferromagnetic coupling in the dimeric species.

I.8 References

(1) Hobbs, A. J.; Ignarro, L. J. Nitric Oxide-Cyclic GMP Signal Transduction System. *Methods Enzymol.* **1996**, *269*, 134–148.

(2) Ford, P. C.; Pereira, J. C. M.; Miranda, K. M. Mechanisms of Nitric Oxide Reactions Mediated by Biologically Relevant Metal Centers. *Structure and Bonding*. **2013**, *154*, 99-136

(3) Krishnan, S. M.; Kraehling, J. R.; Eitner, F.; Bénardeau, A.; Sandner, P. The Impact of the Nitric Oxide (NO)/Soluble Guanylyl Cyclase (sGC) Signaling Cascade on Kidney Health and Disease: A Preclinical Perspective. *Int. J. Molec. Sci.* **2018**, *19*(6), 1712

(4) Korhonen, R.; Lahti, A.; Kankaanranta, H.; Moilanen, E. Nitric Oxide Production and Signaling in Inflammation. *Current Drug Targets: Inflammation and Allergy*. Curr Drug Targets Inflamm Allergy August 2005, pp 471–479.

(5) Tonzetich, Z. J.; McQuade, L. E.; Lippard, S. J. Detecting and Understanding the Roles of Nitric Oxide in Biology. *Inorg. Chem.* **2010**, *49* (14), 6338–6348.

(6) Hayton, T. W.; Legzdins, P.; Sharp, W. B. Coordination and Organometallic Chemistry of Metal-NO Complexes. *Chem. Rev.* **2002**, *102* (4), 935–991.

(7) Li, L. Some Coordination Chemistry of Non-Heme Iron Nitrosyl Complexes. *Comments Inorg. Chem.* **2002**, *23* (5), 335–353.

(8) Ford, P. C.; Lorkovic, I. M. Mechanistic Aspects of the Reactions of Nitric Oxide with Transition-Metal Complexes. *Chem. Rev.* **2002**, *102* (4), 993–1017.

(9) Roncaroli, F.; Videla, M.; Slep, L. D.; Olabe, J. A. New Features in the Redox Coordination Chemistry of Metal Nitrosyls {M-NO+; M-NO·; M-NO-(HNO)}. *Coord. Chem. Rev.* **2007**, *251* (13), 1903–1930..

(10) Mason, D. T.; Zelis, R.; Amsterdam, E. A. Actions of the Nitrites on the Peripheral Circulation and Myocardial Oxygen Consumption: Significance in the Relief of Angina Pectoris. *Chest* **1971**, *59* (3), 296–305.

(11) Tinker, J. H.; Michenfelder, J. D. Sodium Nitroprusside: Pharmacology, Toxicology and Therapeutics. *Anesthesiology* **1976**, *45* (3), 340–354.

(12) Furchgott, R. F.; Ehrreich, S. J.; Greenblatt, E. The Photoactivated Relaxation of Smooth Muscle of Rabbit Aorta. *J. Gen. Physiol.* **1961**, *44*, 499–519.

(13) Furchgott, R. F.; Vanhoutte, P. M. Endothelium-Derived Relaxing and Contracting Factors. *FASEB.* **1991**, 405–411.

(14) De Mel, A.; Murad, F.; Seifalian, A. M. Nitric Oxide: A Guardian for Vascular Grafts? *Chem. Rev.* **2011**, *111* (9), 5742–5767.

(15) Mujoo, K.; Krumenacker, J. S.; Murad, F. Nitric Oxide-Cyclic GMP Signaling in Stem Cell Differentiation. *Free Radic. Biol. Med.* **2011**, *51* (12), 2150–2157.

(16) Rajfer, J.; Aronson, W. J.; Bush, P. A.; Dorey, F. J.; Ignarro, L. J. Nitric Oxide as a Mediator of Relaxation of the Corpus Cavernosum in Response to Nonadrenergic, Noncholinergic Neurotransmission. *N. Engl. J. Med.* **1992**, *326* (2), 90–94.

(17) Ignarro, L. J.; Bush, P. A.; Buga, G. M.; Wood, K. S.; Fukuto, J. M.; Rajfer, J. Nitric Oxide and Cyclic GMP Formation upon Electrical Field Stimulation Cause Relaxation of Corpus Cavernosum Smooth Muscle. *Biochem. Biophys. Res. Commun.* **1990**, *170* (2), 843–850.

(18) Vanin, A. F. Dinitrosyl Iron Complexes with Thiol-Containing Ligands as a "Working Form" of Endogenous Nitric Oxide. *Nitric Oxide* **2016**, *54*, 15–29.

(19) Furchgott, R. F.; Zawadzki, J. V. The Obligatory Role of Endothelial Cells in the Relaxation of Arterial Smooth Muscle by Acetylcholine. *Nature* **1980**, *288* (5789), 373–376.

(20) Arnold, W. P.; Mittal, C. K.; Katsuki, S.; Murad, F. Nitric Oxide Activates Guanylate Cyclase and Increases Guanosine 3':5'-Cyclic Monophosphate Levels in Various Tissue Preparations. *Proc. Natl. Acad. Sci.* **1977**, *74* (8), 3203–3207.

(21) Ignarro, L. J.; Buga, G. M.; Wood, K. S.; Byrns, R. E.; Chaudhuri, G. Endothelium-Derived Relaxing Factor Produced and Released from Artery and Vein Is Nitric Oxide. *Proc. Natl. Acad. Sci.* **1987**, *84* (24), 9265–9269.

(22) Zhao, Y.; Brandish, P. E.; Ballou, D. P.; Marletta, M. A.; Howard, S.; Walsh, C. T. A Molecular Basis for Nitric Oxide Sensing by Soluble Guanylate Cyclase. *Proc. Natl. Acad. Sci.* **1999**, *96* (26), 14753–14758.

(23) Lancaster, J. R.; Hibbs, J. B. EPR Demonstration of Iron-Nitrosyl Complex Formation by Cytotoxic Activated Macrophages. *Proc. Natl. Acad. Sci. U. S. A.* **1990**, *87* (3), 1223–1227.

(24) Nathan, C. F.; Hibbs, J. B. Role of Nitric Oxide Synthesis in Macrophage Antimicrobial Activity. *Curr. Opin. Immunol.* **1991**, *3* (1), 65–70.

(25) Weigert, A.; von Knethen, A.; Fuhrmann, D.; Dehne, N.; Brüne, B. Redox-Signals and Macrophage Biology. *Mol. Aspects Med.* **2018**, *63*, 70–87.

(26) Doulias, P. T.; Greene, J. L.; Greco, T. M.; Tenopoulou, M.; Seeholzer, S. H.; Dunbrack, R. L.; Ischiropoulos, H. Structural Profiling of Endogenous S-Nitrosocysteine Residues Reveals Unique Features That Accommodate Diverse Mechanisms for Protein S-Nitrosylation. *Proc. Natl. Acad. Sci.* **2010**, *107* (39), 16958–16963.

(27) Brozovich, F. V; Nicholson, C. J.; Degen, C. V; Gao, Y. Z.; Aggarwal, M.; Morgan, K. G. Mechanisms of Vascular Smooth Muscle Contraction and the Basis for Pharmacologic Treatment of Smooth Muscle Disorders. *Pharmacol. Rev.* **2016**, *68*, 476–532.

(28) Carpenter, A. W.; Schoenfisch, M. H. Nitric Oxide Release Part II. Therapeutic Applications. *Chem. Soc. Rev.* **2012**, *41* (10), 3742–3752.

(29) Bosworth, C. A.; Toledo Jr., J. C.; Zmijewski, J. W.; Li, Q.; Lancaster Jr., J. R. Dinitrosyliron Complexes and the Mechanism(s) of Cellular Protein Nitrosothiol Formation from Nitric Oxide. *Proc. Natl. Acad. Sci.* **2009**, *106* (12), 4671–4676.

(30) Li, Q.; Li, C.; Mahtani, H. K.; Du, J.; Patel, A. R.; Lancaster Jr., J. R. Nitrosothiol Formation and Protection against Fenton Chemistry by Nitric Oxide-Induced

Dinitrosyliron Complex Formation from Anoxia-Initiated Cellular Chelatable Iron Increase. *J. Biol. Chem.* **2014**, *289* (29), 19917–19927.

(31) Bocedi, A.; Fabrini, R.; Farrotti, A.; Stella, L.; Ketterman, A. J.; Pedersen, J. Z.; Allocati, N.; Lau, P. C. K.; Grosse, S.; Eltis, L. D.; et al. The Impact of Nitric Oxide Toxicity on the Evolution of the Glutathione Transferase Superfamily: A Proposal for an Evolutionary Driving Force. *J. Biol. Chem.* **2013**, *288* (34), 24936–24947.

(32) Severina, I. S.; Bussygina, O. G.; Pyatakova, N. V.; Malenkova, I. V.; Vanin, A. F. Activation of Soluble Guanylate Cyclase by NO Donors - S-Nitrosothiols, and Dinitrosyl-Iron Complexes with Thiol-Containing Ligands. *Nitric Oxide.* **2003**, *8* (3), 155–163.

(33) Andreyev-Andriyevsky, A. A.; Mikoyan, V. D.; Serezhenkov, V. A.; Vanin, A. F. Penile Erectile Activity of Dinitrosyl Iron Complexes with Thiol-Containing Ligands. *Nitric Oxide* **2011**, *24* (4), 217–223.

(34) Sahni, S.; Hickok, J. R.; Thomas, D. D. Nitric Oxide Reduces Oxidative Stress in Cancer Cells by Forming Dinitrosyl Iron Complexes. *Nitric Oxide* **2018**, *76*, 37–44.

(35) Tinberg, C. E.; Tonzetich, Z. J.; Wang, H.; Do, L. H.; Yoda, Y.; Cramer, S. P.; Lippard, S. J. Characterization of Iron Dinitrosyl Species Formed in the Reaction of Nitric Oxide with a Biological Rieske Center. *J. Am. Chem. Soc* **2010**, *132*, 18168–18176.

(36) Schiewer, C. E.; Müller, C. S.; Dechert, S.; Bergner, M.; Wolny, J. A.; Schünemann, V.; Meyer, F. Effect of Oxidation and Protonation States on [2Fe−2S] Cluster Nitrosylation Giving $\{Fe(NO)_2\}^9$ Dinitrosyl Iron Complexes (DNICs). *Inorg. Chem.* **2018**, *58*, 769–784.

(37) Chen, L.; Liu, P.; Gao, H.; Sun, B.; Chao, D.; Wang, F.; Zhu, Y.; Ran Hedenstierna, G.; Wang, C. G. Inhalation of Nitric Oxide in the Treatment of Severe Acute Respiratory Syndrome: A Rescue Trial in Beijing. *Clin. Infect. Dis.* **2004**, *39*, 1531–1535.

(38) Kilbourn, R. G.; Gross, S. S.; Jubran, A.; Adams, J.; Griffith, O. W.; Levi, R.; Lodato, R. F. NG-Methyl-L-Arginine Inhibits Tumor Necrosis Factor-Induced Hypotension: Implications for the Involvement of Nitric Oxide. *Proc. Natl. Acad. Sci.* **1990**, *87* (9), 3629–3632.

(39) Ataei Ataabadi, E.; Golshiri, K.; Jüttner, A.; Krenning, G.; Danser, A. H. J.; Roks, A. J. M. Nitric Oxide-CGMP Signaling in Hypertension: Current and Future Options for Pharmacotherapy. *Hypertension* **2020**, *76* (4), 1055–1068.

(40) Roy, H. S.; Singh, R.; Ghosh, D. Recent Advances in Nanotherapeutic Strategies That Target Nitric Oxide Pathway for Preventing Cartilage Degeneration. *Nitric Oxide* **2021**, *109–110*, 1–11.

(41) Shamnova, E. V.; Bichan, O. D.; Drozd, E. S.; Gorudko, I. V.; Chizhik, S. A.; Shumaev, K. B.; Cherenkevich, S. N.; Vanin, A. F. Regulation of the Functional

and Mechanical Properties of Platelet and Red Blood Cells by Nitric Oxide Donors. *Biophysics (Oxf).* **2011**, *56* (2), 237–242.

(42) Chiesa, J. J.; Baidanoff, F. M.; Golombek, D. A. Don't Just Say NO: Differential Pathways and Pharmacological Responses to Diverse Nitric Oxide Donors. *Biochem. Pharmacol.* **2018**, *156*, 1–9.

(43) Münzel, T.; Daiber, A. Inorganic Nitrite and Nitrate in Cardiovascular Therapy: A Better Alternative to Organic Nitrates as Nitric Oxide Donors? *Vascul. Pharmacol.* **2018**, *102*, 1–10.

(44) Abaffy, P.; Tomankova, S.; Naraine, R.; Kubista, M.; Sindelka, R. The Role of Nitric Oxide during Embryonic Wound Healing. *BMC Genomics* **2019**, *20* (1).

(45) Anastasio, A. T.; Paniagua, A.; Diamond, C.; Ferlauto, H. R.; Fernandez-Moure, J. S. Nanomaterial Nitric Oxide Delivery in Traumatic Orthopedic Regenerative Medicine. *Front. Bioeng. Biotechnol.* **2021**, *8*.

(46) Yang, Y.; Huang, Z.; Li, L. L. Advanced Nitric Oxide Donors: Chemical Structure of NO Drugs, NO Nanomedicines and Biomedical Applications. *Nanoscale* **2021**, *13* (2), 444–459.

(47) Chiarelli, L. R.; Degiacomi, G.; Egorova, A.; Makarov, V.; Pasca, M. R. Nitric Oxide-Releasing Compounds for the Treatment of Lung Infections. *Drug Discov. Today* **2021**, *26* (2), 542–550.

(48) Vong, L. B.; Nagasaki, Y. Nitric Oxide Nano-Delivery Systems for Cancer Therapeutics: Advances and Challenges. *Antioxidants* **2020**, *9* (9), 1–14.

(49) Pieretti, J. C.; Pelegrino, M. T.; Nascimento, M. H. M.; Tortella, G. R.; Rubilar, O.; Seabra, A. B. Small Molecules for Great Solutions: Can Nitric Oxide-Releasing Nanomaterials Overcome Drug Resistance in Chemotherapy? *Biochem. Pharmacol.* **2020**, *176*.

(50) Danielak, A.; Wallace, J. L.; Brzozowski, T.; Magierowski, M. Gaseous Mediators as a Key Molecular Targets for the Development of Gastrointestinal-Safe Anti-Inflammatory Pharmacology. *Front. Pharmacol.* **2021**, *12*, 1–17.

(51) Ignarro, L. J.; Fukuto, J. M.; Griscavage, J. M.; Rogers, N. E.; Byrns, R. E. Oxidation of Nitric Oxide in Aqueous Solution to Nitrite but Not Nitrate: Comparison with Enzymatically Formed nitric oxide from L-arginine (nitric oxide synthase/oxidative metaboism). *Proc. Natl. Acad. Sci.* **1993**, 90, 8103-8107.

(52) Jin, H.; Yang, L.; Ahonen, M. J. R.; Schoenfisch, M. H. Nitric Oxide-Releasing Cyclodextrins. *J. Am. Chem. Soc* **2018**, *140*, 52.

(53) Tobias, J. D.; Naguib, A.; Simsic, J.; Krawczeski, C. D. Pharmacologic Control of Blood Pressure in Infants and Children. *Pediatric Cardiology*. **2020**, *41* (7). 1301–1318.

(54) Dyer, R. R.; Ford, K. I.; Robinson, R. A. S. The Roles of S-Nitrosylation and S-Glutathionylation in Alzheimer's Disease. *Methods Enzymol.* **2019**, *626*, 499–538.

(55) Vanin, A. F. What Is the Mechanism of Nitric Oxide Conversion into Nitrosonium Ions Ensuring S-Nitrosating Processes in Living Organisms. *Cell Biochem. Biophys.* **2019**, *77* (4), 279–292.

(56) Kayki-Mutlu, G.; Koch, W. J. Nitric Oxide and S-Nitrosylation in Cardiac Regulation: G Protein-Coupled Receptor Kinase-2 and β-Arrestins as Targets. *Int. J. Mol. Sci.* **2021**, *22* (2), 1–17.

(57) Hickok, J. R.; Sahni, S.; Shen, H.; Arvind, A.; Antoniou, C.; Fung, L. W. M.; Thomas, D. D. Dinitrosyliron Complexes Are the Most Abundant Nitric Oxide-Derived Cellular Adduct: Biological Parameters of Assembly and Disappearance. *Free Radic Biol Med* **2011**, *51* (8), 1558–1566.

(58) F.Z. Roussin, Ann. Chim. Phys. **1852**. *52*, 285-303.

(59) Cheng, H.-Y.; Chang, S. Density Functional Theory of the Iron-Nitrosyl (S = 3/2) Complex. *Int. J. Quantum Chem.* **2005**, *105* (5), 511–517.

(60) D'Autréaux, B.; Horner, O.; Oddou, J. L.; Jeandey, C.; Gambarelli, S.; Berthomieu, C.; Latour, J. M.; Michaud-Soret, I. Spectroscopic Description of the Two Nitrosyl-Iron Complexes Responsible for Fur Inhibition by Nitric Oxide. *J. Am. Chem. Soc.* **2004**, *126* (19), 6005–6016.

(61) White, C. J.; Speelman, A. L.; Kupper, C.; Demeshko, S.; Meyer, F.; Shanahan, J. P.; Alp, E. E.; Hu, M.; Zhao, J.; Lehnert, N. The Semireduced Mechanism for Nitric Oxide Reduction by Non-Heme Diiron Complexes: Modeling Flavodiiron Nitric Oxide Reductases. *J. Am. Chem. Soc.* **2018**, *140* (7), 2562–2574.

(62) Enemark, J. H.; Feltham, R. D. Principles of Structure, Bonding, and Reactivity for Metal Nitrosyl Complexes. *Coord. Chem. Rev.* **1974**, *13* (4), 339–406.

(63) Yeh, S. W.; Lin, C. W.; Liu, B. H.; Tsou, C. C.; Tsai, M. L.; Liaw, W. F. Chelate-Thiolate-Coordinate Ligands Modulating the Configuration and Electrochemical Property of Dinitrosyliron Complexes (DNICs). *Chem. - A Eur. J.* **2015**, *21* (45), 16035–16046.

(64) Ye, S.; Neese, F. The Unusual Electronic Structure of Dinitrosyl Iron Complexes. *J. Am. Chem. Soc.* **2010**, *132* (11), 3646–3647.

(65) Ghosh, P.; Ding, S.; Chupik, R. B.; Quiroz, M.; Hsieh, C. H.; Bhuvanesh, N.; Hall, M. B.; Darensbourg, M. Y. A Matrix of Heterobimetallic Complexes for Interrogation of Hydrogen Evolution Reaction Electrocatalysts. *Chem. Sci.* **2017**, *8* (12), 8291–8300.

(66) Pectol, D.; Khan, S.; Elsabahy, M.; Wooley, K.; Lim, S.-M.; Darensbourg, M. Effects of Glutathione and Histidine on NO Release from a Dimeric Dinitrosyl Iron Complex (DNIC). *Inorg. Chem.* **2020**, *59* (23), 16998–17008.

(67) Vithayathil, A. J.; Ternberg, J. L.; Commoner, B. P. Changes in Electron Spin Resonance Signals of Rat Liver During Chemical Carcinogensis. *Nature* **1965**, *207*, 1246–1249.

(68) Mallard, J. R.; Kent, M. Differences Observed between Electron Spin Resonance Signals from Surviving Tumour Tissues and from Their Corresponding Normal Tissues. *Nature* **1964**, *204*, 1192.

(69) Vanin A.F.; Nalbandyan R.M. Free radical species with unpaired electron localization on sulfur atom in yeast cells, *Biofizika (Rus)*. **1966**, *11*, 178-179.

(70) Birchall, T.; Tun, K. M. Reinvestigation of Some Iron Dinitrosyl Complexes with Thio-Ligands. *Dalt. Trans.* **1973**, *7* (22), 2521–2523.

(71) Jezowska-Trezebiatowska, B.; Jezierski, A. Electron Spin Resonance Spectroscopy of Iron Nitrosyl Complexes with Organic Ligands. *J. Mol. Struct.* **1973**, *19* (2), 635–640.

(72) McDonald, C. C.; Phillips, W. D.; Mower, H. F. An Electron Spin Resonance Study of Some Complexes of Iron, Nitric Oxide, and Anionic Ligands. *J. Am. Chem. Soc.* **1965**, *87* (15), 3319–3326.

(73) Truzzi, D. R.; Augusto, O.; Iretskii, A. V; Ford, P. C. Dynamics of Dinitrosyl Iron Complex (DNIC) Formation with Low Molecular Weight Thiols. *Inorg. Chem.* **2019**, *50*, 13446–13456.

(74) Deponte, M., The Incomplete Glutathione Puzzle: Just Guessing at Numbers and Figures? *Antioxid. Redox Signal.* **2017,** *27* (15), 1130-1161.

(75) Kumar, C.; Igbaria, A.; D'Autreaux, B.; Planson, A.-G.; Junot, C.; Godat, E.; Bachhawat, A. K.; Delaunay-Moisan, A.; Toledano, M. B., Glutathione revisited: a vital function in iron metabolism and ancillary role in thiol-redox control. *EMBO J.* **2011,** *30* (10), 2044-2056.

(76) Lu, C.-Y.; Liaw, W.-F., Formation Pathway of Roussin's Red Ester (RRE) via the Reaction of a $\{Fe(NO)_2\}^{10}$ Dinitrosyliron Complex (DNIC) and Thiol: Facile Synthetic Route for Synthesizing Cysteine-Containing DNIC. *Inorganic Chemistry* **2013,** *52*, 13918-13926.

(77) Vanin, A. F., Dinitrosyl iron complexes with thiolate ligands: Physico-chemistry, biochemistry and physiology. *Nitric Oxide.* **2009**, *21*, 1-13.

(78) Vanin, A. F.; Borodulin, R. R.; Mikoyan, V. D., Dinitrosyl iron complexes with natural thiol-containing ligands in aqueous solutions: Synthesis and some physico-chemical characteristics (A methodological review). *Nitric Oxide*. **2017**, *66*, 1-9.

(79) Tsou, C. C.; Lu, T. Te; Liaw, W. F. EPR, UV - Vis, IR, and X-Ray Demonstration of the Anionic Dimeric Dinitrosyl Iron Complex [(NO)2Fe(μ-StBu) 2Fe(NO)2]-: Relevance to the Products of Nitrosylation of Cytosolic and Mitochondrial Aconitases, and High-Potential Iron Proteins. *J. Am. Chem. Soc.* **2007**, *129* (42), 12626–12627.

(80) Foster, M. W.; Cowan, J. A. Chemistry of Nitric Oxide with Protein-Bound Iron Sulfur Centers. Insights on Physiological Reactivity. *J. Am. Chem. Soc* **1999**, *121* (17), 4093–4100.

(81) Cheng, Z.; Landry, A. P.; Wang, Y.; Ding, X. H. Binding of Nitric Oxide in CDGSH-Type [2Fe-2S] Clusters of the Human Mitochondrial Protein Miner2. *J. Biol. Chem.* **2017**, *292* (8), 3146–3153.

(82) Yang, W.; Rogers, P. A.; Ding, H. Repair of Nitric Oxide-Modified Ferredoxin [2Fe-2S] Cluster by Cysteine Desulfurase (IscS). *J. Biol. Chem.* **2002**, *277* (15), 12868–12873.

(83) Rogers, P. A.; Eide, L.; Klungland, A.; Ding, H. Reversible Inactivation of E. Coli Endonuclease III via Modification of Its [4Fe-4S] Cluster by Nitric Oxide. *DNA Repair (Amst).* **2003**, *2* (7), 809–817.

(84) Duan, X.; Yang, J.; Ren, B.; Tan, G.; Ding, H. Reactivity of Nitric Oxide with the [4Fe-4S] Cluster of Dihydroxyacid Dehydratase from Escherichia Coli. *Biochem. J.* **2009**, *417* (3), 783–789.

(85) Ekanger, L. A.; Oyala, P. H.; Moradian, A.; Sweredoski, M. J.; Barton, J. K. Nitric Oxide Modulates Endonuclease III Redox Activity by a 800 MV Negative Shift upon [Fe4S4] Cluster Nitrosylation. *J. Am. Chem. Soc* **2018**, *140*, 11800–11810.

(86) Tsai, M. L.; Chen, C. C.; Hsu, I. J.; Ke, S. C.; Hsieh, C. H.; Chiang, K. A.; Lee, G. H.; Wang, Y.; Chen, J. M.; Lee, J. F.; et al. Photochemistry of the Dinitrosyl Iron Complex [S5Fe(NO) 2]- Leading to Reversible Formation of [S 5Fe(μ-S)2FeS5]2- : Spectroscopic Characterization of Species Relevant to the Nitric Oxide Modification and Repair of [2Fe-2S] Ferredoxins. *Inorg. Chem.* **2004**, *43* (16), 5159–5167.

(87) Kim, Y.-M.; Chung, H.-T.; Simmons, R. L.; Billiar, T. R. Cellular Non-Heme Iron Content Is a Determinant of Nitric Oxide-Mediated Apoptosis, Necrosis, and Caspase Inhibition. *J. Biol. Chem.* **2000**, *275* (15), 10954–10961.

(88) Mocellin, S.; Bronte, V.; Nitti, D. Nitric Oxide, a Double Edged Sword in Cancer Biology: Searching for Therapeutic Opportunities. *Med. Res. Rev.* **2007**, *27* (3), 317–352.

(89) Tsou, C. C.; Liaw, W. F. Transformation of the {Fe(NO) 2} 9 Dinitrosyl Iron Complexes (DNICs) into S-Nitrosothiols (RSNOs) Triggered by Acid-Base Pairs. *Chem. - A Eur. J.* **2011**, *17* (47), 13358–13366.

(90) Thomas, D. D.; Heinecke, J. L.; Ridnour, L. A.; Cheng, R.; Kesarwala, A. H.; Switzer, C. H.; Mcvicar, D. W.; Roberts, D. D.; Glynn, S.; Fukuto, J. M.; et al. Signaling and Stress: The Redox Landscape in NOS2 Biology HHS Public Access. *Free Radic. Biol. Med.* **2015**, *87*, 204–225.

(91) Cesareo, E.; Parker, L. J.; Pedersen, J. Z.; Nuccetelli, M.; Mazzetti, A. P.; Pastore, A.; Federici, G.; Caccuri, A. M.; Ricci, G.; Adams, J. J.; Parker M. W.; Lo Bello M. Nitrosylation of human glutathione transferase P1-1 with dinitrosyl diglutathionyl iron complex in vitro and in vivo. *J. Biol. Chem.* **2005**. *280* (51). 42172-42180.

(92) Keese, M. A.; Böse, M.; Mülsch, A.; Schirmer, R. H.; Becker, K. Dinitrosyl-Dithiol-Iron Complexes, Nitric Oxide (NO) Carriers in Vivo, as Potent Inhibitors of Human Glutathione Reductase and Glutathione-S-Transferase. *Biochem. Pharmacol.* **1997**, *54* (12), 1307–1313.

(93) Tsugawa, S.; Noda, Y.; Tarumi, R.; Mimura, Y.; Yoshida, K.; Iwata, Y.; Elsalhy, M.; Kuromiya, M.; Kurose, S.; Masuda, F.; et al. Glutathione Levels and Activities of Glutathione Metabolism Enzymes in Patients with Schizophrenia: A Systematic Review and Meta-Analysis. *J. Psychopharmacol.* **2019**, *33* (10), 1199–1214.

(94) Oestreicher, J.; Morgan, B. Glutathione: Subcellular Distribution and Membrane Transport. *Biochem. Cell Biol.* **2019**, *97* (3), 270–289.

(95) Graff Van Creveld, S.; Rosenwasser, S.; Schatz, D.; Koren, I.; Vardi, A. Early Perturbation in Mitochondria Redox Homeostasis in Response to Environmental Stress Predicts Cell Fate in Diatoms. *ISME J.* **2015**, *9*, 385–395.

(96) López-Mirabal, H. R.; Winther, J. R. Redox Characteristics of the Eukaryotic Cytosol. *Biochim. Biophys. Acta - Mol. Cell Res.* **2008**, *1783* (4), 629–640.

(97) Kojer, K.; Bien, M.; Gangel, H.; Morgan, B.; Dick, T. P.; Riemer, J. Glutathione Redox Potential in the Mitochondrial Intermembrane Space Is Linked to the Cytosol and Impacts the Mia40 Redox State. *EMBO J.* **2012**, *31* (14), 3169–3182.

(98) Gu, F.; Chauhan, V.; Chauhan, A. Glutathione Redox Imbalance in Brain Disorders. *Curr. Opin. Clin. Nutr. Metab. Care.* **2015**, *18* (1), 89–95.

(99) Carlberg, I.; Mannervik, B. Glutathione Reductase. *Methods Enzymol.* **1985**, *113* (C), 484–490.

(100) Thieme, R.; Pai, E. F.; Schirmer, R. H.; Schulz, G. E. Three-Dimensional Structure of Glutathione Reductase at 2 Å Resolution. *J. Mol. Biol.* **1981**, *152* (4), 763–782.

(101) Robaczewska, J.; Kedziora-Kornatowska, K.; Kozakiewicz, M.; Zary-Sikorska, E.; Pawluk, H.; Pawliszak, W.; Kedziora, J. Role of Glutathione Metabolism and Glutathione-Related Antioxidant Defense Systems in Hypertension. *J. Physiol. Pharmacol.* **2016**, *67* (3), 331–337.

(102) Lok, H. C.; Sahni, S.; Jansson, P. J.; Kovacevic, Z.; Hawkins, C. L.; Richardson, D. R. A Nitric Oxide Storage and Transport System That Protects Activated Macrophages from Endogenous Nitric Oxide Cytotoxicity. *J. Biol. Chem.* **2016**, *291* (53), 27042–27061.

(103) Pae, H. O.; Lee, Y. C.; Jo, E. K.; Chung, H. T. Subtle Interplay of Endogenous Bioactive Gases (NO, CO and H2S) in Inflammation. *Arch. Pharm. Res.* **2009**, *32* (8), 1155–1162.

(104) Kapelko, V. I.; Lakomkin, V. L.; Abramov, A. A.; Lukoshkova, E. V.; Undrovinas, N. A.; Khapchaev, A. Y.; Shirinsky, V. P. Protective Effects of Dinitrosyl Iron Complexes under Oxidative Stress in the Heart. *Oxid. Med. Cell. Longev.* **2017**, *2017*, 1–10.

(105) Kovacevic, Z.; Sahni, S.; Lok, H.; Davies, M. J.; Wink, D. A.; Richardson, D. R. Regulation and Control of Nitric Oxide (NO) in Macrophages: Protecting the "Professional Killer Cell" from Its Own Cytotoxic Arsenal via MRP1 and GSTP1. *Biochim. Biophys. Acta* **2017**, *1861* (5), 995–999.

(106) Toyokuni, S.; Ito, F.; Yamashita, K.; Okazaki, Y.; Akatsuka, S. Iron and Thiol Redox Signaling in Cancer: An Exquisite Balance to Escape Ferroptosis. *Free Radic. Biol. Med.* **2017**, *108*, 610–626.

(107) Richardson, D. R.; Lok, H. C. The Nitric Oxide-Iron Interplay in Mammalian Cells: Transport and Storage of Dinitrosyl Iron Complexes. *Biochim. Biophys. Acta* **2008**, *1780* (4), 638–651.

(108) Rubino, F. M. Toxicity of Glutathione-Binding Metals: A Review of Targets and Mechanisms. *Toxics* **2015**, *3*, 20–62.

(109) Mintz, J.; Vedenko, A.; Rosete, O.; Shah, K.; Goldstein, G.; Hare, J. M.; Ramasamy, R.; Arora, H. Current Advances of Nitric Oxide in Cancer and Anticancer Therapeutics. *Vaccines* **2021**, *9* (2), 94.

(110) Köberle, B.; Schoch, S. Platinum Complexes in Colorectal Cancer and Other Solid Tumors. *Cancers (Basel).* **2021**, *13* (9).

(111) Turella, P.; Pedersen, J. Z.; Caccuri, A. M.; De Maria, F.; Mastroberardino, P.; Lo Bello, M.; Federici, G.; Ricci, G. Glutathione Transferase Superfamily Behaves Like Storage Proteins for Dinitrosyl-Diglutathionyl-Iron Complex in Heterogeneous Systems. *J. Biol. Chem.* **2003**, *278* (43), 42294–42299.

(112) Liu, T.; Zhang, M.; Terry, M. H.; Schroeder, H.; Wilson, S. M.; Power, G. G.; Li, Q.; Tipple, T. E.; Borchardt, D.; Blood, A. B. Hemodynamic Effects of Glutathione-Liganded Binuclear Dinitrosyl Iron Complex: Evidence for Nitroxyl Generation and Modulation by Plasma Albumin. *Mol. Pharmacol.* **2018**, *93* (5), 427–437.

(113) Frey, R.; Becker, C.; Saleh, S.; Unger, S.; van der Mey, D.; Mück, W. Clinical Pharmacokinetic and Pharmacodynamic Profile of Riociguat. *Clin. Pharmacokinet.* **2018**, *57*, 647–661.

(114) Thomas, D. D.; Liu, X.; Kantrow, S. P.; Lancaster, J. R. The Biological Lifetime of Nitric Oxide: Implications for the Perivascular Dynamics of NO and O_2. *PNAS* **2001**, *98* (1).

(115) Bryan, N. S.; Grisham, M. B. Methods to Detect Nitric Oxide and Its Metabolites in Biological Samples. *Free Radic. Biol. Med.* **2007**, *43* (5), 645–657.

(116) Shumaev, K. B.; Gorudko, I. V; Kosmachevskaya, O. V; Grigorieva, D. V; Panasenko, O. M.; Vanin, A. F.; Topunov, A. F.; Terekhova, M. S.; Sokolov, A. V; Cherenkevich, S. N.; et al. Protective Effect of Dinitrosyl Iron Complexes with Glutathione in Red Blood Cell Lysis Induced by Hypochlorous Acid. *Oxi. Med. Cell. Longev.* **2019**, 1–12.

(117) Burgova, E. N.; Tkachev, N. A.; Adamyan, L. V.; Mikoyan, V. D.; Paklina, O. V.; Stepanyan, A. A.; Vanin, A. F. Dinitrosyl Iron Complexes with Glutathione Suppress Experimental Endometriosis in Rats. *Eur. J. Pharmacol.* **2014**, *727* (1), 140–147.

(118) Vanin, A. F. Dinitrosyl Iron Complexes with Thiol-Containing Ligands as a Base for Developing Drugs with Diverse Therapeutic Activities: Physicochemical and Biological Substantiation. *Biophysics (Oxf).* **2017**, *62* (4), 629–656.

(119) A.B. Shekhter, T.G. Rudenko, L.P. Istranov, A.E. Guller, R.R. Borodulin, A.F. Vanin, Dinitrosyl iron complexes with glutathione incorporated into acollagen matrix as a base for the design of drugs accelerating skin wound healing, *Eur. J. Pharmaceutical Sci.* **2015**, *78*, 8-18.

(120) A.F. Vanin, L.A. Ostrovskaya, D.B. Korman, R.R. Boriodulin, L.N. Kubrina, M.M. Fomina, N.V. Bluchterova, V.A. Rykova, Anti-tumor activity of dinitrosyl iron complexes with glutathione , *Biophysics (Oxf)*, **2014**, *59*, 415-419.

(121) A.F. Vanin, L.A. Ostrovskaya, D.B. Korman, V.D. Mikoyan, L.N. Kubrina, R.R. Borodulin, M.M. Fomina, N.V. Bluchterova, V.A. Rykova, An anti-nitrosative system as a factor of malignant tumor resistance to the cytotoxic effect of nitrogen monoxide, *Biophysics (Oxf)*, **2015**, *60*, 121-125.

(122) A.F. Vanin, L.A. Ostrovskaya, D.B. Korman, L.N. Kubrina, R.R,. Borodulin, M.M. Fomina, N.V. Bluchterova, V.A. Rykova, A.A. Timoshin, The anti-tumor activity of the S-nitrosoglutathione and dinitrosyl iron complexes with glutathione: comparative studies, *Biophysics (Oxf)*, **2015**, *60*, 121-125.

(123) A.F. Vanin, L.A. Ostrovskaya, D.B. Korman, V.A. Rykova, N.V. Bluchterova, M.M. Fomina, The anti-tumor effect of dinitrosyl iron complexes with glutathione in murine solid-tumor model, *Biophysics (Oxf)*, **2017**, *62*, 479-484.

(124) Wu, S.-C.; Lu, C.-Y.; Chen, Y.-L.; Lo, F.-C.; Wang, T.-Y.; Chen, Y.-J.; Yuan, S.-S.; Liaw, W.-F.; Wang, Y.-M. Water-Soluble Dinitrosyl Iron Complex (DNIC): A Nitric Oxide Vehicle Triggering Cancer Cell Death via Apoptosis. *Inorg. Chem* **2016**, *55*, 54.

(125) Kim, M.; Knoefler, D.; Quarles, E.; Jakob, U.; Bazopoulou, D. Automated Phenotyping and Lifespan Assessment of a C. Elegans Model of Parkinson's Disease. *Transl. Med. Aging* **2020**, *4*, 38–44.

(126) Naß, J.; Abdelfatah, S.; Efferth, T. Induction of Stress Resistance and Extension of Lifespan in Chaenorhabditis Elegans Serotonin-Receptor Knockout Strains by Withanolide A. *Phytomedicine* **2021**, *84*, 153482.

(127) Huang, H.-W.; Lin, Y.-H.; Lin, M.-H.; Huang, Y.-R.; Chou, C.-H.; Hong, H.-C.; Wang, M.-R.; Tseng, Y.-T.; Liao, P.-C.; Chung, M.-C.; et al. Extension of C. Elegans Lifespan Using the ·NO-Delivery Dinitrosyl Iron Complexes. *J. Biol. Inorg. Chem.* **2018**, *23* (3), 775–784.

(128) Lu, T.-T.; Wang, Y.-M.; Hung, C.-H.; Chiou, S.-J.; Liaw, W.-F. Bioinorganic Chemistry of the Natural $[Fe(NO)_2]$ Motif: Evolution of a Functional Model for NO-Related Biomedical Application and Revolutionary Development of a Translational Model. *Inorg. Chem.* **2018**, *57*, 12425–12443.

(129) Conrado, C. L.; Wecksler, S.; Egler, C.; Magde, D.; Ford, P. C. Synthesis and Photochemical Properties of a Novel Iron−Sulfur−Nitrosyl Cluster Derivatized with the Pendant Chromophore Protoporphyrin IX. *Inorg. Chem.* **2004**, *43*, 5543–5549.

(130) Skodje, K. M.; Kwon, M. Y.; Chung, S. W.; Kim, E. Coordination-Triggered NO Release from a Dinitrosyl Iron Complex Leads to Anti-Inflammatory Activity. *Chem. Sci.* **2014**, *5* (6), 2374-2378

(131) Wecksler, S. R.; Hutchinson, J.; Ford, P. C. Toward Development of Water Soluble Dye Derivatized Nitrosyl Compounds for Photochemical Delivery of NO. *Inorg. Chem.* **2006**, *45* (3), 1192–1200.

(132) Wecksler, S. R.; Mikhailovsky, A.; Korystov, D.; Ford, P. C. A Two-Photon Antenna for Photochemical Delivery of Nitric Oxide from a Water-Soluble, Dye-Derivatized Iron Nitrosyl Complex Using NIR Light. *J. Am. Chem. Soc.* **2006**, *128* (11), 3831–3837.

(133) Giuc Tran, N.; Kalyvas, H.; Skodje, K. M.; Hayashi, T.; Moënne-Loccoz, P.; Callan, P. E.; Shearer, J.; Kirschenbaum, L. J.; Kim, E. Phenol Nitration Induced by a $\{Fe(NO)_2\}^{10}$ Dinitrosyl Iron Complex. *J. Am. Chem. Soc.* **2011**. *133*(5). 1184-1187.

(134) Skodje, K. M.; Williard, P. G.; Kim, E. Conversion of $\{Fe(NO)_2\}^{10}$ Dinitrosyl Iron to Nitrato Iron(III) Species by Molecular Oxygen. *Dalt. Trans* **2012**, *41*, 7849.

(135) Meczynska, S.; Lewandowska, H. Variable Inhibitory Effects on the Formation of Dinitrosyl Iron Complexes by Deferoxamine and Salicylaldehyde Isonicotinoyl Hydrazone in K562 Cells. *Hemoglobin* **2008**, *32*, 157–163.

(136) Lok, H. C.; Rahmanto, Y. S.; Hawkins, C. L.; Kalinowski, D. S.; Morrow, C. S.; Townsend, A. J.; Ponka, P.; Richardson, D. R. Nitric Oxide Storage and Transport in Cells Are Mediated by Glutathione S-Transferase P1-1 and Multidrug Resistance Protein 1 via Dinitrosyl Iron Complexes. *J. Biol. Chem.* **2012**, *287* (1), 607–618.

(137) De Maria, F.; Pedersen, J. Z.; Caccuri, A. M.; Antonini, G.; Turella, P.; Stella, L.; Lo Bello, M.; Federici, G.; Ricci, G. The Specific Interaction of Dinitrosyl-Diglutathionyl-Iron Complex, a Natural NO Carrier, with the Glutathione

Transferase Superfamily: Suggestion for an Evolutionary Pressure in the Direction of the Storage of Nitric Oxide. *J. Biol. Chem.* **2003**, *278* (43), 42283–42293.

(138) Cho, S.-L. L., Cheng-Jhe; Lu, Tsai-Te, Synthetic Methodology for Preparation of Dinitrosyl Iron Complexes. *J. Bio. Inorg. Chem.* **2019,** *24*, 495-515.

(139) Harrop, T. C.; Song, D.; Lippard, S. J. Interaction of Nitric Oxide with Tetrathiolato Iron(II) Complexes: Relevance to the Reaction Pathways of Iron Nitrosyls in Sulfur-Rich Biological Coordination Environments. *J. Am. Chem. Soc.* **2006**, *128* (11), 3528–3529.

(140) Ghosh, P.; Quiroz, M.; Pulukkody, R.; Bhuvanesh, N.; Darensbourg, M.Y. Bridging cyanides from cyanoiron metalloligands to redox-active dinitrosyl iron units. *Dalton Trans*. **2018**, *47*, 11812 - 11819.

(141) Pulukkody, R.; Chupik, R. B.; Montalvo, S. K.; Khan, S.; Bhuvanesh, N.; Lim, S.-M.; Darensbourg, M. Y. Toward Biocompatible Dinitrosyl Iron Complexes: Sugar-Appended Thiolates. *Chem. Commun* **2017**, *53*, 1180–1183.

(142) Tsai, M.-L.; Hsieh, C.-H.; Liaw, W.-F. Dinitrosyl Iron Complexes (DNICs) Containing S/N/O Ligation: Transformation of Roussin's Red Ester into the Neutral $\{Fe(NO)_2\}^{10}$ DNICs. *Inorg. Chem.* **2007**, *46*, 5110–5117.

(143) Tseng, Y.; Ching, W.; Liaw, W.; Lu, T. Dinitrosyl Iron Complex [K-18-crown-6-ether][$(NO)_2Fe(^{Me}PyrCO_2)$]: Intermediate for Capture and Reduction of Carbon Dioxide. *Angew. Chemie Int. Ed.* **2020**, *59* (29), 11819–11823.

(144) Kindermann, N.; Schober, A.; Demeshko, S.; Lehnert, N.; Meyer, F. Reductive Transformations of a Pyrazolate-Based Bioinspired Diiron-Dinitrosyl Complex. *Inorg. Chem.* **2016**, *55* (21), 11538–11550.

(145) Atkinson, F. L.; Blackwell, H. E.; Brown, N. C.; Connelly, N. G.; Crossley, J. G.; Orpen, A. G.; Rieger, A. L.; Rieger, P. H. Synthesis of the 17-Electron Cations [FeL(L′)(NO)2]+ (L, L′ = PPh3, OPPh3): Structure and Bonding in Four-Co-Ordinate Metal Dinitrosyls, and Implications for the Identity of Paramagnetic Iron Dinitrosyl Complex Catalysts. *J. Chem. Soc. - Dalt. Trans.* **1996**, *17*, 3491–3502.

(146) Dillinger, S. A. T.; Schmalle, H. W.; Fox, T.; Berke, H. Developing Iron Nitrosyl Complexes as NO Donor Prodrugs. *Dalt. Trans.* **2007**, *32*, 3562–3571.

(147) Li, L.; Li, L. Recent Advances in Multinuclear Metal Nitrosyl Complexes. *Coord. Chem. Rev.* **2016**, *306*, 678–700.

(148) Chen, Y.-J.; Ku, W.-C.; Feng, L.-T.; Tsai, M.-L.; Hsieh, C.-H.; Hsu, W.-H.; Liaw, W.-F.; Hung, C.-H.; Chen, Y.-J. Nitric Oxide Physiological Responses and Delivery Mechanisms Probed by Water-Soluble Roussin's Red Ester and $\{Fe(NO)_2\}^{10}$ DNIC. *J. Am. Chem. Soc.* **2008**, *130*, 10929–10938.

(149) Ke, C. H.; Chen, C. H.; Tsai, M. L.; Wang, H. C.; Tsai, F. Te; Chiang, Y. W.; Shih, W. C.; Bohle, D. S.; Liaw, W. F. $\{Fe(NO)_2\}^9$ Dinitrosyl Iron Complex Acting as a Vehicle for the NO Radical. *J. Am. Chem. Soc.* **2017**, *139* (1), 67–70.

(150) Atkinson, F. L.; Brown, N. C.; Connelly, N. G.; Orpen, A. G.; Rieger, A. L.; Rieger, P. H.; Rosair, G. M. Paramagnetic Tetrahedral Dinitrosyliron Complexes

Containing Redox-Active Cyanomanganese Ligands. *Dalton Trans.* **1996**, No. 9, 1959–1966.

(151) Yeh, S. W.; Lin, C. W.; Li, Y. W.; Hsu, I. J.; Chen, C. H.; Jang, L. Y.; Lee, J. F.; Liaw, W. F. Insight into the Dinuclear $\{Fe(NO)_2\}^{10}$-$\{Fe(NO)_2\}^{10}$ and Mononuclear $\{Fe(NO)_2\}^{10}$ Dinitrosyliron Complexes. *Inorg. Chem.* **2012**, *51* (7), 4076–4087.

(152) Lu, T. Te; Chen, C. H.; Liaw, W. F. Formation of the Distinct Redox-Interrelated Forms of Nitric Oxide from Reaction of Dinitrosyl Iron Complexes (DNICs) and Substitution Ligands. *Chem. - A Eur. J.* **2010**, *16* (27), 8088–8095.

(153) Hsieh, C. H.; Brothers, S. M.; Reibenspies, J. H.; Hall, M. B.; Popescu, C. V.; Darensbourg, M. Y. Ambidentate Thiocyanate and Cyanate Ligands in Dinitrosyl Iron Complexes. *Inorg. Chem.* **2013**, *52* (4), 2119–2124.

(154) Liu, P. H.; Tsai, F. Te; Chen, B. H.; Hsu, I. J.; Hsieh, H. H.; Liaw, W. F. Insight into Chalcogenolate-Bound {Fe(NO)2}9 Dinitrosyl Iron Complexes (DNICs): Covalent Character: Versus Ionic Character. *Dalt. Trans.* **2019**, *48* (18), 6040–6050.

(155) Lo, F. C.; Ho, Y. C.; Chang, P. Y.; Lee, G. H.; Kuo, T. S.; Chen, J. L.; Chen, C. H. New Members of a Class of Monomeric $\{Fe(NO)_2\}^{10}$ Dinitrosyliron Complexes and a Dimeric $\{Fe(NO)_2\}^{10}$-$\{Fe(NO)_2\}^{10}$ Dinitrosyliron Complex. *Eur. J. Inorg. Chem.* **2014**, *2014* (22), 3499–3509.

(156) Hsiao, H. Y.; Chung, C. W.; Santos, J. H.; Villaflores, O. B.; Lu, T. Te. Fe in Biosynthesis, Translocation, and Signal Transduction of NO: Toward Bioinorganic Engineering of Dinitrosyl Iron Complexes into NO-Delivery Scaffolds for Tissue Engineering. *Dalt. Trans.* **2019**, *48* (26), 9431–9453.

(157) Tsai, M. C.; Tsai, F. Te; Lu, T. Te; Tsai, M. L.; Wei, Y. C.; Hsu, I. J.; Lee, J. F.; Liaw, W. F. Relative Binding Affinity of Thiolate, Imidazolate, Phenoxide, and Nitrite toward the ($Fe(NO)_2$) Motif of Dinitrosyl Iron Complexes (DNICs): The Characteristic Pre-Edge Energy of $\{Fe(NO)_2\}^9$ DNICs. *Inorg. Chem.* **2009**, *48* (19), 9579–9591.

(158) Jo, D. H.; Chiou, Y. M.; Que, J. Models for Extradiol Cleaving Catechol Dioxygenases: Syntheses, Structures, and Reactivities of Iron(II)-Monoanionic Catecholate Complexes. *Inorg. Chem.* **2001**, *40* (13), 3181–3190.

(159) Burns, K. T.; Marks, W. R.; Cheung, P. M.; Seda, T.; Zakharov, L. N.; Gilbertson, J. D. Uncoupled Redox-Inactive Lewis Acids in the Secondary Coordination Sphere Entice Ligand-Based Nitrite Reduction. *Inorg. Chem.* **2018**, *57* (16), 9601–9610.

(160) Kwon, Y. M.; Delgado, M.; Zakharov, L. N.; Seda, T.; Gilbertson, J. D. Nitrite Reduction by a Pyridinediimine Complex with a Proton-Responsive Secondary Coordination Sphere. *Chem. Commun.* **2016**, *52* (73), 11016–11019.

(161) Tsai, F. Te; Chen, P. L.; Liaw, W. F. Roles of the Distinct Electronic Structures of the {Fe(NO) 2}9 and {Fe(NO)2}10 Dinitrosyliron Complexes in Modulating

Nitrite Binding Modes and Nitrite Activation Pathways. *J. Am. Chem. Soc.* **2010**, *132* (14), 5290–5299.

(162) Chen, C. H.; Ho, Y. C.; Lee, G. H. Synthesis and Reactivity of the Five-Coordinate {Fe(NO)2}9 [(TMEDA)Fe(NO)2I]. *J. Organomet. Chem.* **2009**, *694* (21), 3395–3400.

(163) Wang, R.; Wang, X.; Sundberg, E. B.; Nguyen, P.; Grant, G. P. G.; Sheth, C.; Zhao, Q.; Herron, S.; Kantardjieff, K. A.; Li, J. Synthesis, Structures, Spectroscopic and Electrochemical Properties of Dinitrosyl Iron Complexes with Bipyridine, Terpyridine, and 1, 10-Phenathroline. *Inorg. Chem.* **2009**, *48* (20), 9779–9785.

(164) Wang, R.; Camacho-Fernandez, M. A.; Xu, W.; Zhang, J.; Li, L. Neutral and Reduced Roussin's Red Salt Ester [Fe2(μ-RS) 2(NO)4] (R = n-Pr, t-Bu, 6-Methyl-2-Pyridyl and 4,6-Dimethyl-2-Pyrimidyl): Synthesis, X-Ray Crystal Structures, Spectroscopic, Electrochemical and Density Functional Theoretical Investigations. *Dalt. Trans.* **2009**, *5*, 777–786.

(165) Hsieh, C. H.; Pulukkody, R.; Darensbourg, M. Y. A Dinitrosyl Iron Complex as a Platform for Metal-Bound Imidazole to N-Heterocyclic Carbene Conversion. *Chem. Commun.* **2013**, *49* (81), 9326–9328.

(166) Hess, J. L.; Hsieh, C. H.; Reibenspies, J. H.; Darensbourg, M. Y. N-Heterocyclic Carbene Ligands as Mimics of Imidazoles/Histidine for the Stabilization of Di-and Trinitrosyl Iron Complexes. *Inorg. Chem.* **2011**, *50* (17), 8541–8552.

(167) Hsieh, C. H.; Darensbourg, M. Y. A {Fe(NO)3}10 Trinitrosyliron Complex Stabilized by an N-Heterocyclic Carbene and the Cationic and Neutral {Fe(NO)2} 9/10 Products of Its NO Release. *J. Am. Chem. Soc.* **2010**, *132* (40), 14118–14125.

(168) Lo, F. C.; Li, Y. W.; Hsu, I. J.; Chen, C. H.; Liaw, W. F. Insight into the Reactivity and Electronic Structure of Dinuclear Dinitrosyl Iron Complexes. *Inorg. Chem.* **2014**, *53* (20), 10881–10892.

(169) Tsai, M.-L.; Tsou, C.-C.; Liaw, W.-F. Dinitrosyl Iron Complexes (DNICs): From Biomimetic Synthesis and Spectroscopic Characterization toward Unveiling the Biological and Catalytic Roles of DNICs. *Acc. Chem. Res.* **2015**, *48*, 1184–1193.

(170) Denny, J. A.; Darensbourg, M. Y. Approaches to Quantifying the Electronic and Steric Properties of Metallodithiolates as Ligands in Coordination Chemistry. *Coord. Chem. Rev.* **2016**, *324*, 82–89.

(171) Pulukkody, R.; Darensbourg, M. Y. Synthetic Advances Inspired by the Bioactive Dinitrosyl Iron Unit. *Acc. Chem. Res.* **2015**, *48* (7), 2049–2058.

(172) Pinder, T. A.; Montalvo, S. K.; Hsieh, C. H.; Lunsford, A. M.; Bethel, R. D.; Pierce, B. S.; Darensbourg, M. Y. Metallodithiolates as Ligands to Dinitrosyl Iron Complexes: Toward the Understanding of Structures, Equilibria, and Spin Coupling. *Inorg. Chem.* **2014**, *53* (17), 9095–9105.

(173) Hsieh, C. H.; Chupik, R. B.; Pinder, T. A.; Darensbourg, M. Y. Dinitrosyl Iron Adducts of (N2S2)M(NO) Complexes (M = Fe, Co) as Metallodithiolate Ligands. *Polyhedron* **2013**, *58*, 151–155.

(174) Hsieh, C. H.; Chupik, R. B.; Brothers, S. M.; Hall, M. B.; Darensbourg, M. Y. Cis-Dithiolatonickel as Metalloligand to Dinitrosyl Iron Units: The Di-Metallic Structure of Ni(μ-SR)[Fe(NO)2] and an Unexpected, Abbreviated Metalloadamantyl Cluster, Ni2(μ-SR) 4[Fe(NO)2]3. *Dalt. Trans.* **2011**, *40* (22), 6047–6053.

(175) Brothers, S. M.; Darensbourg, M. Y.; Hall, M. B. Modeling Structures and Vibrational Frequencies for Dinitrosyl Iron Complexes (DNICs) with Density Functional Theory. *Inorg. Chem.* **2011**, *50* (17), 8532–8540.

(176) Ghosh, P.; Ding, S.; Quiroz, M.; Bhuvanesh, N.; Hsieh, C. H.; Palacios, P. M.; Pierce, B. S.; Darensbourg, M. Y.; Hall, M. B. Structural and Electronic Responses to the Three Redox Levels of Fe(NO)N2S2-Fe(NO)2. *Chem. - A Eur. J.* **2018**, *24* (60), 16003–16008.

(177) Speelman, A. L.; Zhang, B.; Silakov, A.; Skodje, K. M.; Alp, E. E.; Zhao, J.; Hu, M. Y.; Kim, E.; Krebs, C.; Lehnert, N. Unusual Synthetic Pathway for an {Fe(NO) 2 } 9 Dinitrosyl Iron Complex (DNIC) and Insight into DNIC Electronic Structure via Nuclear Resonance Vibrational Spectroscopy. *Inorg. Chem.* **2016**, *55*, 5485–5501.

(178) Lu, T. Te; Lai, S. H.; Li, Y. W.; Hsu, I. J.; Jang, L. Y.; Lee, J. F.; Chen, I. C.; Liaw, W. F. Discrimination of Mononuclear and Dinuclear Dinitrosyl Iron Complexes (DNICs) by S K-Edge X-Ray Absorption Spectroscopy: Insight into the Electronic Structure and Reactivity of DNICs. *Inorg. Chem.* **2011**, *50* (12), 5396–5406.

(179) Dai, R. J.; Ke, S. C. Detection and Determination of the {Fe(NO)2} Core Vibrational Features in Dinitrosyl-Iron Complexes from Experiment, Normal Coordinate Analysis, and Density Functional Theory: An Avenue for Probing the Nitric Oxide Oxidation State. *J. Phys. Chem. B* **2007**, *111* (9), 2335–2346.

(180) Tonzetich, Z. J.; Wang, H.; Mitra, D.; Tinberg, C. E.; Do, L. H.; Jenney, F. E.; Adams, M. W. W.; Cramer, S. P.; Lippard, S. J. Identification of Protein-Bound Dinitrosyl Iron Complexes by Nuclear Resonance Vibrational Spectroscopy. *J. Am. Chem. Soc.* **2010**, *132* (20), 6914–6916.

(181) Grabarczyk, D. B.; Ash, P. A.; Vincent, K. A. Infrared Spectroscopy Provides Insight into the Role of Dioxygen in the Nitrosylation Pathway of a [2Fe2S] Cluster Iron-Sulfur Protein. *J. Am. Chem. Soc.* **2014**, *136* (32), 11236–11239.

(182) Lin, Z. S.; Lo, F. C.; Li, C. H.; Chen, C. H.; Huang, W. N.; Hsu, I. J.; Lee, J. F.; Horng, J. C.; Liaw, W. F. Peptide-Bound Dinitrosyliron Complexes (DNICs) and Neutral/Reduced-Form Roussin's Red Esters (RREs/RRREs): Understanding Nitrosylation of [Fe-S] Clusters Leading to the Formation of DNICs and RREs Using a de Novo Design Strategy. *Inorg. Chem.* **2011**, *50* (20), 10417–10431.

(183) Wang, X.; Sundberg, E. B.; Li, L.; Kantardjieff, K. A.; Herron, S. R.; Lim, M.; Ford, P. C. A Cyclic Tetra-Nuclear Dinitrosyl Iron Complex $[Fe(NO)_2(Imidazolate)]_4$: Synthesis, Structure and Stability. *Chem. Commun.* **2005**, *4*, 477–479.

(184) Lu, T. Te; Weng, T. C.; Liaw, W. F. X-Ray Emission Spectroscopy: A Spectroscopic Measure for the Determination of NO Oxidation States in Fe-NO Complexes. *Angew. Chemie - Int. Ed.* **2014**, *53* (43), 11562–11566.

(185) Tseng, Y. T.; Chen, C. H.; Lin, J. Y.; Li, B. H.; Lu, Y. H.; Lin, C. H.; Chen, H. T.; Weng, T. C.; Sokaras, D.; Chen, H. Y.; et al. To Transfer or Not to Transfer? Development of a Dinitrosyl Iron Complex as a Nitroxyl Donor for the Nitroxylation of an FeIII-Porphyrin Center. *Chem. - A Eur. J.* **2015**, *21* (49), 17570–17573.

(186) Tsou, C. C.; Chiu, W. C.; Ke, C. H.; Tsai, J. C.; Wang, Y. M.; Chiang, M. H.; Liaw, W. F. Iron(III) Bound by Hydrosulfide Anion Ligands: NO-Promoted Stabilization of the [Fe^{III}-SH] Motif. *J. Am. Chem. Soc.* **2014**, *136* (26), 9424–9433.

(187) Wu, W. Y.; Hsu, C. N.; Hsieh, C. H.; Chiou, T. W.; Tsai, M. L.; Chiang, M. H.; Liaw, W. F. NO-to-[N2O2]2--to-N2O Conversion Triggered by {Fe(NO)2}10-{Fe(NO)2}9 Dinuclear Dinitrosyl Iron Complex. *Inorg. Chem.* **2019**, *58* (15), 9586–9591.

(188) Lu, T. Te; Huang, H. W.; Liaw, W. F. Anionic Mixed Thiolate Sulfide-Bridged Roussin's Red Esters [(NO) 2Fe(μ-SR)(μ-S)Fe(NO)2]- (R = Et, Me, Ph): A Key Intermediate for Transformation of Dinitrosyl Iron Complexes (DNICs) to [2Fe-2S] Clusters. *Inorg. Chem.* **2009**, *48* (18), 9027–9035.

(189) Pectol, D.; Khan, S.; Chupik, R.; Elsabahy, M.; Wooley, K.; Darensbourg, M.; Lim, S.-M. Toward the Optimization of Dinitrosyl Iron Complexes as Therapeutics for Smooth Muscle Cells. *Mol. Pharm.* **2019**, *16* (7), 3178–3187.

(190) Pisarenko, O.; Studneva, I.; Timoshin, A.; Veselova, O. Protective Efficacy of Dinitrosyl Iron Complexes with Reduced Glutathione in Cardioplegia and Reperfusion. *Eur. J. Physiol.* **2019**, *471* (4), 583–593.

CHAPTER II : EXPERIMENTAL SECTION FOR CHAPTERS IV-VI*

II.1 General experimental parameters

Materials & Characterizations: Chemical syntheses were performed under an N_2 atmosphere using standard Schlenk techniques. Dry solvents used were purified using a Bruker solvent system. The purities of the complexes were confirmed by solution FT-IR spectroscopy (Bruker 37 Tensor FT-IR spectrometer, CaF_2 window, pathlength = 0.2 mm) and $ESI^{+/-}$-MS (Thermo Scientific Q Exactive Focus. Flow rate = 10 μL/min. Spray voltage = 3.75 kV, and the sheath gas and auxiliary gas flow rates were set to 7 and 0 arbitrary units, respectively. The transfer capillary temperature was held at 250 °C and the S-Lens RF level was set at 50 v. Exactive Series 2.8 SP1/Xcalibur 4.0 software was used for data acquisition and processing). Clear, sterile, flat-bottomed, 96-well tissue culture plates were used for all BCA, Griess and MTS assays. All synthesized or purchased complexes that were used as cell treatments were filtered through sterile 0.2-micron PVDF filters before application to cells. The TGTA-RRE, SPhRRE, SGlucNHC, SPhNHC, and [Na(18-crown-6)][$Fe(CO)_3(NO)$] were synthesized following published procedures.[1]

---

* Sections II.1, II.2 Reprinted with permission from Pectol, D.; Khan, S.; Chupik, R.; Elsabahy, M.; Wooley, K.; Darensbourg, M.; Lim, S.-M. Toward the Optimization of Dinitrosyl Iron Complexes as Therapeutics for Smooth Muscle Cells. *Mol. Pharm*. **2019**, *16* (7), 3178–3187, and II.3 from Pectol, D.; Khan, S.; Elsabahy, M.; Wooley, K.; Lim, S.-M.; Darensbourg, M. Effects of Glutathione and Histidine on NO Release from a Dimeric Dinitrosyl Iron Complex (DNIC). *Inorg. Chem*. **2020**, *59* (23), 16998–17008.

II.2 Experimental Procedures for Chapter III

Cell culture: Vascular smooth muscle cells were kindly gifted by Dr. Andrea Trache at Texas A&M Health Science Center. Cells were isolated from rat cremaster arterioles and were cultured in 5% CO_2 at 37 °C in Dulbecco's Modified Eagle Medium (DMEM/F12) supplemented with 10% fetal bovine serum, 10 mM HEPES (Sigma, St. Louis, MO), 2 mM L-glutamine, 1 mM sodium pyruvate, 100 U/ml penicillin, 100 mg/mL streptomycin and 0.25 mg/mL amphotericin B. Unless otherwise specified, all reagents were purchased from Thermo Fisher Scientific (Waltham, MA).

Griess Assay: The Griess Reagent Kit was purchased from Biotium and used as directed. The SMCs were plated to confluence in half of the 96 wells on the plate. Clear, sterile, flat-bottomed, 96-well tissue culture plates were used. Media was aspirated and replaced with the following reagents in each well: 20 µL Griess Reagent, 150 µL 1% DMSO in phenol-free DMEM/F12 solution containing varying concentrations of DNIC, and 130 µL DMEM/F12 (total 300 µL/well). Absorbance readings at 548 nm of each well after 2, 24 and 48 h of incubation were obtained. The absorbance readings from the wells without cells or Griess reagent were used as the blanks and subtracted from all absorbance readings.

MTS Assay: The 96 well plate colorimetric measurements were performed on a Molecular Devices SpectraMax M5. CellTiter 96® AQ One Solution Cell Proliferation Assay was purchased from Promega and used without modification, as described previously.[44] SMCs were grown to confluency, and then were incubated at 37 °C with

DNIC for 72 h. A 20 µL aliquot of MTS reagent was added to each well and incubated for 2 h. Absorbance was recorded at 490 nm.

Intracellular NO detection using end point fluorescence: The 96 well plate fluorometric measurements were performed on a Molecular Devices SpectraMax M5. The OxiSelect^{TM} Intracellular Nitric Oxide (NO) Assay Kit (Fluorometric) was purchased from Cell Biolabs and used according to the instructions provided in the kit. The plates used were 96 well Griener Bio-One Black, F-bottom, Fluorotrac, high binding, sterile plates. SMCs were plated at 100k/mL and grown overnight in 10% FBS. The following day the media was aspirated, and the SMCs were incubated with 1-1.5 µL DNIC and 1x NO Fluorometric probe in phenol-free DMEM/F12 for 2 h in the dark at 37 ^{o}C. Fluorometric measurements for the NO probe were obtained (Ex – 480 nm / Em – 530 nm). Afterwards, NucRed live nuclear stain was added to each well per the instructions provided with the kit and allowed to incubate for 30 min. The fluorometric measurements were then obtained (Ex – 638 nm / Em – 686 nm). The experimental set-up is visualized in Figure II-1. For the DNIC pre-incubation experiments, DNIC was added 2, 24 and 48 h before incubation with the NO probe for 2 h. DNIC was applied after 2 h NO probe incubation for the NO release profile experiments. Cell fluorescence was also imaged with a laser scanning confocal microscope (Olympus FV 1000) with 10× objective. Cells were plated on 8 Well µ-Slides (ibidi, Germany) and treated as described above.

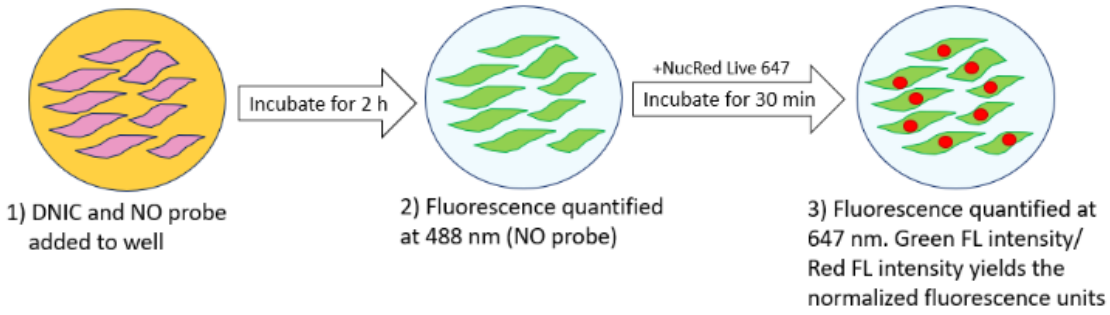

Figure II-1: Method of quantification used in detection and normalization of Intracellular NO.

Multiplex immunotoxicity assay: The endotoxin contents of the various DNIC samples were measured by using the Pierce Limulus Amebocyte Lysate Chromogenic Endotoxin Quantitation Kit (Thermo Fisher Scientific Inc., Rockford, IL), according to the manufacturer instructions, as described previously.[2] RAW 264.7 cells were treated with medium (control), DEANO, neoDNIC, SGluNHC, SGluRRE, SPhNHC and SPhRRE at 5 μM for 24 h. RAW 264.7 cells were treated with medium (control), SGluNHC, SGluRRE and 1-thio-β-D-glucose tetraacetate (thioglucose) at 10 μM for 24 h. The supernatants were then collected and centrifuged for 10 min at 13,000 rpm. Serial dilutions of standards of cytokines were also prepared in the same diluent utilized for the samples (*i.e.* cell-culture medium). Control, standards and treated samples (50 μL) were incubated with antibody-conjugated magnetic beads for 30 min in the dark. After washing the beads, the detection antibody was added to the wells and incubated in the dark for another 30 min under continuous shaking (300 rpm). After washing the beads again, streptavidin-phycoerythrin was added to every well and incubated while protected from

light for 10 min under same shaking conditions. Finally, after several washings with re-suspension in the assay buffer and shaking, the expression of the mouse cytokines, interleukin (IL)-1α, IL-1β, IL-2, IL-3, IL-4, IL-5, IL-6, IL-9, IL-10, IL-12 (P40), IL-12 (P70), IL-13, IL-17, Eotaxin, granulocyte-colony-stimulating factor (G-CSF), granulocyte macrophage-colony-stimulating factor (GM-CSF), interferon-γ (IFN-γ), keratinocyte-derived chemokine (KC), monocyte chemotactic protein (MCP)-1, macrophage inflammatory protein (MIP)-1α, MIP-1β, regulated upon activation normal T-cell expressed and presumably secreted (RANTES) and tumor necrosis factor-α (TNF-α) was measured immediately using Bio-plex 200 system with HTF and Pro II Wash station and the data were analyzed using the Bio-plex Data Pro software (Bio-Rad Laboratories, Hercules, CA).

II.3 Experimental Procedures for Chapter IV

FT-IR: For the FT-IR experiments, 10.0 mg (10.4 μmol) of SGlucRRE was dissolved in 25 mL solvent, and the spectrum was recorded at the desired timepoint. For the SGlucRRE treated with different concentrations of ligand, 2, 10 or 50 molar equivalents of GSH or HisF were added to the reaction vessel before the solvent was added. All IR measurements were recorded on a Bruker 37 Tensor FT-IR spectrometer with an IR cell equipped with a CaF_2 window, pathlength = 0.2 mm.

EPR: The solvents used for these experiments were DMSO (GSH and HisF), DCM (HisF), and 1% DMSO in DMEM/F12 (Histidine and GSH). All solutions were sonicated to ensure solubility. For the EPR experiments, 10.0 mg (10.4 μmol) of SGlucRRE was

dissolved in 10 mL solvent along with 20.8 μmol, 104 μmol, or 521 μmol of GSH, HisF, or histidine. Aliquots, 300 μL, of the reaction mixture, were transferred using a syringe equipped with a thin needle to EPR tubes under an N_2 atmosphere. EPR tubes were then frozen in liquid N_2. All measurements were performed on X-band Bruker Elexsys EPR cooled to 4 K.

MS: Samples of SGlucRRE were stirred overnight with 1, 2, 10, or 50 molar equivalents of exogenous ligand (His, HisF, or GSH). Conditions using the Thermo Scientific Q Exactive Focus were as follows: Flow rate = 10 μL/min, Spray voltage = 3.75 kV, the sheath gas and auxiliary gas flow rates were set to 7 and 0 arbitrary units, respectively. The transfer capillary temperature was held at 250 °C and the S-Lens RF level was set at 50 v. Exactive Series 2.8 SP1/Xcalibur 4.0 software was used for data acquisition and processing. The mass spectra were processed to generate the figures using the mMass program. For LC-MS, the following column conditions were for 5 minutes; from 5-15 minutes, the concentration of MeCN was increased linearly until reaching 100% MeCN (an increase of 5% per minute); 100% MeCN from 15-23 minutes; and then from 23-30 minutes, the column was flushed with 50% MeCN in water. The flow rate over the course of the experiment was 300 μL/min. The in-line UV-Vis detector was set to 350 nmused: 50% acetonitrile (MeCN) in water.

Cell culture: Vascular smooth muscle cells were gifted by Dr. Andrea Trache at the Texas A&M Health Science Center. Cells were isolated from rat cremaster arterioles and were cultured in 5% CO_2 at 37 °C in Dulbecco's Modified Eagle Medium (DMEM/F12),

supplemented with 10% fetal bovine serum, 10 mM HEPES (Sigma, St. Louis, MO), 2 mM L-glutamine, 1 mM sodium pyruvate, 100 U/ml penicillin, 100 mg/mL streptomycin and 0.25 mg/mL amphotericin B. All culturing reagents were purchased from Thermo Fisher Scientific (Waltham, MA).

Griess Assay: The Griess Reagent Kit was purchased from Biotium and used as directed. The following reagents were placed in each well: 20 µL Griess Reagent, 150 µL 1% DMSO in phenol-free DMEM/F12 solution containing varying concentrations of the dimeric DNIC, exogenous ligand (His or GSH), and 130 µL water (total 300 µL/well). Absorbance readings at 548 nm of solutions in each well after 0.5, 1, 2, 6, and 18 h of incubation were obtained. The absorbance readings from the wells with Griess reagent and DMEM/F12 were used as the blanks and subtracted from all absorbance readings. Clear, sterile, flat-bottomed, 96-well tissue culture plates were used for all of the treatment conditions (Griener Bio-One Clear, F-bottom, sterile plates).

Intracellular NO detection using end point fluorescence: The OxiSelect^{TM} Intracellular Nitric Oxide (NO) Assay Kit (Fluorometric – Cell Biolabs) was used according to the instructions provided in the kit. Smooth muscle cells were plated on 96 well Griener Bio-One Black, F-bottom, Fluorotrac, high binding, sterile plates at 100,000 cells/mL. The SMC were grown overnight in 10% FBS. The following day the media was aspirated, washed 3x with DPBS, and then incubated with 1x NO Fluorometric probe in phenol-free DMEM/F12 for 2 h in the dark at 37 ^{o}C. DNIC samples were prepared as concentrated DMSO solutions. One µL of DNIC with 2x, 10x, or 50x molar equivalents of histidine or

GSH in phenol-free DMEM/F12 were added to the SMC. Fluorometric measurements were obtained (Ex – 480 nm / Em – 530 nm). Time = 0 for each treatment condition was recorded when the DNIC-DMSO solution was applied to the cells. Afterwards, NucRed live nuclear stain (NucRed™ Live 647 ReadyProbes™ Reagent – Invitrogen) was added to each well per the instructions provided with the kit and allowed to incubate for 30 min; then the red fluorescence was detected (Ex – 638 nm / Em – 686 nm).

II.4 Experimental Procedures for Chapter V

Chemical syntheses were performed under an N_2 atmosphere using standard Schlenk techniques. Solvents were purified using a Bruker solvent system. The TGTA-RRE and [Na(18-crown-6)][$Fe(CO)_3(NO)$] were synthesized following published procedures.[1] All IR measurements were recorded on a Bruker 37 Tensor FT-IR spectrometer with an IR cell equipped with a CaF_2 window, pathlength = 0.2 mm. Mass spectra were collected with a Thermo Scientific Q Exactive Focus using the following conditions: Flow rate = 10 µL/min, Spray voltage = 3.75 kV, the sheath gas and auxiliary gas flow rates were set to 7 and 0 arbitrary units. The transfer capillary temperature was held at 250 °C and the S-Lens RF level was set at 50 v. Exactive Series 2.8 SP1/Xcalibur 4.0 software was used for data acquisition and processing. The mass spectra were processed to generate the figures using the mMass program.

SCy-RRE synthesis: [Na(18-crown-6)][$Fe(CO)_3(NO)$] (476 mg, 1.04 mmol), and $NOBF_4$ (116 mg, 1.00 mmol) were dissolved in approximately 20 mL dry THF and reacted for 15

minutes yielding a orange-brown solution. The solvent and approximately 1 mmol $Fe(CO)_2(NO)_2$ were removed via vacuum and collected using a liquid N_2 trap. Dicyclohexyl disulfide (104 mg, 0.45 mmol) was dissolved in ~10 mL dry THF and added to the thawed $Fe(CO)_2(NO)_2$ solution. The resulting orange solution was reacted overnight at RT yielding a brown solution the next day. The THF was removed *in vacuo*, and the resulting solid was washed three times with cold, dry pentane, redissolved in 15 mL ether, and filtered through a pad of celite. The resulting filtrate was dried under a gentle purge of N_2 overnight yielding X-ray diffraction quality crystals from the concentrated Et_2O solution (177 mg, 85.1 % yield). The features in the FT-IR spectrum were as follows: ν(NO): (w) 1815 cm^{-1}, (s) 1786 cm^{-1}, (s) 1755 cm^{-1}. Resulting FT-IR spectrum and X-Ray data are found in Figures II-2, II-3 and Tables II-1–II-6).

X-Ray Crystallography for SCyRRE: A Leica MZ 75 microscope was used to identify a suitable brown block with very well defined faces with dimensions (max, intermediate, and min) 0.152 x 0.047 x 0.024 mm^3 from a representative sample of crystals of the same habit. The crystal mounted on a nylon loop was then placed in a cold nitrogen stream (Oxford) maintained at 110 K.

A BRUKER Quest X-ray (fixed-Chi geometry) diffractometer with a PHOTON II detector was employed for crystal screening, unit cell determination, and data collection. The goniometer was controlled using the APEX3 software suite.[3] The sample was optically centered with the aid of a video camera such that no translations were observed as the crystal was rotated through all positions. The X-ray radiation employed was generated

from a Mo-Iμs X-ray tube (Kα = 0.71073Å). 45 data frames were taken at widths of 1°. These reflections were used to determine the unit cell. The unit cell was verified by examination of the *h k l* overlays on several frames of data. No super-cell or erroneous reflections were observed. After careful examination of the unit cell, an extended data collection procedure (6 sets) was initiated using omega and phi scans.

Integrated intensity information for each reflection was obtained by reduction of the data frames with the program APEX3.[3] The integration method employed a three dimensional profiling algorithm and all data were corrected for Lorentz and polarization factors, as well as for crystal decay effects. Finally the data was merged and scaled to produce a suitable data set. The absorption correction program SADABS[4] was employed to correct the data for absorption effects.

Systematic reflection conditions and statistical tests of the data suggested the space group $P2_{1/c}$. A solution was obtained readily (Z=2; Z'=0.5) using XT/XS in APEX3.[3,4] Hydrogen atoms were placed in idealized positions and were set riding on the respective parent atoms. All non-hydrogen atoms were refined with anisotropic thermal parameters. Elongated ellipsoids on the C1 – C6 group suggested disorder which was modeled between two positions each with an occupancy ratio of 0.62:0.38. Appropriate restraints and constraints were added to keep the bond distances, angles, and thermal ellipsoids of the disordered group meaningful. Elongated ellipsoids of the NO groups also suggested disorder. However, our trials to model the disorder did not improve the results. Absence

of additional symmetry and voids were confirmed using PLATON (ADDSYM).[5] The structure was refined (weighted least squares refinement on F2) to convergence.[4]

Olex2 was employed for the final data presentation and structure plots.[6]

TG-RRE synthesis: [Na(18-crown-6)][$Fe(CO)_3(NO)$] (472 mg, 1.03 mmol), $NOBF_4$ (234 mg, 2.00 mmol), and Sodium 1-Thio-β-D-glucose (232 mg, 1.06 mmol) were dissolved in 25 mL dry MeOH yielding a brownish solution. The reaction was stirred overnight at room temperature, then filtered through a pad of celite the following day. Reaction completion was determined via disappearance of ν(CO) features in the FT-IR spectrum (~2000 – 1850 cm^{-1}). The resulting filtrate was dried *in vacuo* and washed 3 times with Et_2O. The brown solid was redissolved in MeOH and precipitated with Et_2O, discarding the supernatant. The precipitation process was repeated 3 times, yielding a brown solid (274 mg, 44% yield). The features in the FT-IR spectrum were as follows: ν(NO): (w) 1804 cm^{-1}, (s) 1770 cm^{-1}, (s) 1747 cm^{-1}. APCI-MS (m/z): 620.92 - **$C_{12}H_{21}Fe_2N_4O_{14}S_2$ [TG-RRE -H]$^-$** . Resulting FT-IR and HRMS spectra are found in Figures II-2, II-4, II-5).

FRET protease assay: Recombinant SC2Mpro protein was expressed and purified according to literature protocol.[Chris4A] The protein was then changed into buffer A (20 mM HEPES, 10 mM NaCl, pH 7.8) using a spin desalting column (Zeba). The purified SC2Mpro was diluted to 10 μM in buffer A and stored at -80 °C. The inhibition assay was based on the established fluorescent peptide assay system[7refchris]. The FRET-based tetradecapeptide substrate (DABCYL-Lys-Thr-Ser-Ala-Val-Leu-Gln-Ser-Gly-Phe-Arg-

Lys-Met-Glu-EDANS) was purchased from Bachem and stored as a 1 mM solution in 100% DMSO. All inhibitors were stored as 10 mM in 100% DMSO solutions in -20 °C freezer. The final inhibition assay contained 50 nM MPro, 10 μM substrate, and varying concentrations of inhibitors. Enzyme and substrate stock solutions were diluted using buffer A. Inhibitors were diluted into varying concentrations maintaining 10% DMSO in buffer A. 40 μL of a 62.5 nM SC2MPro solution was added to each well in a 96-well plate, and 5 μL of inhibitor solution with varying concentrations was added. After a brief shaking, the plate was incubated at 37°C for 15 min. Then 5 μL of a 100 μM substrate solution was added to initiate the activity analysis. The EDANS fluorescence with excitation at 336 nm and emission at 490 nm from the cleaved substrate was detected. GraphPad 8.0 was used to analyze the data and the standard error.

Computational Methods: AutoDock4 was used for blind docking and for the generation of binding poses. The protein used in this study was the monomer of the COVID-19 main protease (PDB:6W63)[7] with the inhibitor X77 and water removed. For each potential inhibitor the genetic algorithm-based calculation was performed with 20 runs for the blind docking, 200 runs for the active site docking for the DNICs, 2000 runs for the peptidic substrates, and 5000 for the glutathione transferase standardization to PDB:1ZGN,[8] with the output for all runs in Lamarckian Genetic Algorithm form. All rotations excluding amide rotations were kept active. The rest of the parameters are as follows: Population Size: 150, Max. number of evaluations: 2.5 million, Max. number of generations 27,000, rate of crossover: 0.8. The dimeric coordinates for TGTA-RRE and TG-RRE used in these

simulations were generated by the addition of the alcohol or acetyl groups onto the SCyRRE crystal structure. The structures were optimized using the Structure Editing tools in UCSF Chimera. The monomeric structures used were based on a previously obtained crystal structure of the N-heterocyclic carbene cleaved TGTA-RRE: [(1,3-bis(2,4,6-trimethylphenyl)imidazolidine)Fe(NO)$_2$(1-thio-β-D-glucose tetraacetate)].[1] The NHC was removed to generate the TGTA DNIC monomer, and then the acetates were truncated to alcohols for the TG DNIC monomer, and then further truncated to generate the SCy DNIC monomer. To generate the charges on the atoms of the free ligands, the RRE DNICs, and the proteins, the AM1-BCC forcefield was used. For the monomeric DNICs, the charges were assigned to the DNIU and ligand separately, with the ligand bearing the -1 charge, and the iron of the DNIU carrying the +1 charge.

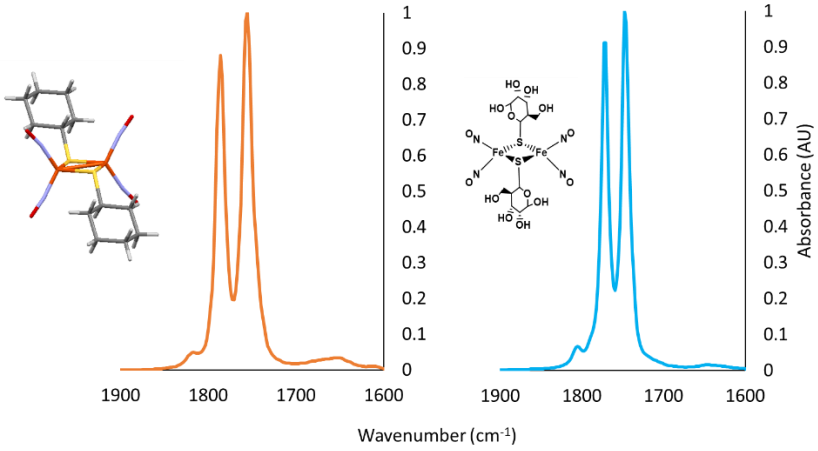

Figure II-2: FT-IR spectra for SCyRRE (left-orange) and TG-RRE (right-blue). The crystal structure for SCyRRE and the expected structure for TG-RRE, are shown in the inlay. The spectra have been normalized (AU = 1) to the highest absorbance from 1900 cm^{-1} to 1600 cm^{-1}.

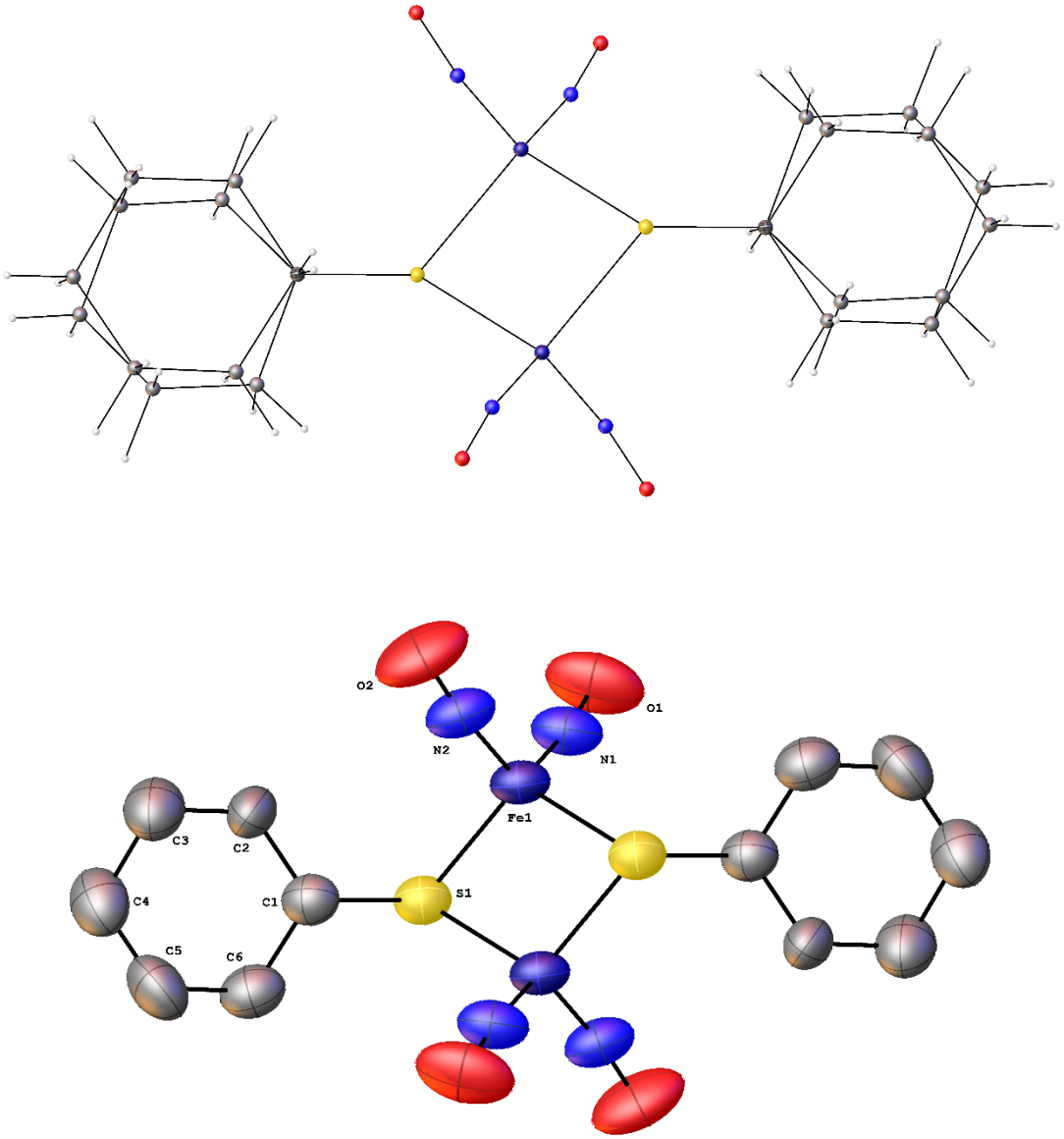

Figure II-3: Representation of the coordinates for the crystal structure of SCyRRE. [Top] Ball and stick representation of the two different DNIC isomers that constitute the crystal lattice. [Bottom] Thermal ellipsoid of the two crystal structures overlaid including the atom labels.

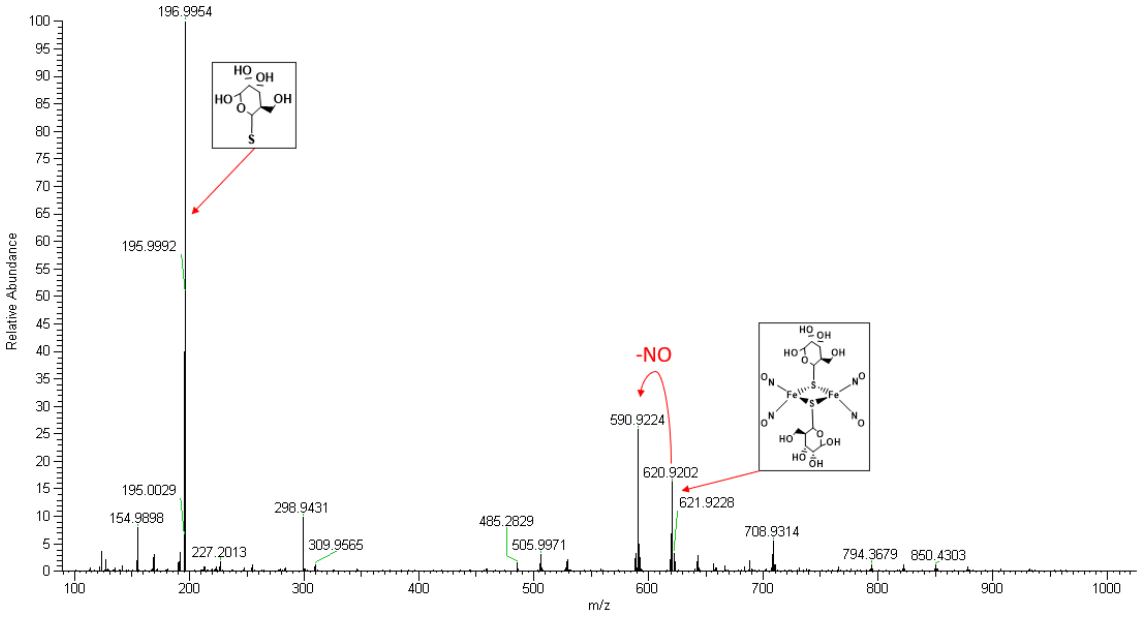

Figure II-4: ESI⁻-MS of TG-RRE. Relevant peaks labeled with their corresponding predicted molecular structure

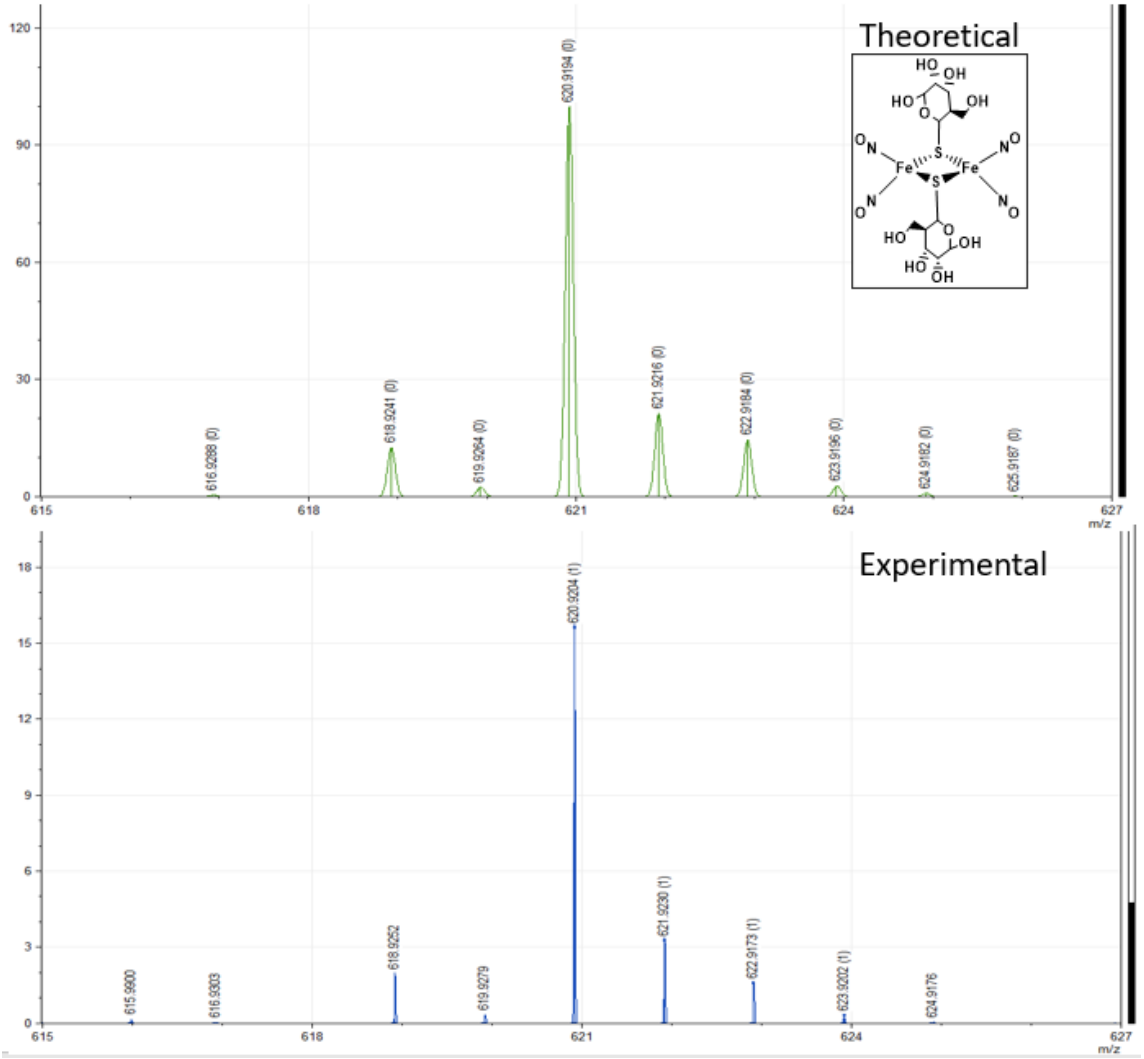

Figure II-5: Theoretical m/z for the [TG-RRE]-H fragment: $C_{12}H_{21}Fe_2N_4O_{14}S_2$ – 620.9194 m/z, in the range of 615-627 m/z. Zoomed in spectra from 615-627 m/z for the mass spectrum shown in Figure II-4.

Table II-1 Crystal data and structure refinement for SCyDNIC.

Empirical formula	C12 H22 Fe2 N4 O4 S2
Formula weight	462.15
Temperature	110.0 K
Wavelength	0.71073 Å
Crystal system	Monoclinic
Space group	P 1 21/c 1
Unit cell dimensions	a = 5.1194(12) Å α= 90°
	b = 14.355(4) Å β= 90.134(8)°
	c = 13.107(3) Å γ = 90°
Volume	963.3(4) $Å^3$
Z	2
Density (calculated)	1.593 Mg/m^3
Absorption coefficient	1.745 mm^{-1}
F(000)	476
Crystal size	0.152 x 0.047 x 0.024 mm^3
Theta range for data collection	3.108 to 24.997°.
Index ranges	-6<=h<=6, -17<=k<=16, -15<=l<=15
Reflections collected	12757
Independent reflections	1677 [R(int) = 0.0205]
Completeness to theta = 24.997°	99.6 %
Absorption correction	Semi-empirical from equivalents
Max. and min. transmission	0.7457 and 0.6207
Refinement method	Full-matrix least-squares on F^2
Data / restraints / parameters	1677 / 97 / 155
Goodness-of-fit on F^2	1.042
Final R indices [I>2sigma(I)]	R1 = 0.0350, wR2 = 0.0690
R indices (all data)	R1 = 0.0376, wR2 = 0.0702
Extinction coefficient	n/a
Largest diff. peak and hole	0.373 and -0.279 $e.Å^{-3}$

Table II-2 Bond lengths [Å] and angles [°] for SCyDNIC. Symmetry transformations used to generate equivalent atoms: #1 -x+1,-y+1,-z+1

Selected Bond	Bond length
Fe(1)-S(1)	2.2493(10)
Fe(1)-S(1)#1	2.2537(10)
Fe(1)-N(1)	1.654(3)
Fe(1)-N(2)	1.655(3)
S(1)-C(1)	1.840(3)
S(1)-C(1A)	1.840(3)
O(1)-N(1)	1.165(4)
O(2)-N(2)	1.161(3)
C(1)-H(1)	1.0000
C(1)-C(2)	1.522(7)
C(1)-C(6)	1.537(6)
C(2)-H(2A)	0.9900
C(2)-H(2B)	0.9900
C(2)-C(3)	1.499(8)
C(3)-H(3A)	0.9900
C(3)-H(3B)	0.9900
C(3)-C(4)	1.519(10)
C(4)-H(4A)	0.9900
C(4)-H(4B)	0.9900
C(4)-C(5)	1.507(11)
C(5)-H(5A)	0.9900
C(5)-H(5B)	0.9900
C(5)-C(6)	1.499(8)
C(6)-H(6A)	0.9900
C(6)-H(6B)	0.9900
C(1A)-H(1A)	1.0000
C(1A)-C(2A)	1.521(6)
C(1A)-C(6A)	1.537(6)
C(2A)-H(2AA)	0.9900

C(2A)-H(2AB)	0.9900
C(2A)-C(3A)	1.499(8)
C(3A)-H(3AA)	0.9900
C(3A)-H(3AB)	0.9900
C(3A)-C(4A)	1.520(10)
C(4A)-H(4AA)	0.9900
C(4A)-H(4AB)	0.9900
C(4A)-C(5A)	1.507(11)
C(5A)-H(5AA)	0.9900
C(5A)-H(5AB)	0.9900
C(5A)-C(6A)	1.499(8)
C(6A)-H(6AA)	0.9900
C(6A)-H(6AB)	0.9900
Selected Bonds	Bond angle
S(1)-Fe(1)-S(1)#1	106.21(3)
N(1)-Fe(1)-S(1)	106.66(10)
N(1)-Fe(1)-S(1)#1	109.59(12)
N(1)-Fe(1)-N(2)	117.79(13)
N(2)-Fe(1)-S(1)	109.35(12)
N(2)-Fe(1)-S(1)#1	106.69(10)
Fe(1)-S(1)-Fe(1)#1	73.79(3)
C(1)-S(1)-Fe(1)#1	109.67(11)
C(1)-S(1)-Fe(1)	109.57(11)
C(1A)-S(1)-Fe(1)	109.57(11)
S(1)-C(1)-H(1)	109.8
C(2)-C(1)-S(1)	108.3(8)
C(2)-C(1)-H(1)	109.8
C(2)-C(1)-C(6)	109.0(10)
C(6)-C(1)-S(1)	110.2(7)
C(6)-C(1)-H(1)	109.8

C(1)-C(2)-H(2A)	109.0
C(1)-C(2)-H(2B)	109.0
H(2A)-C(2)-H(2B)	107.8
C(3)-C(2)-C(1)	113.0(14)
C(3)-C(2)-H(2A)	109.0
C(3)-C(2)-H(2B)	109.0
C(2)-C(3)-H(3A)	109.5
C(2)-C(3)-H(3B)	109.5
C(2)-C(3)-C(4)	110.8(15)
H(3A)-C(3)-H(3B)	108.1
C(4)-C(3)-H(3A)	109.5
C(4)-C(3)-H(3B)	109.5
C(3)-C(4)-H(4A)	109.6
C(3)-C(4)-H(4B)	109.6
H(4A)-C(4)-H(4B)	108.2
C(5)-C(4)-C(3)	110.1(15)
C(5)-C(4)-H(4A)	109.6
C(5)-C(4)-H(4B)	109.6
C(4)-C(5)-H(5A)	109.4
C(4)-C(5)-H(5B)	109.4
H(5A)-C(5)-H(5B)	108.0
C(6)-C(5)-C(4)	111.0(14)
C(6)-C(5)-H(5A)	109.4
C(6)-C(5)-H(5B)	109.4
C(1)-C(6)-H(6A)	109.6
C(1)-C(6)-H(6B)	109.6
C(5)-C(6)-C(1)	110.4(12)
C(5)-C(6)-H(6A)	109.6
C(5)-C(6)-H(6B)	109.6
H(6A)-C(6)-H(6B)	108.1
O(1)-N(1)-Fe(1)	170.5(3)
O(2)-N(2)-Fe(1)	170.3(3)

S(1)-C(1A)-H(1A)	109.2
C(2A)-C(1A)-S(1)	109.4(6)
C(2A)-C(1A)-H(1A)	109.2
C(2A)-C(1A)-C(6A)	112.3(7)
C(6A)-C(1A)-S(1)	107.4(5)
C(6A)-C(1A)-H(1A)	109.2
C(1A)-C(2A)-H(2AA)	109.5
C(1A)-C(2A)-H(2AB)	109.5
H(2AA)-C(2A)-H(2AB)	108.1
C(3A)-C(2A)-C(1A)	110.6(8)
C(3A)-C(2A)-H(2AA)	109.5
C(3A)-C(2A)-H(2AB)	109.5
C(2A)-C(3A)-H(3AA)	109.8
C(2A)-C(3A)-H(3AB)	109.8
C(2A)-C(3A)-C(4A)	109.5(10)
H(3AA)-C(3A)-H(3AB)	108.2
C(4A)-C(3A)-H(3AA)	109.8
C(4A)-C(3A)-H(3AB)	109.8
C(3A)-C(4A)-H(4AA)	109.4
C(3A)-C(4A)-H(4AB)	109.4
H(4AA)-C(4A)-H(4AB)	108.0
C(5A)-C(4A)-C(3A)	111.1(10)
C(5A)-C(4A)-H(4AA)	109.4
C(5A)-C(4A)-H(4AB)	109.4
C(4A)-C(5A)-H(5AA)	109.3
C(4A)-C(5A)-H(5AB)	109.3
H(5AA)-C(5A)-H(5AB)	107.9
C(6A)-C(5A)-C(4A)	111.8(11)
C(6A)-C(5A)-H(5AA)	109.3
C(6A)-C(5A)-H(5AB)	109.3
C(1A)-C(6A)-H(6AA)	109.6
C(1A)-C(6A)-H(6AB)	109.6

C(5A)-C(6A)-C(1A)	110.4(9)
C(5A)-C(6A)-H(6AA)	109.6
C(5A)-C(6A)-H(6AB)	109.6
H(6AA)-C(6A)-H(6AB)	108.1

II.5 References

(1) Pulukkody, R.; Chupik, R. B.; Montalvo, S. K.; Khan, S.; Bhuvanesh, N.; Lim, S.-M.; Darensbourg, M. Y. Toward Biocompatible Dinitrosyl Iron Complexes: Sugar-Appended Thiolates. *Chem. Commun.* **2017**, *53*, 1180–1183.

(2) Elsabahy, M.; Samarajeewa, S.; Raymond, J. E.; Clark, C.; Wooley, K. L., Shell-crosslinked Knedel-like Nanoparticles Induce Lower Immunotoxicity than their Non-crosslinked Analogs. *J. Mater. Chem. B Mater. Biol. Med.* **2013,** *1* (39)

(3) APEX3 "Program for Data Collection on Area Detectors" BRUKER AXS Inc., 5465 East Cheryl Parkway, Madison, WI 53711-5373 USA

(4) Sheldrick, G.M. (2008). *Acta Cryst*. A64, 112-122. Sheldrick, G. M. (2015), *Acta Cryst*. A71, 3-8. Sheldrick, G. M. (2015). *Acta Cryst*. C71, 3-8. XT, XS, BRUKER AXS Inc., 5465 East Cheryl Parkway, Madison, WI 53711-5373 USA.

(5) Spek, A. L., PLATON - A Multipurpose Crystallographic Tool. *J. Appl. Cryst.* **2003**, *36*, 7-13.

(6) Dolomanov, O. V, Bourhis, L. J., Gildea, R. J., Howard, J. A. K., and Puschmann, H. OLEX2: A Complete Structure Solution, Refinement and Analysis Program, *J. Appl. Cryst.* **2009**, *42*, 339-341.

(7) RCSB PDB - 6W63: Structure of COVID-19 main protease bound to potent broad-spectrum non-covalent inhibitor X77 https://www.rcsb.org/structure/6W63 (accessed May 13, 2021).

(8) Cesareo, E.; Parker, L. J.; Pedersen, J. Z.; Nuccetelli, M.; Mazzetti, A. P.; Pastore, A.; Federici, G.; Caccuri, A. M.; Ricci, G.; Adams, J. J.; et al. Nitrosylation of Human Glutathione Transferase P1-1 with Dinitrosyl Diglutathionyl Iron Complex in Vitro and in Vivo. *J. Biol. Chem.* **2005**, *280* (51), 42172–42180.

CHAPTER III : TOWARDS THE OPTIMIZATION OF DINITROSYL IRON COMPLEXES AS THERAPEUTICS FOR SMOOTH MUSCLE CELLS[†]

III.1 Introduction

Nitric oxide has achieved celebrity status in the last decades for its myriad functions, such as gaseous signaling in mammalian, plant, and bacterial cells that control such things as blood vessel dilation, muscle relaxation, nervous system function, immune response, memory, cell signaling, and post translational modification of proteins.[1-2] Nitric oxide is clearly of importance to physiological/biological chemistry, but it is also a well-studied ligand in coordination chemistry due to its multiple accessible redox levels and its ability to participate in d_{π}-π^* bonding. To account for this delocalization, a notation was created that enumerates the total number, n, of electrons within the d_{π}-π^* manifold: $\{M(NO)_x\}^n$ where x is the number of nitrosyl ligands.[3] The functions of nitric oxide in an organism are largely dependent on its concentration. In the pM to nM range, NO has therapeutic effects, such as smooth muscle relaxation, wound healing, nervous system signaling, and proliferation of certain cell types. However, at μM levels, NO can trigger apoptosis, damage DNA, indiscriminately nitrosylate protein thiols, and generate reactive oxygen and nitrogen species (ROS and RNS, respectively).[4]

[†] Text and Figures reprinted with permission from Pectol, D.; Khan, S.; Chupik, R.; Elsabahy, M.; Wooley, K.; Darensbourg, M.; Lim, S.-M. Toward the Optimization of Dinitrosyl Iron Complexes as Therapeutics for Smooth Muscle Cells. *Mol. Pharm*. **2019**, *16* (7), 3178–3187.

The main cellular targets for nitric oxide are cysteine, thiols, tyrosine, oxygen, Fe-S clusters, and metal hemes.[5-7] Endogenously generated NO arises from three enzymes: endothelial nitric oxide synthase (eNOS) is the primary source of NO for smooth muscle cells; inducible NOS (iNOS) is involved in immune response; and neuronal NOS (nNOS) is used for nervous system signaling. All forms of NOS generate NO from L-arginine and oxygen in an NAD(P)H-dependent process.[8-9] Hence, efforts to study the effect of exogeneous NO are to be approached with caution as concomitant changes in endogenous production in response to the treatment can render interpretation of the results ambiguous.

Nitric oxide is a ubiquitous signaling molecule, with the main target of NO produced from eNOS being soluble guanylate cyclase (sGC).[5] sGC is an Fe-heme containing protein that catalyzes the formation of 3',5'-cyclic guanosine monophosphate (cGMP) from guanosine triphosphate (GTP), which is initiated by NO in smooth muscle cells.[7] The resultant cascade of events ultimately causes smooth muscle relaxation. Nitric oxide is not directly delivered to the smooth muscle cells but diffuses from the endothelial cells to the smooth muscle cells in response to shear stress. Therefore, finding new therapeutics that can deliver a controlled amount of NO would be useful for treating ailments, such as hypertension, asthma, erectile dysfunction, diabetes, or other disorders linked to improper function of vasculature.[10]

Nitric oxide release molecules (NORMs) are one method of treating these disorders. Organic-based small molecule NORMs, including NONOates and S-nitrosothiols are challenged by short half-lives ($t_{1/2}$) of NO release (on the order of minutes

for SNAP,[11] DEANO[12] and similar derivatives) and temperature/light sensitivity (*S*-nitrosoglutathioine, GSNO, must be stored in the dark at -80ºC). The incorporation of NONOates into larger macrocycles has been shown to abrogate such shortcomings of organic NORMs.[13] Metal-based NORMs exist and have been used as emergency treatments for rapid induction of hypotension, but the most widely used complex, sodium nitroprusside ($Na_2[Fe(NO)(CN)_5]$), has hazardous side effects, namely cyanide poisoning.[14]

The interplay between iron and nitric oxide in biology is extensive, including the Fe(NO)-heme and the lesser known dinitrosyl iron complexes (DNICs). The DNICs were first observed in 1964-5, in tissues isolated from rats that had been under oxidative stress. A characteristic EPR signal at *g*-value 2.03 would later be identified as a monomeric $\{Fe(NO)_2\}^9$ DNIC with the formula $[(RS)_2Fe(NO)_2]^-$, where SR^- = cysteine/glutathione.[15-17] The chemical composition of an EPR-silent type of DNIC is a dimer of $\{Fe(NO)_2\}^9$ DNIUs with bridging thiolates (Roussin's Red Ester - RRE)[18] which are spin coupled to achieve diamagnetism. Another well-known derivative is Roussin's Black Salt - RBS[19] existing in the form of Fe_4S_3 clusters that contain three DNIUs and one mononitrosyl iron unit (MNIU) all bridged by sulfides. The connection between such chemical and biological dinitrosyl compositions has been bridged by Cowan *et al.* and Ding *et al*. who demonstrated that the NO reacts with Fe_xS_x clusters to produce protein-bound DNICs that are transformed back into Fe_xS_x clusters with the aid of cysteine desulfurase,[20-21] which has been corroborated by chemical experiments.[22] An extensive and recent review of the

history and application of DNICs to biological systems has been assembled by W-F. Liaw and co-workers.[23] As DNICs are expected to be NO storage and transfer agents in biology,[24] the question we chose to address is whether synthetic analogues could serve as an exogenous, long-lasting source of NO.

In fact, DNICs are postulated to be the "working form" of nitric oxide within the cell.[24-27] Chemically, the DNIC can act as a donor of NO^+, NO and NO^-,[28] and S-nitrosate protein thiols in anaerobic and aerobic environments.[29-31] The enhanced stability that the iron imparts to the reactive nitrosyl, and its versatility as a NO donor, might allow for phenotypes that were not available for organic based NO-donors or such FDA-approved drugs like Adempas[32] emulate the release of nitric oxide by increasing sGC activity.

Related to our specific choice of ligands in the DNICs of Figure III-1 is a report that water-soluble $\{Fe(NO)_2\}^9$ DNICs and RRE-type complexes interact with endothelial cells, HSP70[33], decrease tumor size in an *in vivo* rat study,[34] and extend the lifespan of *c. elegans*.[35] Extensive *in vivo* work has shown that glutathionyl DNICs reduce pain in rats,[36-37] as well as influence platelet aggregation and red blood cell levels.[38] Efforts have also been made to synthesize a photo-activated NORM using a DNIC.[39] It has also been reported that DNICs can chemically interact with biological analogues of cysteine, Rieske type iron-sulfur clusters, and tyrosine.[40-41] In fact, the only x-ray structure of a protein-containing DNIC was obtained from a loading of synthetic glutathione-based RRE-DNIC into glutathione transferase.[42]

In earlier work, we demonstrated that DNICs containing sugar-appended thiolates increased total nitrite concentration the cellular media in the presence and absence of endothelial cells, and that SGluRRE provided a sustained source of released nitrite into media over 24 h. The NHC-based complexes and neoDNIC decomposed quickly in an aerobic, aqueous environment.[43] Despite the significance of the effect of NO on SMCs *vide supra*, DNIC pro-drug investigations have relied on endothelial cells.

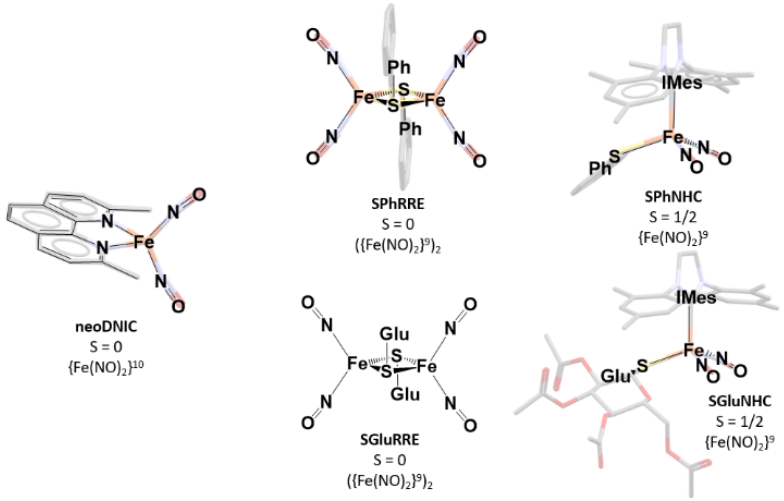

Figure III-1. Chemical representations of the DNICs used in this and previous studies.[43] SGlu = 1-thio-β-D-glucose tetraacetate; SPh = thiophenol; IMes = 1,3-bis(2,4,6-trimethylphenyl)imidazolidene. S is the total electronic spin on the complex. The two S = ½ $\{Fe(NO)_2\}^9$ DNIUs in the RRE DNICs are antiferromagnetically coupled.

The array of five DNICs used in this *in vitro* SMC study is shown in Figure III-1. With them, we explore whether NO will be released from its carrier molecule and delivered into the cytosol of smooth muscle cells. We probe the coordination environment and oxidation state by contrasting the NHC-based complexes, monomeric $\{Fe(NO)_2\}^9$

species with the reduced $\{Fe(NO)_2\}^{10}$ neoDNIC. The enhanced stability of the dimeric complexes, based on μ-SPh and μ-SGlu, offer opportunity to contrast the effect of dinuclearity on NO release; however, dimer splitting by *in situ* cellular compounds may alter such expectations.[43] Finally, contrast of the effect of RS^- hydrophilicity is possible for both NHC and RRE based DNICs. The goal of this research is to study of the biological effects of DNICs on smooth muscle and RAW 264.7 cells, and gain a fundamental understanding of the chemical properties of these DNICs that will ultimately lead to effective delivery of NO to the therapeutic target of NO release.

III.2 Total nitrite detected using the Griess Assay in presence and absence of SMCs:

In vitro detection of formation of nitrite in the cellular media was achieved using the Griess assay, a colorimetric detection of an azo-dye that is only formed in the presence of nitrite. It is established that NO, in the presence of oxygen and water converts into NO_2^-,[45] but it is also possible that a NO^+ ion is hydrolyzed from the DNIC to form nitrite.[25] An assay was designed to compare the amount of dye formed in the presence and absence of SMCs. Figure III-2 displays the concentration of nitrite detected in the media following incubation of the DNIC at different time periods (2, 24 and 48 h). The amount of nitrite detected from the monomeric NHC DNICs remained constant throughout the time course of the experiment, and there was no difference in the nitrite detected in the presence and absence of SMCs which is consistent with our findings in the endothelial cell study.[43]

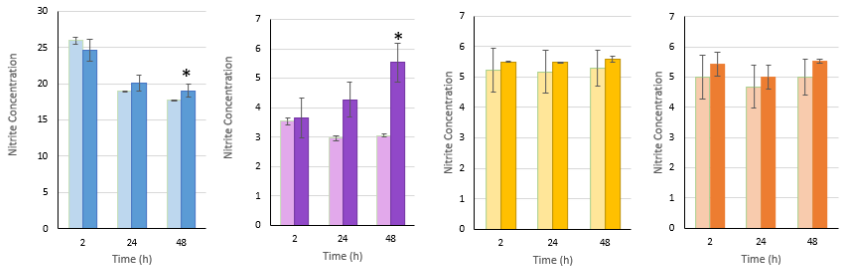

Time (h)	SPhRRE [NO_2^-] w/ SMC	SPhRRE [NO_2^-] no SMC	SGluRRE [NO_2^-] w/ SMC	SGluRRE [NO_2^-] no SMC	SPhNHC [NO_2^-] w/ SMC	SPhNHC [NO_2^-] no SMC	SGluNHC [NO_2^-] w/ SMC	SGluNHC [NO_2^-] no SMC
2	25.9(5)	24(1)	3.5(1)	3.6(7)	5.2(5)	5.50(2)	5.0(7)	5.4(4)
24	18.9(1)	20(1)	2.96(7)	4.2(6)	5.2(5)	5.48(1)	4.7(7)	5.0(4)
48	17.7(1)	19(1)	3.05(4)	5.5(6)	5.3(4)	5.6(1)	5.0(6)	5.5(1)

Figure III-2: Griess assay results for four DNICs used in this study. The y-axis is the concentration of nitrite (μM) detected in the media. The DNIC concentrations for each trial are 30 μM. In this figure and throughout the manuscript: (SPhRRE = blue, SGluRRE = purple, SPhNHC = yellow, SGluNHC = orange) The absorbance was recorded at three separate time points (2, 24 and 48 h) for two separate treatment conditions (without SMCs – dark, with SMCs – light). The same plate was used for the duration of the study. Numbers in parenthesis indicated standard deviation from n = 3 trials. Asterisk indicates $p < 0.05$ when comparing the concentration of nitrite detected in the presence and absence of cells at that time point and concentration.

In contrast, the RRE DNICs showed a significant increase ($p < 0.05$) in the amount of nitrite detected in the absence of cells after 24 h (SPhRRE) or 48 h (SGluRRE). Besides the statistically higher amount of nitrite detected without cells, each dimer showed a different release profile to the SMCs. SGluRRE exhibited a steady increase in the concentration of nitrite detected in the absence of cells, but in the presence of cells, the amount of nitrite detected remained constant. The other dimeric complex SPhRRE, did not show the same increase in nitrite concentration over time, but in the absence of SMCs the [NO_2^-] was higher than in the presence of SMCs. This study provides information about the amount of nitrite present in the extracellular environment upon treatment with

DNICs but provides no information regarding NO transfer into the cells. From these data, we can conclude that the DNICs result in nitrite detection in the extracellular environment, and that the presence of SMCs causes a decrease in the amount of nitrite detected for the RRE DNICs.

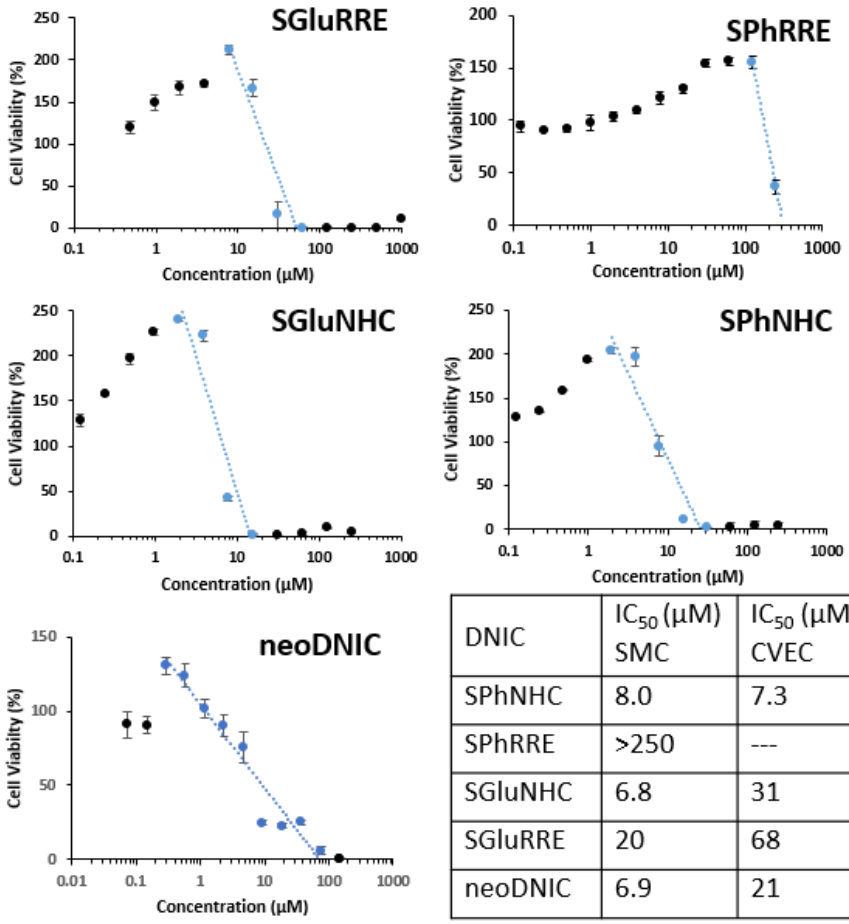

DNIC	IC_{50} (μM) SMC	IC_{50} (μM) CVEC
SPhNHC	8.0	7.3
SPhRRE	>250	---
SGluNHC	6.8	31
SGluRRE	20	68
neoDNIC	6.9	21

Figure III-3 Results of viability assay for SMCs treated with DNICs. Trials shown are representative of three independent trials. IC_{50} values in the table are calculated based on the plots shown in this figure. The trendlines were used to calculate the IC_{50}. Values from previous study with coronary venular endothelial cells (CVEC) are compared.[43]

III.3 Effect of the DNIC treatments on cell viability

In the next set of experiments, we investigated which features of the DNICs had the greatest effect on the viability of SMCs. The viability was determined colorimetrically by observing the presence of a formazan dye which is reduced from a tetrazole in the MTS assay by mitochondrial reductases. Unexpectedly, the DNICs and/or their by-products resulted in significant increases in viabilities at relatively low concentrations. Therefore, the experiments were conducted in triplicate for three separate runs for each DNIC. The viability curves shown in Figure III-5 are representative of three independent trials, the only exception being SPhRRE (see Figure III-4). To account for the apparent systematic increases in viabilities, the IC_{50} values were calculated from fitting logarithmic trendlines through the linear effect ranges with the IC_{50} concentrations being calculated at half of the maximum observed viabilities.

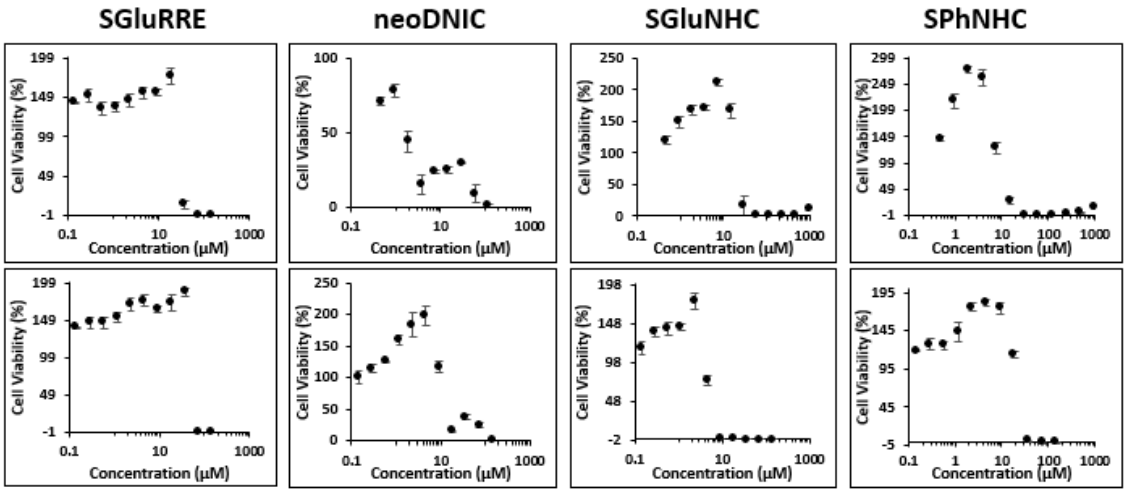

Figure III-4 MTS viability assay curves for SMC grown to 20k/well treated with DNIC's at varying concentrations. Each trial is a set of biological triplicate**s.**

The monomeric DNICs (neoDNIC, SGluNHC, SPhNHC) have similar IC_{50}'s regardless of coordination environment, thiol functionality, or oxidation state of the DNIC source. The higher IC_{50} values of the dimeric DNICs as compared to the monomeric DNICs is attributed to the stability of the dimeric DNIU in solution compared to the monomeric counterparts. The single outstanding difference was thiol functionality on the RREs. By changing the thiol identity from thiophenol to thioglucose the IC_{50} decreased approximately ten-fold from >250 μM (SPhRRE) to 20 μM (SGluRRE). It is notable that the IC_{50} values from the CVEC study[43] are generally higher

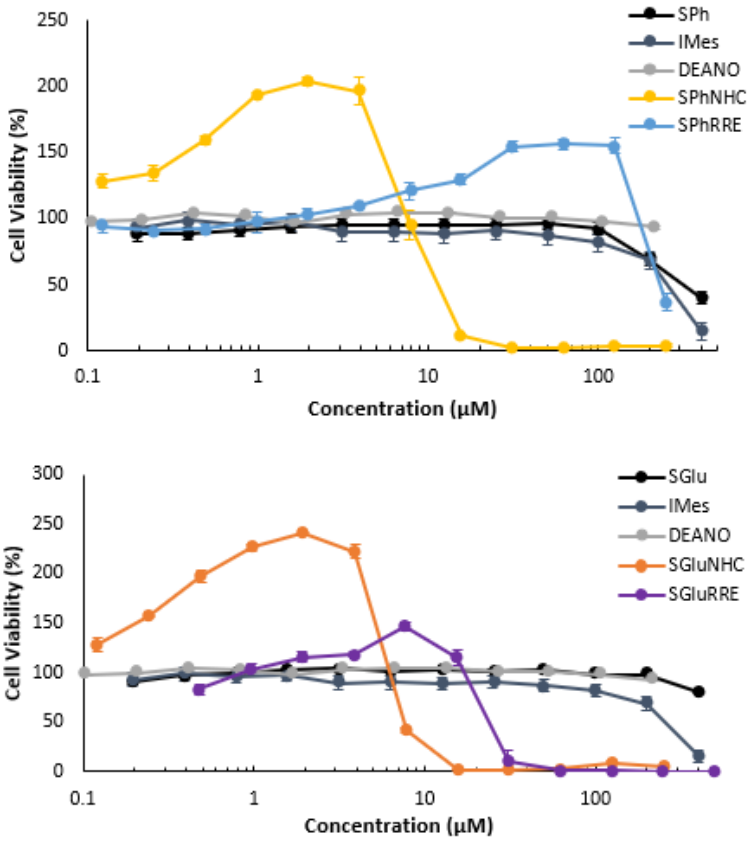

Figure III-5 Overlaid results of the viability assay for SMC treated with DNICs and their decomposition products. The thio-glucose containing DNICs are in the top panel, and the thiophenol DNICs are on the bottom. IMes, SGlu and SPh are the ligands used to synthesize the DNICs as shown in Fig. 1

compared to the SMCs study, with the sole exception being SPhNHC. A supposition is that since the endothelial cells generate NO from eNOS, they are more resistant to RNS when compared to SMCs, which are the ultimate therapeutic target of the endothelial cell-generated NO. It was established that the observed increase and decrease in viability was due to the DNIC and not its major decomposition products (Figure III-5). The carbene and the thiols relevant to the DNIC, and DEANO, the positive control for NO release, are

overlaid with the DNIC viability curves. Those decomposition products do not result in an increase in viability of the cells; in fact they become toxic to the SMC at higher concentrations (~500 μM). In contrast, all of the DNIC treatments exhibit an increase in viability followed by a stark, concomitant decrease. While the mechanism by which these DNICs increase cell viability is undetermined, we can say that in SMCs the DNIU is responsible for the observed increase in mitochondrial reductase activity.

III.4 Investigations of the effect of DNICs on immune system activity

The use of DNICs as drugs requires an understanding of how they affect the viability of individual cells, and in addition, how the DNICs might stimulate the immune system towards action. Cytokines are known to be involved with communication between different actors in the immune system. Measurement of the expression of various cytokines[46] is usually utilized to demonstrate the ability of biomaterials to interact with the immune system, either *in vitro* or *in vivo*.[44, 47-50] For example, a number of the interleukin cytokines could be responsible for recruiting macrophages, starting an inflammatory response, or activating T-cells towards action.[51] Recently, an immunotoxicity index was developed to facilitate interpretation of the expression of cytokines from biological systems.[52] After measurement of cytokines for different treatments, overexpression of cytokines was compared to the control untreated group ($p < 0.05$). Values exceeding 1 (*i.e.*, higher than the control) are summed and used as numerical theoretical values for evaluating the immunotoxicity of the tested materials (*i.e.,* the higher the index value, the higher the predicted immunotoxicity). It is worth mentioning that the

concentration of DNIC at which the immunotoxicity index is calculated must be provided because the index value depends on the concentration of the tested materials. The concentration used for these immunotoxicity assays was determined using the IC_{50}'s for the array of DNIC complexes on RAW 264.7 cells (Figure III-6). Also, the duration of the treatment must be fixed. In this particular study, there was no need to evaluate the potential adsorption of the measured cytokines onto the tested materials because the materials tested here are small molecules rather than particles, which are unlikely to result in significant adsorption of the measured cytokines.[53-54]

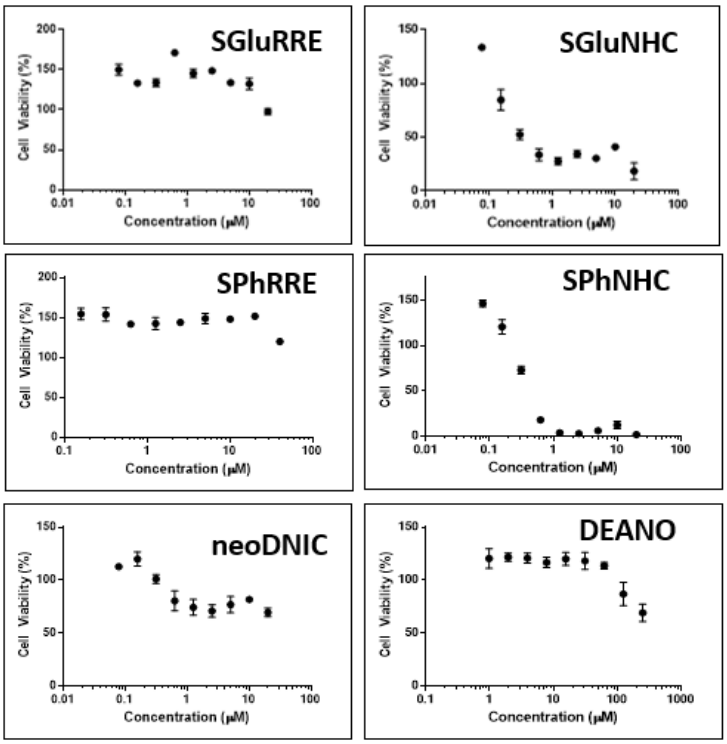

DNIC/NO source	IC_{50} (μM) RAW 264.7
SPhNHC	0.29
SPhRRE	>250
SGluNHC	0.12
SGluRRE	210
neoDNIC	0.37
DEANO	110

Figure III-6 MTS viability assay curves for RAW 264.7 cells grown to 20k/well treated with DNIC's at varying concentrations. Each trial is a set of biological triplicates. The table on the right contains the IC_{50} data for the corresponding graphs on the left.

From the viability curves (Figure III-6), it was determined that the monomeric DNICs (neoDNIC, SGlu/SPhNHC) were highly toxic to macrophages, with IC_{50}'s in the high nanomolar range (Table 1). On the other hand, the dimeric DNICs SGlu/SPhRRE were less toxic, with IC_{50}'s in the high micromolar range. In contrast to the behavior of SMCs treated with DNICs, the macrophages did not exhibit an increase in viability upon DNIC treatment.

No detectable amounts of endotoxins were identified in the DNIC samples (data not shown). The DEANO, neoDNIC, SGluNHC, SGluRRE, SPhNHC and SPhRRE had immunotoxicity indices of 2.5, 0, 0, 12.6, 0 and 7.7, respectively, at concentration of 5 μM (Figure III-7). Based on previous testing of various drugs and polymeric materials, an immunotoxicity index below 15 is considered to have minimal immunotoxicity, from 15-45 is moderate, and above 45 would be considered severe. Out of the 23 measured cytokines, slight induction was observed only for RANTES (T-cell recruitment) and TNF-α (apoptosis signal) after treatment with SGluRRE and SPhRRE (Figure III-7), whereas no cytokines were significantly induced after treatment with neoDNIC, SGluNHC and SPhNHC. Based on previously published data and other tested materials, these complexes at the tested concentrations are considered to have minimal immunotoxicity.[44, 47-50] It is worth mentioning that the low IC_{50} measured in RAW 264.5 macrophages following treatment with the neoDNIC, SGluNHC and SPhNHC, might have contributed to the observed decease in the production of the cytokines, as compared to the control untreated cells. Based on preliminary experiments, concentration of 5 μM was the minimal

concentration that can be utilized to observe an increase in cytokines release in response to the treatment with the complexes, as compared to the control untreated cells. Values in Figure III-7 are presented as mean ± SD of three replicates. Significant differences between two groups were evaluated by Student's t test (unpaired) or between more than two groups by one-way ANOVA followed by Tukey's multiple comparison tests. Differences between different groups were considered significant for *p* values less than 0.05.

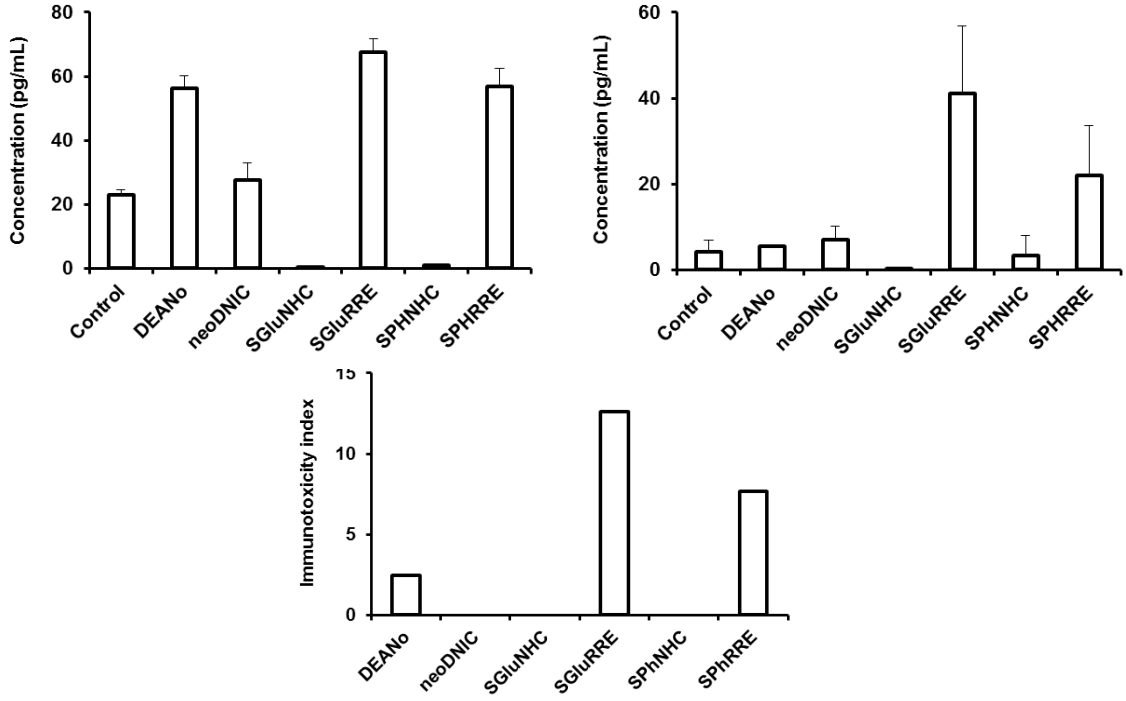

Figure III-7 The expression of the mouse cytokines, regulated upon activation normal T-cell expressed and presumably secreted (RANTES) (A) and tumor necrosis factor-α (TNF-α) (B), following the treatment of RAW 264.7 cells with media (control), DEANO, neoDNIC, SGluNHC, SGluRRE, SPhNHC and SPhRRE at 5 μM for 24 h. All cytokines tested besides TNF-α and RANTES did not show any induction of cytokines. (C) Calculated immunotoxicity index for the induction of mouse cytokines IL-1α, IL-1β, IL-2, IL-3, IL-4, IL-5, IL-6, IL-9, IL-10, IL-12 (P40), IL-12 (P70), IL-13, IL-17, eotaxin, G-CSF, GM-CSF, IFN-γ, KC, MCP-1, MIP-1α, MIP-1β, RANTES, and TNF-α following the treatment of RAW 264.7 cells with DEANO, neoDNIC, SGluNHC, SGluRRE, SPhNHC and SPhRRE

III.5 Fluorometric methodology and analysis of intracellular nitric oxide

a) Confocal Microscopy

The OxiSelect™ Nitric Oxide probe was used to examine the hypothesis that the difference in observed nitrite in presence *vs*. in the absence of SMCs from the Griess assay might be due to some loss of the nitric oxide payload *via* delivery and ultimately consumption inside the cells. The DNICs that exhibited a statistically significant increase

(SGluRRE, SPhRRE) in nitrite detected in the absence of cells would be expected to show an increase in intracellular NO concentration. None of the compounds absorbed or emitted in such a way that would interfere with the fluorescence measurements. In order to better visualize the intracellular NO probe, the SMCs in Figure III-8 were pretreated with NOS inhibitor L-NNA. The resulting fluorometric images show the holistic differences between SMC populations treated with NO probe and DNIC for 2 h (Figure S4). The most obvious difference was observed for the neoDNIC, where after treatment, there was a visible increase in intensity with the cells being marked by bright green puncta. The monomeric NHC DNICs and the SPhRRE did not show a difference that could be detected without the aid of further quantification (Figure III-8). There were some brighter patches of green fluorescence visible in the confocal images of SMCs treated with SGluRRE. In order to properly quantify the amount of fluorescence, the needed normalization factors for the total number of cells were obtained from fluorometric assay, as described below.

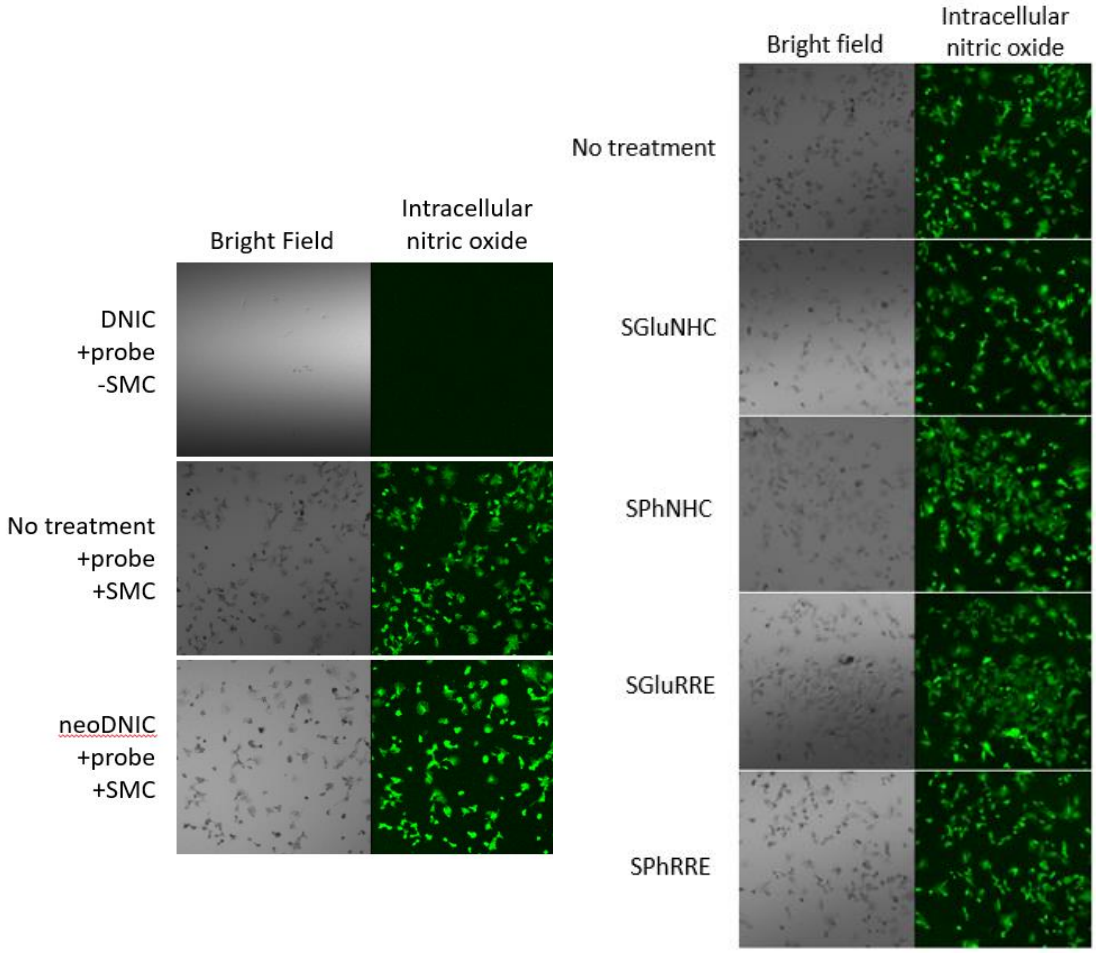

Figure III-8: Confocal microscopy images collected with a 10x objective (image size 1.3 µm × 1.3 µm). The brighter the green fluorescence, the more nitric oxide present. Concentrations of DNIC are as follows. 30 µM: SPhRRE, SGluRRE; 3 µM: SPhNHC, SGluNHC. To aid in visualization, 100 µM L-NNA (L-nitroarginine), an NOS inhibitor, was added to each well. No treatment indicates that only L-NNA was present and no DNIC treatments were added.

.

b) Quantification of intracellular NO from fluorometric assay

Figure II-1 represents the method adopted for detection and quantification of intracellular nitric oxide. Normally for such assays, a cell counting step is incorporated at

the end of the experiment; however, since these fluorescence assays take place in an opaque, black-bottomed 96-well plate, the normal colorimetric spectroscopic methods cannot be implemented. Hence, in order to quantify the total cell population in these conditions, a nuclear stain for live cells with an excitation and emission well beyond the range of the green fluorescent probe was used (NucRed647). By dividing the total green fluorescence (amount of intracellular NO detected by the probe) by the red fluorescence (number of nuclei present in each sample well) the average intracellular NO per individual cell was obtained.. This approach does not determine whether the DNIC enters the cytosol, but it does provide a definitive conclusion about the released NO. It has been established that DNICs can liberate $[NO]^+$, NO, or $[NO]^-$ depending on the identity of the ligand that exchanges or displaces the NO on iron. with NO.[28]

By using this normalized total fluorescence, the difference between the fluorescence signal generated by SMCs that received no treatment and those that received DNIC treatment could be determined. Three general methods were applied (Figure III-9A). Co-incubation is described as simultaneous application of the DNIC and NO probe to the SMCs (Figure III-9B and III-9C). For pre-incubation, the DNIC was applied to the SMCs 2, 24 or 48 h before the NO probe was added (Figure III-9D). Lastly, in the NO release profile experiments, NO probe was incubated with SMCs for 2 h, then the DNIC was

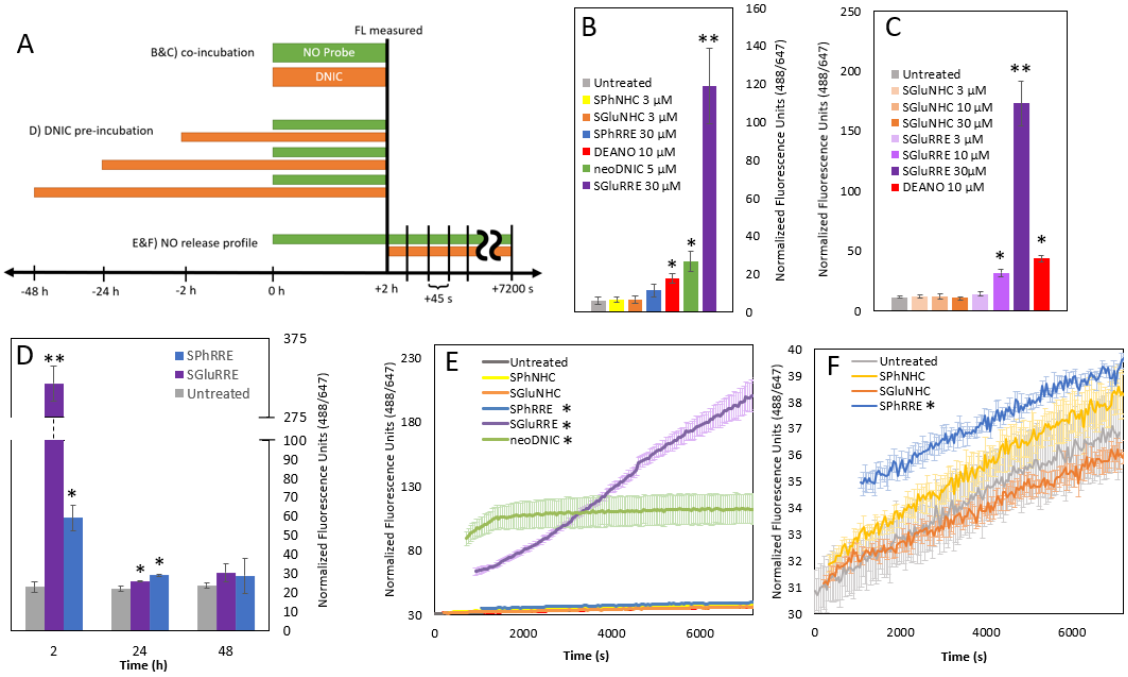

Figure III-9 Fluorometric detection and quantification of intracellular nitric oxide using the OxiSelect™ IntraNO probe. (A) Diagram of difference in incubation timeline for different DNIC treatments. (B & C) Quantification of intracellular NO via co-incubation with 100 µM L-NNA (NOS inhibitor). Cells were incubated with the probe and the DNIC treatment for 2 h at 37 ˚C. Differences in cell population were normalized with NucRed Live stain. (D) Time-dependent fluorescence quantification of DNIC pre-incubation for 2, 24 or 48 h. (E & F) NO release profile of the five DNICs with the same concentrations used in the previous experiment. Time = 0 indicates the time point which SMCs were initially treated with DNIC. Asterisk indicates $p < 0.05$ when comparing the fluorescence values to control. Double asterisk indicates $p < 0.01$.

added to the SMC and fluorescence was measured every 45 s after DNIC treatment (Figure III-9E and III-9F). Ten μM DEANO was used as the positive control for NO release for these experiments. In Figure III-9B, the normalized fluorescence (488 nm/647 nm) was observed after 2 h treatment with the five DNICs in this study.

Based on the results, neither the SGluNHC nor the SPhNHC caused a change in the total intracellular NO. While the method by which these complexes elicit a lethal response in the SMC requires further investigation, we can conclude from these data that the NHC-based DNICs did not deliver their NO payload inside the cell. Based on the Griess assay (Figure III-2) and the data presented in Figure III-9B and III-9C, we posit that either the NHC-based DNICs released/degraded too quickly and did not gain entry into the cytosol even at higher concentrations (Figure III-9C), or the NHC-based complexes, upon entry into the cell, could have generated a nitroso-iron species that was unable to liberate NO. The liberated NO could have diffused from solution,[55] or decomposed in the extracellular matrix, but it did not enter the cell as nitric oxide.

In contrast, the dimeric RRE complexes delivered nitric oxide into the cytosol, and the thiosugar appended SGluRRE imported approximately 6x more NO into the cell after 2 h than did the simple thiophenol-appended SPhRRE (Figure III-9B). The SPhRRE apparently produced an increase in intracellular NO, however it was not statistically significant. With SGluRRE and neoDNIC there were significant increases in the intracellular NO concentration. This import or delivery was also concentration dependent (Figure III-9C). If the SMCs were preincubated with DNIC before treatment with the NO

probe, a statistically significantly higher intracellular NO concentration remained present 24 h after treatment with DNIC. After 48 h, there was no longer a difference between the intracellular NO concentrations (Figure III-9D). SGluRRE produced a higher concentration inside the cell compared to SPhRRE at the 2 h timepoint, but after 24 h, the intracellular NO concentrations from both complexes were similar. The thiosugar moiety on the SGluRRE led to the DNIC treatment releasing more of its NO into the cytosol. It is expected that the sugar group caused the DNIC to be actively transported into the cell, a supposition that is supported by the drastic increase of intracellular NO at 2 h. Observing the NO release profiles of

the five tested DNICs shows definitively that SGlu/SPhNHC do not release NO into the cytosol, and SPhRRE treatment causes a small increase in the intracellular NO (Figure III-9F). The neoDNIC-treated cells reached their maximum at 1500 s , further reinforcing that it delivers its NO rapidly. On the other hand, SGluRRE provided a sustained release of NO over the 2-hour observation period (Figure III-9E).

Table III-1 - Summary of the structure/function relationships of the five DNIC complexes. Highlighted columns represent DNIC-based therapeutics of greatest promise.

	SGluRRE	SGluNHC	SPhRRE	SPhNHC	neoDNIC
Redox level of DNIC source	$\{Fe(NO)_2\}^9$	$\{Fe(NO)_2\}^9$	$\{Fe(NO)_2\}^9$	$\{Fe(NO)_2\}^9$	$\{Fe(NO)_2\}^{10}$
Nuclearity	Dimer	Monomer	Dimer	Monomer	Monomer
Thiol identity	Glucose	Glucose	Phenyl	Phenyl	N/A
SMC IC_{50} (μM)	20	6.8	>250	7.3	6.9
RAW 264.7 IC_{50} (μM)	210	0.12	>250	0.29	0.37
NO into cytosol	Yes	No	Yes	No	Yes
Immunotoxicity index	Minimal (12.6)	None (0)	Minimal (7.7)	None (0)	None (0)

III.6 Comments and Conclusion

From this study, we conclude that both dimeric complexes, SGluRRE and SPhRRE, are more promising pro-drug systems than are the NHC-based monomeric counterparts. Although their ultimate fate is unknown, it is understood that the dimeric complexes provide a source of NO to SMCs that is sustained over 24 h, while exhibiting limited cytotoxicity and generating minimal immunotoxic effects. The thioglucose functionality of SGluRRE gave increased NO delivery to the cytosol vs. SPhRRE, with only minor reduction in IC_{50}. Moreover, SGluRRE induced no cytokine response from RAW 264.7 cells, and the monomeric SGluNHC induced a cytokine response minimally. From this we conclude that there is no artificial stimulation of the immune system for

these complexes (Table III-1). For mononuclear DNICs, the reduced $\{Fe(NO)_2\}^{10}$ source (neoDNIC) is a more effective vehicle for NO delivery in an *in vitro* environment when compared to the oxidized DNIC sources (SGlu/SPhNHC). The Griess Assay determined that the concentration of NO-derived nitrite in the media decreased in the presence of cells, leading to the conclusion that the smooth muscle cells consume the DNICs.

This study offers initial clues into the rational design of small molecule DNICs appropriate for NO delivery. For this series, the stability provided by the multinuclear nature of the RRE DNICs is the determining factor for sustained release of NO. Since the RRE-type complexes are neutral, their *in vitro* reactivity can be modified by altering the substituents on the thiol. Appending more polar groups to the thiol should aid in its water solubility which may be of importance in developing therapeutics. Additionally, lipophilic moieties or compounds known to be actively transported across cell membranes might be added to increase the DNICs cell permeability. Such derivatives await future studies.

What is evident from these experiments is that the dimeric DNICs and neoDNIC are prodrugs for NO release, and these specific NHC-based DNICs are not. The composition of the complex responsible for ultimately releasing the NO (*i.e.* intact RRE dimer, some derivative of the diiron species, or a monomeric DNIC generated *in situ*) has yet to be identified. We continue to develop hypotheses and experiments to probe the nature of the active species.

Although not all of the DNIC derivatives delivered NO into the cytosol, all increased the viability in SMC that was shown to be an NO independent process.

However, the toxicity of the monomeric NHC-based DNICs to macrophages would be a hindrance for their development as proliferative therapeutic agents. In contrast, SGluRRE was shown to be an order of magnitude less toxic to RAW 264.7 when compared to SMC, so it could be used as a proliferative therapeutic without deleterious effects to the immune system. Furthermore, SGluRRE (and maybe other DNICs pending the results of the Immunotoxicity Assay) are not artificially stimulating a cytokine response. From these data, the dimeric RRE-DNIC scaffold seems to be the optimal vehicle for NO release and DNIU-based therapeutics, and the monomeric, reduced DNIU could potentially be developed further as a vehicle for rapid delivery of nitric oxide.

III.7 References

1. Leon, L.; Jeannin, J.-F.; Bettaieb, A., Post-translational Modifications Induced by Nitric Oxide (NO): Implication in Cancer Cells Apoptosis. *Nitric Oxide* **2008,** *19* (2), 77-83.
2. Carpenter, A. W.; Schoenfisch, M. H., Nitric Oxide Release Part II. Therapeutic Applications. *Chem Soc Rev* **2012,** *40* (10), 3742-3752.
3. Enemark, J. H.; Feltham, R. D., Principles of Structure, Bonding, and Reactivity for Metal Nitrosyl Complexes. *Coord Chem Rev* **1974,** *13* (4), 339-406.
4. Mocellin, S.; Bronte, V.; Nitti, D., Nitric Oxide, a Double Edged Sword in Cancer Biology: Searching for Therapeutic Opportunities. *Med Res Rev* **2007,** *27* (3), 317-352.

5. Martin, E.; Berka, V.; Bogatenkova, E.; Murad, F.; Tsai, A.-L., Ligand Selectivity of Soluble Guanylyl Cyclase Effect of the Hydrogen-bonding Tyrosine in the Distal Heme Pocket on Binding of Oxygen, Nitric Oxide, and Carbon Monoxide. *J Biol Chem* **2006,** *281* (38), 27836-27845.

6. Kumar, S.; Singh, R. K.; Bhardwaj, T. R., Therapeutic Role of Nitric Oxide as Emerging Molecule. *Biomed Pharmacother* **2017,** *85*, 182-201.

7. Zhao, Y.; Brandish, P. E.; Ballou, D. P.; Marletta, M. A.; Howard; Walsh, C. T., A Molecular Basis for Nitric Oxide Sensing by Soluble Guanylate Cyclase. *Proc Nat Acad Sci* **1999,** *96* (26), 14753-14758.

8. Bogdan, C., Nitric Oxide Synthase in Innate and Adaptive Immunity: an Update. *Trends Immunol* **2015,** *36* (3).

9. Förstermann, U.; Sessa, W. C., Nitric Oxide Synthases: Regulation and Function. *Eur Heart J* **2012,** *33*, 829-837.

10. Brozovich, F. V.; Nicholson, C. J.; Degen, C. V.; Gao, Y. Z.; Aggarwal, M.; Morgan, K. G., Mechanisms of Vascular Smooth Muscle Contraction and the Bsis for Parmacologic Treatment of Smooth Muscle Disorders. *Pharmacol Rev* **2016,** *68*, 476-532.

11. Mathews, W. R.; Kerr, S. W., Biological Activity of S-nitrosothiols: the Role of Nitric Oxide. *J Pharmacol Exp Ther* **1993,** *267* (3), 1529-1537.

12. Huerta, S.; Chilka, S.; Bonavida, B., Nitric Oxide Donors: Novel Cancer Therapeutics. *Intl J Oncol* **1992,** *33* (5), 909-927.

13. Jin, H.; Yang, L.; Ahonen, M. J. R.; Schoenfisch, M. H., Nitric Oxide-Releasing Cyclodextrins. *J Am Chem Soc* **2018,** *140*, 52-52.

14. Tinker, J. H.; Michenfelder, J. D., Sodium Nitroprusside: Pharmacology, Toxicology and Therapeutics. *Anesthesiology* **1976,** *45* (3), 340-354.

15. Mallard, J. R.; Kent, M., Differences Observed Between Electron Spin Resonance Signals from Surviving Tumour Tissues and from their Corresponding Normal Tissues. *Nature* **1964,** *204*, 1192-1192.

16. Lloveras, J.; Vincensini, P.; Ribbes, G.; Record, M.; Ferre, G.; Douste-Blazy, L.; Pescia, J., Subcellular Localization and Paramagnetic Properties of Signals Observed in Krebs II Ascites Cells by Electron Spin Resonance Spectroscopy. *Radiat Res* **1980,** *82* (1), 45-54.

17. Vithayathil, A. J.; Ternberg, J. L.; Commoner, B. P., Changes in Electron Spin Resonance Signals of Rat Liver During Chemical Carcinogensis. *Nature* **1965,** *207*, 1246-1249.

18. Lu, C.-Y.; Liaw, W.-F., Formation Pathway of Roussin's Red Ester (RRE) via the Reaction of a $\{Fe(NO)_2\}^{10}$ Nitrosyliron Complex (DNIC) and Thiol: Facile Synthetic Route for Synthesizing Cysteine-containing DNIC. *Inorg Chem* **2013,** *52*, 13918-13926.

19. Hamilton-Brehm, S. D.; Schut, G. J.; Adams, M. W. W., Antimicrobial Activity of the Iron-sulfur Nitroso Compound Roussin's Black Salt $[Fe_4S_3(NO)_7]$ on the

Hyperthermophilic Archaeon Pyrococcus Furiosus. *Appl Environ Microbiol* **2009,** *75* (7), 1820-1825.

20. Foster, M. W.; Cowan, J. A., Chemistry of Nitric Oxide with Protein-bound Iron Sulfur Centers. Insights on Physiological Reactivity. *J Am Chem Soc* **1999,** *121* (17), 4093-4100.

21. Rogers, P. A.; Eide, L.; Klungland, A.; Ding, H., Reversible Inactivation of E. coli Endonuclease III via Modification of its [4Fe-4S] Cluster by Nitric Oxide. *DNA Repair* **2003,** *2*, 809-817.

22. Schiewer, C. E.; Muller, C. S.; Dechert, S.; Bergner, M.; Wolny, J. A.; Schunemann, V.; Meyer, F., Effect of Oxidation and Protonation States on [2Fe-2S] Cluster Nitrosylation Giving $\{Fe(NO)2\}^9$ Dinitrosyl Iron Complexes (DNICs). *Inorg Chem* **2018**.

23. Lu, T.-T.; Wang, Y.-M.; Hung, C.-H.; Chiou, S.-J.; Liaw, W.-F., Bioinorganic Chemistry of the Natural $[Fe(NO)_2]$ Motif: Evolution of a Functional Model for NO-related Biomedical Application and Revolutionary Development of a Translational Model. *Inorg Chem* **2018,** *57* (20), 12425-12443.

24. Hickok, J. R.; Sahni, S.; Shen, H.; Arvind, A.; Antoniou, C.; Fung, L. W. M.; Thomas, D. D., Dinitrosyliron Complexes are the Most Abundant Nitric Oxide-Derived Cellular Adduct: Biological Parameters of Assembly and Disappearance. *Free Radic Biol Med* **2011,** *51* (8), 1558-1566.

25. Vanin, A. F., Dinitrosyl Iron Complexes with Thiol-containing Ligands as a "Working Form" of Endogenous Nitric Oxide. *Nitric Oxide* **2016,** *54*, 15-29.

26. Vanin, A. F., Dinitrosyl Iron Complexes with Thiol-containing Ligands as a Base for New-generation Drugs. *Open Conf. Proc. J.* **2013,** *4*, 47-53.

27. Drapier, J.-C.; Pellat, C.; Henry, Y., Generation of EPR-detectable Nitrosyl-iron Complexes in Tumor Target Cells Cocultured with Activated Macrophages. *J. Biol. Chem.* **1991,** *266* (16), 10162-10167.

28. Lu, T. T.; Chen, C. H.; Liaw, W. F., Formation of the Distinct Redox-interrelated Forms of Nitric Oxide from Reaction of Dinitrosyl Iron Complexes (DNICs) and Substitution Ligands. *Chem Eur J* **2010,** *16* (27), 8088-8095.

29. Keszler, A.; Diers, A. R.; Ding, Z.; Hogg, N., Thiolate-based Bidinitrosyl Iron Complexes: Decomposition and Detection and Differentiation from S-nitrosothiols. *Nitric Oxide* **2017,** *65*, 1-9.

30. Bosworth, C. A.; Toledo Jr, J. C.; Zmijewski, J. W.; Li, Q.; Lancaster Jr, J. R., Dinitrosyliron Complexes and the Mechanism(s) of Cellular Protein Nitrosothiol Formation from Nitric Oxide. *Proc. Natl. Acad. Sci.* **2009,** *106*, 4671-4676.

31. Li, Q.; Li, C.; Mahtani, H. K.; Du, J.; Patel, A. R.; Lancaster Jr, J. R., Nitrosothiol Formation and Protection Against Fenton Chemistry by Nitric Oxide-induced Dinitrosyliron Complex Formation from Anoxia-initiated Cellular Chelatable Iron Increase. *J. Biol. Chem.* **2014,** *289* (29), 19917-19927.

32. Frey, R.; Becker, C.; Saleh, S.; Unger, S.; van der Mey, D.; Mück, W., Clinical Pharmacokinetic and Pharmacodynamic Profile of Riociguat. *Clin. Pharmacokinet.* **2018,** *57*, 647-661.

33. Chen, Y.-J.; Ku, W.-C.; Feng, L.-T.; Tsai, M.-L.; Hsieh, C.-H.; Hsu, W.-H.; Liaw, W.-F.; Hung, C.-H.; Chen, Y.-J., Nitric Oxide Physiological Responses and Delivery Mechanisms Probed by Water-soluble Roussin's Red Ester and $\{Fe(NO)_2\}^{10}$ DNIC. *J Am Chem Soc* **2008,** *130*, 10929-10938.

34. Wu, S.-C.; Lu, C.-Y.; Chen, Y.-L.; Lo, F.-C.; Wang, T.-Y.; Chen, Y.-J.; Yuan, S.-S.; Liaw, W.-F.; Wang, Y.-M., Water-soluble Dinitrosyl Iron Complex (DNIC): a Nitric Oxide Vehicle Triggering Cancer Cell Death via Apoptosis. *Inorg Chem* **2016,** *55* (18), 9383-9392.

35. Huang, H.-W.; Lin, Y.-H.; Lin, M.-H.; Huang, Y.-R.; Chou, C.-H.; Hong, H.-C.; Wang, M.-R.; Tseng, Y.-T.; Liao, P.-C.; Chung, M.-C.; Ma, Y.-J.; Wu, S.-C.; Chuang, Y.-J.; Wang, H.-D.; Wang, Y.-M.; Huang, H.-D.; Lu, T.-T.; Liaw, W.-F., Extension of C. elegans Lifespan Using the ·NO-delivery Dinitrosyl Iron Complexes. *J Biol Inorg Chem* **2018,** *23* (3), 775-784.

36. Adamyan, L. V.; Burgova, E. N.; Tkachev, N. A.; Mikoyan, V. D.; Stephanyan, A. A.; Sonova, M. M.; Galkin, A. V.; Vanin, A. F., Dinitrosyl Iron Complexes with Glutathione Largely Relieve Rats of Experimental Endometriosis. *Biophys J* **2013,** *58* (2), 222-227.

37. Burgova, E. N.; Tkachev, N. A.; Adamyan, L. V.; Mikoyan, V. D.; Paklina, O. V.; Stepanyan, A. A.; Vanin, A. F., Dinitrosyl Iron Complexes with Glutathione Suppress Experimental Endometriosis in Rats. *Eur J Pharmacol* **2014,** *727* (1), 140-147.

38. Shamova, E. V.; Bichan, O. D.; Drozd, E. S.; Gorudko, I. V.; Chizhik, S. A.; Shumaev, K. B.; Cherenkevich, S. N.; Vanin, A. F., Regulation of the Functional and Mechanical Properties of Platelet and Red Blood Cells by Nitric Oxide Donors. *Biophys J* **2011,** *56* (2), 237-242.

39. Conrado, C. L.; Wecksler, S.; Egler, C.; Magde, D.; Ford, P. C., Synthesis and Photochemical Properties of a Novel Iron−sulfur−nitrosyl Cluster Derivatized with the Pendant Chromophore Protoporphyrin IX. *Inorg Chem* **2004,** *43*, 5543-5549.

40. Fitzpatrick, J.; Kalyvas, H.; Filipovic, M. R.; Ivanović, I.; Burmazović, B. I.; Macdonald, J. C.; Shearer, J.; Kim, E., Transformation of a Mononitrosyl Iron Complex to a [2Fe-2S] Cluster by a Cysteine Analogue. *J Am Chem Soc* **2014,** *136*, 7229-7232.

41. Giuc Tran, N.; Kalyvas, H.; Skodje, K. M.; Hayashi, T.; Moënne-Loccoz, P.; Callan, P. E.; Shearer, J.; Kirschenbaum, L. J.; Kim, E., Phenol Nitration Induced by a $\{Fe(NO)_2\}^{10}$ Dinitrosyl Iron Complex. *J Am Chem Soc* **2011,** *133* (5), 1184-1187.

42. Cesareo, E.; Parker, L. J.; Pedersen, J. Z.; Nuccetelli, M.; Mazzetti, A. P.; Pastore, A.; Federici, G.; Caccuri, A. M.; Ricci, G.; Adams, J. J.; Parker, M. W.; Lo Bello, M., Nitrosylation of Human Glutathione Transferase P1-1 with Dinitrosyl Diglutathionyl Iron Complex in vitro and in vivo. *J Biol Chem* **2005,** *280* (51), 42172-80.

43. Pulukkody, R.; Chupik, R. B.; Montalvo, S. K.; Khan, S.; Bhuvanesh, N.; Lim, S.-M.; Darensbourg, M. Y., Toward Biocompatible Dinitrosyl Iron Complexes: Sugar-Appended Thiolates. *Chem Comm* **2017,** *53*, 1180-1183.

44. Elsabahy, M.; Samarajeewa, S.; Raymond, J. E.; Clark, C.; Wooley, K. L., Shell-crosslinked Knedel-like Nanoparticles Induce Lower Immunotoxicity than their Non-crosslinked Analogs. *J Mater Chem B Mater Biol Med* **2013,** *1* (39).

45. Ignarro, L. J.; Fukuto, J. M.; Griscavage, J. M.; Rogers, N. E.; Byrns, R. E., Oxidation of Nitric Oxide in Aqueous Solution to Nitrite but not Nitrate: Comparison with Enzymatically Formed Nitric Oxide from L-arginine (nitric oxide synthase/oxidative metaboism). *Proc Nat Acad Sci* **1993,** *90*, 8103-8107.

46. Guven-Maiorov, E.; Ece Acuner-Ozbabacan, S.; Keskin, O.; Gursoy, A.; Nussinov, R., Structural Pathways of Cytokines may Illuminate their Roles in Regulation of Cancer Development and Immunotherapy. *Cancers* **2014,** *6*, 663-683.

47. Elsabahy, M.; Li, A.; Zhang, F.; Sultan, D.; Liu, Y.; Wooley, K. L., Differential Immunotoxicities of Poly(ethylene glycol)- vs. Poly(carboxybetaine)-coated Nanoparticles. *J Control Release* **2013,** *172* (3), 641-52.

48. Elsabahy, M.; Shrestha, R.; Clark, C.; Taylor, S.; Leonard, J.; Wooley, K. L., Multifunctional Hierarchically Assembled Nanostructures as Complex Stage-wise Dual-delivery Systems for Coincidental yet Differential Trafficking of siRNA and Paclitaxel. *Nano Lett* **2013,** *13* (5), 2172-81.

49. Elsabahy, M.; Wooley, K. L., Cytokines as Biomarkers of Nanoparticle Immunotoxicity. *Chem Soc Rev* **2013,** *42* (12), 5552-76.

50. Elsabahy, M.; Zhang, S.; Zhang, F.; Deng, Z. J.; Lim, Y. H.; Wang, H.; Parsamian, P.; Hammond, P. T.; Wooley, K. L., Surface Charges and Shell Crosslinks Each Play Significant Roles in Mediating Degradation, Biofouling, Cytotoxicity and Immunotoxicity for Polyphosphoester-based Nanoparticles. *Sci Rep* **2013,** *3*, 3313.

51. Stenken, J. A.; Poschenrieder, A. J., Bioanalytical Chemistry of Cytokines - a Review. *Anal Chim Acta* **2015,** *853*, 95-115.

52. Elsabahy, M.; Wooley, K. L., Data Mining as a Guide for the Construction of Cross-linked Nanoparticles with Low Immunotoxicity via Control of Polymer Chemistry and Supramolecular Assembly. *Acc Chem Res* **2015,** *48* (6), 1620-30.

53. Elsabahy, M.; Wooley, K. L., Reassessment of Nanomaterials Immunotoxicity. *Nano Today* **2018,** *20*, 10-12.

54. Elsabahy, M.; Wooley, K. L.; Hendricksen, A.; Oh, K., Multiplexing Techniques for Measurement of the Immunomodulatory Effects of Particulate Materials: Precautions when Testing Micro- and Nano-particles. *Methods* **2019,** *158*, 81-85.

55. He, W.; Frost, M. C., Direct Measurement of Actual Levels of Nitric Oxide (NO) in Cell Culture Conditions Using Soluble NO Donors. *Redox Biol* **2016,** *9*, 1-14.

CHAPTER IV : EFFECTS OF GLUTATHIONE AND HISTIDINE ON NO RELEASE FROM A DIMERIC DINITROSYL IRON COMPLEX (DNIC)‡

IV.1 Introduction

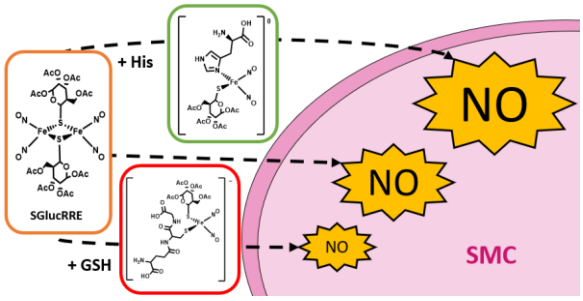

Figure IV-1 Depiction of the modulation of NO release from SGlucRRE through the addition of exogenous biocompatibile agents.

Nitric oxide (NO) is a ubiquitous signaling molecule in mammalian biology that is involved in immune response, neuronal transmission, cardiovascular health and a litany of other functions. Endogenous production of NO utilizes three isozymes (endothelial, neuronal, and inducible nitric oxide synthase (eNOS, nNOS and iNOS)).[1] The cellular target destinations of NO can be Fe-S clusters, metal hemes, protein thiols, and tyrosine.[2-7] Therapeutic sources of NO vary from benign nutritional supplements (for pulmonary and respiratory health), to inhalable NO gas. Despite the dangers of administering nitric oxide as a poisonous gas, NO has been most recently used as a treatment for the SARS-CoV disease;[8-9] it is even known as a therapy for premature newborns with respiratory failure.[10] Controllable molecular reservoirs of NO are obviously desirable.

---

‡ Reprinted with permission from Pectol, D.; Khan, S.; Elsabahy, M.; Wooley, K.; Lim, S.-M.; Darensbourg, M. Effects of Glutathione and Histidine on NO Release from a Dimeric Dinitrosyl Iron Complex (DNIC). *Inorg. Chem*. **2020**, *59* (23), 16998–17008. © 2021 American Chemical Society

Nitric oxide released endogenously within cells either diffuses as gaseous NO or may be transferred as an adduct to its target because of its high reactivity and short half-life as a free radical in an aerobic, aqueous environment.[11-12] While abundant cellular thiols such as free cysteine or glutathione are generally expected to be the major carriers as *S*-nitrosothiols (SNOs), nitric oxide also reacts with a combination of the chelatable iron pool (CIP) and available natural donor ligands to generate dinitrosyl iron complexes (DNICs) as tetrahedral $L_2Fe(NO)_2$ or $X_2Fe(NO)_2^-$ species.[13-17] Convincing arguments are made that DNICs are the likely working form of NO *in vivo* due to enhanced stability within the highly electron-delocalized, and redox level variability of the dinitrosyl iron unit (DNIU).[18-23] They are also inspiration for biomimetics and development in the design of NO-releasing molecules, NORMs (Figure IV-2A).[24-29] For this reason a rich literature has evolved around DNICs and many aspects of electronic structure effects on physical characteristics and function are known.[30-32]

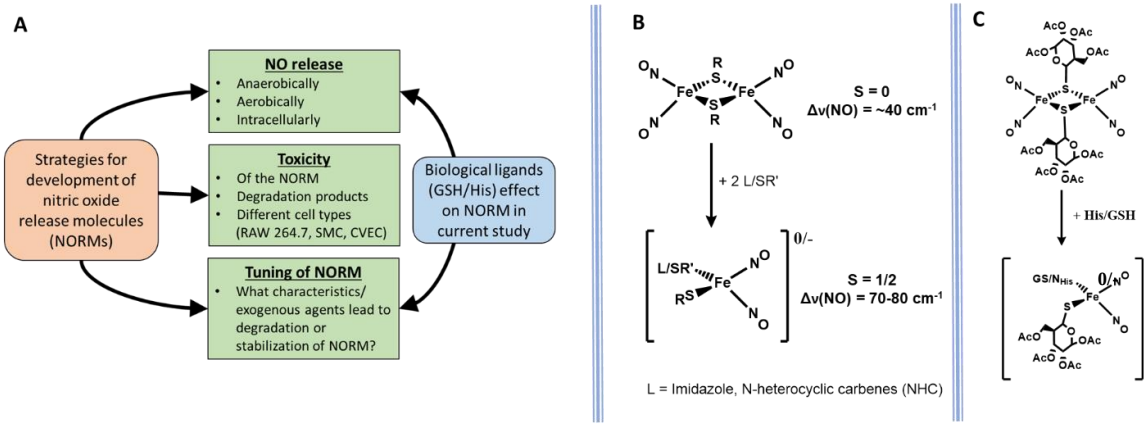

Figure IV-2 (A) Chart representing factors considered for development of NO release molecules (NORMs) as therapeutics. (B) Known reactions for cleavage of dimeric $\{Fe(NO)_2\}^9$ RRE-DNICs as well as the spectroscopic signatures of cleavage products.[36] (C) The general reaction mechanism for SGlucRRE that are investigated in this work

It is the enormity of unintentional reactions with media or other biomolecules that discourage ventures into a field where traditional analytical probes are not definitive. However, there is a rich synthetic inorganic background for DNICs that allow us to predict the likely ligands in the biological milieu that would offer exploitable outcomes as it relates to the stability of the DNIU. Vanin, et al. and Liaw, et al. have shown that dimeric, diamagnetic $[(\mu\text{-SR})Fe(NO)_2]_2$ exist in equilibria with paramagnetic $[(SR)_2Fe(NO)_2]^-$, where in biology SR may be glutathione, cysteine or any protein thiol.[33-35] From synthetic inorganic chemistry it is known that N-donor ligands such as imidazoles (surrogates for histidine), N-heterocyclic carbenes, and phosphines form isolable, stable complexes.[36-38]

	SGlucRRE	SGluNHC	SPhRRE	SPhNHC	neoDNIC
SMC IC_{50} (μM)	20	6.8	>250	7.3	6.9
RAW 264.7 IC_{50} (μM)	210	0.12	>250	0.29	0.37
Intracellular NO release	Yes	No	Yes	No	Yes
NO release in media	Yes	Yes	Yes	Yes	Yes

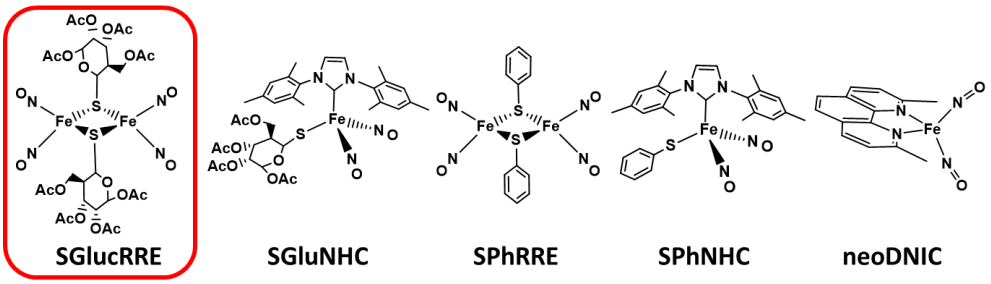

Figure IV-3: Tabular summation of previous results of DNIC studies published in Ref 24. The cell types used in the study were rat arteriolar smooth muscle cells (SMC), and murine RAW 264.7 macrophages. Structures of the DNICs used in that study are shown below, and the DNIC employed in this manuscript, SGlucRRE, is circled in red.

In previous studies, we emulated these naturally occurring DNIC motifs within an array of five complexes, Figure IV-2, in attempts to determine which molecule might serve as the most promising therapeutic source of NO for smooth muscle cells (SMCs), chosen for study as appropriate prototypes of vascular relaxation (See Figure IV-2 for overall strategic goals).[24] Features of such NORMs attractive for development would be their stability or tendency to degrade, liberating NO payloads, concomitant with relatively non-toxic decomposition products. From the complexes shown in Figure IV-2, the dimeric thioglucose-bridged DNIC, SGlucRRE, was found to provide sustained release of NO over 24 hours with less cytotoxicity and immunotoxicity when compared to the other DNICs assayed. In the current study, instead of beginning a large synthetic effort to design entirely novel DNICs, we have opted to generate different DNICs by altering the coordination sphere *in situ* by cleaving SGlucRRE with the safe, ubiquitous biologically relevant ligands histidine and glutathione.

IV.2 Experimental Design/Rationale

To facilitate identification of possible cleavage products and to emulate the *in vivo* concentrations of His and GSH, 100-300 μM[39] and 1-10 mM[40,41] respectively, 30 μM samples of SGlucRRE were treated with 2, 10 and 50 equiv. of His and GSH. The solvent chosen for each chemical experiment was dependent on the co-solubility of the exogenous ligand and SGlucRRE. Analysis of products by infrared spectroscopy assessed whether the dimeric complex was cleaved by comparing the difference in wavenumber of the

symmetric and asymmetric ν(NO) stretches; ESI⁻-MS characterized the charged products generated in the cleavage reaction, and EPR spectroscopy was used to detect the generation of a characteristic S = ½, g = 2.03, signal for $\{Fe(NO)_2\}^9$ species derived from the cleaved dimer.[32,42,43]

To determine whether molecular NO (gas) is released/transferred in these reactions, the Griess assay was employed to determine if the presence of an exogenous ligand hastens the generation of nitrite from NO in an aerobic, aqueous environment; a fluorometric intracellular NO probe surveyed the release profile of NO into the cytosol of smooth muscle cells.

Pursuing the hypothesis that cleavage of the dimeric RRE DNICs into monomeric derivatives moderate NO release, chemical studies under similar conditions to the biological milieu provide the foundation for this report. Cleavage of dimeric RRE DNICs requires a nucleophile stronger than the L-type, μ-SR thiolates present in the complex; examples are *N*-heterocyclic carbenes,[25] imidazoles,[37] aryl- and alkyl-thiolates (Figure IV-2B).[36] Based on available ligands in the media and the cytosol, the most biologically ubiquitous thiolate, glutathione, and nature's imidazole, histidine, were chosen for reactivity studies with SGlucRRE (Figure IV-2C).

IV.4 Assessing the chemical reactivity of SGlucRRE with glutathione.

The possible sites for metal center ligation on glutathione include one amine, two amides, one thiol, and two carboxylic acid groups. The reactivity of the glutathione was

initially probed by the change in the FT-IR spectra upon addition of ligand to SGlucRRE. Stoichiometric amounts of GSH in DMSO cleaved the SGlucRRE within 15 min and the products were assigned according to the ratio of the NO stretching frequency intensity and the $\Delta\nu$(NO) of those stretches (Figure IV-4C). After five minutes, numerous signals in the 1800-1600 cm^{-1} region implied that multiple nitrosyl-containing species were generated, some of which were attributed to glutathione (Figure IV-4C). After 15 min, the signals coalesced into three main features at 1741 cm^{-1}, 1664 cm^{-1}, and 1527 cm^{-1}. Due to the overlap of amide and carboxylate stretches of glutathione in region where ν(NO) stretches are expected, the FT-IR spectra are inconclusive regarding the nuclearity of the DNIU.[34] However, the growth of an EPR signal at g = 2.02 when SGlucRRE was treated with stoichiometric amounts of glutathione in DMSO, supports the conclusion that

under anaerobic conditions, glutathione cleaves the dimeric DNIC (Figure IV-4D) and produces the EPR active monomeric DNICs.

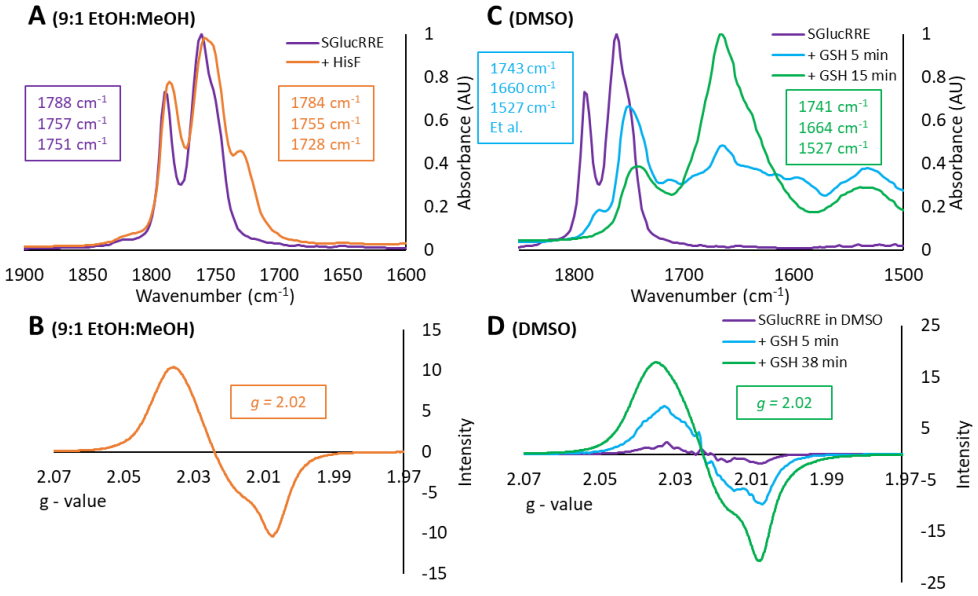

Figure IV-4: Comparison of FT-IR and EPR spectra upon reaction of SGlucRRE with exogenous biological ligands, HisF and glutathione under anerobic conditions and solvents as on the figures. Results of prominent features in the FT-IR and EPR spectra are labeled in the boxes corresponding to the color of the spectra. (A) FT-IR absorbance spectra in diatomic region of SGlucRRE (purple), and SGlucRRE treated with two equivalents of HisF (orange) in a 9:1 EtOH:MeOH solvent mixture. (B) X-band EPR spectra recorded at 4K of SGlucRRE treated with two equivalents of HisF in 9:1 EtOH:MeOH at t = 60 min (orange). (C)) FT-IR absorbance spectra of SGlucRRE (purple), and SGlucRRE treated with two equiv. of GSH at t = 5 min (blue) and t = 15 min (green) in DMSO. (D) X-band EPR spectra recorded at 4K of SGlucRRE treated with two equivalents of GSH at t = 0 (purple), t = 5 (blue), and t = 38 (green) minutes in DMSO.

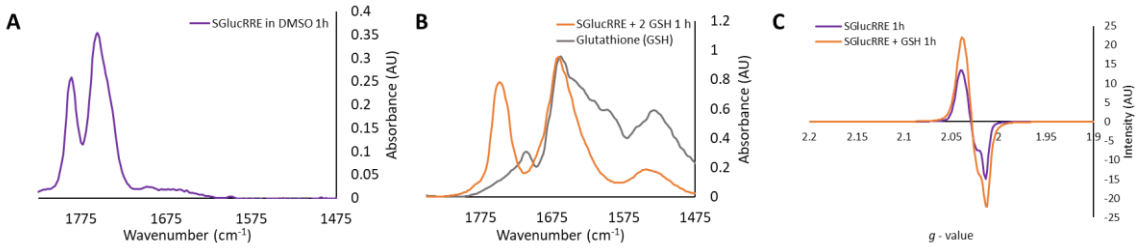

Figure IV-5: Comparison of the reactivity of DMSO and glutathione in DMSO using EPR and FT-IR. (A) FT-IR spectrum of SGlucRRE dissolved in DMSO after 1 h (purple). (B) FT-IR spectra of SGlucRRE treated with 2 equivalents of GSH after 1 h (orange) with the spectra of glutathione (grey) provided as a reference. (C) X-band EPR spectra collected at 4K for SGlucRRE in DMSO (purple), and SGlucRRE with 2 equivalents of glutathione in DMSO.

Dimer cleavage of SGlucRRE by DMSO to generate the characteristic $\{Fe(NO)_2\}^9$ EPR signal has been reported,[25] however, we assert this increase in spin as detected by EPR and change in FT-IR spectrum can be primarily contributed to glutathione in our studies. Emphasizing the results described above, Figure IV-4C and IV-5 displays the IR spectrum of SGlucRRE dissolved in DMSO and recorded after one hour. It has the same ν(NO) stretching pattern and position as were observed in DCM or MeOH and other solvents, indicating that SGlucRRE is still intact. When treated with two equivalents of GSH, there is a noticeable change in the FT-IR spectrum, Figure IV-5B. As a more sensitive probe for dimer cleavage and the production of radical monomers, the EPR spectrum of the pure SGlucRRE collected in DMSO shows a signal at g = 2.02 (Figure IV-5C) without addition of glutathione, but grows in intensity as is added. We proceed with the hypothesis that the dominant factor for the reactivity of SGlucRRE is glutathione

and not DMSO. Controls with SGlucRRE in DMSO are provided for the *in vitro* portion of the study to delineate the reactivity of DMSO to that of the exogenous ligands.

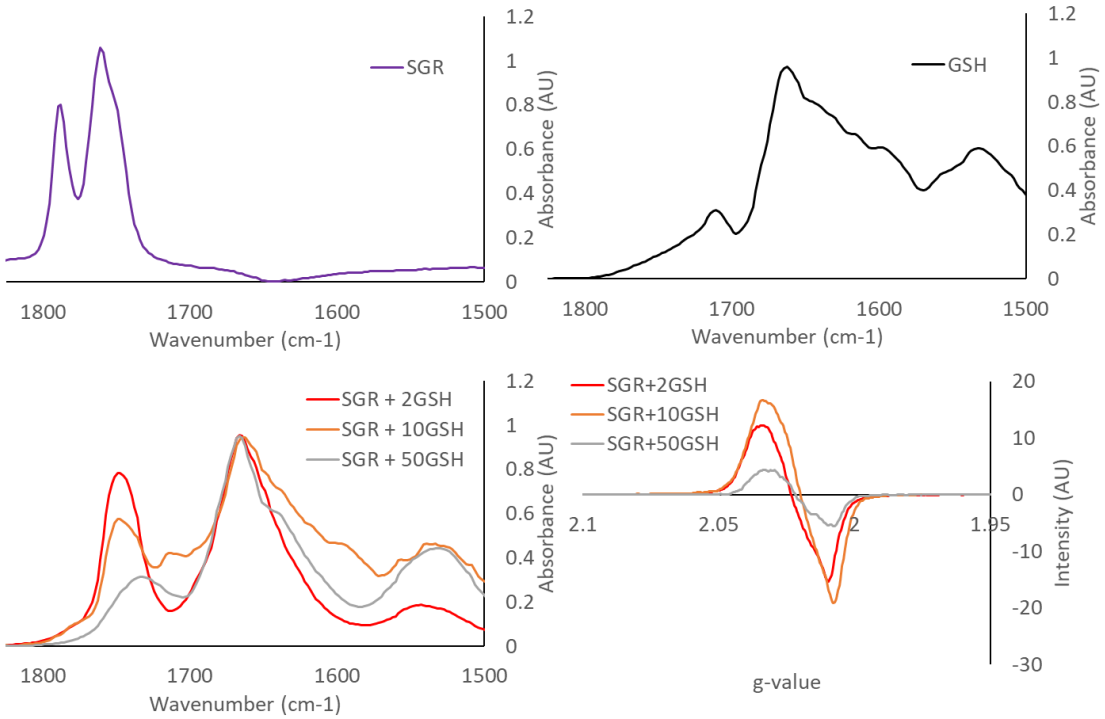

Figure IV-6 FT-IR absorbance spectra of [Top left] SGlucRRE (purple), [Top right] glutathione, and [Bottom left] SGlucRRE after treatment of 2 (red), 10 (orange), or 50 (grey) equivalents of glutathione in DMSO. Spectra A-C were normalized to the highest intensity peak in the 1850-1500 cm^{-1} range. [Bottom right] X-band EPR spectra recorded at 4K of SGlucRRE treated with 2 (red), 10 (orange), or 50 (grey) equivalents of glutathione in DMSO.

In order to assess the effect of increasing GSH concentration (2, 10 or 50 molar equivalents of GSH ligand) on SGlucRRE dimer cleavage, FT-IR, EPR, and ESI^{-}-MS spectral monitors were employed for overnight reactions at room temperature in DMSO. With increasing concentrations of GSH, red-shifted FT-IR signals were observed, and the intensity of the S = ½ signal indicative of a monomeric $\{Fe(NO)_2\}^9$ DNIC was more

intense with 10 vs. 2 equiv. (Figure IV-6). When treated with one and two equivalents of glutathione, there was evidence of dimer cleavage to form monomeric $\{Fe(NO)_2\}^9$ DNICs with formula $[(SGluc)(SG)Fe(NO)_2]^-$ as well as the formation of RRE-type DNICs with μ-S thioglucose and glutathione, $[(\mu\text{-}SGluc)(\mu\text{-}SG)(Fe(NO)_2)_2]^-$ (Figures IV-8 – IV-11). The LC-MS data suggested that this mixed thiolate product was not merely an artifact generated during the ionization process, but was a discrete, chromatographically separated and identified complex (Figures IV-12 – IV-14). With larger excesses, 50 equiv. of GSH (Figure IV-6), the species that produces the S = 1/2 EPR signal decreases significantly. In this case there is a loss of SGlucRRE as corroborated by ESI$^-$-MS (Figure IV-7)

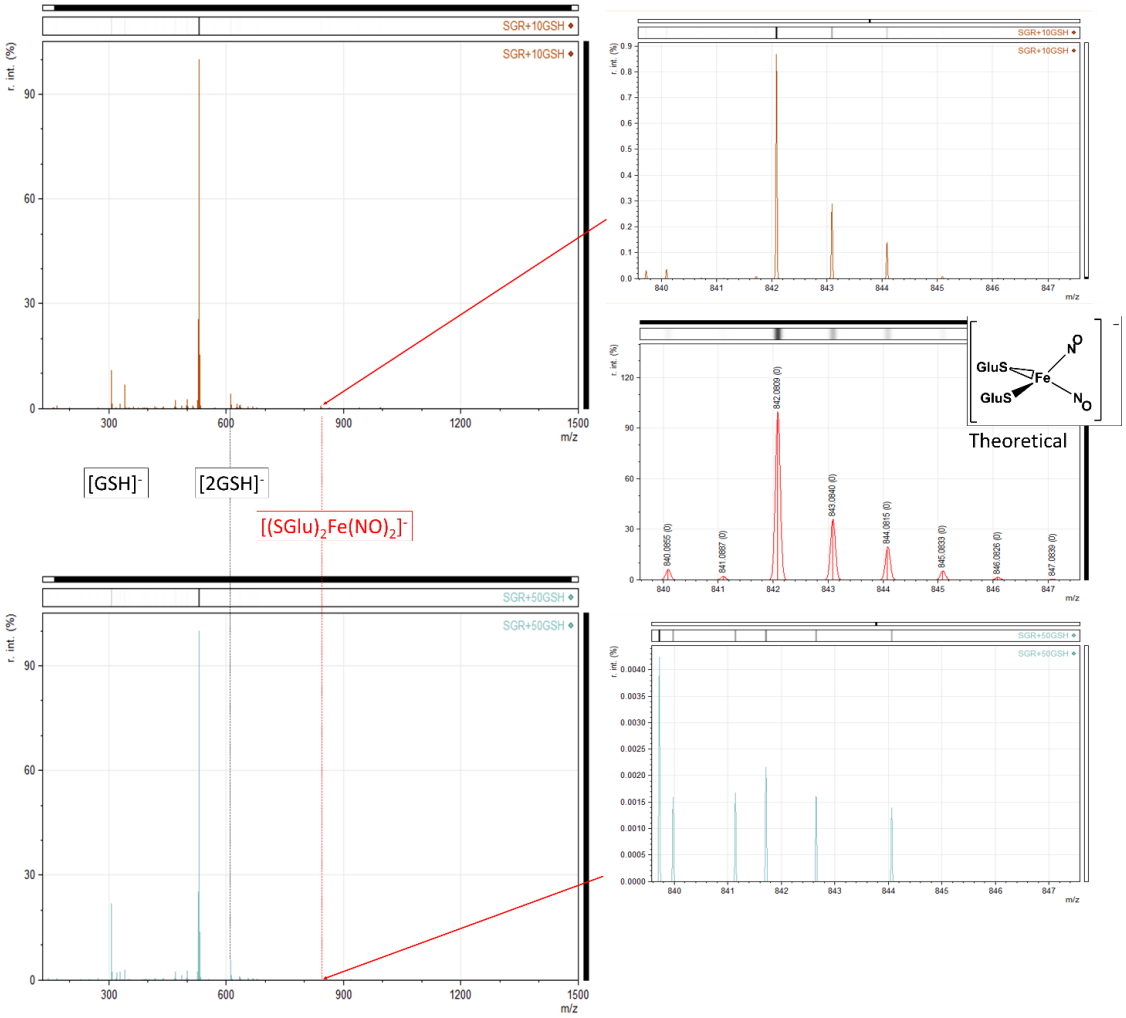

Figure IV-7 ESI⁻-MS of SGlucRRE treated with 10 (brown – top left) and 50 (cyan – bottom left) molar equivalents of glutathione. (Left) Full spectra with identifiable isotopic bundles labelled. (Right) Zoomed in spectra from 839.5-848 m/z for both the 10x (Top right) and 50x (Bottom right) GSH treatments. Theoretical isotopic bundle (red – middle right) is for $[(SGluc)_2Fe(NO)_2]^-$, $C_{28}H_{38}FeN_2O_{20}S_2$, the cleaved monomer of SGlucRRE is shown for comparison.

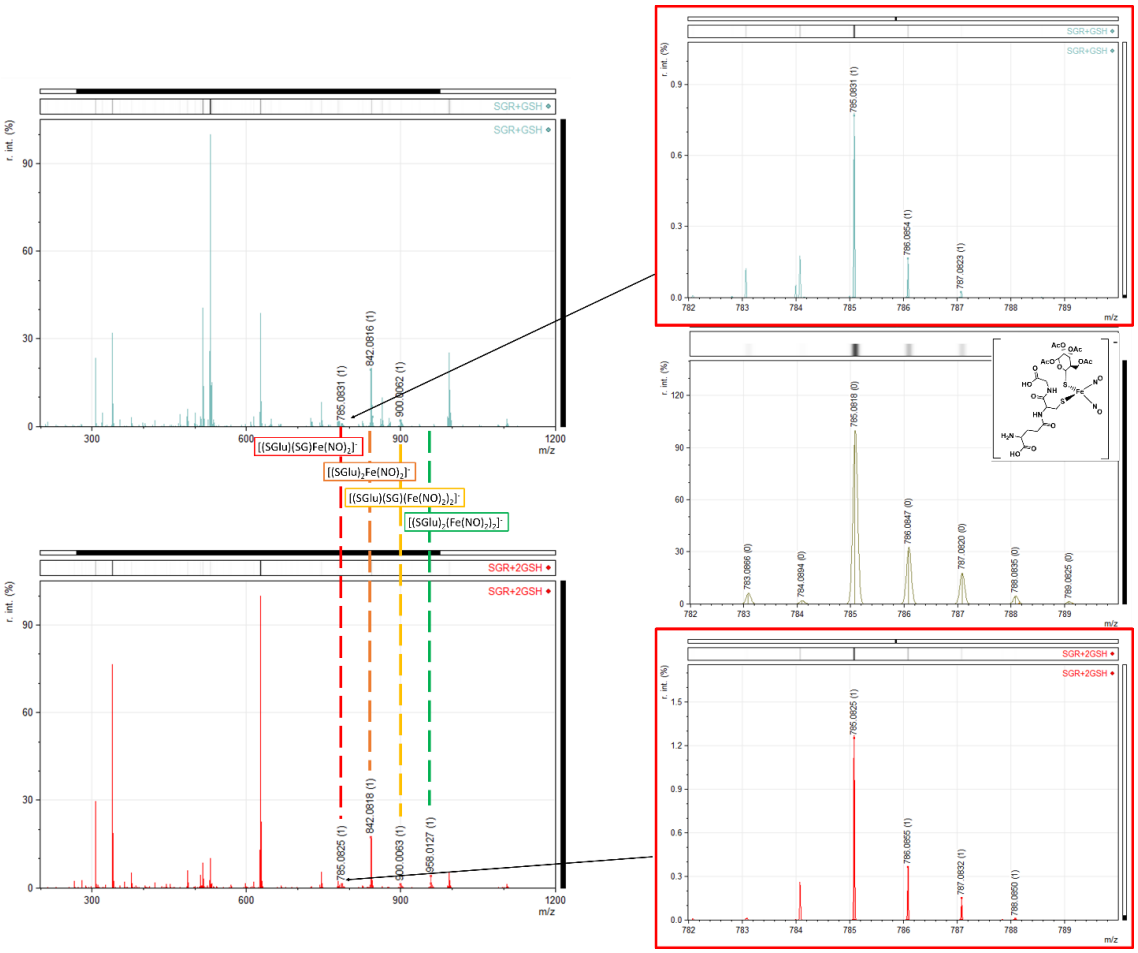

Figure IV-8: ESI⁻-MS of SGlucRRE treated with 1 (teal – top left) and 2 (red – bottom left) molar equivalents of glutathione. (Right) Zoomed in spectra from 782-790 m/z for both the 1x (Top right) and 2x (Bottom right) GSH treatments. Theoretical isotopic bundle (middle right) is for $[(SGluc)(SG)Fe(NO)_2]^-$, $C_{24}H_{35}FeN_5O_{17}S_2$.

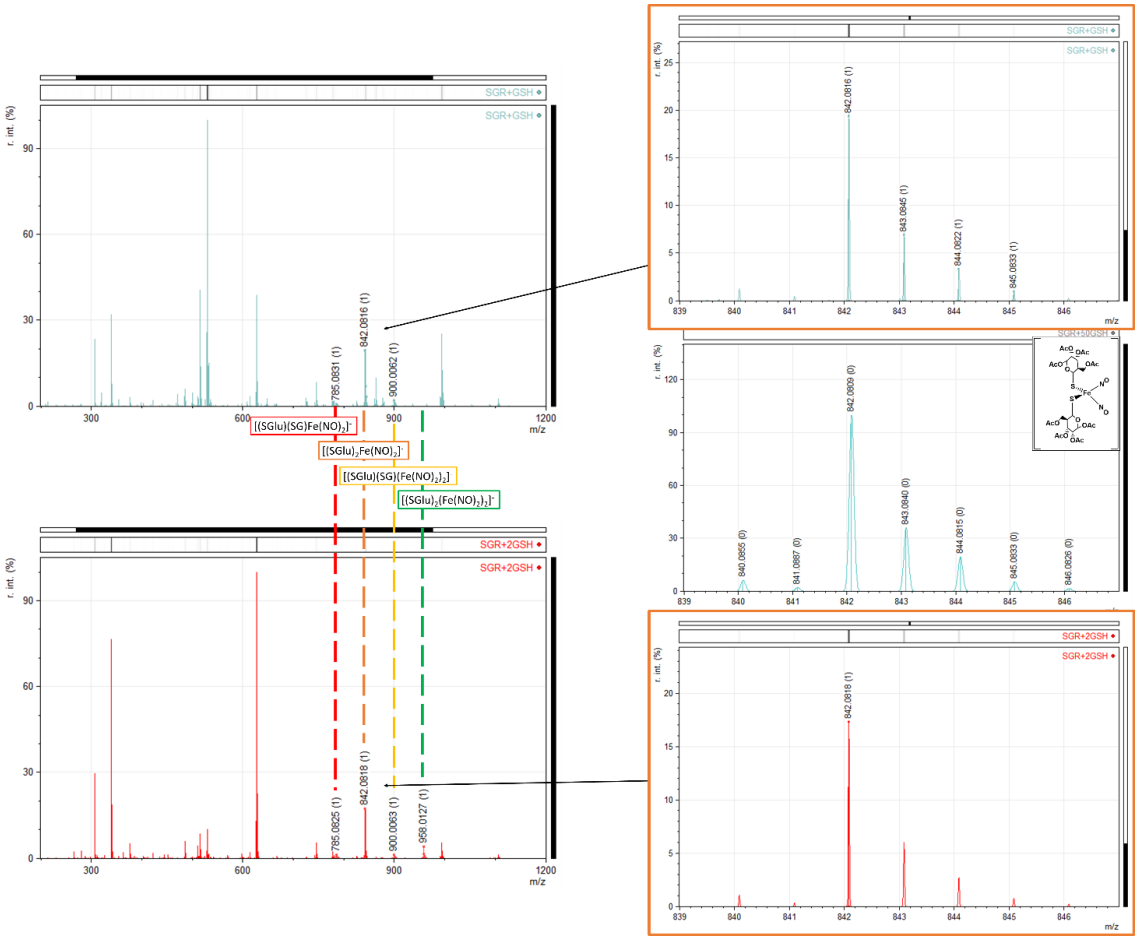

Figure IV-9 ESI⁻-MS of SGlucRRE treated with 1 (teal – top left) and 2 (red – bottom left) molar equivalents of glutathione. (Right) Zoomed in spectra from 839-847 m/z for both the 1x (Top right) and 2x (Bottom right) GSH treatments. Theoretical isotopic bundle (middle right) is for $[(SGluc)_2Fe(NO)_2]^-$, $C_{28}H_{38}FeN_2O_{20}S_2$.

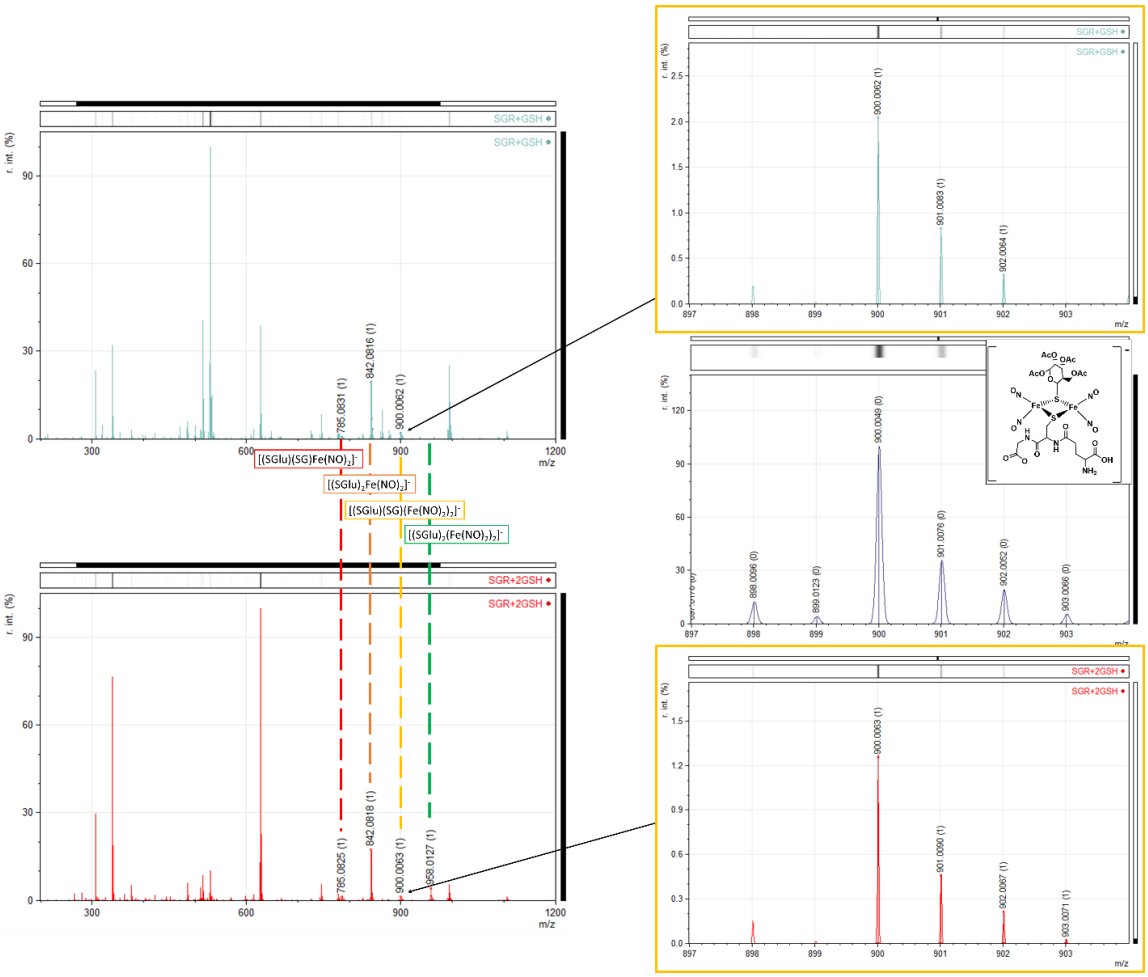

Figure IV-10: ESI⁻-MS of SGlucRRE treated with 1 (teal – top left) and 2 (red – bottom left) molar equivalents of glutathione. (Right) Zoomed in spectra from 897-904 m/z for both the 1x (Top right) and 2x (Bottom right) GSH treatments. Theoretical isotopic bundle (middle right) is for $[(SGluc)(SG)(Fe(NO)_2)_2]^-$, $C_{24}H_{35}Fe_2N_7O_{19}S_2$.

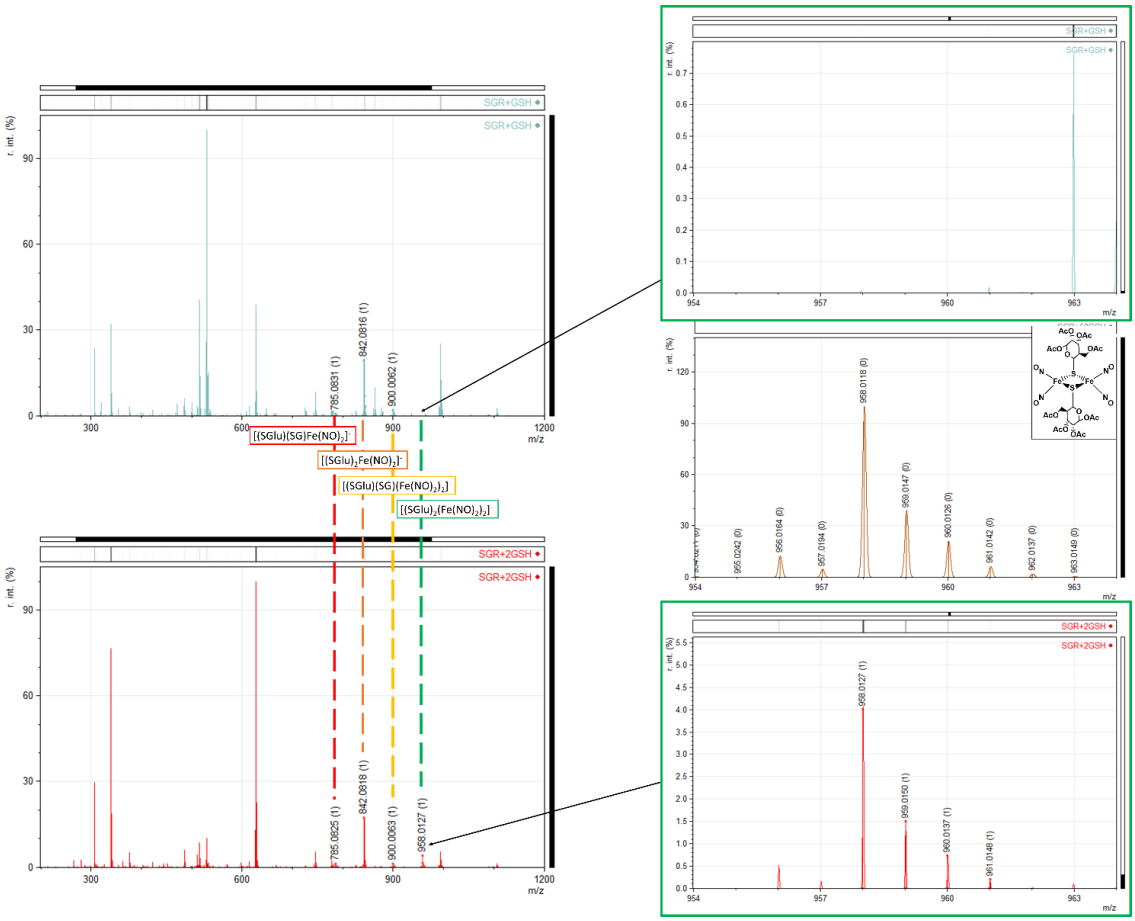

Figure IV-11: ESI⁻-MS of SGlucRRE treated with 1 (teal – top left) and 2 (red – bottom left) molar equivalents of glutathione. (Right) Zoomed in spectra from 954-964 m/z for both the 1x (Top right) and 2x (Bottom right) GSH treatments. Theoretical isotopic bundle (middle right) is for $[(SGluc)_2(Fe(NO)_2)_2]^-$, $C_{28}H_{38}Fe_2N_4O_{22}S_2$.

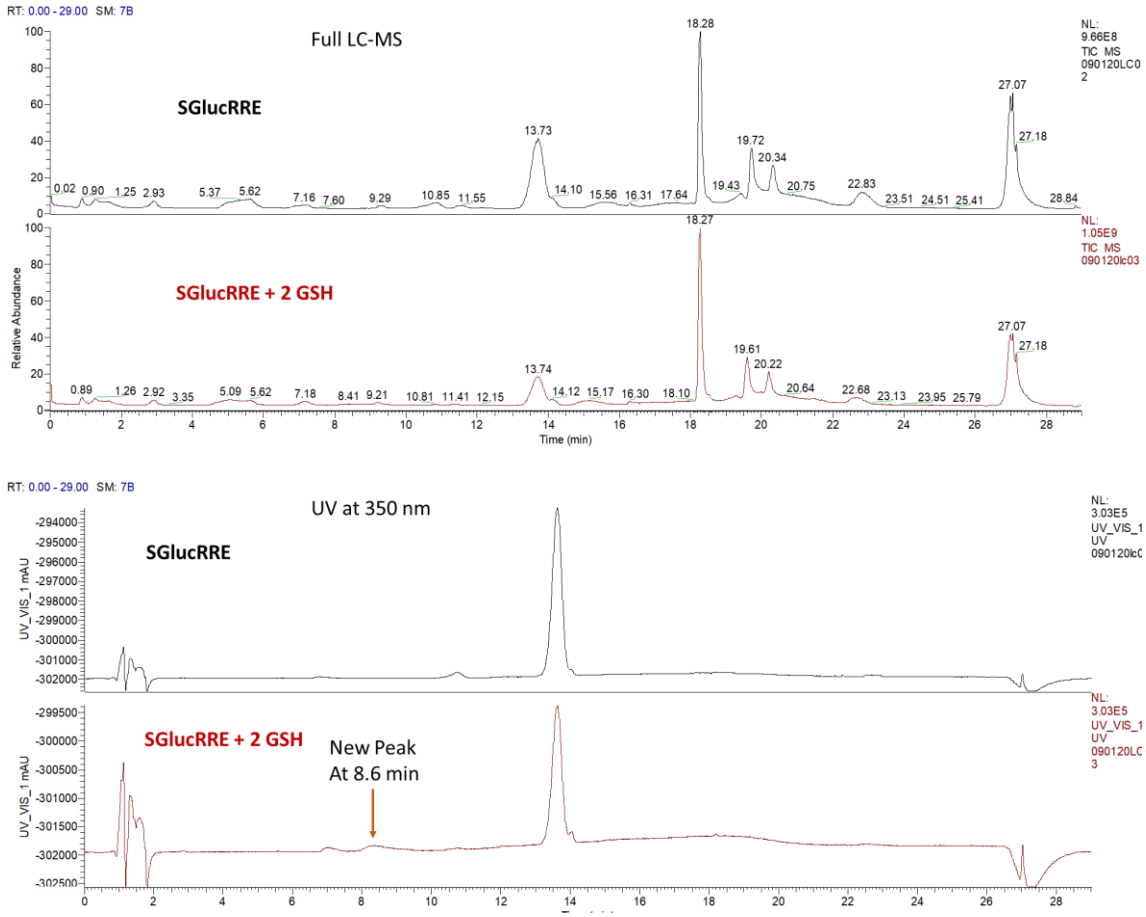

Figure IV-12 Full LC-MS spectra corresponding to SGlucRRE (black trace), and SGlucRRE + 2x glutathione (red trace). A UV-Vis detector was in-line with the LC-MS before ionization and was set to 350 nm, a common absorbance for DNICs. [Top] Full LC-MS chromatogram, and [bottom] chromatogram following the absorbance at 350 nm.

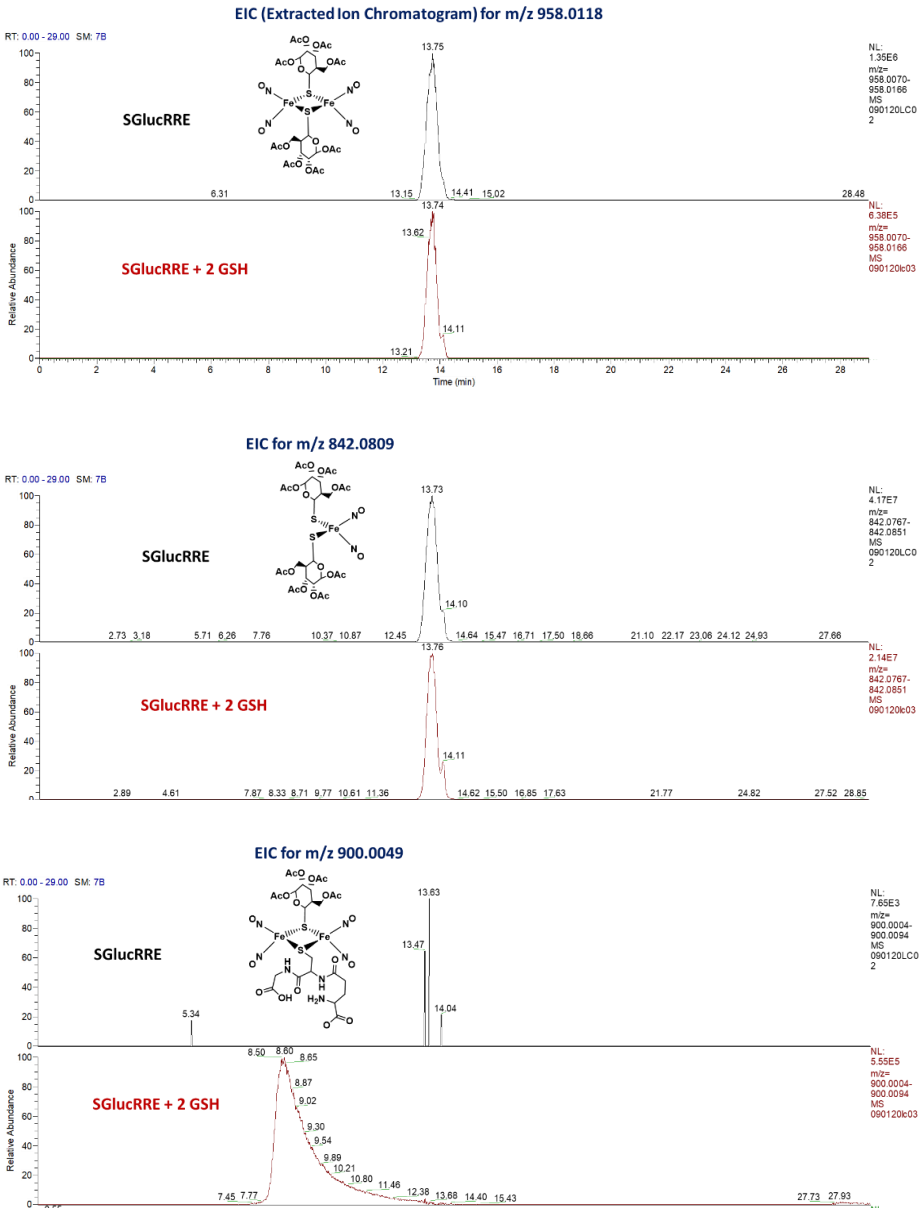

Figure IV-13 Extracted Ion Chromatograms (EIC) for relevant isotopic bindles that correlate to peaks detected in the UV-Vis chromatograms in the LC-MS in Figure IV-12. The intensity of the relative absorbances as well as the m/z range detected is shown in the text to the right of each chromatogram. The EIC's presented, along with a graphical chemical representation, are as follows: [Top]: $[(SGluc)_2(Fe(NO)_2)_2]^-$, $C_{28}H_{38}Fe_2N_4O_{22}S_2$, 958.0118 m/z [Middle]: $[(SGluc)_2Fe(NO)_2]^-$, $C_{28}H_{38}FeN_2O_{20}S_2$, 842.0809 m/z , [Bottom]: $[(SGluc)(SG)(Fe(NO)_2)_2]^-$, $C_{24}H_{35}Fe_2N_7O_{19}S_2$, 900.0049 m/z.

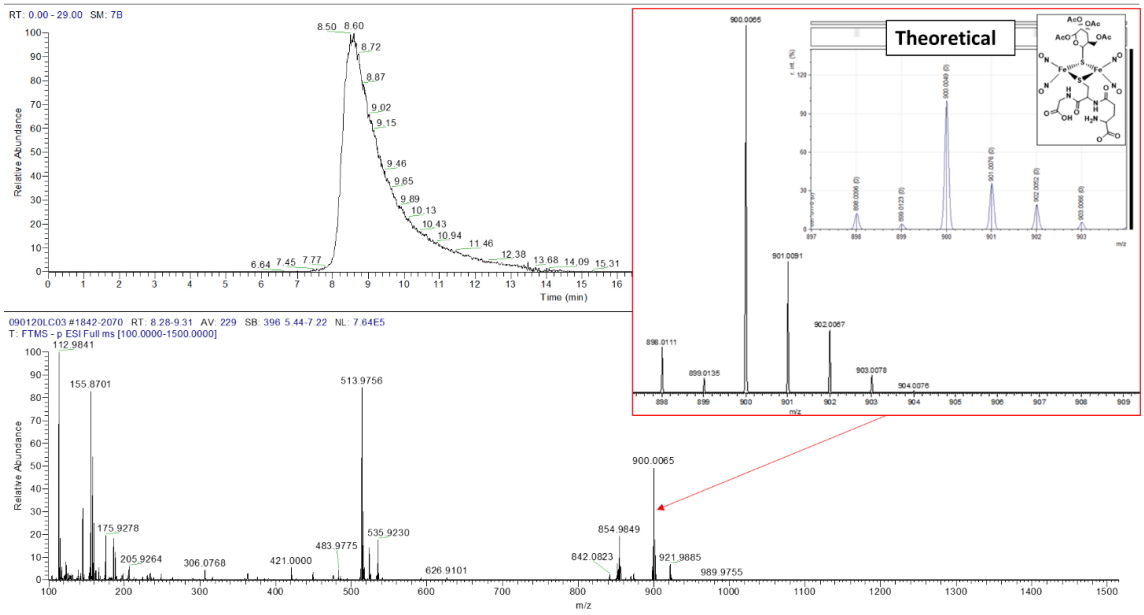

Figure IV-14: Confirmation of the identification of the isotopic bundle of $[(SGluc)(SG)(Fe(NO)_2)_2]^-$. [Top]: UV-Vis chromatogram resulting from LC-MS analysis of SGlucRRE + 2x GSH in DMSO shown in the bottom panel of Figure IV-13. [Bottom]: Full ESI-MS collected from the region shown in the top panel. [Red Inlay]: Zoomed in region corresponding to $[(SGluc)(SG)(Fe(NO)_2)_2]^-$, $C_{24}H_{35}Fe_2N_7O_{19}S_2$, from 897-909 m/z. The theoretical isotopic bundle for$[(SGluc)(SG)(Fe(NO)_2)_2]$ is labeled as such

IV.4 Assessing the chemical reactivity of SGlucRRE with histidinyl derivatives.

As with the above experiments with glutathione, the products from reactions of SGlucRRE with protected (HisF: Nα-FMOC-N(im)-trityl-L-histidine), isopropyl imidazole (IpI), and unprotected histidine (His) were characterized. For isopropylimidazole, the possible ligation are limited to the sp^2 hybridized imidazole nitrogen. With free histidine, both imidazole nitrogens, the amide, and carboxylic acid groups of the peptide backbone are available for reactivity, but the protected HisF eliminates possible amide and imidazole ligation. These different histidinyl derivatives

were analyzed in DCM for FT-IR and MS detection with IpI and HisF. HisF treat DNIC was characterized in 9:1 MeOH:EtOH for EPR evaluation. The unprotected histidine was characterized using MS in 1% DMSO in water.

A less drastic change in the FT-IR spectrum was observed upon treatment of SGlucRRE with HisF as compared to glutathione (Figure IV-4A). A small shoulder appeared at 1728 cm^{-1}, and the absorption that corresponds to the SGlucRRE starting material (1788 cm^{-1}) did not show a significant decrease in intensity, implying that there may be incomplete cleavage of the dimer. The same trend in reactivity was shown by the FT-IR spectra was shown for the IpI treated DNIC when compared to the HisF treated SGlucRRE (Figure IV-19). An increase in the g = 2.02 EPR signal was seen upon treatment with HisF which supports the presence of a histidine-cleaved monomer (Figure IV-4B).

Upon 10x and 50x HisF treatments, the isotopic bundle that corresponds to the HisF cleaved monomer of composition $[(SGluc)(N_{HisF})Fe(NO)_2]^0$ was detected (Figure IV-15). At 10x and 50x unprotected histidine concentrations in 1% DMSO in water, the only species detected was ionized histidine (data not shown), but when treated with stoichiometric amounts of histidine, monomeric DNICs were detected with the formula $[(N_{His})(SGluc)Fe(NO)_2]^-$ (Figure IV-16). Based on the totality of this data, histidine cleaves the SGlucRRE dimer with its imidazole, generating a monomeric DNIC.

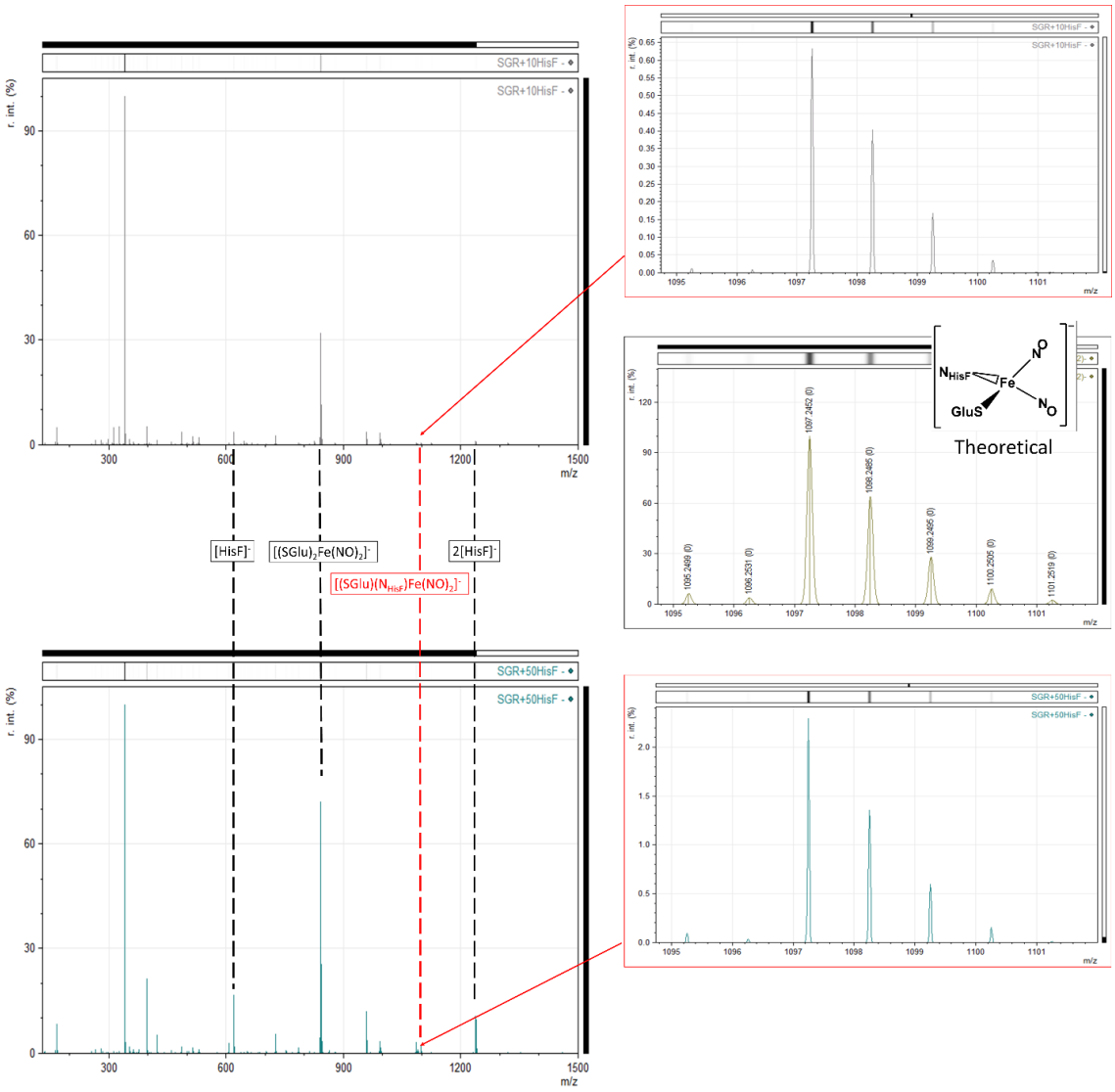

Figure IV-15: (Left) Full ESI⁻-MS of SGlucRRE treated with 10 (black – top left) and 50 (blue – bottom left) molar equivalents of HisF with m/z range from 100 - 1500. Identifiable isotopic bundles are labelled. (Right) Zoomed in spectra from 1094.5 - 1102 m/z for both the 10x (Top Right) and 50x HisF (Bottom right) treatments. Theoretical isotopic bundle for $[(SGluc)(N_{HisF})Fe(NO)_2]^-$, $C_{54}H_{51}FeN_5O_{15}S$ (1097.25 m/z), and the structure of HisF cleaved monomer is shown middle left.

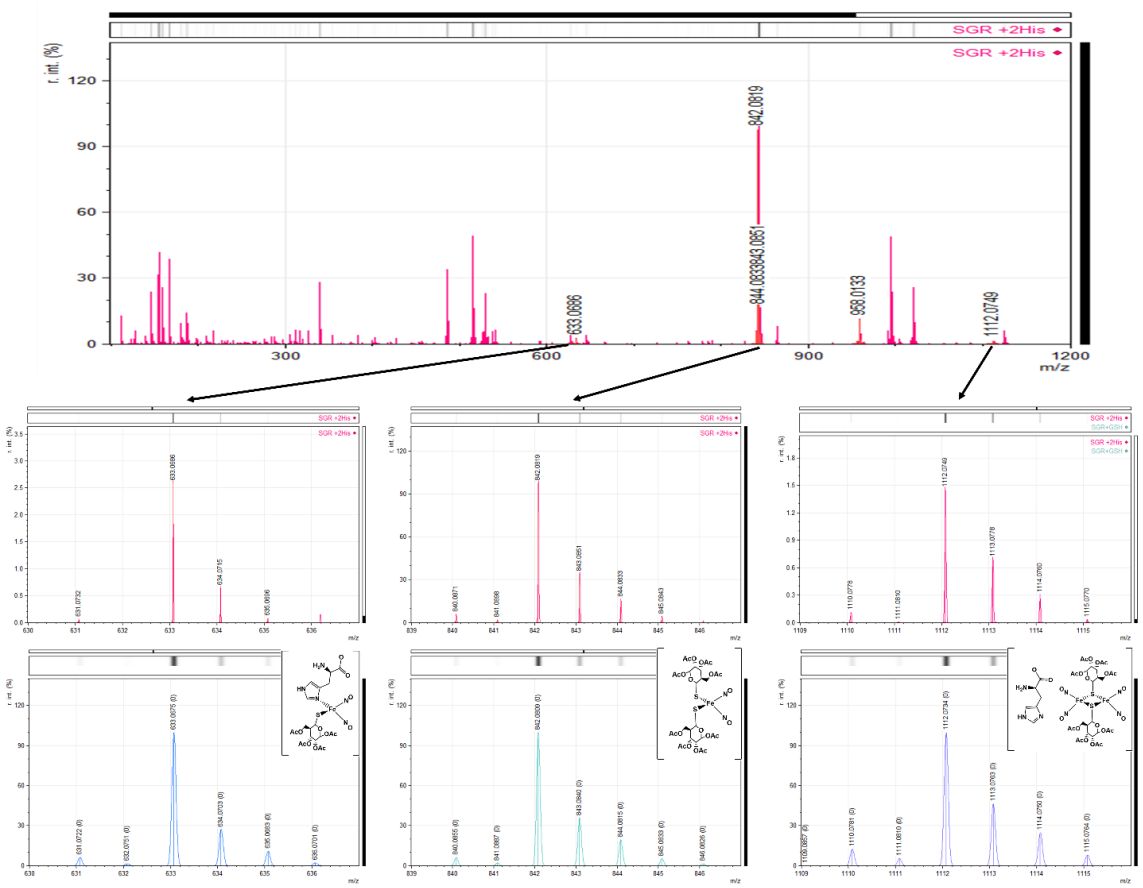

Figure IV-16: Cleavage of SGlucRRE as detected by ESI-MS. (Top) Full ESI⁻-MS of SGlucRRE treated with 2 molar equivalents of histidine with m/z range from 100 - 1200. Identifiable isotopic bundles are labelled. (Bottom left) Zoomed in spectrum from 630 - 637 m/z, and below, the theoretical spectrum and structure of $[(His)(SGluc)Fe(NO)_2]^-$, $C_{20}H_{27}FeN_5O_{13}S$. (Bottom middle) Zoomed in spectrum from 839 – 847 m/z, and below, the theoretical spectrum for $[(SGluc)_2Fe(NO)_2]^-$, $C_{28}H_{38}FeN_2O_{20}S_2$. (Bottom right) Zoomed in spectrum from 1109 – 1116 m/z.

IV.5 The effect of glutathione and histidine on SGlucRRE stability in DMEM/F12.

The above studies in DMSO and in the absence of water and oxygen provide evidence that the thiolate sulfur of glutathione and the sp^2 imidazole nitrogen of histidine interacts with the SGlucRRE. In order to establish the reactivity of SGlucRRE in the

solvent mixture used for the *in vitro* smooth muscle cell experiments, EPR spectroscopy was performed in 1% DMSO in DMEM/F12 growth media upon treatment with increasing concentrations of GSH and His (Figure IV-17). Even without the addition of His or GSH, an isotropic g = 2.0, S = ½ EPR signal indicated that some reagent in the media had cleaved the RRE DNIC. Upon addition of up to 10 molar equivalents of histidine, the intensity of this signal is enhanced, but then decreases at 50 molar equiv. (Figure IV-17A-B). An explanation for the disappearance of the S = ½ signal is indicated in the higher g-value portion of the spectrum. Without additional histidine, there is no signal at g = 4, but one appears and intensifies with increasing concentrations of histidine (Figure IV-17C). As signals at g = 4 are characteristic of "junk iron" or high-spin Fe^{III},[44,45] it is reasonable to conclude that excess histidine decomposes the monomeric DNIC, whatever it might be, into unidentified ferric species. In contrast to the histidine treatment, addition of glutathione in aqueous media find no EPR signals develop in the g = 2 and g = 4 region (Figure IV-17D-F). From this we conclude that monomeric DNICs are not being formed, there is no degradation into Fe^{III} , and GSH, through some mechanism, protects the SGlucRRE from cleavage and degradation in aqueous media. Notably the results of the LC-MS experiment (Figures IV-12 – IV-14), which showed the formation of mixed thiolate RRE's on treatment of SGlucRRE with glutathione in DMSO/air, support the conclusion that the species in the media are in an antiferromagnetically coupled, EPR-silent, dimeric RRE form.

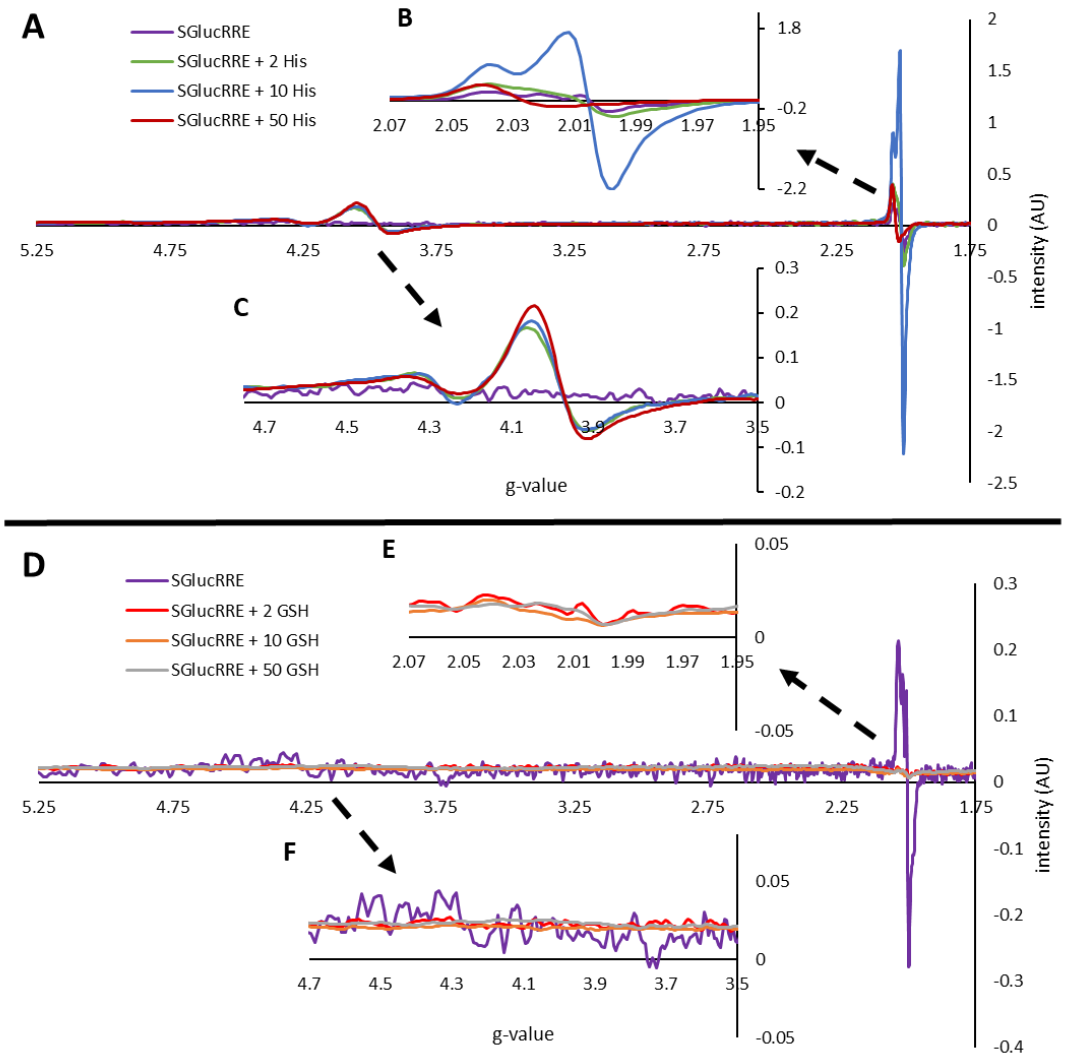

Figure IV-17: X-band EPR spectra collected at 4 K of SGlucRRE (100 μM) treated with increasing concentrations of histidine (A-C) or GSH (D-F) in 1% DMSO in phenol-free DMEM-F12. Solutions were sonicated prior to measurement after reaction for 30 minutes to ensure solubility. (A) Full EPR spectra of SGlucRRE (purple, g = 2.00), SGlucRRE treated with 2 (green g = 2.00, 3.98), 10 (blue g = 2.00, 3.98), or 50 (maroon g = 2.03, 3.98) molar equivalents of histidine. B and C are the zoomed in g = 2 and g = 4 regions respectively. (D) Full EPR spectra of SGlucRRE (purple), SGlucRRE treated with 2 (red), 10 (orange), and 50 (grey) molar equivalents of GSH. E and F are the zoomed in g = 2 and g = 4 regions emphasizing the lack of detectable signals in at those positions in the EPR spectra. In E, the EPR spectrum of SGlucRRE with no treatment (purple) is omitted for clarity.

Another hypothesis for the elimination of the S = ½ signal might be due to reduction of the DNIC with the ubiquitous cellular redox regulator glutathione. To further examine the role of DNIC reduction, another common cellular reductant, ascorbate, was used (Figure IV-18).[46,47] Upon reaction with 2 molar equivalents of ascorbate for 15 minutes, as was the case with histidine, a signal in the g = 4 region was observed that was attributed to ferric iron. As expected, when treated with 10 molar equivalents of ascorbate, the Fe^{III} signal is eliminated, likely reduced to ferrous iron. Curiously, upon treatment with 50 equiv. ascorbate, a signal around g = 4 re-emerges, but at higher g value. From the treatment with stoichiometric ascorbate, it appears that the DNIC has decomposed into a ferric species, implying DNIC degradation, at the higher concentrations of ascorbate, the final fate of the DNIC cannot be determined based solely on the EPR results.

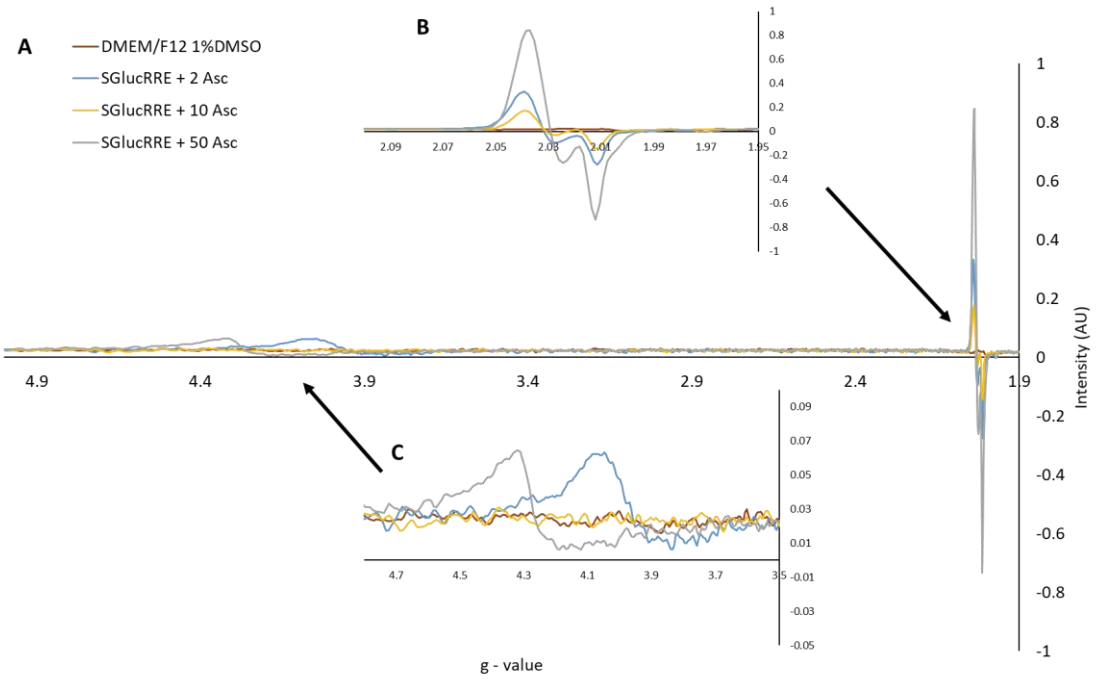

Figure IV-18 X-band EPR spectra collected at 4 K of SGlucRRE (100 μM) treated with increasing concentrations of ascorbate in 1% DMSO in phenol-free DMEM-F12. (A) Full EPR spectra of SGlucRRE treated with 2 (blue), 10 (yellow), or 50 (grey) molar equivalents of ascorbate. B and C are the zoomed in $g = 2$ and $g = 4$ regions respectively. The EPR spectrum of DMEM/F12 in 1% DMSO is provided for comparison (brown).

IV.6 Effect of imidazoles on NO transfer to CoTPP from SGlucRRE

To probe if this cleavage of SGlucRRE by exogenous imidazoles, generating Fe^{III}, has an effect on NO release/transfer from the DNIC, an NO trap, cobalt(II)tetraphenylporphyrin (CoTPP) was added to this solution. The DNIC was stirred in DCM over a course of 4 days in the presence of IpI, HisF, or without any exogenous imidazole, and the growth of the ν(NO) feature at 1682 cm^{-1} corresponding to (NO)CoTPP[48,49] was monitored using FT-IR (Figure IV-19). The decomposition of SGlucRRE and transfer of its NO to CoTPP in the presence of IpI, was observed by the loss of the stretch from the SGlucRRE starting

material at 1788 cm^{-1} and the growth of the signal at 1682 cm^{-1}. The protected histidine also caused the NO to transferred from SGlucRRE to CoTPP, but did not as completely as the IpI treated DNIC since the stretch at 1788 cm^{-1} remains in the FT-IR spectrum. This can be attributed to the large amount of steric bulk flanking HisF when compared to IpI. Both conditions resulted in enhanced transfer of NO to CoTPP than the untreated DNIC in DCM when comparing the relative absorbances of the ν(NO) feature at 1682 cm^{-1} (Figure IV-19E). Combined with the EPR/IR evidence (Figures IV-4, IV-17), we conclude that the cleavage of the SGlucRRE by the imidazole derivatives is responsible for the enhancement of the transfer of NO from SGlucRRE to (NO)CoTPP.

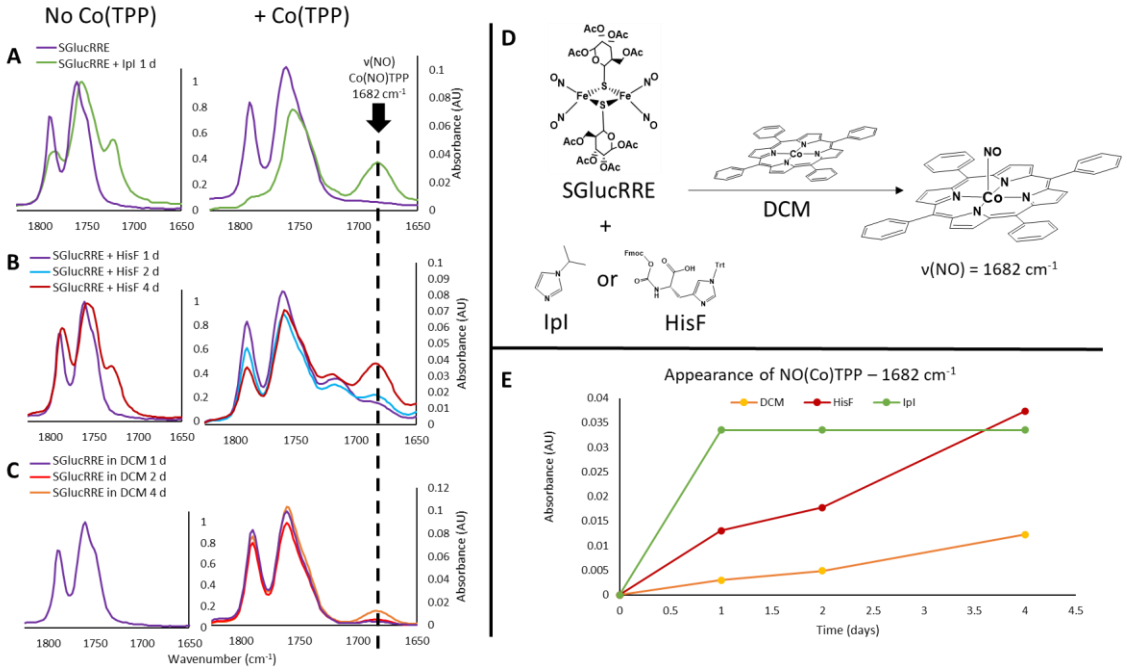

Figure IV-19 Using Co(II)Tetraphenylporphyrin (CoTPP) to monitor the transfer of NO from SGlucRRE in the presence of imidazole derivatives to generate (NO)CoTPP. All of the reactions monitored are in dichloromethane (DCM). For A-C the spectra on the left are given as shown in the legend, and the spectra on the right are in identical conditions except for the presence of four equivalents of CoTPP. The presence of (NO)CoTPP is monitored by the growth of the stretch at 1682 cm^{-1}. (A) FT-IR spectra collected after treatment of SGlucRRE with stoichiometric amounts of isopropylimidazole (IpI). (B) FT-IR spectra collected of SGlucRRE treated with two equivalents of HisF, and (C) FT-IR spectra collected of SGlucRRE in DCM without any additional exogenous ligands. (D) The general scheme for the CoTPP experiment performed int his figure. (E) Tracking the growth of the absorbance related to the ν(NO)-(NO)CoTPP at 1682 cm^{-1} for the different conditions; green – IpI, red – HisF, yellow – DCM.

IV.7 Probing NO transfer/release.

For the first assessment of NO release, the Griess assay was adopted to monitor the conversion of NO to nitrite in an aerobic, aqueous environment when treated with 2, 10, or 50 molar equivalents of glutathione or histidine (Figure IV-20). After 30 minutes,

increasing concentrations of nitrite are detected in all of the histidine treatment conditions when compared to untreated SGlucRRE; the nitrite levels converge after 18 hours (Fig. IV-20A-B). Initially after 30 minutes, more nitrite is detected in all treatment conditions (Fig. IV-20C); however, after 1 h all of the GSH treatment conditions diverge (Fig. IV-20D). The 2x GSH-treated SGlucRRE had higher nitrite concentrations at every timepoint. The 10x GSH-treated sample from the 1 h mark onward was statistically the

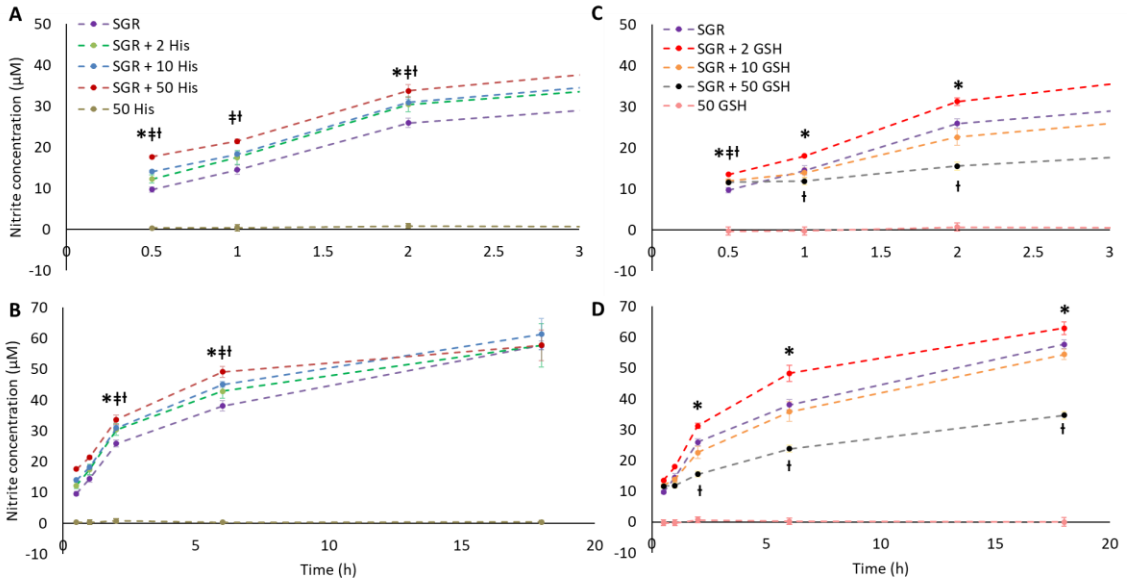

Figure IV-20: Griess assay data for determination of nitrite concentration using 30 μM SGlucRRE (SGR) in DMEM/F12 with differing concentrations of exogenous ligand at 0.5, 1, 2, 6, and 18 h. The different treatment conditions are as follows: SGlucRRE (purple), abbreviated SGR, SGlucRRE + 2 His (green), + 10 His (blue), + 50 His (maroon), + 2 GSH (red), + 10 GSH (orange), + 50 GSH (grey), 50 His only (tan), and 50 GSH only (pink). The number in front of the exogenous ligand indicates the molar equivalents with reference to the DNIC (2 = 60 μM, 10 = 300 μM, 50 = 1.5mM). (A): The first three hours of the Griess assay data collected for SGlucRRE and all histidine treatment conditions, and (B), the full 18 hours of the experiment. (C) The first three hours of Griess assay data collected for SGlucRRE and all GSH treatment conditions, and (D)(Bottom right) the full-time course of the experiment. * = ($p < 0.05$) when comparing +2(His/GSH) to the untreated SGlucRRE, ǂ = ($p < 0.05$) when comparing +10(His/GSH) to SGlucRRE, and ł = ($p < 0.05$) when comparing +50(His/GSH) to SGlucRRE.

same as the untreated SGlucRRE, and the 50x GSH treated sample from the 2 h mark onward was trend as the histidine-treated samples, showing that stoichiometric amounts of exogenous glutathione increase the rate of NO released from the DNIC. However, with excesses of glutathione (10x or 50x) the softer thiolate imparts protection to the $Fe(NO)_2$ unit, diminishing the rate of NO release in aerobic, aqueous conditions.

To observe if chemical reduction of the DNIC is a factor of this protective effect that dampens the release rate of NO, ascorbate was used (Figure IV-21). Upon treatment with ascorbate, the amount of nitrite detected is drastically reduced from 25 μM nitrite detected without reductant to 3.4 μM with reductant. This decrease is more pronounced upon treatment with increased equivalents of reductant, going as low as the limit of detection for the Griess assay upon treatment with 50 equivalents of ascorbate (~1 μM).

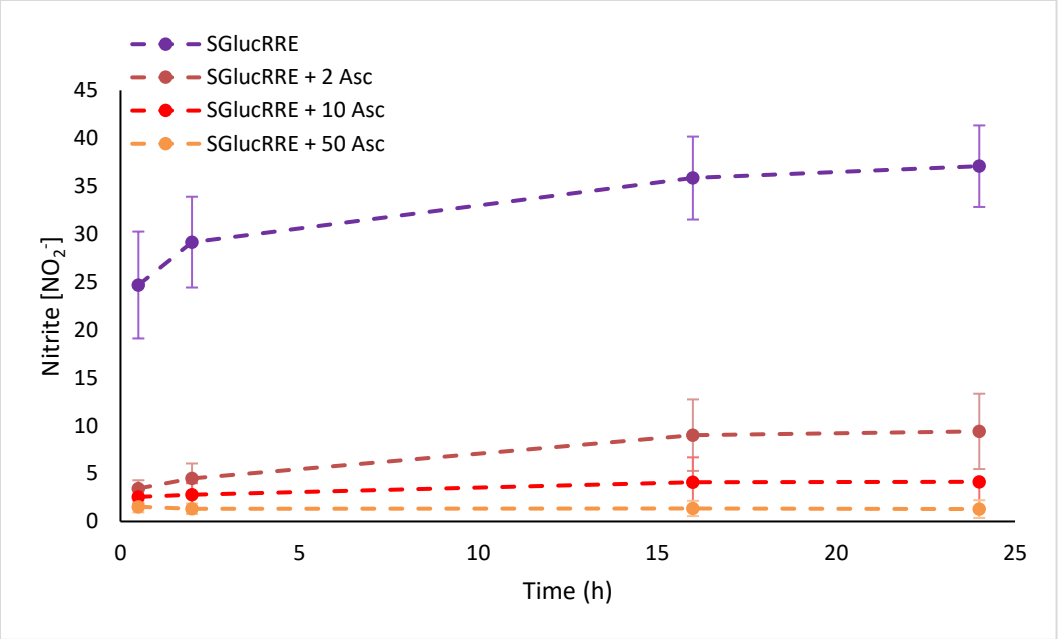

Figure IV-21 Griess assay data for determination of nitrite concentration using 30 μM SGlucRRE in DMEM/F12 with differing concentrations of ascorbate at 0.5, 2, 16, and 24 h. The treatment conditions are as follows: SGlucRRE without any additional reductant (purple), SGlucRRE with 2 equiv. (orange), 10 equiv. (red), and 50 equiv. (green) of ascorbate. Error bars represent standard deviation of n = 3 trials.

The final assessment of NO release, the intracellular NO assay, was utilized to determine whether the same trend established by the Griess assay was consistent with the amount of NO that was delivered into the cytosol of smooth muscle cells. Each of the different treatment conditions (SGlucRRE + 2x, 10x, and 50x GSH/His) were compared to that of the untreated DNIC, SGlucRRE (Fig. IV-22). Upon treatment with 2 equiv. histidine (Fig. IV-22A), the intracellular NO release time profile does not change, but as more histidine is added, increased amounts of NO are released in the cytosol. The amount of NO detected in SGlucRRE and the SGlucRRE +10x histidine and +50x histidine treated

smooth muscle cells diverged at 1900 s. At 3200 s the DNIC with 50 molar equivalents of histidine no longer provides a statistically higher amount of intracellular NO; the same was true for the DNIC +10x His at 4100 s (Fig. IV-22B-C). As was seen in the Griess assay, eventually, all of the histidine treatment conditions converge to the same amount of detectable NO.

The amount of intracellular NO was decreased upon treatment of DNIC with increasing concentrations of exogenous glutathione (Figure IV-22D-F). With stoichiometric treatment of GSH, just as with the histidine, there was not a significant change in the amount of intracellular nitric oxide. However, when treated with 10 or 50 molar equivalents of GSH, the intracellular NO is drastically decreased starting around 2000 s after DNIC treatment. Over the course of the experiment, the amount of intracellular NO remained statistically higher than that of untreated smooth muscle cells, which validates the results from the Griess assay.

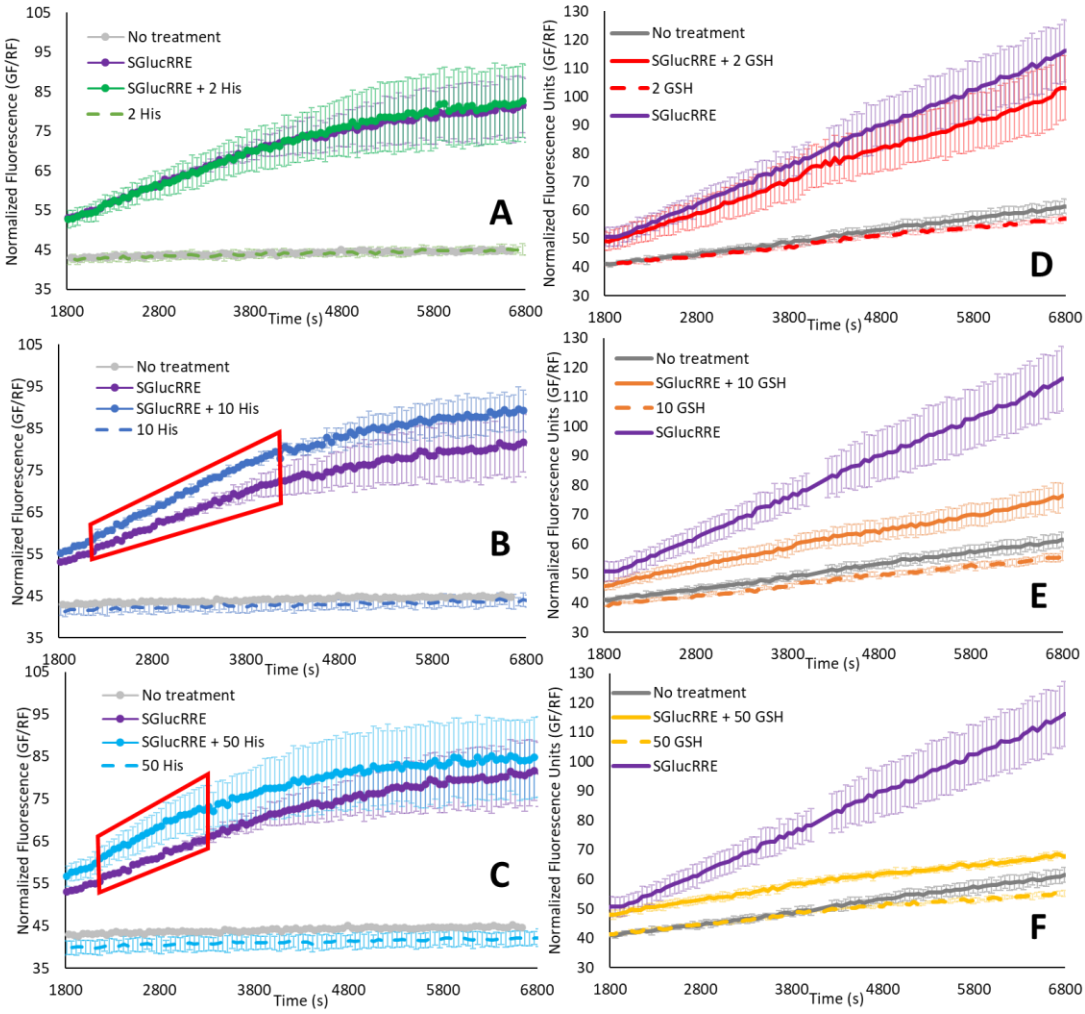

Figure IV-22: Intracellular NO release profile for smooth muscle cells treated with 30 μM SGlucRRE (purple) with or without increasing molar equivalents of histidine and/or glutathione. (A) 30 μM SGlucRRE (purple), compared to SGlucRRE + 2 molar equivalents of His (green), 2x His (dashed green), and untreated SMC (grey). B&C have identical treatment conditions as A with the exception of increasing histidine treatment concentrations (10x histidine in B [blue] and 50x histidine in C [cyan]). (D) 30 μM SGlucRRE (purple), compared to SGlucRRE + 2 molar equivalents of GSH (red), 2x His (dashed red), and untreated SMC (grey). E&F have identical treatment conditions as D with the exception of increasing glutathione treatment concentrations (10x GSH in E [orange] and 50x GSH in F [yellow]). Time = 0 indicates the time point at which SMCs were initially treated with DNIC. Red boxes indicate a significant increase ($p < 0.05$) in the intracellular NO detected due to exogenous ligand compared to SMC treated with SGlucRRE only.

To further corroborate that the decrease in detected nitrite is not solely due to reduction by glutathione, SGlucRRE was treated with increasing concentrations of the common cellular reductant ascorbate (Figure IV-23). With the addition of ascorbate, no NO is released into the cytosol regardless of ascorbate concentration. Upon reduction of the DNIC, the presence of nitrite in solution is almost completely abolished, implying that the role of glutathione in effecting the release of NO is primarily based on coordination.

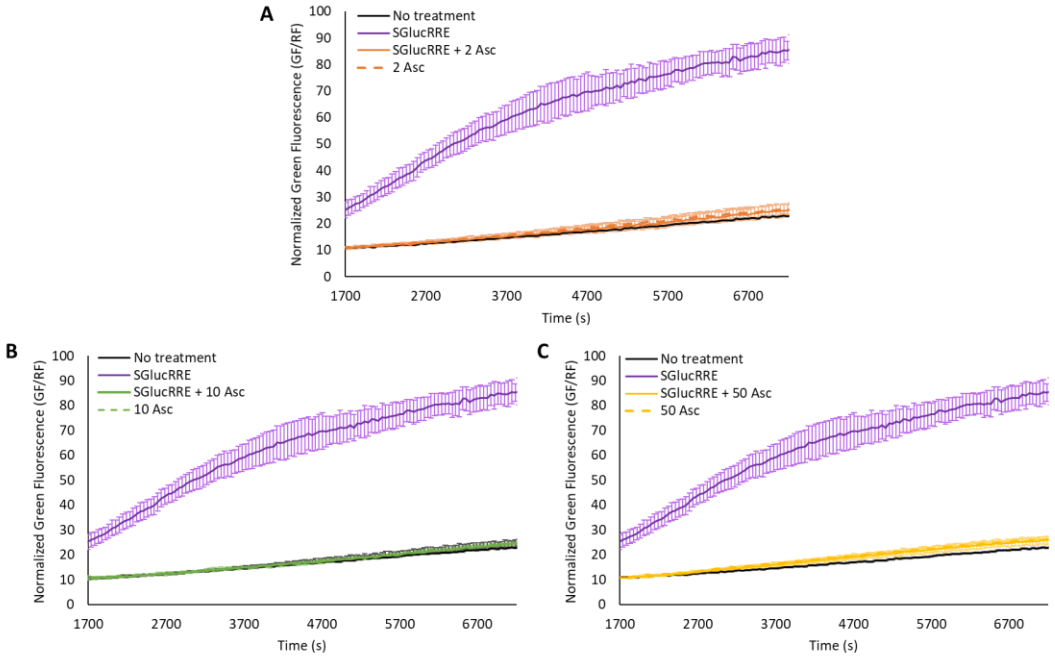

Figure IV-23: Intracellular NO release profile for smooth muscle cells treated with 30 μM SGlucRRE (purple) with or without increasing molar equivalents of ascorbate. (A) 30 μM SGlucRRE (purple), compared to SGlucRRE + 2 molar equivalents of ascorbate (orange), 2x His (dashed orange), and untreated SMC (black). B&C have identical treatment conditions as A with the exception of increasing ascorbate treatment concentrations (10x ascorbate in B [green, solid with DNIC, dashed without DNIC] and 50x histidine in C [yellow, solid with DNIC, dashed without]). Time = 0 indicates the time point at which SMC's were initially treated with DNIC.

IV.8 Discussion

Our previous study found that a synthetic RRE-type DNIC could provide a sustained source of intracellular NO to smooth muscle cells, in contrast to the NHC-cleaved monomer which did not increase intracellular NO.[15] The current study shows that addition of exogenous biological ligands cleaves the dimeric DNIC to form a new NORM, which alters intracellular NO release by changing the coordination environment about iron with the use of "safe" biological additives. This provides insight as to how the DNIC might function once inside the cell.

Based on the spectroscopic observation of RRE cleavage by histidine and GSH, data from the Griess assay, and the detection of RRE-type DNICs with mixed thiolates in the mass spectra, the following hypothesis is proposed and visualized in Figure IV-2. From the data presented in this paper, the synthetic DNIC SGlucRRE is cleaved by histidine. Additionally, EPR measurements in aqueous media show that the DNIC is not only split with histidine to generate a S = ½ DNIC, but it subsequently degrades into an unidentified Fe^{III} complex. In conjunction with the NO release studies, these results indicate that the harder N-donor histidine ligand destabilizes the DNIU leading to its eventual decomposition into Fe^{III} and NO, a conclusion that was corroborated by the data collected in the Griess assay and intracellular NO fluorescence probes (Figure IV-24).

In contrast to histidine, the rate of NO release is decreased when GSH is used as the exogenous cleaving ligand. The softer thiolates of glutathione and thioglucose are better suited for stabilization of the electronically diffuse DNIU. As implicated from the

combination of FT-IR, EPR and MS, glutathione also cleaves SGlucRRE. In addition to the monomeric DNICs, dimeric RRE-type DNICs with mixed thiolates were also detected by MS. This observation is taken as evidence for dimeric DNICs reforming after cleavage by the exogenous thiol. This same stabilizing effect that glutathione has on the DNIU was observed in the Griess assay and the intracellular NO probe. As more GSH was added to SGlucRRE, less NO was detected.

By comparing the NO release rate from SGlucRRE treated with GSH (gradual decrease in NO detected intracellularly) to SGlucRRE treated with ascorbate (which results in complete loss of intracellular NO), it can be concluded that this decrease in NO release in this study can be attributed to the coordinative interactions between glutathione and the DNIU. Reduction may play a part in the intracellular decomposition of SGlucRRE, due to the elevated intracellular concentration of endogenous glutathione, but there are still questions surrounding the role of DNIU redox level related to the liberation of NO and transport of DNICs in biology.

In the current study, we find that both the histidine and glutathione cleaved SGlucRRE produce monomeric DNICs that deliver NO into the cytosol. Nitric oxide is released in the cytosol at higher concentrations at earlier time-points when the histidine is the additive to smooth muscle cells, but NO release is depressed upon treatment with glutathione. The significant increase in intracellular NO begins at 1900 s, but converges back to the untreated SGlucRRE after a little more than an hour (3200-4100 s). An excess of GSH has an even more drastic effect on the amount of NO that is delivered into the

cytosol of SMCs from SGlucRRE when compared to those treated with histidine. Stoichiometric GSH treatments with SGlucRRE is largely the same as untreated SGlucRRE. However, as more exogenous GSH is added, significantly less intracellular NO is detected. This could be due to the combination of exogenous and endogenous GSH imparting stabilizing to the DNIC, slowing its NO release. Additionally, it appears that the decrease in NO release in the cytosol upon glutathione treatment is not solely because of reduction, and more than likely occurs through some combination of coordination to iron and reduction by glutathione once inside the cytosol (Figure IV-24). On the other hand, there are ubiquitously expressed export systems for glutathione complexes that involve both Glutathione transferase (GST) and Multidrug Resistance Protein 1 (MRP1); either or both could be ultimately responsible for the drastic decrease in intracellular NO upon treatment with exogenous GSH.[50,51]

This data further supports the hypothesis by Vanin, et al., based on EPR evidence that endogenous thiolates and the DNIU establish an equilibrium between dimeric RRE-type DNICs and monomeric DNICs.[20] Importantly, by working with isolated and well characterized DNICs, we can conclude that the known interrelation results of the CIP, NO and GSH can be explained by the transport of intact DNICs.[17,50-55] Ruuge et al.[29] reported that DNICs, not GSH or NO, protected red blood cells from lysing by abrogating oxidative stress and inflammation. This interrelation between Fe, NO, and GSH was also observed by Richardson, et al.[13,21,53,55] who reported that inhibition of GSH synthesis resulted in loss of DNIC efflux from cells via MRP1; they postulated that intracellular DNIC

concentrations were responsible for NO storage, transport, and generation. To reinforce this hypothesis, the only known crystal structure of a DNIC bound to a protein was reported when Ricci, et al.[56] published their structure of GST P1-1.[57] Taken altogether we conclude that when smooth muscle cells are presented with a synthetic, RRE-type DNIC, the NO and the Fe in the DNIC are incorporated into the cell's interrelated pathways with the aid of endogenously produced glutathione.

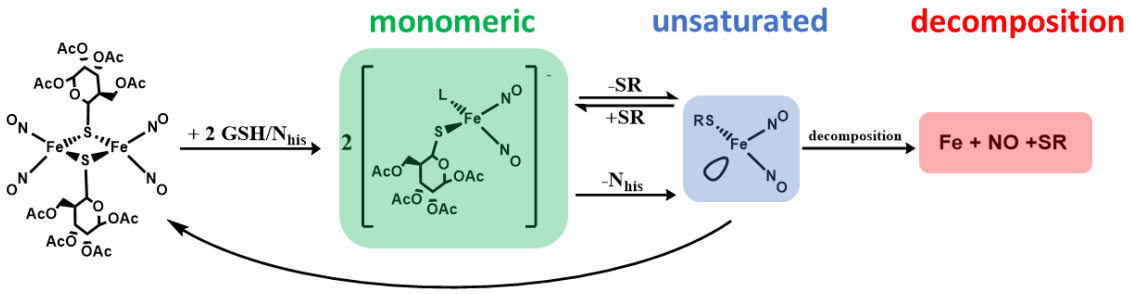

Figure IV-24: Putative mechanism of the SGlucRRE reactivity with the two biological ligands used in this study. Green indicates the cleaved monomer that is generated upon treatment with ligand, blue is complex with one of the ligands from the cleaved state dissociated, and the red is the decomposition of the complex to liberate NO. SR = 1-thio β-D-Glucose tetraacetate or glutathione; L = Histidine or Glutathione.
.

IV.9 Conclusions

This investigation in search of an active NO release molecule demonstrated that a stable, synthetic, dimeric RRE-type DNIC, SGlucRRE, readily reacts with glutathione and histidine to form cleaved monomeric DNICs. These same monomeric DNICs are likely formed when the intact RRE reacts in the cytosol with endogenously available glutathione or with the histidine in DMEM/F12. These DNIC complexes are hypothesized to be the active intracellular NORMs. The NO-release rate of this new NORM is altered by the

addition of an exogenous ligand. When treated with greater than 10 equivalents or more of histidine, NO is released faster in the cytosol and into the media due to cleavage of the dimeric RRE DNIC and the instability of the resultant His-DNIC monomer. Conversely, when treated with 10 equiv. or more of glutathione, NO is more slowly released due to the ability of GSH to stabilize the DNIU through binding to iron and reforming mixed thiolate RRE-DNICs. This result could also be attributed to the SMCs' innate machinery that identifies and stabilizes DNIC-GSH complexes. Our work highlights the complexities and strengths of metal coordination complexes as potential therapeutics since the efficacy of a metallodrug can be drastically altered with intentional ligand substitution *in vitro*.

IV.10 References

1. Förstermann, U.; Sessa, W. C. Nitric Oxide Synthases: Regulation and Function. *Eur. Heart J.* **2012**, *33*, 829–837.
2. Leon, L.; Jeannin, J.-F.; Bettaieb, A., Post-translational modifications induced by nitric oxide (NO): Implication in cancer cells apoptosis. *Nitric Oxide* **2008,** *19* (2), 77-83.
3. Carpenter, A. W.; Schoenfisch, M. H., Nitric Oxide Release Part II. Therapeutic Applications. *Chem. Soc. Rev.* **2012,** *40* (10), 3742-3752.
4. Zhao, Y.; Brandish, P. E.; Ballou, D. P.; Marletta, M. A.; Howard; Walsh, C. T., A molecular basis for nitric oxide sensing by soluble guanylate cyclase. *Proc. Natl. Acad. Sci.* **1999,** *96* (26), 14753-14758.

5. Schiewer, C. E.; Müller, C. S.; Dechert, S.; Bergner, M.; Wolny, J. A.; Schünemann, V.; Meyer, F., Effect of Oxidation and Protonation States on [2Fe−2S] Cluster Nitrosylation Giving $\{Fe(NO)_2\}^9$ Dinitrosyl Iron Complexes (DNICs). *Inorg. Chem.* **2018,** *58*, 769-784.

6. Rogers, P. A.; Eide, L.; Klungland, A.; Ding, H., Reversible inactivation of E. coli endonuclease III via modification of its [4Fe-4S] cluster by nitric oxide. *DNA Repair* **2003,** *2*, 809-817.

7. Giuc Tran, N.; Kalyvas, H.; Skodje, K. M.; Hayashi, T.; Moënne-Loccoz, P.; Callan, P. E.; Shearer, J.; Kirschenbaum, L. J.; Kim, E., Phenol Nitration Induced by a $\{Fe(NO)_2\}^{10}$ Dinitrosyl Iron Complex. *J. Am. Chem. Soc.* **2011,** *133* (5), 1184-1187.

8. Chen, L.; Liu, P.; Gao, H.; Sun, B.; Chao, D.; Wang, F.; Zhu, Y.; Hedenstierna, G.; Wang, C. G. Inhalation of Nitric Oxide in the Treatment of Severe Acute Respiratory Syndrome: A Rescue Trial in Beijing. *Clin. Infect. Dis.* **2004**, *39*, 1531–1535.

9. Akerstrom, S.; Gunalan, V.; Keng, C. T.; Tan, Y.-J.; Mirazimi, A. Dual Effect of Nitric Oxide on SARS-CoV Replication: Viral RNA Production and Palmitoylation of the S Protein Are Affected. *Virology* **2009**, *395*, 1–9.

10. Lai, M.-Y.; Chu, S.-M.; Lakshminrusimha, S.; Lin, H.-C.; Lin, H.-C. Beyond the Inhaled Nitric Oxide in Persistent Pulmonary Hypertension of the Newborn. *Pediatr. Neonatol.* **2018**, *59*, 15–23.

11. Ignarro, L. J.; Fukuto, J. M.; Griscavage, J. M.; Rogers, N. E.; Byrns, R. E. Oxidation of nitric oxide in aqueous solution to nitrite but not nitrate: Comparison with enzymatically formed nitric oxide from L-arginine. *Proc. Natl. Acad. Sci.* **1993**, *90*, 8103-8107.

12. Thomas, D. D.; Liu, X.; Kantrow, S. P.; Lancaster, J. R. The Biological Lifetime of Nitric Oxide: Implications for the Perivascular Dynamics of NO and O_2. *Proc. Natl. Acad. Sci.* **2001**, *98* (1) 355-360.

13. Truzzi, D. R.; Augusto, O.; Iretskii, A. V.; Ford, P. C., Dynamics of Dinitrosyl Iron Complex (DNIC) Formation with Low Molecular Weight Thiols. *Inorg. Chem.* **2019,** *50*, 13446-13456.

14. Lok, H. C.; Sahni, S.; Jansson, P. J.; Kovacevic, Z.; Hawkins, C. L.; Richardson, D. R., A Nitric Oxide Storage and Transport System That Protects Activated Macrophages from Endogenous Nitric Oxide Cytotoxicity. *J. Biol. Chem.* **2016,** *291* (53), 27042-27061.

15. Wynia-Smith, S. L.; Smith, B. C. Nitrosothiol Formation and S-Nitrosation Signaling through Nitric Oxide Synthases. *Nitric Oxide* **2017**, *63*, 52–60.

16. Keszler, A.; Diers, A. R.; Ding, Z.; Hogg, N., Thiolate-based bidinitrosyl iron complexes: Decomposition and detection and differentiation from S-nitrosothiols. *Nitric Oxide* **2017,** *65*, 1-9.

17. Bosworth, C. A.; Toledo Jr., J. C.; Zmijewski, J. W.; Li, Q.; Lancaster Jr., J. R. Dinitrosyliron Complexes and the Mechanism(s) of Cellular Protein Nitrosothiol Formation from Nitric Oxide. *Proc. Natl. Acad. Sci.* **2009**, *106* (12), 4671–4676.

18. Hickok, J. R.; Sahni, S.; Shen, H.; Arvind, A.; Antoniou, C.; Fung, L. W. M.; Thomas, D. D., Dinitrosyliron complexes are the most abundant nitric oxide-derived cellular adduct: biological parameters of assembly and disappearance. *Free Radic. Biol. Med.* **2011,** *51*, 1558-1566.

19. Vanin, A. F., Dinitrosyl Iron Complexes with Thiol-containing Ligands as a Base for New-Generation Drugs. *Open Conf. Proc. J.* **2013,** *4*, 47-53.

20. Vanin, A. F., Dinitrosyl iron complexes with thiol-containing ligands as a "working form" of endogenous nitric oxide. *Nitric Oxide* **2016,** *54*, 15-29.

21. Hawkins, N.; Ponka, C.; Richardson, P., Nitrogen Monoxide (NO) Storage and Transport by Dinitrosyl-Dithiol-Iron Complexes: Long-lived NO That Is Trafficked by Interacting Proteins. *J. Biol. Chem* **2012,** *287* (10), 6960-6968.

22. Enemark, J. H.; Feltham, R. D. Principles of Structure, Bonding, and Reactivity for Metal Nitrosyl Complexes. *Coord. Chem. Rev.* **1974**, *13* (4), 339–406.

23. Ye, S.; Neese, F. The Unusual Electronic Structure of Dinitrosyl Iron Complexes. *J. Am. Chem. Soc.* **2009**, *132*, 3646–3647.

24. Pectol, D.; Khan, S.; Chupik, R.; Elsabahy, M.; Wooley, K.; Darensbourg, M.; Lim, S.-M., Toward the Optimization of Dinitrosyl Iron Complexes as

Therapeutics for Smooth Muscle Cells. *Molecular Pharmaceutics* **2019,** *16* (7), 3178-3187.

25. Pulukkody, R.; Chupik, R. B.; Montalvo, S. K.; Khan, S.; Bhuvanesh, N.; Lim, S.-M.; Darensbourg, M. Y., Toward biocompatible dinitrosyl iron complexes: sugar-appended thiolates. *Chem. Commun* **2017,** *53*, 1180-1183.

26. Chen, Y.-J.; Ku, W.-C.; Feng, L.-T.; Tsai, M.-L.; Hsieh, C.-H.; Hsu, W.-H.; Liaw, W.-F.; Hung, C.-H.; Chen, Y.-J. Nitric Oxide Physiological Responses and Delivery Mechanisms Probed by Water-Soluble Roussin's Red Ester and $\{Fe(NO)_2\}^{10}$ DNIC. *J. Am. Chem. Soc.* **2008**, *130*, 10929–10938.

27. Remizova, M. I.; Kochetygov, N. I.; Gerbout, K. A.; Lakomkin, V. L.; Timoshin, A. A.; Burgova, E. N.; Vanin, A. F. Effect of Dinitrosyl Iron Complexes with Glutathione on Hemorrhagic Shock Followed by Saline Treatment. *Eur. J. Pharmacol.* **2011**, No. 662, 40–46.

28. Vanin, A. F., Dinitrosyl Iron Complexes with Thiol-Containing Ligands as a Base for Developing Drugs with Diverse Therapeutic Activities: Physicochemical and Biological Substantiation. *Biophysics* **2017,** *62* (4), 629-656.

29. Shumaev, K. B.; Gorudko, I. V.; Kosmachevskaya, O. V.; Grigorieva, D. V.; Panasenko, O. M.; Vanin, A. F.; Topunov, A. F.; Terekhova, M. S.; Sokolov, A. V.; Cherenkevich, S. N.; Ruuge, E. K., Protective Effect of Dinitrosyl Iron Complexes with Glutathione in Red Blood Cell Lysis Induced by Hypochlorous Acid. *Oxid. Med. Cell. Longev.* **2019**. 1-12.

30. Jones, M. W.; Powell, D. R.; Richter-Addo, G. B. Synthesis, Characterization, and Fiber-Optic Infrared Reflectance Spectroelectrochemical Studies of Some Dinitrosyl Iron Diphosphine Complexes $Fe(NO)_2L_2$ (L = $P(C_6H_4X)_3$). *J. Organomet. Chem.* **2014**, *754*, 63–74.

31. Speelman, A. L.; Zhang, B.; Silakov, A.; Skodje, K. M.; Alp, E. E.; Zhao, J.; Hu, M. Y.; Kim, E.; Krebs, C.; Lehnert, N. Unusual Synthetic Pathway for an $\{Fe(NO)_2\}^9$ Dinitrosyl Iron Complex (DNIC) and Insight into DNIC Electronic Structure via Nuclear Resonance Vibrational Spectroscopy. *Inorg. Chem.* **2016**, *55*, 5485–5501.

32. Tinberg, C. E.; Tonzetich, Z. J.; Wang, H.; Do, L. H.; Yoda, Y.; Cramer, S. P.; Lippard, S. J. Characterization of Iron Dinitrosyl Species Formed in the Reaction of Nitric Oxide with a Biological Rieske Center. *J. Am. Chem. Soc* **2010**, *132*, 18168–18176.

33. Lu, C.-Y.; Liaw, W.-F., Formation Pathway of Roussin's Red Ester (RRE) via the Reaction of a $\{Fe(NO)_2\}^{10}$ Dinitrosyliron Complex (DNIC) and Thiol: Facile Synthetic Route for Synthesizing Cysteine-Containing DNIC. *Inorganic Chemistry* **2013,** *52*, 13918-13926.

34. Vanin, A. F., Dinitrosyl iron complexes with thiolate ligands: Physico-chemistry, biochemistry and physiology. *Nitric Oxide.* **2009**, *21*, 1-13.

35. Vanin, A. F.; Borodulin, R. R.; Mikoyan, V. D., Dinitrosyl iron complexes with natural thiol-containing ligands in aqueous solutions: Synthesis and some physico-chemical characteristics (A methodological review). *Nitric Oxide*. **2017**, *66*, 1-9.

36. Cho, S.-L. L., Cheng-Jhe; Lu, Tsai-Te, Synthetic Methodology for Preparation of Dinitrosyl Iron Complexes. *J. Bio. Inorg. Chem.* **2019,** *24*, 495-515.

37. Tsai, M.-L.; Hsieh, C.-H.; Liaw, W.-F., Dinitrosyl Iron Complexes (DNICs) Containing S/N/O Ligation: Transformation of Roussin's Red Ester into the Neutral $\{Fe(NO)_2\}^{10}$ DNICs. *Inorg. Chem.* **2007,** *46*, 5110-5117.

38. Lewandowska, H.; Stepkowski, T. M.; Sadło, J.; Wójciuk, G. P.; Wójciuk, K. E.; Rodger, A.; Kruszewski, M., Coordination of iron ions in the form of histidinyl dinitrosyl complexes does not prevent their genotoxicity. *Bioorg. Med. Chem.* **2012**, *20*, 6732-6738.

39. Hu, H.; Gu, Y.; Xu, L.; Zou, Y.; Wang, A.; Tao, R.; Chen, X.; Zhao, Y.; Yang, Y., A genetically encoded toolkit for tracking live-cell histidine dynamics in space and time. *Sci. Rep.* **2017,** 7: 43479.

40. Deponte, M., The Incomplete Glutathione Puzzle: Just Guessing at Numbers and Figures? *Antioxid. Redox Signal.* **2017,** *27* (15), 1130-1161.

41. Kumar, C.; Igbaria, A.; D'Autreaux, B.; Planson, A.-G.; Junot, C.; Godat, E.; Bachhawat, A. K.; Delaunay-Moisan, A.; Toledano, M. B., Glutathione revisited: a vital function in iron metabolism and ancillary role in thiol-redox control. *EMBO J.* **2011,** *30* (10), 2044-2056.

42. Tsai, M.-L.; Tsou, C.-C.; Liaw, W.-F. Dinitrosyl Iron Complexes (DNICs): From Biomimetic Synthesis and Spectroscopic Characterization toward Unveiling the Biological and Catalytic Roles of DNICs. *Acc. Chem. Res.* **2015**, *48*, 1184–1193.

43. Fitzpatrick, J.; Kim, E. Synthetic Modeling Chemistry of Iron−Sulfur Clusters in Nitric Oxide Signaling. *Acc. Chem. Res* **2015**, *48*.

44. Klencsár, Z.; Köntös Z. EPR Analysis of Fe^{3+} and Mn^{2+} Complexation Sites in Fulvic Acid Extracted from Lignite. *J. Phys. Chem. A.* **2018**, *122*, 3190–3203.

45. Miano, T.; Provenzano, M.; Brunetti, G. Reference and Standard Fulvic and Humic Acids of Various Origin. *Sci. Total Environ.* **1989**, *81*, 143–156.

46. Przybyło, M.; Langner, M. On the Physiological and Cellular Homeostasis of Ascorbate. *Cell. Mol. Biol. Lett.* **2020**, *25* (32), 1–17.

47. Tu, Y.-J.; Njus, D.; Schlegel, H. B. Organic & Biomolecular Chemistry A Theoretical Study of Ascorbic Acid Oxidation and $HOO^{\bullet}$ /$O_2^{\bullet-}$ Radical Scavenging. *Org. Biomol. Chem.* **2017**, *15*, 4417.

48. Buchner, F.; Seufert, K.; Auwä, W.; Heim, D.; Barth, J. V; Flechtner, K.; Gottfried, J. M.; Steinrü, H.-P.; Marbach, H. NO-Induced Reorganization of Porphyrin Arrays. *ACS Nano* **2009**, *3* (7), 1789–1794.

49. Shiba, S.; Yamada, K.; Matsuguchi, M. Humidity-Resistive Optical NO Gas Sensor Devices Based on Cobalt Tetraphenylporphyrin Dispersed in Hydrophobic Polymer Matrix. *Sensors* **2020**, *20* (1295).

50. Hawkins, N.; Ponka, C.; Richardson, P., Nitrogen Monoxide (NO) Storage and Transport by Dinitrosyl-Dithiol-Iron Complexes: Long-lived NO That Is Trafficked by Interacting Proteins. *J. Biol. Chem* **2012,** *287* (10), 6960-6968.

51. Lok, H. C.; Sahni, S.; Jansson, P. J.; Kovacevic, Z.; Hawkins, C. L.; Richardson, D. R., A Nitric Oxide Storage and Transport System That Protects Activated Macrophages from Endogenous Nitric Oxide Cytotoxicity. *J. Biol. Chem.* **2016,** *291* (53), 27042-27061.

52. Adamyan, L. V.; Burgova, E. N.; Tkachev, N. A.; Mikoyan, V. D.; Stephanyan, A. A.; Sonova, M. M.; Galkin, A. V.; Vanin, A. F., Dinitrosyl Iron Complexes with Glutathione Largely Relieve Rats of Experimental Endometriosis. *Biophysics* **2013,** *58* (2), 222-227.

53. Burgova, E. N.; Tkachev, N. A.; Adamyan, L. V.; Mikoyan, V. D.; Paklina, O. V.; Stepanyan, A. A.; Vanin, A. F., Dinitrosyl iron complexes with glutathione suppress experimental endometriosis in rats. *Eur. J. Pharmacol.* **2014,** *727* (1), 140-147.

54. Van Faassen, E.; Vanin, A. F., Radicals for Life: The Various Forms of Nitric Oxide. Van Faassen, E.; Vanin, A. F., Eds. Elsevier B. V.: 2007; 9-73.

55. Lewandowska, H.; Sadło, J.; Męczyńska, S.; Stępkowski, T. M.; Wójciuk, G.; Kruszewski, M., Formation of glutathionyl dinitrosyl iron complexes protects against iron genotoxicity. *Dalton Transactions* **2015,** *44*, 12640-12640.

56. De Maria, F.; Pedersen, J. Z.; Maria Caccuri, A.; Antonini, G.; Turella, P.; Stella, L.; Lo Bello, M.; Federici, G.; Ricci, G. The Specific Interaction of Dinitrosyl-Diglutathionyl-Iron Complex, a Natural NO Carrier, with the Glutathione Transferase Superfamily: Suggestion for an Evolutionary Pressure in the Direction of the Storage of Nitric Oxide. *J. Biol. Chem.* **2003**. *276* (48), 42283-42293.

57. Cesareo, E.; Parker, L. J.; Pedersen, J. Z.; Nuccetelli, M.; Mazzetti, A. P.; Pastore, A.; Federici, G.; Caccuri, A. M.; Ricci, G.; Adams, J. J.. Nitrosylation of Human Glutathione Transferase P1-1 with Dinitrosyl Diglutathionyl Iron Complex in Vitro and in Vivo. *J. Biol. Chem.* **2005**, *280* (51), 42172–42180.

CHAPTER V : DETERMINING METHOD OF INHIBITION OF SARS-COV-2 VIRAL REPLICATION FOR RRE DNICS

V.1 Introduction

Based on the viral genome of SARS-CoV-2 (SC2), there are a number of druggable chokepoints that can prevent the virus from replicating properly; the chymotrypsin-like main protease (nsp5/M^{pro}) is one of those targets.[1-2] Fortunately, homologous cysteine proteases with high sequence similarity (> 80%) are expressed in other viruses and therapeutics have previously been investigated for the SARS, MERS, Hepatitis E, Ebola, and other variations of this protease.[3-5] The protease specific to COVID-19 has a catalytic dyad that consists of a cysteine and histidine which work in concert to cleave the viral peptide chain synthesized at the host cell ribosomes to generate the proteins necessary for viral replication. Inhibitors for this complex can inactivate the enzyme by covalent attachment of an electron acceptor (e.g., an epoxide or Michael acceptor) to the catalytic thiolate in the active site, by outcompeting the substrate for binding at the active site, or via allosteric inhibition.[6-10] One intriguing study involved the use of Zn(toluene-dithiolate) coordination complexes as inhibitors.[11] The metal-containing inhibitor coordinated to the catalytic His-Cys dyad, rendering the enzyme inactive.

Dinitrosyl Iron Complexes (DNICs), contain $Fe(NO)_2$ units, typically with two additional donor ligands, including anionic thiolates and neutral N-donors such as imidazoles, thus rendering the iron in a tetrahedral environment.[12] Dinitrosyl iron complexes have been explored as therapeutics for many NO-related disease states where NO homeostasis is likely important; these include diabetic wound healing, erectile

dysfunction, and asthma, amongst others.[13-20] DNICs have been identified as degradation products from addition of NO to iron-sulfur clusters.[21] The known stability (relative to RSNOs and free NO) of the dinitrosyl iron unit (DNIU), which is capable of transfer from one donor ligand to another, is key to its identification as the working form of NO in physiology. The iron in the DNIU is regarded as a coordinatively unsaturated electropositive center which has been shown to attract myriad donor ligands, including *N*- and *S*- donors. Figure V-1 displays the potential for dimeric DNICs to provide a DNIU for coordinative to one or both of the Cys/His dyad of M^{pro}.

The most promising lead for a DNIC-based therapeutic was identified as a dimeric DNIC with thioglucosetetraacetate bridging ligands (TGTA-RRE), of formula $[(\mu\text{-TGTA})Fe(NO)_2]_2$ (TGTA = 1-thio-β-d-glucose tetraacetate), that enhanced concentrations of NO (relative to endogeneous) for up to 24. The dimeric DNIC abrogated the cytotoxicity of the DNIU with IC_{50}'s from 20 – 210 μM in *in vitro* tissue culture. Out of an array of 26 cytokines, TGTA-RRE minimally induced RANTES (T-cell recruitment) and TNF-α (apoptosis).[22] Furthermore, treatment of TGTA-RRE with biological sources of thiols and imidazoles, namely glutathione and histidine, led to the cleavage of the dimer generating $[(TGTA)(N_{His})Fe(NO)_2]^0$ and $[(TGTA)(GS)Fe(NO)_2]^-$.[23] Herein we pursue a reliable foundation for repurposing DNIC-based therapeutics as potential $SC2M^{pro}$ inhibitors.

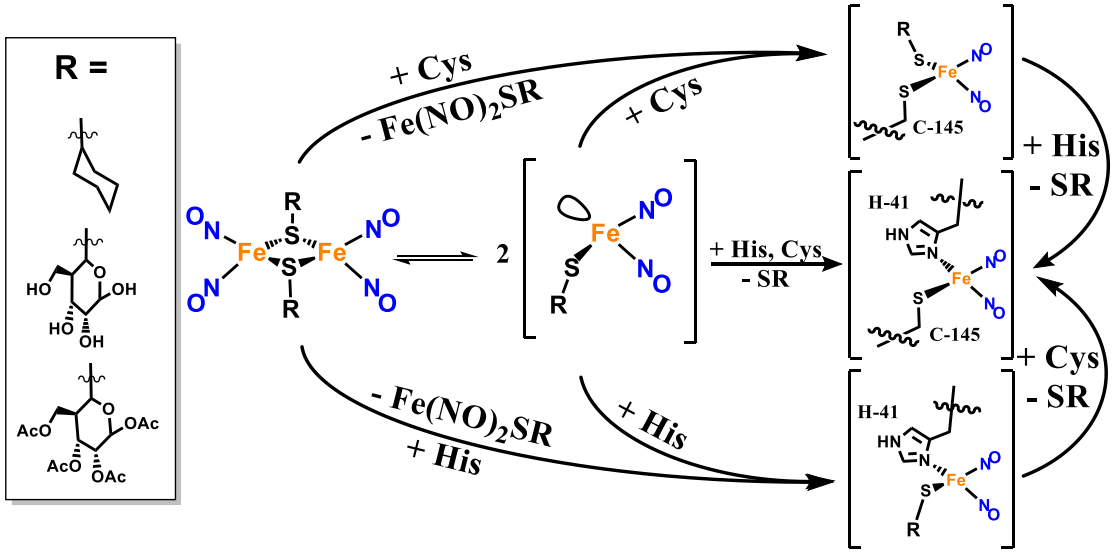

Figure V-1: Outline of potential modes of inhibition for a DNIC-based SC2Mpro therapeutic. [Left] R-groups used to generate the DNICs used in this study. The dimeric DNICs (TGTA-RRE, TG-RRE, and SCy-RRE), unsaturated monomeric DNICs (TGTA-m, TG-m, and SCy-m), and free ligands (TGTA, TG, and SCy) were evaluated *in silico* as potential inhibitors. [Right] Postulated mechanisms for inhibition of $SC2M^{pro}$ by DNICs. SR corresponds to the three different thiolate groups shown in the left panel.. Solvent or a weakly coordinating ligand in the cellular milieu occupies the vacant site on the monomeric SR DNIC in the center. His-41 and Cys-145 are the residues that constitute the catalytic dyad in $SC2M^{pro}$.

Key to providing a fundamental computational base for our study is a protein crystal structure in 2005 that established the binding pocket of glutathione transferase could accept a glutathione-$Fe(NO)_2$ adduct upon ligand displacement by a tyrosine *O*-donor at the active site, forming a tetrahedral DNIC.[24] This ternary protein-ligand-DNIU complex provides validation for computational studies of the binding of a DNIC to the $SC2M^{pro}$ active site pocket and inspires this *in vitro* study of a series of DNICs as inhibitors for M^{pro}. Computational modelling of the interaction of intact DNIC dimer, and the cleaved monomer, for three DNIC derivatives, TGTA-RRE, thioglucose TG-RRE, and and cyclohexyl (SCy-RRE) groups with the $SC2M^{pro}$ was carried out using the well-

known molecular simulation computational package, AutoDock.[25] A FRET assay for the protease activity *in vitro* was used to experimentally interrogate the most promising DNIC leads derived from the *in silico* studies.[26]

V.2 Validation of peptidic substrate with *in silico* chemistry:

Computational protein docking programs such as AutoDock, and its derivative software suites, including AutoDock4.2.6, MGLTools-1.5.6, CADD – 1.5.6, and PMV-1.5.6, which uses a free energy force field that accounts for dispersive, electrostatic, hydrogen bonding, and desolvation energies, have guided development of covalent drugs as inhibitors of proteases including $SC2M^{pro}$. The presumption of DNIC-based $SC2M^{pro}$ inhibition is that the intact DNIC migrates to the active site and outcompetes the substrate for binding. To properly make that comparison using AutoDock, the final docked energies of the DNICs are compared to that of the peptidic substrate. Obtaining a crystal structure of the natural substrate of the protease docked at the active site is nigh impossible since the peptide chains are designed to be cleaved by the enzyme. In lieu of this, truncated peptidic chains based on a commercially available FRET protease activity probe (FRET probe peptide: DABCYL-Lys-Thr-Ser-Ala-Val-Leu-Gln-Ser-Gly-Phe-Arg-Lys-Met-Glu-EDANS; computational peptides: Val-Lys-Gln-Ser [VLQS] and Ala-Val-Lys-Gln-Ser [AVLQS]) were computationally docked into the active site using the parameters listed in the experimental section (Figure V-2). The final binding energies of these poses are as follows: -8.21 kcal/mol for VLQS, -7.46 kcal/mol for AVLQS. Such results provide useful references as to the association of residue sidechains with subsections of the

substrate binding pocket; as well it indicates the feasibility of AutoDock predictions of organic molecule binding poses.[26-27] The S2 and S3 clefts are well fitted to interact with the larger hydrophobic groups on the Leu, and Val sidechains. The S1 pocket is narrower and contains H-bonding partners for glutamine, and the size of the S1' pocket prohibits occupation by anything larger than a serine.

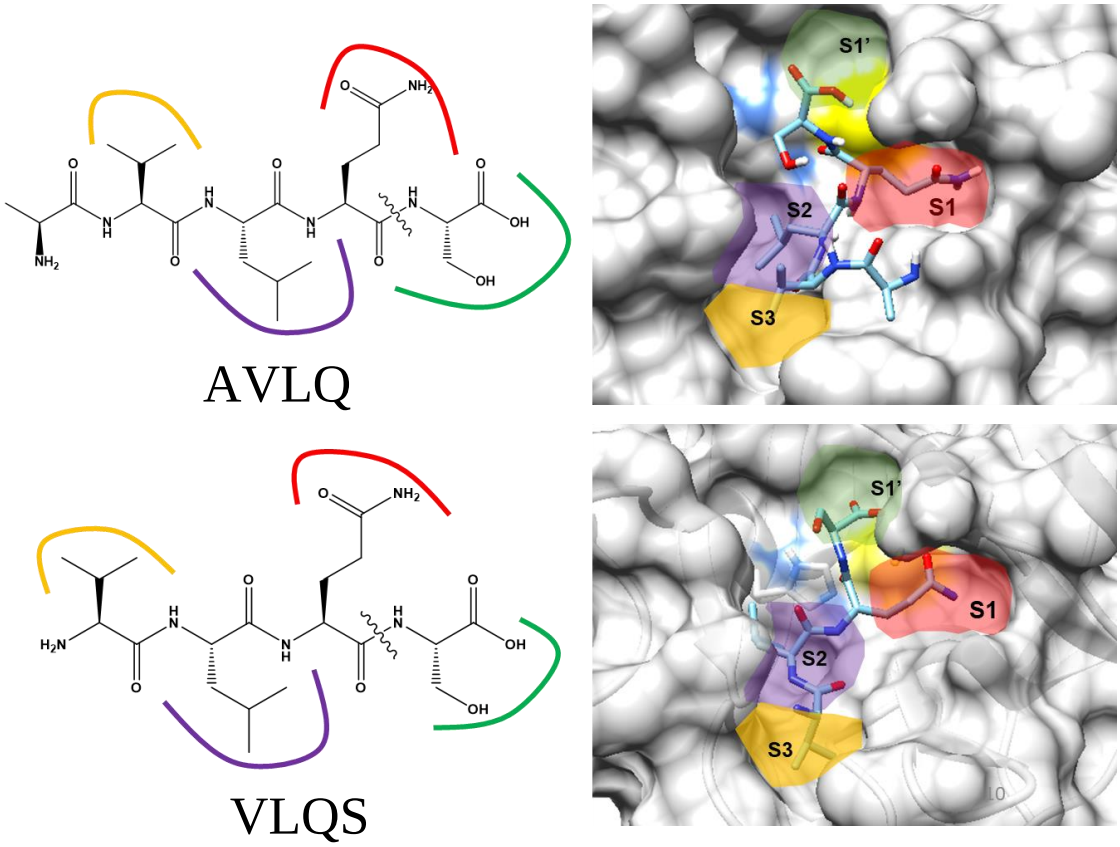

Figure V-2: Computational docking of peptidic substrates to the active site of the SARS-CoV-2 main protease (PDB: 6W63). [Left] The peptides, their single letter abbreviations, and their corresponding binding pockets as determined by the *in silico* docking (colored arcs which correspond to the shaded areas in the images on the right) are shown. [Right] Likely binding poses generated from AutoDock4 calculations to the moecular surface of the SC2M^{pro}. The peptide is shown in cyan, and the catalytic dyad of His_{41} (blue) and Cys_{145} (yellow) are labeled using their three letter designators.

V.3 Benchmarking coordinatively unsaturated DNIU's to GST P1-1 using AutoDock4

Although it has been demonstrated numerous times that AD4 works well for generating potential binding poses for molecular organic inhibitors, the accuracy of results from AD4 for predicting the electrostatic/covalent interactions between metal-containing inhibitors and proteins remains uncertain. It has been demonstrated that AD4 can reliably predict inhibitor binding poses of coordinatively saturated metal complexes in which the metal is completely encased in its ligand field with largely organic linkers available and susceptible to intermolecular interactions.[28-30] However, unsaturated metal centers where a reactive site on the metal is exposed does not respond to AutoDock as rigorously as other computational methods. Instead, the best result treats them as charged spheres which allows for metals to still participate in electrostatic interactions with the target protein surface, but does not take into account geometrical preference, orbital overlap, and other parameters associated with higher order computational methods.[32] Using AutoDock as a predictive tool for reactive metal fragments has been attempted with studies of Cu coordination complexes and showed association to the active site of $SC2M^{pro}$.[31] By truncating known crystal structures to generate "active" metal containing fragments, Karges, et al. were able to computationally model cysteinyl inhibition of $SC2M^{pro}$ with a Re^{I} tricarbonyl complex.[32] Applying that same approach to the DNICs used in this study, an *N*-heterocyclic carbene was truncated from a crystal structure obtained in our lab, [(1,3-

bis(2,4,6-trimethylphenyl)imidazolidine)Fe(NO)$_2$(1-thio-β-D-glucose tetraacetate)], to generate a tetrahedral DNIU with an apical vacancy.[33]

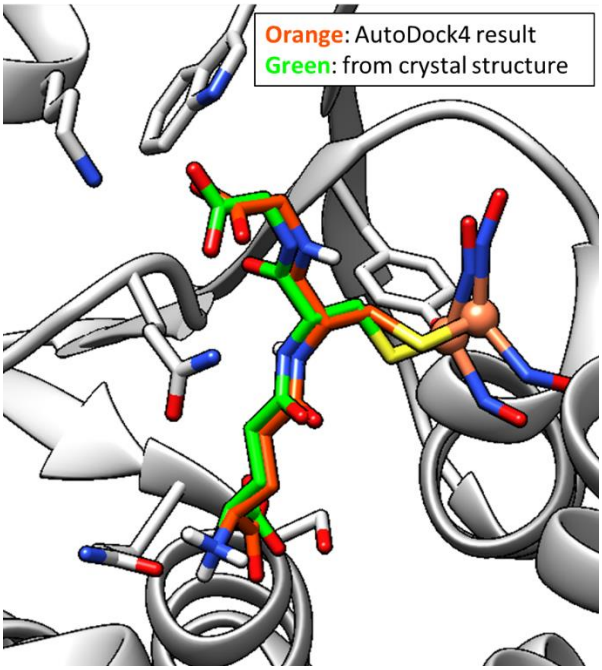

Figure V-3: Overlaid crystal structure of the glutathionyl DNIC (green) bound to GST P1-1 (grey)[24] and the results of the computational docking of the coordinatively unsaturated glutathionyl DNIC using the AutoDock methodology described previously (orange).

Using this modified approach, AutoDock4's ability to predict the protein-metal interactions a coordinatively unsaturated DNIC was benchmarked against the only protein crystal structure containing a DNIU: GST P1-1 (PDB: 1ZGN).[24] Although this method may not be as rigorous as other higher-order computational methods, in this case, as is demonstrated by Figure V-3, the relative simplicity of AutoDock is not a detriment to the resulting data. The DNIU is still situated within binding distance of Tyr$_7$ and the calculated root mean square difference (RMSD) of the DNIC fragment is 1.77 Å from the crystal structure (2.10 Å resolution). Based on this data, AutoDock is accepted as a

predictive tool for coordinatively unsaturated DNIC binding. This same methodology is used for the remainder of the monomeric DNIC calculations.

V.4 Computational docking of DNICs to the active site of SC2M^{pro}

For each of the DNICs, the Final Intermolecular Energy as calculated by AutoDock were compared for the free ligand, the monomeric DNIC, and the dimeric RRE DNICs contain TGTA, TG and SCy thiolates. Using the lowest energy binding pose for each scenario, the distance from the iron in the DNIU to the closest metal binding residue in the binding pocket was measured. For the ligands by themselves, they generally occupied the S2 and S3 pockets, around 7 Å away from the catalytic dyad with poor calculated Final Intermolecular Energies: -4.29, -4.51, and -2.78 kcal/mol for TGTA, TG, and SCy respectively, with almost no electrostatic contribution from the ligand (Figure V-4 &V-5).

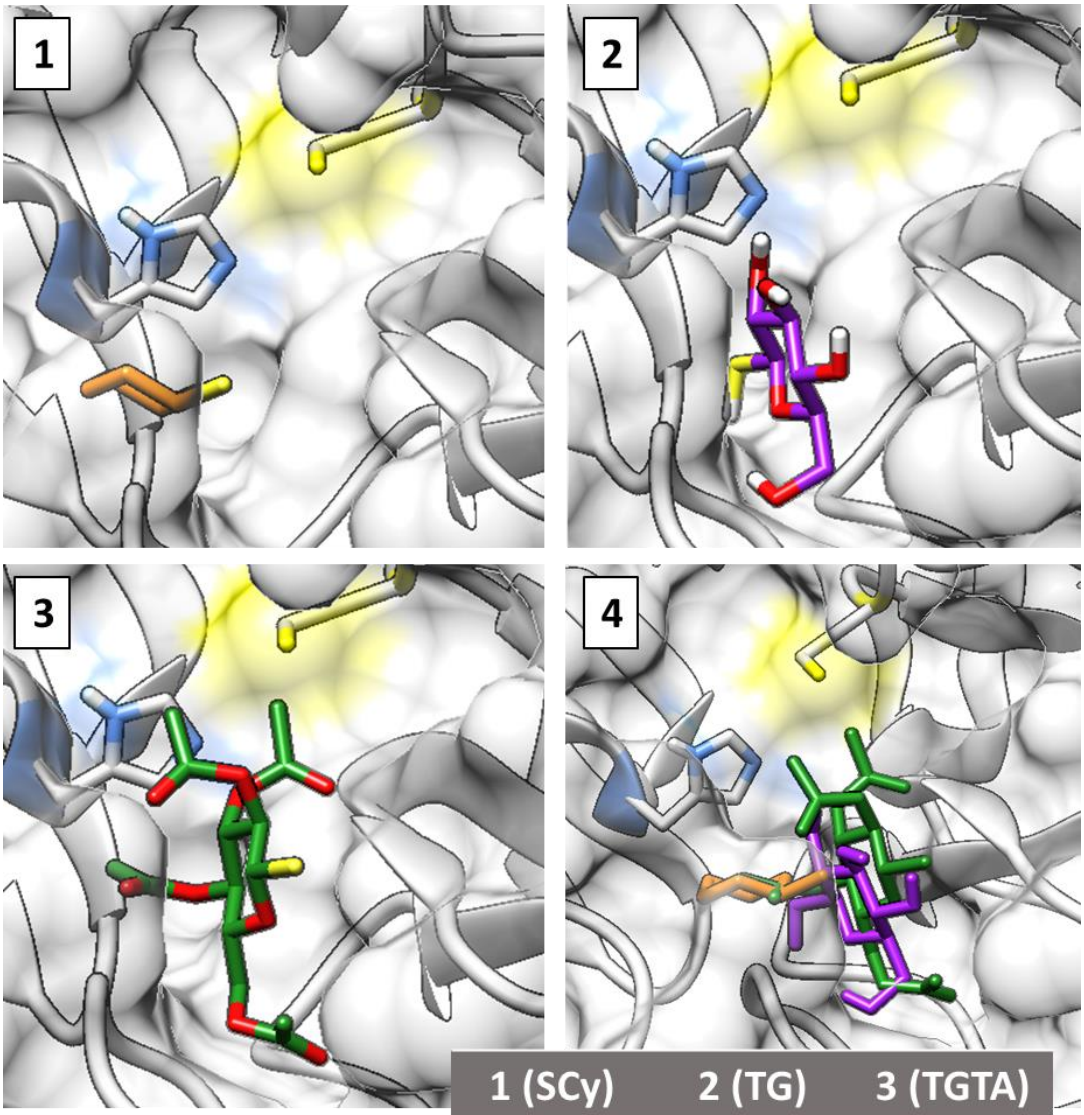

	1 (SCy)	2 (TG)	3 (TGTA)
Final Intermolecular Energy (kcal/mol)	-2.78	-4.51	-4.29

Figure V-4: Most favorable binding poses for the free ligands (1 – SCy, orange; 2 – TG, purple; 3 – TGTA, green) at the active site of SC2Mpro (PDB: 6W63). The final intermolecular energies for the displayed binding poses are given in the table below. All values are in kcal/mol. 4) Overlaid binding poses for the three free ligands emphasizing the fit to the S2 and S3 binding pockets.

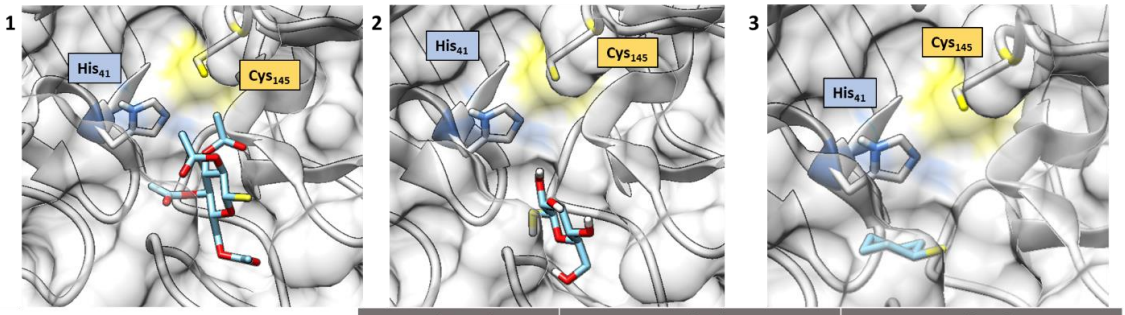

	1 (TGTA)	2 (TG)	3 (SCy)
Estimated Free Energy of Binding	-1.61 kcal/mol	-2.72 kcal/mol	-2.78 kcal/mol
Final Intermolecular Energy	-4.29 kcal/mol	-4.51 kcal/mol	-2.78 kcal/mol
vdW + Hbond + desolv Energ	-4.34 kcal/mol	-4.45 kcal/mol	-3.00 kcal/mol
Electrostatic Energy	+0.05 kcal/mol	-0.06 kcal/mol	+0.22 kcal/mol
Torsional Free Energy	+2.68 kcal/mol	+1.79 kcal/mol	0.00 kcal/mol

Figure V-5: Graphical representation of the binding poses with the lowest free energy generated using AutoDock4 for the free thiolate ligands, TGTA [1], TG [2], and SCy [3], to the active site of SC2Mpro (PDB: 6W63). The catalytic dyad of His41 (blue) and Cys145 (yellow) are labeled in [1, 2, 3]. Binding energies from the calculations are presented in the table below**.**

In the monomeric form, the 6-membered ring of the thiolate shifts to accommodate for the electrostatic interaction between the DNIU and Cys_{145}. For the SCy monomer, instead of occupying the S2 pocket as was the case with the free ligand, the monomeric SCy-m shifts to the S1 pocket (Figures V-6, V-7). The combination of dispersive (-3.88 kcal/mol) and electrostatic (-2.47 kcal/mol) interactions led to an enhancement in the binding energy compared to the ligand by itself. This same trend is seen for the monomeric TGTA-m, but the additional steric bulk on the ring leads to more complete occupation of the substrate binding pocket. As expected, this increase in interaction with the pocket decreases the total energy of binding (-7.72 kcal/mol for TGTA-m vs -6.36 for SCy-m). However, the addition of steric bulk does not always lead to a more favorable interaction with the substrate binding pocket. For TG-m, the addition of the DNIU to

thioglucose disrupted the fit of the free ligand in the S3 pocket. Unable to fit in the most favorable binding pocket for the ligand, the driving force of the interaction became the electrostatic interaction between Cys_{145} and the DNIU. This positioning of the DNIU drastically decreases the dispersive interaction between the TG and the binding pocket (-1.78 kcal/mol for TG-m vs. -4.45 for the free TG). Despite the differences in pocket occupation, each monomeric DNIU is positioned favorably for coordinative inhibition via coordination to Cys_{145} (Figure V-8).

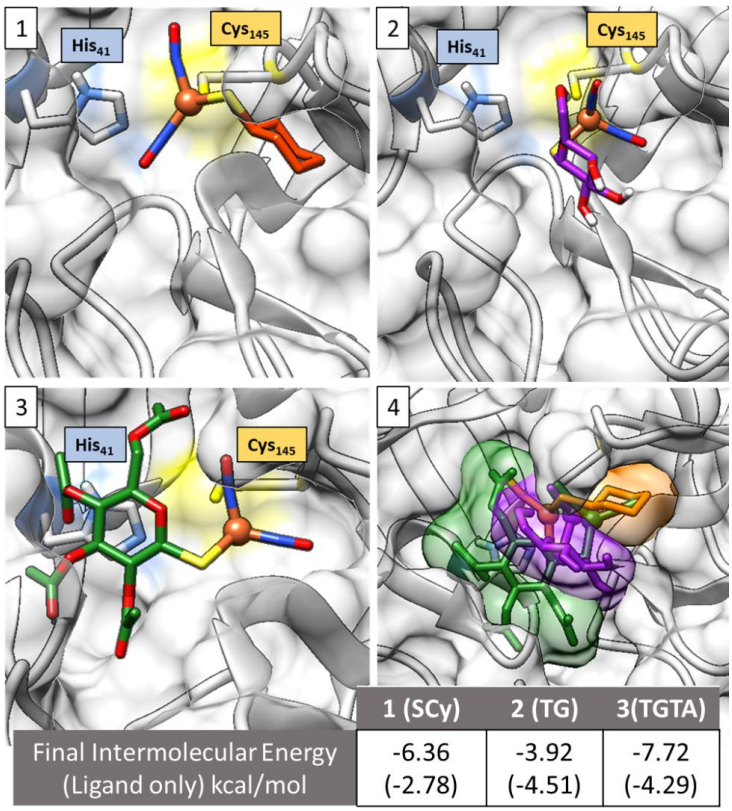

Final Intermolecular Energy (Ligand only) kcal/mol	1 (SCy)	2 (TG)	3(TGTA)
	-6.36 (-2.78)	-3.92 (-4.51)	-7.72 (-4.29)

Figure V-6: Most favorable binding poses for the monomeric DNICs (1 – SCy-DNIC, orange; 2 – TG-DNIC, purple; 3 – TGTA-DNIC, green) at the active site of SC2Mpro (PDB: 6W63). The final intermolecular energies for the displayed binding poses are given in the table below. All values are in kcal/mol, and the resulting energies for the docking of the free thiolate ligands are given in parenthesis. 4) Overlaid binding poses for the three monomeric DNICs emphasizing the fit to the substrate binding pocket by visualizing their calculated molecular surface.

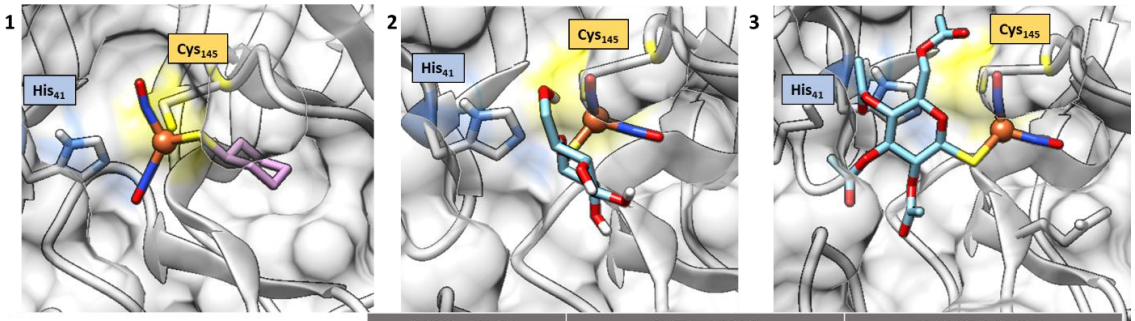

	1 (SCy-DNIC)	2 (TG-DNIC)	3 (TGTA-DNIC)
Estimated Free Energy of Binding	-5.46 kcal/mol	-1.53 kcal/mol	-4.13 kcal/mol
Final Intermolecular Energy	-6.36 kcal/mol	-3.92 kcal/mol	-7.71 kcal/mol
vdW + Hbond + desolv Energ	-3.88 kcal/mol	-1.78 kcal/mol	-6.46 kcal/mol
Electrostatic Energy	-2.47 kcal/mol	-2.14 kcal/mol	-1.25 kcal/mol
Torsional Free Energy	+0.89 kcal/mol	+2.39 kcal/mol	+3.58 kcal/mol

Figure V-7: Graphical representation of the binding poses with the lowest free energy generated using AutoDock4 for the monomeric DNICs, SCy-m [1], TG-m [2], and TGTA-m [3], to the active site of SC2Mpro (PDB: 6W63). The catalytic dyad of His41 (blue) and Cys145 (yellow) are labeled in [1, 2, 3]. Binding energies from the calculations are presented in the table below.

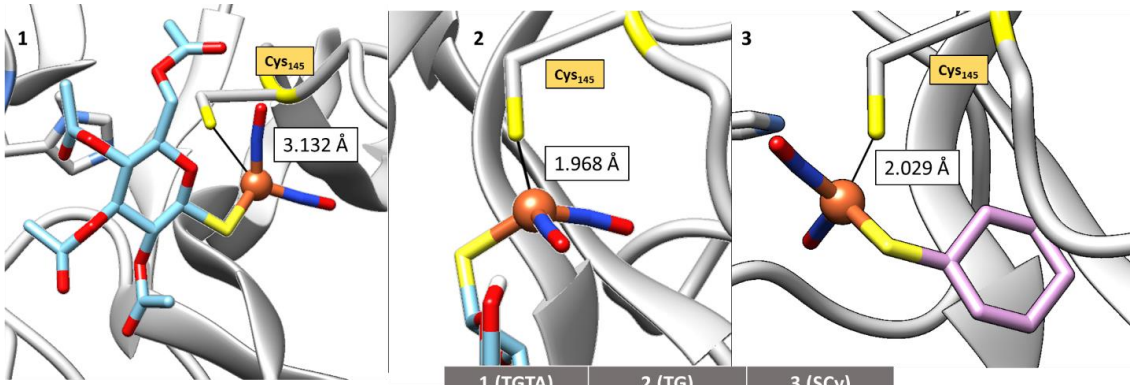

	1 (TGTA)	2 (TG)	3 (SCy)
Distance from Fe to S of Cys145	3.132 Å	1.968 Å	2.029 Å

Figure V-8: Relevant distances from the DNIU to Cys145 of SC2Mpro (PDB: 6W63) as obtained from the AutoDock4 calculations for the cleaved, monomeric DNICs TGTA (1) , TG (2), and SCy (3).

For the dimeric RRE-type DNICs, the identity of the 6-membered thiolate ring alters the general position of the DNIU in the substrate binding pocket (Figure V-9). The DNIUs were situated above the catalytic dyad for TGTA- and TG-RRE, approximately 3.7 Å away from Cys_{145} (Figure V-10). For SCy-RRE, just like in the monomeric case, one of the hydrophobic cyclohexyl groups is situated in the S2 pocket with the DNIU 6.6 Å from the catalytic dyad. The increase in pocket occupation via the increase of steric bulk on TGTA-RRE compared to the other two dimeric DNICs yields final intermolecular energies of -11.18 kcal/mol for TGTA-RRE, -8.10 kcal/mol for TG-RRE, and -7.81 kcal/mol for SCy-RRE (Figure V-11).

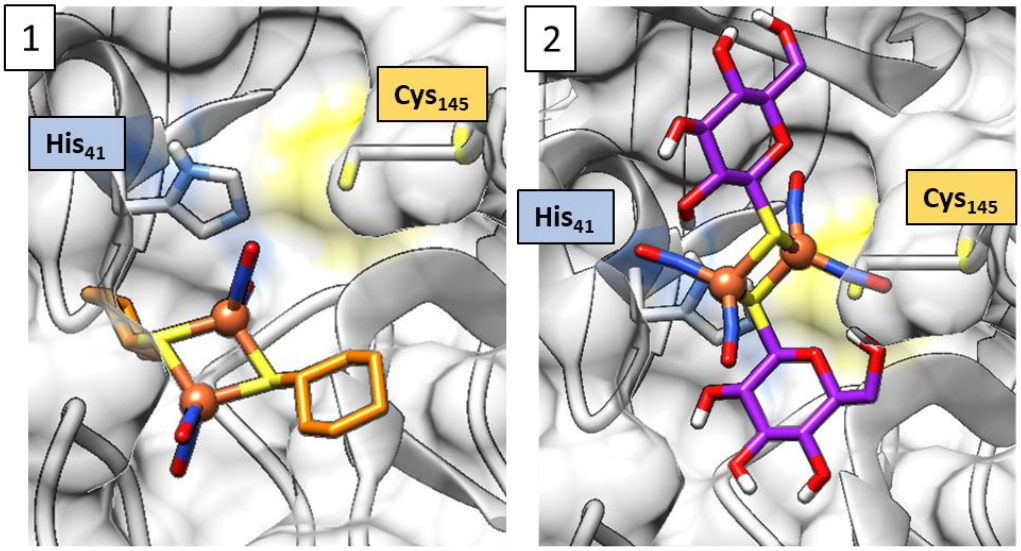

	1 (SCy-RRE)	2 (TG-RRE)	3(TGTA-RRE)
Final Intermolecular Energy (kcal/mol)	-8.61	-8.10	-11.18

Figure V-9: Most favorable binding poses for the dimeric DNICs (1 – SCy-RRE, orange; 2 – TG-RRE, purple; 3 – TGTA-RRE, green) at the active site of SC2Mpro (PDB: 6W63). All values are in kcal/mol. 4) Overlaid binding poses for the three dimers emphasizing the proximity to the dyad for TGTA-RRE and TG-RRE.

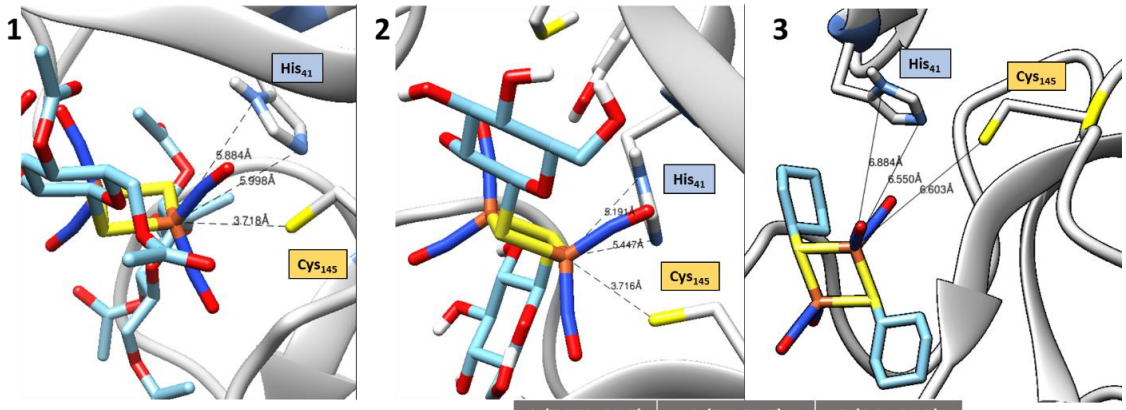

	1 (TGTA-RRE)	2 (TG-RRE)	3 (SCy-RRE)
Distance from Fe to NH of His_{41}	5.884 Å	5.191 Å	6.884 Å
Distance from Fe to N of His_{41}	5.998 Å	5.447 Å	6.550 Å
Distance from Fe to S of Cys_{145}	3.718 Å	3.716 Å	6.603 Å

Figure V-10: : Relevant distances from the DNIU to metal binding residues near the active site of SC2Mpro (PDB: 6W63) as obtained from the AutoDock4 calculations for the dimeric, RRE-type DNICs TGTA-RRE (1) , TG-RRE (2), and SCy-RRE (3).

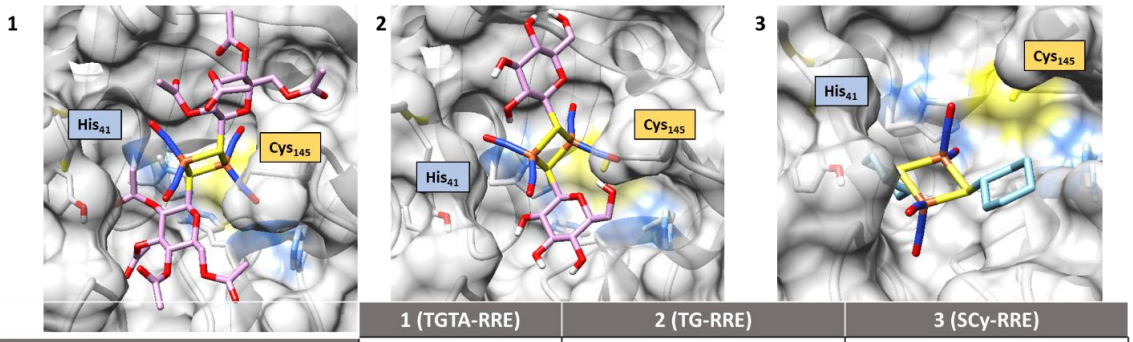

	1 (TGTA-RRE)	2 (TG-RRE)	3 (SCy-RRE)
Estimated Free Energy of Binding	-5.22 kcal/mol	-3.97 kcal/mol	-8.01 kcal/mol
Final Intermolecular Energy	-11.18 kcal/mol	-7.55 kcal/mol	-8.61 kcal/mol
vdW + Hbond + desolv Energ	-11.16 kcal/mol	-7.47 kcal/mol	-8.58 kcal/mol
Electrostatic Energy	-0.02 kcal/mol	-0.08 kcal/mol	-0.02 kcal/mol
Torsional Free Energy	+5.97 kcal/mol	-+3.58 kcal/mol	+0.60 kcal/mol

Figure V-11: Graphical representation of the binding poses with the lowest free energy generated using AutoDock4 for the dimeric DNICs, TGTA-RRE [1], TG-RRE [2], and SCy-RRE [3], to the active site of SC2Mpro (PDB: 6W63). The catalytic dyad of His41 (blue) and Cys145 (yellow) are labeled in [1, 2, 3]. Binding energies from the calculations are presented in the table below.

Table V-1: Results of the AutoDock4 calculations for the free ligand, monomeric and dimeric DNICs.

		Final Intermolecular Energy (kcal/mol)	Fe to S-Cys_{145} (Å)
Ligands	SCy	-2.78	---
	TG	-4.51	---
	TGTA	-4.29	---
Monomers	SCy($Fe(NO)_2$)	-6.36	2.069
	TG($Fe(NO)_2$)	-3.92	1.968
	TGTA($Fe(NO)_2$)	-7.71	3.132
Dimers	SCy-RRE	-8.61	6.603
	TG-RRE	-8.10	3.716
	TGTA-RRE	-11.18	3.718

V.5 Probing DNIC-based inhibition of $SC2M^{pro}$ *in vitro*

Since each of the DNICs positioned the DNIU favorably for coordinative inhibition of Cys_{145}, the two that were most soluble in aqueous media (TG-RRE and TGTA-RRE) were tested *in vitro* to see if the possibility of inhibition as purported by AutoDock is experimentally viable (Table V-1). The Ki's were experimentally determined for the free ligands TG and TGTA, $Fe(III)Cl_3$, $NaNO_2$ (NO control), and the dimeric TG-RRE and TGTA-RRE. The aforementioned FRET protease assay determined that TGTA-RRE and TG-RRE inhibited $SC2M^{pro}$ with an Ki of 38±2.0 and 33±2.0 µM respectively (Figure V-12). These values are about an order of magnitude less than Fe(III), (322.5 µM), the DNIC decomposition product in aqueous media. The free ligands and nitrite did not inhibit the protease activity of the enzyme even at mM concentrations (Figure V-1). This establishes that the inhibition comes from the dinitrosyl iron unit, and

not the thiolate, iron, or NO since the IC_{50}'s of the decomposition products are at least an order of magnitude lower than the DNICs tested. Furthermore, the inactivity of the ligand is consistent with the computational data which suggests that the free ligands are poorer inhibitors than the monomeric or dimeric forms of the DNIC.

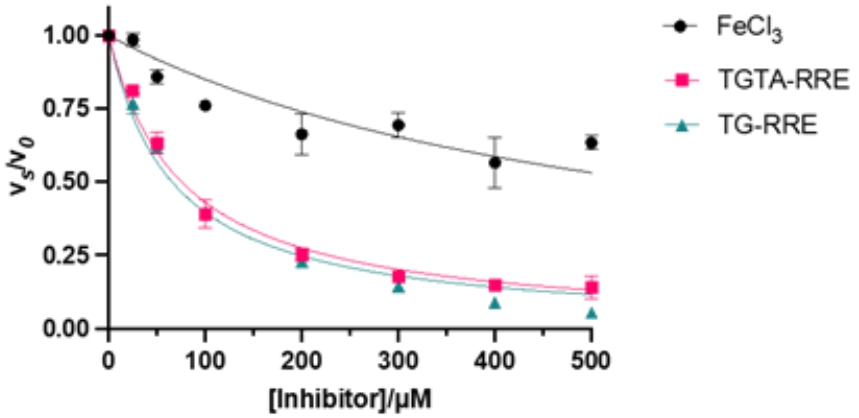

Figure V-12: Kinetic analysis of TGTA-RRE (pink), TG-RRE (green) and $FeCl_3$ (black) on $SC2M^{pro}$. Data processing method is described in supplementary information. K_i values are as follows: TGTA-RRE – 38 ±2.0, TG-RRE – 33 ±2.0, $FeCl_3$ – 284 ±30

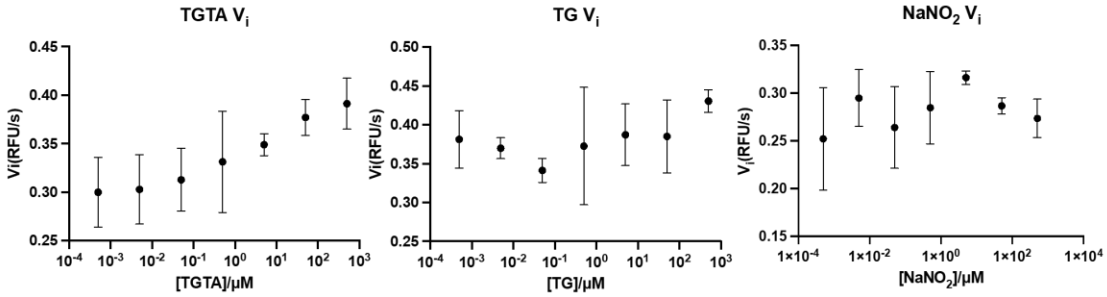

Figure V-13: Concentration vs. velocity plots used to calculate *Ki* for TGTA [Left], TG [Middle], and $NaNO_2$ [Right].

V.6 Discussion

The DNICs were found to inhibit SC2M^{pro} *in vitro*. In conjunction with computational chemistry which found that the dimeric and monomeric complexes associate with the active site of SC2M^{pro}, a reasonable supposition is that the mode of inhibition is due to the interference of substrate binding via occupation by the intact DNIC dimer, or through deactivation of the catalytic dyad by coordination of the monomeric DNIU to the catalytic Cys_{145}.

These assumptions are based on the methodological validation of AutoDock as a predictive tool for coordinatively unsaturated DNICs by recreating the crystal structure of a glutathionyl DNIC bound to GST P1-1. Although the bond distances, and angles of the primary coordination sphere of the DNIU as a result of the AutoDock computation are not perfect, the ease of computation and relative accuracy of the results are promising for predicting the interactions of a DNIU with protein substrates. Ideally, the DNIC would be treated in a more computationally rigorous manner, but DNICs have been notoriously difficult to accurately model computationally due to the extensive delocalization between the Fe *d*-orbitals and the π^* orbitals of the nitrosyl ligands leading to variable oxidation states for the DNIU.[34-38]

Table V-2: Summary of *in vitro* inhibition data derived from treatment of $SC2M^{pro}$ with compounds used in this study. IC_{50} values calculated using: $\boldsymbol{IC_{50}} = \frac{[\boldsymbol{Enzyme}]}{2} + \boldsymbol{Ki}$

Compound	Ki*/μM	IC_{50}
$FeCl_3$	322.5	322.5
$NaNO_2$	N.A	N.A
TGTA-RRE	32.87	32.88
TGTA-ligand only	N.A	N.A
TG-RRE	28.18	28.19
TG-ligand only	N.A	N.A

Based on the computational data, if the dimeric DNIC was the expected active inhibitory complex, TGTA would be the most efficacious inhibitor tested. However, the two dimeric DNICs tested had similar *Ki* values (Table V-2). This implies that the monomer is the likely active inhibitory complex since the only commonality across the molecular simulations was the proximity to the catalytic Cys_{145}. Although AutoDock accounts for electrostatic interactions between the iron and the cysteine, it does not account for any covalent interactions. Therefore we would expect the actual binding energies associated with the monomeric DNIU interaction with Cys_{145} to be more favorable than the AutoDock calculation indicates, i.e. more favorable than -3.9 to -7.7 kcal/mol.

Iron misregulation has been linked to one of the more serious side effects of COVID-19, especially notable in a hyper-inflammatory state known as a "cytokine storm."[39] This flood of IL-6 leads to the generation of hepcidin, which degrades the

ubiquitous iron exporter ferroportin, leading to an increase in intracellular iron. Consequentially, serum levels of ferritin are increased, causing hyperferritinemia. This misregulation of iron leads to a functional iron deficiency which been attributed to symptoms like anosmia and agueusia (loss of smell and taste respectively).[40-45] Building upon the interrelation between thiolates, NO, and iron, the hypothesis is that the excess of intracellular iron associated with a poor COVID prognosis can be converted to DNICs thus dampening the symptoms related to iron toxicity and potentially using the resulting DNICs to inhibit $SC2M^{pro}$.[46-48] The exact formulation required to generate effective DNIC inhibitors *in vivo* remains unknown, but turning the iron misregulation associated with a poor prognosis into an inhibitor of viral replication is a promising therapeutic outcome to pursue.

V.7 Conclusion

Dinitrosyl iron complexes TGTA-RRE and TG-RRE inhibit $SC2M^{pro}$ *in vitro* with a *Ki* of 38 μM and 33 μM, respectively. Based on the *in silico* docking data obtained and the *in vitro* values for inhibition, the likely active inhibitory species is a monomeric DNIC, derived from the splitting of the dimeric RRE-DNIC, bound to the catalytic Cys_{145}. This study presents a simple, but validated, computational method for predicting DNIC-protein interactions, allowing for the modelling of DNICs as potential inhibitors for other enzymes of interest.

V.8 References:

(1) Morse, J. S.; Lalonde, T.; Xu, S.; Liu, W. R. Learning from the Past: Possible Urgent Prevention and Treatment Options for Severe Acute Respiratory Infections Caused by 2019-nCoV. *Chem. Bio. Chem.* **2020**, *21* (5), 730–738.

(2) Dai, W.; Zhang, B.; Su, H.; Li, J.; Zhao, Y.; Xie, X.; Jin, Z.; Liu, F.; Li, C.; Li, Y.; et al. Structure-Based Design of Antiviral Drug Candidates Targeting the SARS-CoV-2 Main Protease. *Science.* **2020**, *368* (6497), 1–9.

(3) Pandey, A.; Nikam, N.; Shreya, A. B.; Mutalik, S. P.; Gopalan, D.; Kulkarni, S.; Singh Padya, B.; Fernandes, G.; Mutalik, S.; Prassl, R. Potential Therapeutic Targets for Combating SARS-CoV-2: Drug Repurposing, Clinical Trials and Recent Advancements. *Life Sci.* **2020**, *256*, 1–20.

(4) Joshi, R. S.; Jagdale, S. S.; Bansode, S. B.; Shiva Shankar, S.; Tellis, M. B.; Kumar Pandya, V.; Chugh, A.; Giri, A. P.; Kulkarni, M. J. Discovery of Potential Multi-Target-Directed Ligands by Targeting Host-Specific SARS-CoV-2 Structurally Conserved Main Protease. *J. Biomol. Struct. Dyn.* **2020**, 16.

(5) Zhang, L.; Lin, D.; Sun, X.; Curth, U.; Drosten, C.; Sauerhering, L.; Becker, S.; Rox, K.; Hilgenfeld, R. Crystal Structure of SARS-CoV-2 Main Protease Provides a Basis for Design of Improved a-Ketoamide Inhibitors. *Science.* **2020**, *368* (6489), 409–412.

(6) Goyal, B.; Goyal, D. Targeting the Dimerization of the Main Protease of Coronaviruses: A Potential Broad-Spectrum Therapeutic Strategy. *ACS Combinatorial Science*. **2020**, 22 (6), 297-305.

(7) Zanetti-Polzi, L.; Smith, M. D.; Chipot, C.; Gumbart, J. C.; Lynch, D. L.; Pavlova, A.; Smith, J. C.; Daidone, I. Tuning Proton Transfer Thermodynamics in SARS-CoV-2 Main Protease: Implications for Catalysis and Inhibitor Design. *J. Phys. Chem. Lett.* **2021**, *12* (17), 4195–4202.

(8) Joshi, R. S.; Jagdale, S. S.; Bansode, S. B.; Shiva Shankar, S.; Tellis, M. B.; Kumar Pandya, V.; Chugh, A.; Giri, A. P.; Kulkarni, M. J. Discovery of Potential Multi-Target-Directed Ligands by Targeting Host-Specific SARS-CoV-2 Structurally Conserved Main Protease. *J. Biomol. Struct. Dyn.* **2020**, 16.

(9) Ramos-Guzmán, C. A.; Ruiz-Pernía, J. J.; Tuñón, I. Unraveling the SARS-CoV-2 Main Protease Mechanism Using Multiscale Methods. *ACS Catal.* **2020**, *10* (21), 12544–12554.

(10) Bzówka, M.; Mitusińska, K.; Raczyńska, A.; Samol, A.; Tuszyński, J. A.; Góra, A. Structural and Evolutionary Analysis Indicate That the Sars-COV-2 Mpro Is a Challenging Target for Small-Molecule Inhibitor Design. *Int. J. Mol. Sci.* **2020**, *21* (9). (1)

(11) Lee, C.-C.; Kuo, C.-J.; Hsu, M.-F.; Liang, P.-H.; Fang, J.-M.; Shie, J.-J.; Wang, A. H.-J. Structural Basis of Mercury- and Zinc-Conjugated Complexes as SARS-CoV 3C-like Protease Inhibitors. *FEBS Lett.* **2007**, *581* (28), 5454–5458.

(12) Cho, S.-L.; Liao, · Cheng-Jhe; Lu, T.-T. Synthetic Methodology for Preparation of Dinitrosyl Iron Complexes. *J. Biol. Inorg. Chem.* **2019**, *24*, 495–515.

(13) Vanin, A. F. Dinitrosyl Iron Complexes with Thiol-Containing Ligands as a Base for New-Generation Drugs (Review). *Open Conf. Proc. J.* **2013**, *4*, 47–53.

(14) Carpenter, A. W.; Schoenfisch, M. H. Nitric Oxide Release Part II. Therapeutic Applications. *Chem. Soc. Rev.* **2012**, *40* (10), 3742–3752.

(15) Vanin, A. F. Dinitrosyl Iron Complexes with Thiolate Ligands: Physico-Chemistry, Biochemistry and Physiology. *Nitric Oxide*. **2009**, *21* (1), 1-13.

(16) Remizova, M. I.; Kochetygov, N. I.; Gerbout, K. A.; Lakomkin, V. L.; Timoshin, A. A.; Burgova, E. N.; Vanin, A. F. Effect of Dinitrosyl Iron Complexes with Glutathione on Hemorrhagic Shock Followed by Saline Treatment. *Eur. J. Pharmacol.* **2011**, No. 662, 40–46.

(17) Burgova, E. N.; Tkachev, N. A.; Adamyan, L. V.; Mikoyan, V. D.; Paklina, O. V.; Stepanyan, A. A.; Vanin, A. F. Dinitrosyl Iron Complexes with Glutathione Suppress Experimental Endometriosis in Rats. *Eur. J. Pharmacol.* **2014**, *727* (1), 140–147.

(18) Shumaev, K. B.; Gorudko, I. V; Kosmachevskaya, O. V; Grigorieva, D. V; Panasenko, O. M.; Vanin, A. F.; Topunov, A. F.; Terekhova, M. S.; Sokolov, A. V; Cherenkevich, S. N.; et al. Protective Effect of Dinitrosyl Iron Complexes with Glutathione in Red Blood Cell Lysis Induced by Hypochlorous Acid. *Oxi. Med. Cell. Longev.* **2019**, 1–12.

(19) Mintz, J.; Vedenko, A.; Rosete, O.; Shah, K.; Goldstein, G.; Hare, J. M.; Ramasamy, R.; Arora, H. Current Advances of Nitric Oxide in Cancer and Anticancer Therapeutics. *Vaccines* **2021**, *9* (2), 94.

(20) Murad, F. Nitric Oxide and Cyclic GMP in Cell Signaling and Drug Development. *N. Engl. J. Med.* **2006**, *355* (19), 2003–2011.

(21) Ekanger, L. A.; Oyala, P. H.; Moradian, A.; Sweredoski, M. J.; Barton, J. K. Nitric Oxide Modulates Endonuclease III Redox Activity by a 800 MV Negative Shift upon [Fe4S4] Cluster Nitrosylation. *J. Am. Chem. Soc* **2018**, *140*, 11800–11810.

(22) Pectol, D.; Khan, S.; Chupik, R.; Elsabahy, M.; Wooley, K.; Darensbourg, M.; Lim, S.-M. Toward the Optimization of Dinitrosyl Iron Complexes as Therapeutics for Smooth Muscle Cells. *Mol. Pharm.* **2019**, *16* (7), 3178–3187.

(23) Pectol, D.; Khan, S.; Elsabahy, M.; Wooley, K.; Lim, S.-M.; Darensbourg, M. Effects of Glutathione and Histidine on NO Release from a Dimeric Dinitrosyl Iron Complex (DNIC). *Inorg. Chem.* **2020**, *59* (23), 16998–17008.

(24) Cesareo, E.; Parker, L. J.; Pedersen, J. Z.; Nuccetelli, M.; Mazzetti, A. P.; Pastore, A.; Federici, G.; Caccuri, A. M.; Ricci, G.; Adams, J. J.; et al. Nitrosylation of Human Glutathione Transferase P1-1 with Dinitrosyl Diglutathionyl Iron Complex in Vitro and in Vivo. *J. Biol. Chem.* **2005**, *280* (51), 42172–42180.

(25) Morris, G. M.; Huey, R.; Lindstrom, W.; Sanner, M. F.; Belew, R. K.; Goodsell, D. S.; Olson, A. J. AutoDock4 and AutoDockTools4: Automated Docking with Selective Receptor Flexibility. *J. Comput. Chem.* **2009**, *30* (16), 2785–2791.

(26) Helgren, T. R.; Seven, E. S.; Chen, C.; Edwards, T. E.; Staker, B. L.; Abendroth, J.; Myler, P. J.; Horn, J. R.; Hagen, T. J. The Identification of Inhibitory Compounds of Rickettsia Prowazekii Methionine Aminopeptidase for Antibacterial Applications. *Bioorganic Med. Chem. Lett.* **2018**, *28* (8), 1376–1380.

(27) Joshi, R. S.; Jagdale, S. S.; Bansode, S. B.; Shiva Shankar, S.; Tellis, M. B.; Kumar Pandya, V.; Chugh, A.; Giri, A. P.; Kulkarni, M. J. Discovery of Potential Multi-Target-Directed Ligands by Targeting Host-Specific SARS-CoV-2 Structurally Conserved Main Protease. *J. Biomol. Struct. Dyn.* **2020**, 16.

(28) Chen, W.; Li, Y.; Cui, Y.; Zhang, X.; Zhu, H. L.; Zeng, Q. Synthesis, Molecular Docking and Biological Evaluation of Schiff Base Transition Metal Complexes as Potential Urease Inhibitors. *Eur. J. Med. Chem.* **2010**, *45* (10), 4473–4478.

(29) Chen, D.; Menche, G.; Power, T. D.; Sower, L.; Peterson, J. W.; Schein, C. H. Accounting for Ligand-Bound Metal Ions in Docking Small Molecules on Adenylyl Cyclase Toxins. *Proteins Struct. Funct. Bioinforma.* **2007**, *67* (3), 593–605.

(30) Kozak, J. J.; Gray, H. B.; Garza-López, R. A. Structural Stability of the SARS-CoV-2 Main Protease: Can Metal Ions Affect Function? *J. Inorg. Biochem.* **2020**, *211*.

(31) G.-L. Roberto A., K. John J., G. Harry B., Copper(II) Inhibition of the SARS-CoV-2 Main Protease, **2020.** *Chemrxiv*

(32) Karges, J.; Kalaj, M.; Gembicky, M.; Cohen, S. M. Re I Tricarbonyl Complexes as Coordinate Covalent Inhibitors for the SARS-CoV-2 Main Cysteine Protease. *Angew. Chemie Int. Ed.* **2021**, *60*, 2–10.

(33) Pulukkody, R.; Chupik, R. B.; Montalvo, S. K.; Khan, S.; Bhuvanesh, N.; Lim, S.-M.; Darensbourg, M. Y. Toward Biocompatible Dinitrosyl Iron Complexes: Sugar-Appended Thiolates. *Chem. Commun.* **2017**, *53*, 1180–1183.

(34) Ghosh, P.; Ding, S.; Quiroz, M.; Bhuvanesh, N.; Hsieh, C. H.; Palacios, P. M.; Pierce, B. S.; Darensbourg, M. Y.; Hall, M. B. Structural and Electronic Responses to the Three Redox Levels of Fe(NO)N2S2-Fe(NO)2. *Chem. - A Eur. J.* **2018**, *24* (60), 16003–16008.

(35) Dong, H. T.; Speelman, A. L.; Kozemchak, C. E.; Sil, D.; Krebs, C.; Lehnert, N. The Fe 2 (NO) 2 Diamond Core: A Unique Structural Motif In Non-Heme Iron–NO Chemistry . *Angew. Chemie* **2019**, *131* (49), 17859–17863.

(36) Banerjee, A.; Sen, S.; Paul, A. Theoretical Investigations on the Mechanistic Aspects of O2 Activation by a Biomimetic Dinitrosyl Iron Complex. *Chem. - A Eur. J.* **2018**, *24* (13), 3330–3339.

(37) Cheng, H.-Y.; Chang, S. Density Functional Theory of the Iron-Nitrosyl (S = 3/2) Complex. *Int. J. Quantum Chem.* **2005**, *105* (5), 511–517.

(38) Emel'Yanova, N. S.; Shestakov, A. F.; Sanina, N. A. DFT Calculations of the Redox Potentials for the Nitrosyl Complexes [Fe2(μ-RS)2(NO)4] with R = Alkyl. *Int. J. Quantum Chem.* **2013**, *113* (5), 740–744.

(39) Mehta, P.; McAuley, D. F.; Brown, M.; Sanchez, E.; Tattersall, R. S.; Manson, J. J. COVID-19: Consider Cytokine Storm Syndromes and Immunosuppression. *Lancet* **2020**, *395*, 1033–1034.

(40) Liu, W.; Zhang, S.; Nekhai, S.; Liu, S. Depriving Iron Supply to the Virus Represents a Promising Adjuvant Therapeutic Against Viral Survival. *Curr. Clin. Microbiol. Reports* **2020**, *7*, 1–7.

(41) Edeas, M.; Saleh, J.; Peyssonnaux, C. Iron: Innocent Bystander or Vicious Culprit in COVID-19 Pathogenesis? *International Journal of Infectious Diseases*. **2020**, 303–305.

(42) Cavezzi, A.; Troiani, E.; Corrao, S.; Marino, S.; Civico, A.; Cristina, D. COVID-19: Hemoglobin, Iron, and Hypoxia beyond Inflammation. A Narrative Review. *Clin. Pract.* **2020**, *10*, 1271.

(43) Perricone, C.; Bartoloni, E.; Bursi, R.; Cafaro, G.; Guidelli, G. M.; Shoenfeld, Y.; Gerli, R. COVID-19 as Part of the Hyperferritinemic Syndromes: The Role of Iron Depletion Therapy. *Immunol. Res.* **2020**, *68*, 213–224.

(44) Taneri, P. E.; Gómez-Ochoa, S. A.; Erand, L.; Raguindin, P. F.; Rojas, L. Z.; Roa-Díaz, Z. M.; Salvador Jr., D.; Groothof, D.; Minder, B.; Kopp-Heim, D.; et al. Anemia and Iron Metabolism in COVID-19: A Systematic Review and Meta-Analysis. *Eur. J. Epidemiol.* **2020**, *35*, 763–773.

(45) Sonnweber, T.; Boehm, A.; Sahanic, S.; Pizzini, A.; Aichner, M.; Sonnweber, B.; Kurz, K.; Koppelstätter, S.; Haschka, D.; Petzer, V.; et al. Persisting Alterations of Iron Homeostasis in COVID-19 Are Associated with Non-Resolving Lung

Pathologies and Poor Patients' Performance: A Prospective Observational Cohort Study. *Respir. Res.* **2020**, *21* (276), 1–9.

(46) Vanin, A. F.; Tronov, V. A.; Borodulin, R. R. Nitrosonium Cation as a Cytotoxic Component of Dinitrosyl Iron Complexes with Thiol-Containing Ligands (Based on the Experimental Work on MCF7 Human Breast Cancer Cell Culture). *Cell Biochem. Biophys.* **2021**, *79* (1), 93–102.

(47) Vanin, A. F.; Pekshev, A. V.; Vagapov, A. B.; Sharapov, N. A.; Lakomkin, V. L.; Abramov, A. A.; Timoshin, A. A.; Kapelko, V. I. Gaseous Nitric Oxide and Dinitrosyl Iron Complexes with Thiol-Containing Ligands as Potential Medicines That Can Relieve COVID-19. *Biophysics (Oxf).* **2021**, *66* (1), 155–163.

(48) Vanin, A. F. Dinitrosyl Iron Complexes with Thiol-Containing Ligands Can Suppress Viral Infections as Donors of the Nitrosonium Cation (Hypothesis). *Biophys.* **2020**, *65* (4), 698–702.

CHAPTER VI : CONCLUSION AND FUTURE DIRECTIONS

Dinitrosyl iron complex research in the chemical and biochemical fields has rapidly expanded since 2016, with 151 new manuscripts published during this time (as of May 2021). Many of the advances have led to the elucidation of the electronic structure of DNICs,[1-4] the clarification of the mechanism of N_2O production as seen in di-iron nitric oxide reductases (NORs),[5] and the ability of the DNIU to catalyze a number of reductive processes.[6-9] The majority of the publications are centered on the discovery of novel roles of DNIC's in biology, further cementing the hypothesis of DNICs as the "working form" of NO,[10,11] as well as investigations of the therapeutic nature of numerous synthetic DNICs.[12-20]

Most of these investigations of DNICs as therapeutics emulate the dimeric, thiolate-bridged motifs observed through biochemical characterization of DNICs. Chapter III describes an investigation of the modification these natural motifs with abiotic tools available only through inorganic synthetic methodologies. The introduction of inorganic ligands was thought to tune the release of NO from the DNIC with the addition of steric bulk and π backbonding via the mesityl-flanked *N*-heterocyclic carbene. By this approach, it was determined μwhich properties of the synthetic DNIC led to NO release both inside and outside smooth muscle cells, the ultimate therapeutic target for nitric oxide. The assumption was that by making monomers with sterically encumbering stabilizing ligands, like bulky *N*-heterocyclic carbenes, should decrease the rate of NO release from the DNIU. In contrast to the expected result, in all cases, the monomeric

DNICs degraded rapidly in aerobic aqueous conditions, and the dimeric DNICs were sustained sources of NO (up to 24 h). In the dimeric form, the DNICs were much less toxic, and did not artificially stimulate the production of cytokines from macrophage cells. The most promising of the potential DNIC-based therapeutics combined thiolates from an FDA approved drug(thioglucosetetraacetate is bound to a Au-phosphine unit in Auranophin[21]) with the naturally occurring dimeric DNIC motif: TGTA-RRE.

Since it was observed, Chapter III, that cleaving the dimer caused the NO to be released more rapidly, it was theorized that some unknown agent inside the cell caused the dimer to liberate NO through cleavage. Building upon this assumption, in Chapter IV, it was postulated that the *in situ* generation of novel cleaved monomeric species could alter the therapeutic nature, i.e., alter the NO release rate, of our most promising therapeutic lead without having to design and synthesize an entirely new series of DNICs. Based on the rich history of DNICs in synthetic inorganic chemistry, its known that imidazoles and thiols could cleave the DNIC dimer to generate a monomer. The most abundant sources of imidazoles and thiolates expected to be in the cell are histidine and glutathione respectively. The dimeric TGTA-RRE was treated with increasing concentrations of histidine and glutathione to observe if there was any change in the rate of NO release. Interestingly, there were two different outcomes. As was expected, upon cleavage with histidine, the DNIU is destabilized, and degrades, causing an increase in the rate of NO release inside and outside the cell. However, upon cleavage with glutathione, the rate of NO release decreases. The idea is that the excess of glutathione cleaves and stabilizes the DNIC for long enough that it is able to reform the more stable dimer in

aerobic aqueous environments. In addition to cleavage by an exogenous agent, reduction of the DNIC drastically reduces the amount of NO released in media, and completely eliminated NO release intracellularly. Since reduction is not the trigger, it was postulated that the cleavage by some harder ligand in the cellular milieu is ultimately the active NORM for dimeric DNICs.

The addition of safe, accessory biological molecules to alter the efficacy of the therapeutic DNIC has applications beyond the release of NO. The active form of many metallotherapeutics, such as platinum-based anti-cancer drugs or silver releasing *N*-heterocyclic carbenes, are generated upon *in situ* ligand substitution.[22-24] By intentionally incubating these therapeutic complexes with increasing concentrations of glutathione or histidine could potentially modulate the efficacy of the drug without having to entirely reformulate the drug and initiate the lengthy and costly process of FDA approval.[25]

Furthermore, the information gathered in Chapter IV supports Vanin's hypothesis that the DNIC is the "working form" of NO.[26] This isolated and characterized system showed the presence of mixed thiolate bridged DNICs upon the addition of glutathione, emphasizing the interrelation of the CIP, NO and GSH. The assumption based on the data provided is that when smooth muscle cells encounter an RRE-type DNIC, the NO and the Fe in the DNIC are incorporated into the cell's interrelated pathways with the aid of endogenously produced glutathione. Judging by the biological importance of the DNIC in nitric oxide storage, transport, and release, it seems counterintuitive that DNICs are spontaneously formed in the cytosol without the aid of a scaffold protein or through some enzymatic process, but to this date, there are no enzymes that catalyze the formation of

dinitrosyl iron complexes. The area of formation, trafficking, and controlled decomposition of DNICs awaits further biochemical investigation. The likely candidates for this enzymatic formation of DNICs would be related to glutathione transport and reduction due to the heavily interrelated nature of Fe, NO, and GSH in biology, and that the only known crystal structure of a DNIC is GST P1-1 bound to a glutathionyl DNIC.[27]

In order to further modulate NO release from the DNIU, instead of altering the primary coordination sphere as was shown in Chapters III & IV, it was postulated that installing the DNIC into a larger macromolecular framework would abrogate the rapid decomposition of the monomeric DNICs, and allow for the fine-tuning of NO release from the DNIU. It is estabilished that the coordination environment of the DNIU dictates its ability to release NO, and with the proper ligation DNICs are sufficiently robust and can provide sustained release of NO for up to 24 hours. However, when the coordination environment of the DNIU contains an N-N or M-N_2S_2 bidentate chelate, the NO payload is released within 30 minutes.[16] There are numerous potential DNIC binding motifs that can be incorporated into a polymeric framework, such at the M-N_2S_2 metallodithiolate, disulfides, and N-N chelates (Figure VI-1).[22]

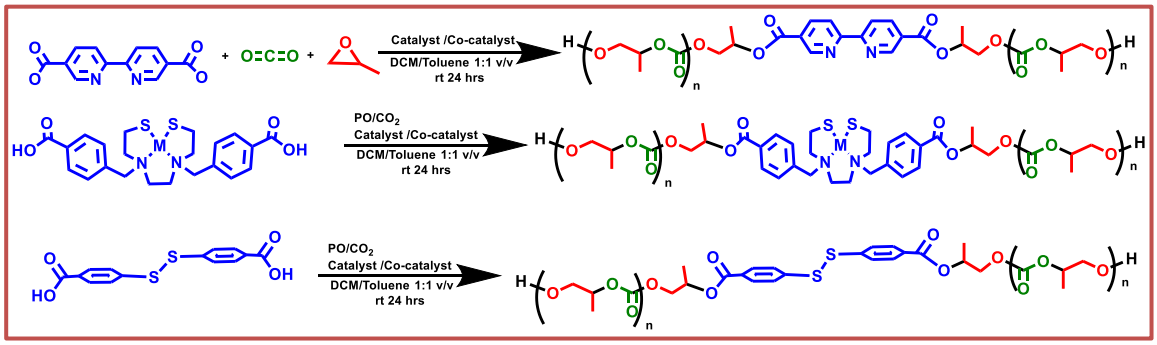

Figure VI-1: Potential DNIC binding motifs incorporated into a polycarbonate polymer. Based on synthesis of bipy polymers outlined in Ref 25.

It is expected that the rapid decomposition seen in the monomeric chelates will be abrogated upon incorporation into the macromolecular scaffold. The polymers were characterized in an analogous manner to the rhenium carbonyl prototype using UV-Vis, FT-IR and NMR spectroscopies.[22-25] Based on preliminary data collected using the bipy-based polymer shown above, the DNIU does not survive polymerization conditions, however, if the DNIU is installed after the ABA triblock polymer is synthesized, NO is liberated from the macromolecule (Figure VI-2). However, the identity/presence of the DNIU is muddled based on the FT-IR spectra (interference due to the polycarbonate, and relative weakness of the DNIC ν(NO) stretches) and EPR spectroscopy (interference due to residual catalyst leads to DNIC S = ½ signal quenching). Still, based on the DNIU synthons that were tested for incorporation into the polymeric framework, the $\{Fe(NO)_2\}^{10}$ DNIU synthon, $Fe(CO)_2(NO)_2$, proved to be the most efficacious at intracellular delivery of NO to SMCs. The other $\{Fe(NO)_2\}^9$ synthons, $Fe(CO)_3(NO)$ + 2 $NOBF_4$ and the trinitrosyl iron complex $[(IMes)Fe(NO)_3]^+$, provided the SMC with a statistically higher concentration of NO lower than the $\{Fe(NO)_2\}^{10}$ synthon. The identity of the polymer bound DNIC has yet to be elucidated.

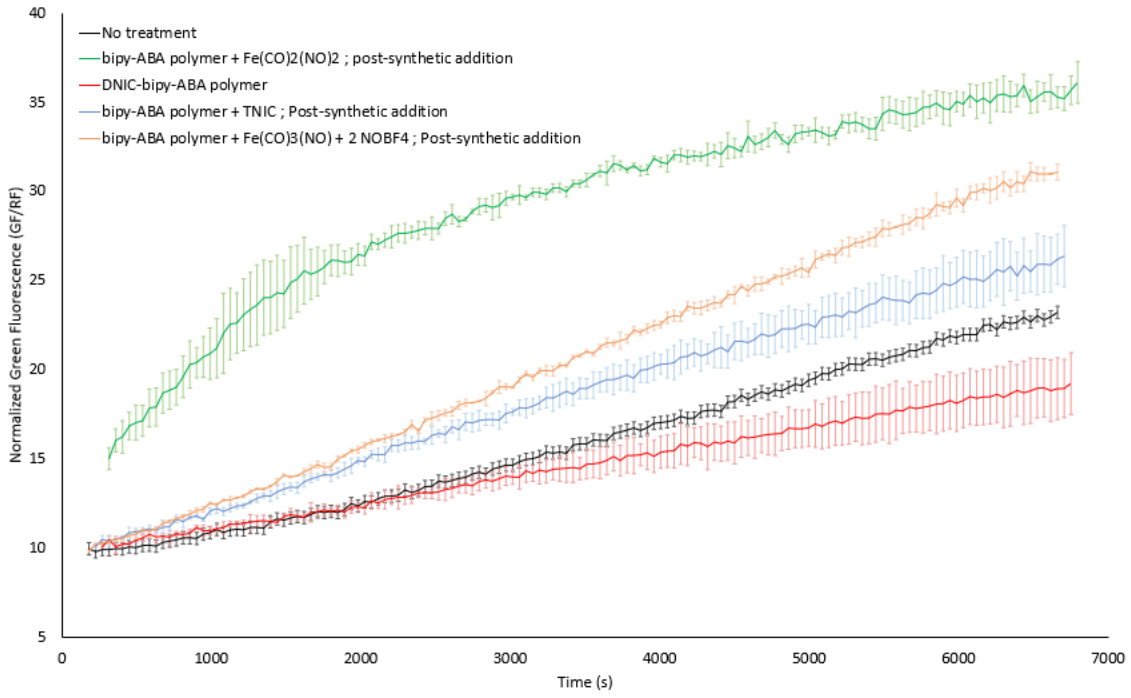

Figure VI-2: Intracellular NO release profile for bipy-based polymers (1 mg bipyCTA/mL) loaded with different DNIU synthons. Post-synthetic synthon addition indicates that the DNIC source was appended to the polymer after completion of polymer synthesis. Time = 0 indicates the time point at which SMCs were initially treated with DNIC.

Scientists are always looking for a way to apply their expertise to glaring societal needs, and that is exactly what we attempted to do with our foray into the field of antiviral research. As was shown above, DNICs have a number of biological interactions with thiolates and imidazoles; so in Chapter V, the main protease of COVID-19, $SC2M^{pro}$, (the active site contains a catalytic cysteine and histidine) was explored as a potential target for inhibition by DNICs. *In silico* chemistry, namely the computational docking program AutoDock4.2.6, was used to confirm the mechanism of DNIC inhibition of the protease. By properly parameterizing the coordinatively unsaturated DNIC, AutoDock reproduced the only reported crystal structure of a DNIC bound to a protein providing us with

confidence in our approach. Using that methodology for modeling the DNIC inhibitors, an array of nine molecules was tested based on three thiolates, thioglucosetetraacetate, thioglucose, and thiocyclohexane. The free thiolate ligand, the monomeric DNIC bound to the thiolate with a vacant coordination site, and the dimeric DNIC were computationally docked for all thiolate derivatives. Based on that collection of data, the free ligands were the poorest inhibitors, the monomeric DNICs were in the middle, then the dimeric DNICs had the most favorable binding energies. We would expect the binding energies for the monomeric DNICs to be lower that what was calculated with AutoDock since the association of the iron with the protein is purely electrostatic. The TGTA- and TG-based DNICs were shown to occupy the substrate binding pocket, provide the lowest binding energies, and position the DNIU for coordinative inhibition of the catalytic Cys_{145} of $SC2M^{pro}$. When tested for efficacy *in vitro,* TGTA-RRE and TG-RRE inhibited $SC2M^{pro}$ with an IC_{50} of 32.9 μM and 28.2 μM, respectively. The thiol ligands, nitrite, and $FeCl_3$ did not inhibit the protease at concentrations up to 100 μM. thus further validating the *in silico* methodology and implicating the monomeric DNIC as the active inhibitory agent.

This computational methodology only accounts for the electrostatic interactions between the iron and the protein, but the reality of the potential chemistries that the DNIU could be involved in far exceeds simple coordination. The only other documented inhibition of a protease by a DNIC was actually due to nitrosylation of a catalytic thiol, and not coordination of the DNIU. Higher order computational methods might provide insight as to how and if RSNO formation occurs via the dinitrosyl iron unit since experimental evidence shows that the formation of DNICs are necessary for intracellular

protein RSNO formation.[26-29] However, the computational modelling of the DNIU has proven to be no trivial task.

Overall, DNICs have proven themselves to be interdisciplinary molecules. The diffuse and fluxional electronic structure of the DNIU has fascinated inorganic and physical chemists. The ability of DNIC clusters to perform two electron chemistry due to their electrochemical reversibility has attracted inorganic and organic chemists. The emergence of DNICs as the true actors in the storage and transport of nitric oxide *in vivo* is emerging as a field of biochemical research, and the therapeutic nature of the DNIU is a relatively unexplored field in pharmaceutical chemistry. We hope that advances outlined in this dissertation have made strides towards the understanding and formulation of safe and effective DNIC-based therapeutics.

References:

(1) Speelman, A. L.; Zhang, B.; Silakov, A.; Skodje, K. M.; Alp, E. E.; Zhao, J.; Hu, M. Y.; Kim, E.; Krebs, C.; Lehnert, N. Unusual Synthetic Pathway for an $\{Fe(NO)_2\}^9$ Dinitrosyl Iron Complex (DNIC) and Insight into DNIC Electronic Structure via Nuclear Resonance Vibrational Spectroscopy. *Inorg. Chem.* **2016**, *55*, 5485–5501.

(2) Dong, H. T.; Speelman, A. L.; Kozemchak, C. E.; Sil, D.; Krebs, C.; Lehnert, N. The $Fe_2(NO)_2$ Diamond Core: A Unique Structural Motif In Non-Heme Iron–NO Chemistry. *Angew. Chemie - Int. Ed.* **2019**, *58* (49), 17695–17699.

(3) White, C. J.; Speelman, A. L.; Kupper, C.; Demeshko, S.; Meyer, F.; Shanahan, J. P.; Alp, E. E.; Hu, M.; Zhao, J.; Lehnert, N. The Semireduced Mechanism for Nitric Oxide Reduction by Non-Heme Diiron Complexes: Modeling Flavodiiron Nitric Oxide Reductases. *J. Am. Chem. Soc.* **2018**, *140* (7), 2562–2574.

(4) Delgado, M.; Gilbertson, J. D. Ligand-Based Reduction of Nitrate to Nitric Oxide Utilizing a Proton-Responsive Secondary Coordination Sphere. *Chem. Commun.* **2017**, *53* (81), 11249–11252.

(5) Wu, W. Y.; Hsu, C. N.; Hsieh, C. H.; Chiou, T. W.; Tsai, M. L.; Chiang, M. H.; Liaw, W. F. NO-to-[N2O2]2--to-N2O Conversion Triggered by $\{Fe(NO)_2\}^{10}$-$\{Fe(NO)_2\}^9$ Dinuclear Dinitrosyl Iron Complex. *Inorg. Chem.* **2019**, *58* (15), 9586–9591.

(6) Tseng, Y.; Ching, W.; Liaw, W.; Lu, T. Dinitrosyl Iron Complex [K-18-crown-6-ether][$(NO)_2Fe(^{Me}PyrCO_2)$]: Intermediate for Capture and Reduction of Carbon Dioxide. *Angew. Chemie Int. Ed.* **2020**, *59* (29), 11819–11823.

(7) Ding, S.; Ghosh, P.; Darensbourg, M. Y.; Hall, M. B. Interplay of Hemilability and Redox Activity in Models of Hydrogenase Active Sites. *Proc. Natl. Acad. Sci. U. S. A.* **2017**, *114* (46), E9775–E9782.

(8) Ding, S.; Ghosh, P.; Lunsford, A. M.; Wang, N.; Bhuvanesh, N.; Hall, M. B.; Darensbourg, M. Y. Hemilabile Bridging Thiolates as Proton Shuttles in Bioinspired H2 Production Electrocatalysts. *J. Am. Chem. Soc.* **2016**, *138* (39), 12920–12927.

(9) Ghosh, P.; Ding, S.; Chupik, R. B.; Quiroz, M.; Hsieh, C. H.; Bhuvanesh, N.; Hall, M. B.; Darensbourg, M. Y. A Matrix of Heterobimetallic Complexes for Interrogation of Hydrogen Evolution Reaction Electrocatalysts. *Chem. Sci.* **2017**, *8* (12), 8291–8300.

(10) Vanin, A. F. Dinitrosyl Iron Complexes with Thiol-Containing Ligands as a "Working Form" of Endogenous Nitric Oxide. *Nitric Oxide* **2016**, *54*, 15–29.

(11) Mikoyan, V. D.; Vanina, L. S.; Vanin, A. F. Dinitrosyl Iron Complexes with Thiol-Containing Ligands in Plant Tissues. *Biophys.* **2017**, *62* (3), 559–564.

(12) Shumaev, K. B.; Gorudko, I. V; Kosmachevskaya, O. V; Grigorieva, D. V; Panasenko, O. M.; Vanin, A. F.; Topunov, A. F.; Terekhova, M. S.; Sokolov, A. V; Cherenkevich, S. N.; et al. Protective Effect of Dinitrosyl Iron Complexes with Glutathione in Red Blood Cell Lysis Induced by Hypochlorous Acid. *Oxi. Med. Cell. Longev.* **2019**, 1–12.

(13) Truzzi, D. R.; Alves, S. V.; Netto, L. E. S.; Augusto, O. The Peroxidatic Thiol of Peroxiredoxin 1 Is Nitrosated by Nitrosoglutathione but Coordinates to the Dinitrosyl Iron Complex of Glutathione. *Antioxidants* **2020**, *9* (4).

(14) Pisarenko, O.; Studneva, I.; Timoshin, A.; Veselova, O. Protective Efficacy of Dinitrosyl Iron Complexes with Reduced Glutathione in Cardioplegia and Reperfusion. *Pflugers Arch. Eur. J. Physiol.* **2019**, *471* (4), 583–593.

(15) Akentieva, N. P.; Sanina, N. A.; Prichodchenko, T. R.; Gizatullin, A. R.; Shkondina, N. I.; Shushanov, S. S.; Stupina, T. S.; Aldoshin, S. M. Anticancer

Activity of Dinitrosyl Iron Complex (NO Donor) on the Multiple Myeloma Cells. *Dokl. Biochem. Biophys.* **2019**, *486* (1), 238–242.

(16) Pectol, D. S.; Khan, S.; Chupik, R. B.; Elsabahy, M.; Wooley, K. L.; Darensbourg, M. Y.; Lim, S.-M. Toward the Optimization of Dinitrosyl Iron Complexes as Therapeutics for Smooth Muscle Cells. *Mol. Pharm.* **2019**, *16* (7).

(17) Huang, H.-W.; Lin, Y.-H.; Lin, M.-H.; Huang, Y.-R.; Chou, C.-H.; Hong, H.-C.; Wang, M.-R.; Tseng, Y.-T.; Liao, P.-C.; Chung, M.-C.; et al. Extension of C. Elegans Lifespan Using the ·NO-Delivery Dinitrosyl Iron Complexes. *J. Biol. Inorg. Chem.* **2018**, *23* (3), 775–784.

(18) Gizatullin, A. R.; Akentieva, N. P.; Sanina, N. A.; Shmatko, N. Y.; Goryachev, N. S.; Shkondina, N. I.; Prichodchenko, T. R.; Zhelev, N.; Aldoshin, S. M. Effect of Dinitrosyl Iron Complexes (NO Donors) on the Metabolic Processes in Human Fibroblasts. *Dokl. Biochem. Biophys.* **2018**, *483* (1), 337–340.

(19) Liu, T.; Zhang, M.; Terry, M. H.; Schroeder, H.; Wilson, S. M.; Power, G. G.; Li, Q.; Tipple, T. E.; Borchardt, D.; Blood, A. B. Hemodynamic Effects of Glutathione-Liganded Binuclear Dinitrosyl Iron Complex: Evidence for Nitroxyl Generation and Modulation by Plasma Albumin. *Mol. Pharmacol.* **2018**, *93* (5), 427–437.

(20) Sahni, S.; Hickok, J. R.; Thomas, D. D. Nitric Oxide Reduces Oxidative Stress in Cancer Cells by Forming Dinitrosyl Iron Complexes. *Nitric Oxide* **2018**, *76*, 37–44.

(21) Mjos, K. D.; Orvig, C. Metallodrugs in Medicinal Inorganic Chemistry. *Chem. Rev.* **2014**, *114*, 4540–4563.

(22) Bhat, G. A.; Rashad, A. Z.; Darensbourg, D. J. Synthesis of Terpyridine-Containing Polycarbonates with Post-Polymerization Providing Water-Soluble and Micellar Polymers and Their Metal Complexes. *Polym. Chem* **2020**, 11, 4699.

(23) Folsom, T. M.; Bhat, G. A.; Rashad, A. Z.; Darensbourg, D. J. Approach for Introducing a Single Metal Complex into a Polymer Chain: Metallo-Chain Transfer Agents in CO_2 or COS/Epoxide Copolymerization Processes. *Macromol.* **2019**, *52*, 5217–5222.

(24) Bhat, G. A.; Luo, M.; Darensbourg, D. J. Catalysis of Carbon Dioxide and Oxetanes to Produce Aliphatic Polycarbonates. *Green Chem.* **2020**, *22*, 7707–7724.

(25) Bhat, G. A.; Darensbourg, M. Y.; Darensbourg, D. J. Copolymerization of Propylene Oxide and $^{13}CO_2$ to Afford Completely Alternating Regioregular ^{13}C-Labeled Poly(Propylene Carbonate). *Polym. J.* **2021**, *53* (1), 215–218.

(26) Köberle, B.; Schoch, S. Platinum Complexes in Colorectal Cancer and Other Solid Tumors. *Cancers*. **2021**, 13 (9), 1-21

(27) Ndagi, U.; Mhlongo, N.; Soliman, M. E. Metal Complexes in Cancer Therapy – An Update from Drug Design Perspective. *Drug Design, Development and Ther* **2017**, 11, 599-616.

(28) De Frémont, P.; Scott, N. M.; Stevens, E. D.; Ramnial, T.; Lightbody, O. C.; Macdonald, C. L. B.; Clyburne, J. A. C.; Abernethy, C. D.; Nolan, S. P. Synthesis of Well-Defined N-Heterocyclic Carbene Silver(I) Complexes. *Organommetallics* **2005**, *24*, 6301–6309.

(29) Rubino, F. M. Toxicity of Glutathione-Binding Metals: A Review of Targets and Mechanisms. *Toxics* **2015**, *3*, 20–62.

(30) Vanin, A. F., Dinitrosyl iron complexes with thiol-containing ligands as a "working form" of endogenous nitric oxide. *Nitric Oxide* **2016,** *54*, 15-29.

(31) Bosworth, Charles, A.; Toledo Jr., J. C.; Zmijewski, J. W.; Li, Q.; Lancaster Jr., J. R. Dinitrosyliron Complexes and the Mechanism(s) of Cellular Protein Nitrosothiol Formation from Nitric Oxide. *Proc. Natl. Acad. Sci.* **2009**, *106*, 4671–4676.

(32) Li, Q.; Li, C.; Mahtani, H. K.; Du, J.; Patel, A. R.; Lancaster Jr., J. R. Nitrosothiol Formation and Protection against Fenton Chemistry by Nitric Oxide-Induced Dinitrosyliron Complex Formation from Anoxia-Initiated Cellular Chelatable Iron Increase. *J. Biol. Chem.* **2014**, *289* (29), 19917–19927.

(33) Keszler, A.; Diers, A. R.; Ding, Z.; Hogg, N. Thiolate-Based Bidinitrosyl Iron Complexes: Decomposition and Detection and Differentiation from S-Nitrosothiols. *Nitric Oxide* **2017**, *65*, 1–9.

(34) Wynia-Smith, S. L.; Smith, B. C. Nitrosothiol Formation and S-Nitrosation Signaling through Nitric Oxide Synthases. *Nitric Oxide* **2017**, *63*, 52–60.